Durham E-Theses

Using the fucosylation mutant sensitive-to-freezing8 (sfr8) to explore the influence of plant cell wall on transpiration

HULME, RACHEL,KATIE

How to cite:

Use policy

Using the fucosylation mutant *sensitive-to-freezing8* (*sfr8*) to explore the influence of plant cell wall on transpiration

Rachel Katie Hulme

Durham University

Submitted for the Degree of Master of Science by Research
Department of Biosciences
March 2022

Abstract

Cell walls have a specialised structure and function in guard cells that surround and control the openness of the stomata, microscopic pores allowing CO_2 uptake and water loss. The *Arabidopsis thaliana senstive-to-freezing8 (sfr8)* mutant loses water more quickly than wildtype and has severely reduced levels of cellular fucose, affecting multiple aspects of cell wall, including xyloglucan, pectin, proteins and mechanical strength. The defective cell wall components of *sfr8* may result in a higher transpiration rate. This study aims to discover how the *sfr8* cell wall mutation influences transpiration.

Arabidopsis mutants affected in different aspects of cell wall were measured for their transpiration rate and stomatal conductance, the rate of stomatal gas exchange. Mutants in fucosylation, pectin abundance, xyloglucan and mechanical stress all had transpiration or stomatal conductance during dehydration stress similar to wildtype. Only one mutant other than *sfr8* had transpiration and stomatal conductance significantly higher than wildtype during drought stress and changing CO_2 concentration; the pectin modification mutant, *reduced wall acetylation2* (*rwa2*). Further measures of stomatal structure and function were taken. *sfr8* had significantly different stomatal development to wildtype and limited stomatal dynamics, whereas, *rwa2* had stomatal size, density and aperture equivalent to wildtype. Mutants were tested for drought tolerance and surprisingly, *sfr8* had a better survival rate than wildtype, which may be attributed to the altered stomatal development.

The results of this study and supporting literature indicate that pectin crosslinking, but not all pectin modification, affects transpiration, stomatal behaviour and drought tolerance. The higher transpiration rate of *rwa2* is probably due to cuticle damage. Moreover, *sfr8* had the highest transpiration of all tested mutants suggesting that other factors may influence *sfr8* transpiration, which are explored. Understanding the mechanistic basis of genes, like *SFR8,* that affect stomatal characteristics and drought tolerance will become increasingly important as drought becomes more prevalent.

Contents

List of figures

List of tables

List of abbreviations

Standard scientific abbreviations are used for units of amount, length, molarity, temperature, time and weight. Standard chemical elements symbols are used. Standard scientific conventions have been used for protein and gene naming: the names of wildtype proteins and genes are in capitals, while mutant names are in lowercase. The names of genes denoted by italics, whereas, protein names are not italicised.

ABA	Abscisic acid
APAP	Arabinoxylan pectin arabinogalactan protein
ARAD	Arabinan deficient
BOR	Requires high boron
CESA	Cellulose synthase
Col	Columbia ecotype
CSC	Cellulose synthase complex
EPF	Epidermal patterning factor
ESMD	Esmeralda
FOC	Fused outer cuticle ledge
FRB	Friable
FUT	Fucosyltransferase
IRGA	Infra-red gas analyser
IRX	Irregular xylem
GA	Gibberellin
GID	Gibberellin Insensitive Dwarf
HG	Homogalacturonan
MS	Murashige and Skoog media
NTC	No template control
PCR	Polymerase chain reaction
PP2C	Protein phosphatases type 2C
PME	Pectin methylesterase
PMR	Powdery mildew resistant
PRO	Procera
QUA	Quasimodo
RGL2	RGA-like 2
RG-I	Rhamnogalacturonan I
RG-II	Rhamnogalacturonan II
RGXT	RG-II specific xylosyltransferase
RWA	Reduced wall acetylation
SCORD	Susceptible-to-coronatine-deficient Pst DC300
SnRK	SNF-related kinase
TBL	Trichome birefringence
Ws	Wassilewskija ecotype
XXT	Xyloglucan xylosyltransferase

Statement of Copyright

The copyright of this thesis rests with the author. No quotation from it should be published without the author's prior written consent and information derived from it should be acknowledged.

Acknowledgements

Firstly, I would like to extend my biggest thanks to my supervisor Dr Heather Knight for her encouragement, support and advice throughout these 18-months. Your kindness and empathy have really helped through a challenging time.

Thank you to Prof Robert Baxter and Dr Ankush Prashar for sharing their equipment, their knowledge and their time. I would also like to thank Maeve Dale, Dr Ashley Pridgeon and Dr Paige Panter for all their advice from afar. Your generosity and expertise are much appreciated.

Many thanks go to all of lab 19 for their guidance, generosity and patience throughout. With special thanks to Nathan and Morgan for giving so much of your time and resources to help me and for doing so with such kindness.

Finally, thank you to my family and friends for their love and support throughout this time and through all the moments that led me here.

Chapter 1: Introduction

The plant cell wall is a dynamic mosaic of polysaccharides and proteins that performs a plethora of functions, including strength, flexibility, development and biotic and abiotic stress tolerance (Jones et al., 2003; Cosgrove, 2015; Houston et al., 2016). Each cell type has unique functions performed by the cell wall, which requires a specialised cell wall structure. Distinct cell wall structures arise from different abundances and modifications of the three main cell wall polysaccharides, which are cellulose, pectin and hemicellulose (Cosgrove, 2005; Keegstra, 2010). Also contributing to the specialised function of cell walls are different proteins, which can be enzymatic, structural, receptor, transport or signalling (Cosgrove, 2016a; Houston et al., 2016).

As cell walls are fundamental to plant cell function, cell wall mutants have a range of phenotypes, such as dwarfism, weak mechanical strength and sensitivity to stresses (Cavalier et al., 2008; MacMillan et al., 2010; Zhang et al., 2019b). The focus of this thesis, *sensitive-to-freezing8* (*sfr8*), is an *Arabidopsis thaliana* (hereafter referred to as Arabidopsis) cell wall mutant. As a result of an inability to synthesise the sugar fucose that is incorporated into many cell wall components, *sfr8* has altered structure of pectins, the hemicellulose xyloglucan and cell wall proteins (Faye et al., 1989; Pauly and Keegstra, 2016; Ndeh et al., 2017; Zentella et al., 2017). Accompanying this change to cell wall structure is a range of mutant phenotypes, including reduced strength and growth (Reiter et al., 1993); shorter petioles and rounder leaves (Gonçalves et al., 2017); as well as decreased stress tolerance (Feng et al., 2018; Zhang et al., 2019b; Panter et al., 2019); and in particular, preliminary experiments indicate *sfr8* may have a transpiration defect (Panter, 2018).

The majority of plant transpiration occurs through the stomata, the microscopic pores on the leaf surface that mediate gas exchange between plant and environment. A huge volume of water passes through the stomata, which can be problematic when the plant has a transpiration defect, like *sfr8* is proposed to have, and is especially precarious when water is scarce, such as during drought periods (Hetherington and Woodward, 2003). Plants can limit transpirational water loss through the stomata by the action of two identical cells that surround the stomata and can open and close the pore, these are guard cells. The guard cell walls, like all cells, have a specialised structure, which balances the strength and flexibility needed to control the openness of the stomata (Shope et al., 2003; Gribaa et al., 2013; Le Gall et al., 2015; Hunt et al., 2017; Novaković et al., 2018). The guard cell walls of *sfr8* are defective and could be causing the proposed water loss defect. This thesis will be investigating the effect cell wall has on leaf transpiration and stomatal characteristics through the use of *sfr8* and other cell wall mutants.

1.1 The Structure and Function of Plant Cell Walls

Cell walls are organelles that form the outer barrier of plant cells, providing strength, protection and a variety of other functions throughout the plant life cycle. Plant cell walls are a complex, dynamic, extracellular mosaic of approximately 90-95% polysaccharides and 5-10% protein (Figure 1.1; McNeil et al., 1984; Fry, 1988). There are three main cell wall polysaccharides; cellulose, pectin and hemicellulose. The linear chains of cellulose are formed of β-4-linked D-glucose residues and bind together to form microfibrils (Keegstra, 2010). Pectins have a backbone of galacturonic acid and are distinguished into three main covalently-linked domains, homogalacturonan, rhamnogalacturonan I and rhamnogalacturonan II (Harholt et al., 2010). Hemicelluloses are characterised by having β-1,4-glycosidic bonds as their dominant linkage and includes xyloglucans, xylans, mannans and β-glucans (Pauly et al., 2013). The polysaccharides interact with each other to form the cell wall matrix, which influences several properties of cell wall function. Cell wall proteins also contribute to the cell wall matrix and are of highly diverse form and function, including enzymatic, receptor, transport, structural and signalling proteins (Cosgrove, 2016a; Houston et al., 2016). The composition and thickness of cell wall varies between species, between tissues and within a cell across the different types of cell wall; primary, secondary and the middle lamella (Cosgrove, 2005; Keegstra, 2010; Houston et al., 2016). Primary cell walls are deposited during cell division in young cells and the matrix is composed of the cellulose, hemicellulose and pectin (Cosgrove and Jarvis, 2012; Zhang et al., 2021). The middle lamella, on the other hand, is deposited after cell division and is rich in pectins, which form a continuous layer between adjacent cells and secondary cell walls (Keegstra, 2010). In contrast, secondary cell walls are laid down in cells that require additional mechanical support once cell growth has stopped. The secondary cell wall matrix consists of cellulose, the hemicellulose xylan and lignin, a fourth cell wall polysaccharide that is highly abundant in secondary cell walls (Cosgrove and Jarvis, 2012; Meents et al., 2018).

Cell walls perform a wide variety of functions for plants including; providing both flexibility and strength to cells, influencing plant development, defence against herbivorous organisms and abiotic stress tolerance. Cell walls are strong, rigid matrices which maintain the structural integrity of cells by combatting internal hydrostatic pressures and by providing mechanical strength to structurally support tissues, such as the stem (Ryden et al., 2003; Chiniquy et al., 2013; Houston et al., 2016). Despite this strength, cell walls can still be flexible organelles that allow changes to cell shape, even after the cell has fully formed. Such flexibility in cell shape is important for specialised cells, notably guard cells which need to regularly change shape to open and close the stomata (Jones et al., 2003; Ralet et al., 2008). Through controlling the shape of cells, cell walls also influence cell morphology which leads to different cell types and tissues (Keegstra, 2010). Cell walls are also involved in cell development by allowing cell growth and differentiation. The connections between cell wall polysaccharides are enzymatically degraded at specific locations, which allows the cell wall components to spread apart and expand the cell size, this is cell wall loosening (Cosgrove, 2014, 2015). Once loosened, new cell wall polysaccharides are synthesised to stabilise the larger cell wall, which leads not only to cell growth but also differentiation into specialised cells, as wall loosening can occur in specific regions of the wall to trigger anisotropic growth (Cosgrove,

2014, 2015). Furthermore, cell walls are essential to forming cell to cell adhesions (Durand et al., 2009; Cosgrove, 2016b). Additionally, cell walls serve as an essential structural barrier to herbivorous organisms through both passive and active defence mechanisms (Houston et al., 2016). On top of their role in biotic stress tolerance, cell walls can be modified to tolerate a variety of abiotic stresses, such as drought, cold, heavy metal and salt stress (Le Gall et al., 2015; Houston et al., 2016; described in further detail on page 32). Moreover, the porosity of the cell wall matrix influences the water uptake and loss from cells, which can be important under osmotic stresses (McCann et al., 1990; Fleischer et al., 1999). Finally, cell walls can also be used to store polysaccharides in seeds to feed germinating plants (Naran et al., 2008).
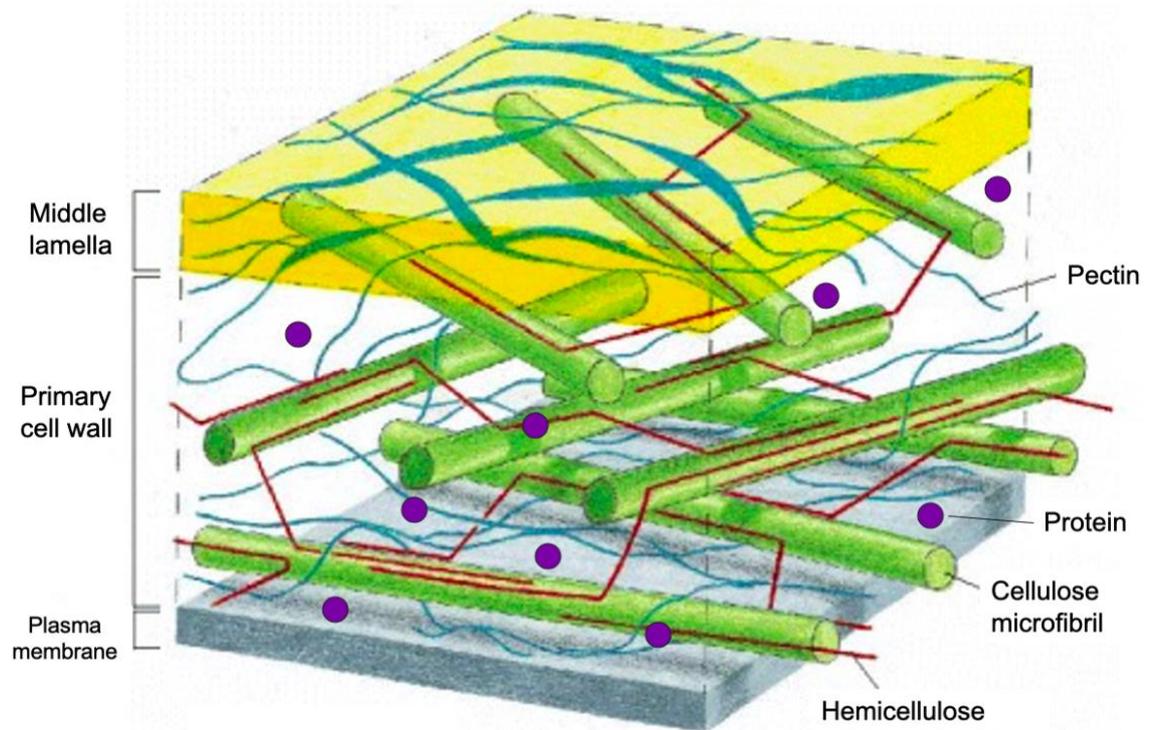
Figure 1.1: Primary cell wall of plants. Green tubes show linear cellulose microfibrils, red lines show hemicellulose and blue lines show pectin. The three polysaccharides interact with each other, forming a matrix. Purple circles show proteins, which are soluble, interact with cell wall polysaccharides or are embedded in the plasma membrane. This is the classic model that is widely used, however, recent work (e.g. Cosgrove 2016b) suggests this model is not wholly accurate. Adapted from: Alberts et al., 2007.

1.1.1 Cellulose

Cellulose is a highly abundant component of cell walls, compromising 20-30% of the dry mass of primary cell wall and 15% of the volume, and as such a large part of plant cells, cellulose is the most abundant polymer on Earth (Roelofsen, 1966). Cellulose has a simple structure, composed entirely of linear β-4-linked D-glucan, and has a high degree of polymerisation, forming chains 7,000 to 15,000 sugars long. Several cellulose chains crystallise to form ribbon-like structure, called a microfibril, which vary in diameter ranging from 3 to 15nm depending on cell type and species (McCann et al., 1990; Cosgrove, 2005; Zhang et al., 2018). The polymerisation reaction of cellulose is catalysed by cellulose synthase, which uses a UDP-glucose substrate to transfer glucose to the elongating cellulose chain (Keegstra, 2010). Cellulose abundance, distribution and chain length differs between primary and secondary cell walls.

Cellulose provides important functions for the cell, such as, providing mechanical strength, forming a polysaccharide matrix and facilitating cell growth.

1.1.1.1 The Synthesis and Structure of Cellulose

Cellulose synthase (CESA) synthesises cellulose as part of cellulose synthase complexes (CSC; Kimura et al., 1999). There are 10 isoforms of CESA, three of which must be present in the same CSC for the CSC to assemble and function normally (Cosgrove, 2005; Meents et al., 2018). A set of three CESAs are limited to vascular tissues and are required for cellulose synthesis in secondary cell walls, these are CESA4, CESA7 and CESA8 (Taylor et al., 2003). In contrast, a different set, CESA1, CESA3 and CESA6, are associated with the primary cell wall and are present in many cell types undergoing expansion, such as the root (Doblin et al., 2002). CSCs are composed of six subunits forming a rosette structure about 25nm in diameter (Doblin et al., 2002). The rosettes are assembled in the Golgi and transported areas of the plasma membrane associated with microtubules (Doblin et al., 2002; Watanabe et al., 2015). CSCs move along microtubules in linear tracks orientated perpendicular to the cell axis, this determines the microfibril orientation.

Within the same CSC, several cellulose chains are produced that associate with each other to form microfibrils. Early work suggested that each of the six rosette subunits contained six CESAs that each produced a single cellulose chain, which rendered 36 cellulose chains, all of which associated with each other to form a 36-chain microfibril (Doblin et al., 2002; Cosgrove, 2005). However, recent molecular modelling has suggested microfibrils are more likely formed of 18 or 24 cellulose chains (Oehme et al., 2015). Therefore, either some of the 36 CESAs present in the CSC are inactive (Oehme et al., 2015) or more likely only 18-24 CESAs are present in CSCs (Meents et al., 2018). An 18-chain model has been proposed, in which there are three CESAs per rosette subunit (Newman et al., 2013).

Microfibrils have hydrophobic flat sides and hydrophilic edges, which form a flat ribbon shape. Microfibrils interact with other microfibrils via hydrogen bonds between edges and Van der Waal forces between flat sides; these microfibril-microfibril crosslinks vary in length from 20 to 40nm (McCann et al., 1990; Kim et al., 2013). Projections based on an 18-chain model give rise to microfibrils that have a variety of cross-sectional shapes with different hydrophobic and hydrophilic surfaces exposed (Newman et al., 2013). The 18-chain model also suggested occasional twinning, in which two microfibrils coalesce (Newman et al., 2013). Previously, microfibrils were commonly presented as having a parallel arrangement perpendicular to the growth axis of the cell and potentially controlling the growth axis of the cell (Gardner and Blackwell, 1974; McNeil et al., 1984). Microfibril coalescence was confirmed with atomic force microscopy in which cellulose was observed at the nanoscale in an undisturbed state. Cellulose distribution was less even than previously thought and in limited regions, microfibrils even came into close contact in tight cellulose-cellulose junctions, which are implicated as biomechanical hotspots (Zhang et al., 2014).

Cellulose is more abundant in secondary cell walls composing 40-50% of wood components, whereas primary cell walls are only composed of about 20-30% cellulose (Roelofsen, 1966; Zhong and Ye, 2015). The CSCs move slowly during primary cell wall formation, meaning the rate of cellulose synthesis is slow as a result the degree of polymerisation in primary cell wall is smaller. However, during secondary cell wall formation, CSCs move faster and there is a higher density of CSCs, consequently cellulose synthesis is very rapid, yielding the high cellulose content (Marx-Figini, 1966; Watanabe et al., 2015). Unlike the disperse arrangement of cellulose in primary cells walls, cellulose microfibrils in secondary cell walls have a more compact arrangement and are wound around the cell in a helix (Cosgrove and Jarvis, 2012).

1.1.1.2 Cellulose Function

Cellulose has several important functions, including forming a polysaccharide matrix, which achieves load bearing for the cell and facilitates interactions with other cell wall components (Wang et al., 2012). Microfibrils have different hydrophilic and hydrophobic surfaces exposed due to the variety of cross-sectional shapes of microfibrils (as proposed by the 18-chain model (Newman et al., 2013)); this provides different affinities for the polysaccharides that cellulose binds, such as hemicelluloses, pectins and lignin (Cosgrove, 2014). The network formed from the tight, irreversible binding between cellulose and the hemicellulose xyloglucan is the dominant load-bearing structure in growing cell walls (Hayashi, 1989; Pauly et al., 1999). In secondary cell walls, xylan, the most abundant hemicellulose, also forms an extensive network with cellulose in via a twofold helical screw conformation (Simmons et al., 2016). A fifth to a half of cellulose exhibits close contact with pectins in the primary cell wall of Arabidopsis (Wang et al., 2012). The extensive crosslinks between cellulose and pectins may involve pectin entrapment in or between microfibrils (Wang et al., 2015). Proteins also bind microfibrils, which has an impact on cell wall properties. For example, cellulose interactions with the glycoprotein extensin determine the mechanical strength of cell wall (Iraki et al., 1989).

Another essential function of cellulose is allowing cell expansion during plant growth and morphogenesis. Cell wall loosening is an important co-ordinated process that drives morphological changes in the cell leading to differentiation and growth. For loosening to occur, cellulose microfibrils must be enzymatically loosened, which allows the microfibrils and other components associated with microfibrils to disperse (Cosgrove, 2014; Zhang et al., 2017). Some wall loosening is mediated by the protein expansin, which binds cellulose of a specific structure that is enriched with xyloglucan (Wang et al., 2015). In the short term, the spread of cell wall components allows growth, without the need to synthesise new wall polymers (Cosgrove, 2014). Later the addition of new wall polymers is needed to maintain cell wall integrity (Cosgrove, 2016b). Similarly, microfibrils can be passively reoriented when the wall is stretched by an external force, which contributes to the axial extension and transverse compression needed for the wall to withstand the force. The microfibril movement is different depending on whether it is for wall loosening for growth or due to an applied force (Zhang et al., 2017). Cellulose microfibrils are also important for consolidating the growth axis after the cell has switched from symmetric to asymmetric growth during morphogenesis (Peaucelle et al., 2015).

1.1.2 Pectin

Another highly abundant cell wall polysaccharide is pectin, which constitutes around 35% of primary cell wall in dicotyledonous plants, such as Arabidopsis, and less than 10% in grasses and woody tissue (Fry, 1988; Mohnen, 2008). As result of their complex branching and many different sugar residues, pectin synthesis requires at least 67 different glycosyltransferases, methyltransferases and acetyltransferases (Mohnen, 2008). Following synthesis in the Golgi, pectin is deposited soon after cell division during the early stages of cell expansion, which leads to a middle lamella rich in pectins (Voragen et al., 2009; Keegstra, 2010; Harholt et al., 2010). Pectin is made up of several covalently linked domains that all share a high content of galacturonic acid (Harholt et al., 2010). The largest of the pectin domains is unbranched homogalacturonan (HG), which comprises about 65% of pectin and makes up almost a quarter of Arabidopsis primary cell wall (Zablackis et al., 1995; Mohnen, 2008). The two other main pectic domains are rhamnogalacturonan I (RG-I) and rhamnogalacturonan II (RG-II), which constitute approximately 20-35% and 10% of pectin content respectively (Zablackis et al., 1995; Mohnen, 2008). There are also minor pectic domains, such as, xylogalacturonan and apiogalacturonan (Zhang et al., 2021). The three main pectin domains can be highly modified. HG can undergo high degree of modification by methyl-esters and O-acetyl esters, giving a variety of HG modification states, which are spatially regulated throughout the cell wall and across tissues (Hafrén et al., 2000; Pelloux et al., 2007; Amsbury et al., 2016; Philippe et al., 2017). RG-I can also be modified by O-acetylation or by side chains of different constitutions (Baldwin et al., 2014; Stranne et al., 2018). Additionally, the side chains of RG-II can be modified by the addition or removal of methyl- and O-acetyl esters (Pabst et al., 2013).

Through forming covalent crosslinks with cellulose and hemicelluloses, pectin is an essential part of maintaining the rigidity and integrity of the cell wall matrix (Popper and Fry, 2008). In the previously accepted tethered network model, there are few pectin-cellulose interactions and pectins have no role in cell wall dynamics, instead only space cellulose microfibrils (Figure 1.2; McCann et al., 1990). However, recent data suggests that there are extensive stable but weak crosslinks between pectin, particularly HG and RG-I, and cellulose microfibrils, more than assumed in the tethered network model (Zykwinska et al., 2005; Wang et al., 2012, 2015; Cosgrove, 2016b). Additionally, because HG can achieve a range of modification states, pectins have been recently implicated as potential control points for cell growth and differentiation, which goes against the tethered network model (Peaucelle et al., 2015). As well as its involvement in normal plant development, modification of pectin is also important for stress tolerance and mechanical strength. For example, pectin side chains highly enriched in arabinose can limit water loss during osmotic stress (Moore et al., 2013) and cold tolerant plants have a higher degree of methylesterification of HG (Baldwin et al., 2014). Similarly for biotic stress, increased pectin accumulation and decreased acetylation of HG increases pathogen resistance (Vogel et al., 2004; Manabe et al., 2011; Nafisi et al., 2015). Moreover, pectins have roles in providing mechanical strength for the cell wall while remaining very dynamic structures (Fry, 1988). Pectin also influences other cell wall properties such as surface charge, pH and porosity (McNeil et al., 1984). Porosity, a factor which determines the rate of water uptake and loss from the cell wall, is increased upon the removal of pectins (McCann et al., 1990).

The crosslinking of pectins are important for maintaining appropriate porosity and the water holding capacity of the cell wall (Einhorn-Stoll et al., 2012). The ability of pectin to allow huge changes in its hydration status mediates many cellular process, such as triggering seed germination and osmotic stress tolerance (Levesque-Tremblay et al., 2015). Additionally, pectins are integral to cell to cell adhesion, as they are rich in the middle lamella and stick together the primary cell wall of adjacent cells (Voragen et al., 2009; Cosgrove, 2016b).
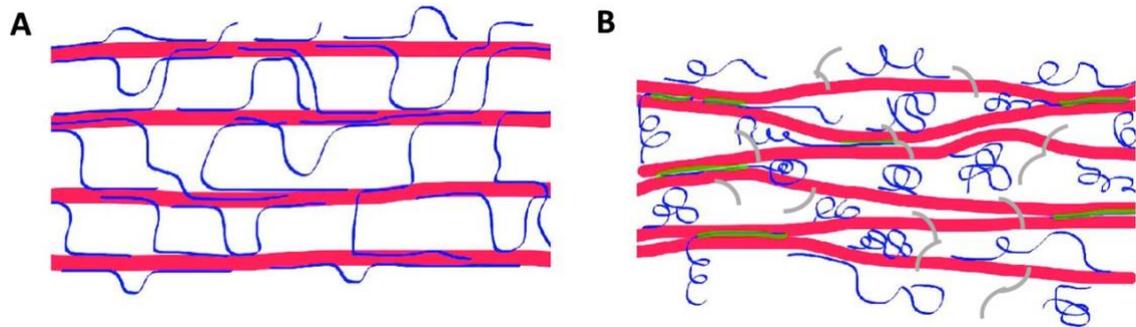
Figure 1.2: A comparison of the tethered network model (A) and the biomechanical hotspot model (B). A: Parallel cellulose microfibrils (shown as red lines) spaced by the hemicellulose xyloglucan (shown as blue lines). B: Tight cellulose-cellulose junctions bonded by xyloglucan (highlighted in green) forming biomechanical hotspots and more abundant pectin-cellulose interactions (shown as grey lines). Adapted from Cosgrove 2016b.

1.1.2.1 Homogalacturonan (HG)

The most abundant domain of pectin, homogalacturonan (HG), is formed of unbranched polymers of 1,4-α-linked D-galacturonic acid, which on average reaches lengths of about 100 residues (Yapo et al., 2007). HG is synthesised by α-1,4-galacturonosyl transferases (GAUTs), which add galacturonic acid residues to the non-reducing end of the growing HG chain (Scheller et al., 1999). HG can undergo a high degree of modification by methylesterification and O-acetylation, with the degree of acetylation ranging from 40-85% depending on tissues (Pelloux et al., 2007; Philippe et al., 2017; Stranne et al., 2018). Methylesterification occurs on C6 carboxyl groups by pectin methyltransferases (Wolf et al., 2009), while O-acetylation occurs at positions O2 and/or O3 by O-acetyltransferases (Perrone et al., 2002). HG is mainly deposited in the cell wall in a methylesterified state, which can de-esterified by pectin methylesterases (PMEs) to create a variety of esterification states (Voragen et al., 2009). De-esterified HG forms crosslinks with adjacent de-esterified HG chains if there are at least 10 consecutive de-esterified HG residues (Levesque-Tremblay et al., 2015). The crosslinks require a divalent cation, of which calcium (Ca^{2+}) is mostly used (Jarvis, 1984). The Ca^{2+} crosslinks between HG chains forms a stable gel (Levesque-Tremblay et al., 2015). The degree of esterification varies between tissues, for example, lignified xylem tissue has a predominantly methylesterified HG (Hafrén et al., 2000), whereas, guard cell walls mostly have de-esterified HG (Amsbury et al., 2016). Esterification states can also range within cells, as stem parenchyma cells have a spatially regulated distribution of a range of many methyl-esterification states of HG within each cell (Willats et al., 2001a). As well as within and between cells, HG modification states can vary

between species, for instance, stem-rust-fungus resistant and susceptible wheat species have different distribution of methyl-esters on HG (Wiethölter et al., 2003).

The phenotypes of mutants with reduced HG content demonstrate that HG is essential to many cellular processes, such as root cell adhesion (Durand et al., 2009) and dehydration tolerance (Bouton et al., 2002). The gel formed from HG Ca^{2+} crosslinks allows vast changes in the hydration status of the matrix and cell wall stiffness, which are essential components of cellular function (Levesque-Tremblay et al., 2015). The HG Ca^{2+} crosslinks also have a load-bearing capacity and because of this strength, increased HG content can compensate for a disrupted cellulose network (Levesque-Tremblay et al., 2015). Moreover, HG modification has many essential functions, such as plant development, defence against stresses, mechanical strength and cell function (Manabe et al., 2011; Orfila et al., 2012; Amsbury et al., 2016). De-methylesterification of HG is necessary to trigger wall loosening (Peaucelle et al., 2015) and deacetylation of HG cause changes to the structure and composition of cell wall polysaccharides with an impact on cell wall extensibility (Gou et al., 2012). Both wall loosening and extensibility are important factors for anisotropic growth (Gou et al., 2012; Peaucelle et al., 2015). Additionally, a change in the distribution of methyl-esterified HG can result in increased resistance to a fungal pathogen (Wiethölter et al., 2003). Furthermore, decreased O-acetylation of HG can also increase the stiffness of plant tissues, such as tubers (Orfila et al., 2012). Similarly, the removal of both methyl- and O-acetyl-ester groups increases the stiffness of cell walls, which has functional ramifications, effecting growth, morphology and stress tolerance (Levesque-Tremblay et al., 2015; Cosgrove, 2018). Finally, the modification state of HG directly impacts the function of guard cells; an increase in methyl-estertified HG in guard cells means they have a reduced capacity to open and close their stomata (Amsbury et al., 2016).

1.1.2.2 Rhamnogalacturonan-I (RG-I)

Rhamnogalacturonan I (RG-I) is the second most abundant pectic domain and the only type of pectin which does not have a backbone of pure galacturonic acid. Instead the backbone is comprised of alternating α-1,4-D-galacturonic acid-α-1,2-L-rhamnose repeats, which can reach a length of up to 600 residues (Harholt et al., 2010). RG-I is a branched structure, containing side chains attached at C4 positions made up of D-galactose, L-arabinose and small amounts of L-fucose, which increases the level of polymerisation to approximately 2000 (McNeil et al., 1984; Lau et al., 1985). These side chains include arabinans, galactans and arabinogalactans. Arabinans are highly branched neutral side chains, containing a backbone of 1,5-linked α-L-arabinose residues, while galactans consists of 1,4-linked β-D-galactose (Lau et al., 1985; Caffall and Mohnen, 2009). RG-I is synthesised by RG-I:rhamnosyltransferases in the Golgi and arabinose is essential to this synthesis (Harholt et al., 2006; Takenaka et al., 2018). Modification of RG-I mainly occurs by changes to the side chains, such as an increase in a particular residue or an increase in branching, and RG-I can be acetylated at the C2 and C3 position by TRICHOME BIREFRINGENCE-LIKE 10 (TBL10; Baldwin et al., 2014; Stranne et al., 2018).

The main functions of RG-I are to provide cell wall flexibility and control the hydration status of the matrix. RG-I is 4-fold more flexible than HG (Ralet et al., 2008). The side chains, mainly arabinans, are responsible for the flexibility through interacting with HG and preventing HG chains forming too tight associations with each other. Arabinan regulation of cell wall flexibility is especially important in guard cells walls, which need flexibility to open and close the stomata to regulate water loss (Jones et al., 2003). Furthermore, arabinans also have a role in drought stress through maintaining and recovering the hydration status of the matrix during and after a water deficit (Gribaa et al., 2013; Moore et al., 2013). Additionally, the galactan side chains of RG-I also modulate the water binding capacity of the cell wall through interactions with the cell wall matrix and altering the spacing of polysaccharides (Komalavilas and Mort, 1989). As a result, drought tolerant species have adapted to increase the number of RG-I side chains when water stressed (Leucci et al., 2008). RG-I also maintains the integrity of the matrix through covalent bonds with other pectic domains and other cell wall polysaccharides, such as xyloglucan, 50% of which is synthesised which attached to RG-I (Popper and Fry, 2008). The side chains are also involved in interactions with other cell wall components, for example, arabinogalactan side chains are associated with arabinogalactan proteins (Voragen et al., 2009). Finally, arabinan side chains also have a role as a storage polymer in seeds and influence seed germination (Harholt et al., 2010).

1.1.2.3 Rhamnogalacturonan-II (RG-II)

The final of the main three pectic domains is rhamnogalacturonan II (RG-II) which, contrary to what the name suggests, is structurally unrelated to RG-I. RG-II is the most structurally complex glycan known, as it is highly branched and composed of 13 different sugar residues connected by at least 21 different glycosidic linkages. The backbone consists of approximately 10 α-1,4-linked D-galacturonic acid residues to which 6 side chains, labelled A to F, are attached (Figure 1.3; Ndeh et al., 2017). The structure of RG-II is highly conserved across the plant kingdom (Pabst et al., 2013), however, modified forms exist. For example, side chain A can be methylesterified and side chain B can be O-acetylated (Pabst et al., 2013). Additionally, side chain A can be truncated or can have the fucose residue replaced by galactose, when fucose is limiting such as in the fucose-deficient mutants, *MURUS1* (*mur1)* and *SENSITIVE-TO-FREEZING8* (*sfr8*; Reuhs et al., 2004; Pabst et al., 2013). The majority of RG-II, more than 90%, is present as a dimer (Funakawa and Miwa, 2015). Two monomeric RG-II molecules spontaneously form a borate-diol ester between the apiosyl residues of each side chain A, which forms dimeric RG-II (Figure 1.3; O'Neill et al., 1996; Ishii et al., 1999). Optimal pH, the presence of borate and the inclusion of fucose in side chain A are essential to dimer formation (O'Neill et al., 1996, 2001). Dimeric RG-II is formed during RG-II synthesis and secretion into the cell wall (Chormova et al., 2014). RG-II synthesis is dependent on several enzymes with a variety of functions including; sugar synthesis, e.g. GDP-D-mannose-4,6-dehydratase which is involved in the synthesis of fucose (Bonin et al., 1997); sugar transfer, e.g. RG-II SPECIFIC XYLOSYLTRANSFERASEs (RGXTs) which transfer xylosyl residues onto side chain A of RG-II (Voragen et al., 2009); and borate transport, e.g. REQUIRES HIGH BORON2 (BOR2) is involved in the synthesis of dimeric RG-II (Miwa et al., 2013).

Dimeric RG-II is a very important component in cell walls, with roles in maintaining the integrity, strength, thickness and pore size of the cell wall (Fleischer et al., 1999; Ishii et al., 2001; Ryden et al., 2003; Sechet et al., 2018). The borate diol ester between dimeric RG-II is essential to the formation and stabilisation of the pectin network (Fleischer et al., 1999). When the proportion of RG-II in the dimeric form is decreased, the tensile strength of the cell wall is reduced and the cell wall thickness is increases, indicating the role of dimeric RG-II in regulating these important factors of cell wall function (Ishii et al., 2001; Ryden et al., 2003). Dimeric RG-II regulates cell wall pore size, as when monomeric RG-II is more abundant, such as when grown in boron-deficient conditions, cell wall pore size increases, which has an impact on the hydration status of the matrix (Fleischer et al., 1999). The inefficient regulation of these cell wall properties in dimeric RG-II deficient plants results in dwarfism, abnormal development and reduced cell wall integrity (O'Neill et al., 2001; Sechet et al., 2018).
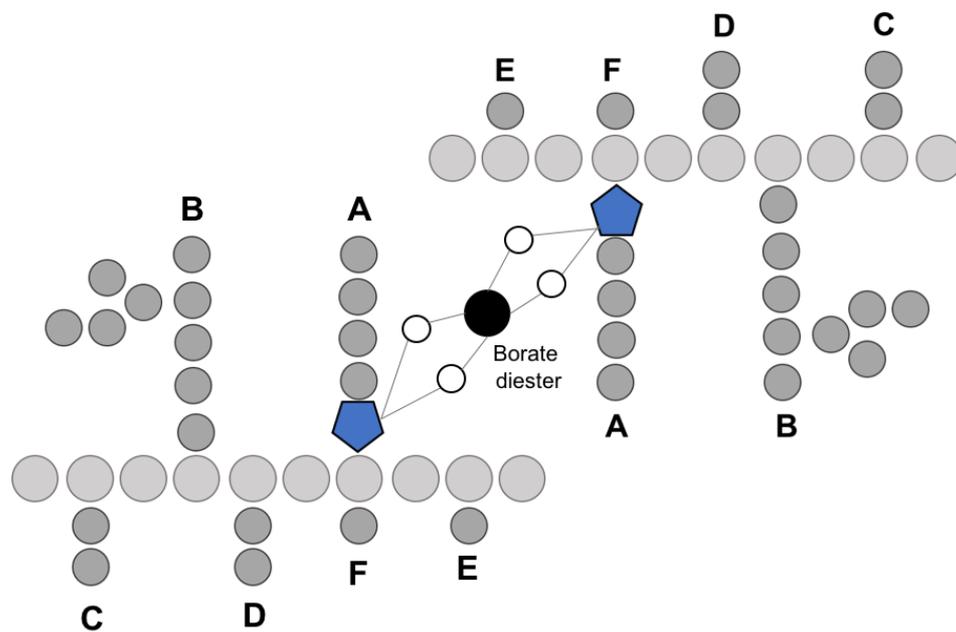
Figure 1.3: The structure of dimeric RG-II. The backbone of 10 α-1,4-linked D-galacturonic acid residues is shown as light grey circles. The 6 side chains are shown as dark grey circles and labelled A-F. The adipose residue on side chain A is shown as a blue hexagon. The borate diester covalently links the two adipose residues and is shown as white and black circles. Adapted from O'Neill *et al.* 2001 and Ndeh *et al.* 2017.

1.1.3 Hemicellulose

Hemicellulose is another large component of cell walls, composing approximately one-third of the cell wall (Fry, 1988; Pauly and Keegstra, 2008). Hemicelluloses are a group of non-cellulosic polysaccharides which have β-1,4-glycosidic bonds as their dominant linkage, this includes xyloglucan, xylan, mannan and β-glucan (Pauly et al., 2013). Xyloglucan is highly abundant in primary cell walls, conversely, xylan is the major hemicellulose of secondary cell walls (Zablackis et al., 1995; Ebringerová and Heinze, 2000). The synthesis of hemicellulose occurs in the Golgi by cellulose synthase-like proteins and glycosyltransferases (Pauly et al., 2013). Like pectin, hemicelluloses can undergo O-acetylation by members of the REDUCED WALL ACETYLATION (RWA) (Manabe et al., 2011, 2013) and TRICHOME BIREFRINGENCE-LIKE (TBL) families of O-acetyltransferases (Gille et al., 2011; Xiong et al., 2013). As a polysaccharide group of diverse

structure, hemicelluloses have a wide variety of functions, including; maintaining cell wall matrix integrity (Popper and Fry, 2008; Harholt et al., 2010; Simmons et al., 2016; Xiao et al., 2016), providing mechanical strength (Chiniquy et al., 2013), influencing cell wall mechanics (Park and Cosgrove, 2012a) and a minor role as storage polymer in some species (Naran et al., 2008). The degree of O-acetylation also influences these functions, particularly in xylan (Zhang et al., 2019a).

1.1.3.1 Xyloglucan

Xyloglucan is present in the cell walls of all land plants and accounts for about 20% of dicot cell walls (Zablackis et al., 1995). The backbone consists of β-1,4-linked glucose residues that are regularly substituted with α-linked xylose residues at the C6 position. Further modification can occur by addition of other residues, mainly galactose and fucose. The modification of xyloglucan depends on tissue and species and generates a branched structure (Pauly and Keegstra, 2016). Xyloglucan is synthesised in the Golgi by xyloglucan xylosyltransferases (XXTs) and cellulose synthase like-C proteins (Cavalier et al., 2008; Kim et al., 2020). Other proteins are involved in xyloglucan synthesis, for example, FUCOSYLTRANSFERASE1 (FUT1) adds fucose to terminal galactose residues of side chains (Perrin et al., 2003). Half of xyloglucan is synthesised attached to pectic polysaccharides, which is most likely the RG-I domain, generating a negative change, whereas the remaining xyloglucan is synthesised as free forms with a neutral charge (Popper and Fry, 2008). Xyloglucan undergoes O-acetylation mainly on the O6 position of the galactose residue, a process which involves O-acetyltransferases, such as RWA proteins and TBL27 (Kiefer et al., 1989; Gille et al., 2011; Manabe et al., 2011). Another protein, ALTERED XYLOGLUCAN9 (AXY9), is required for the O-acetylation of xyloglucan, as it transfers the O-acetyl group from RWA proteins to TBL proteins (Bray, 2004).

The functional significance of xyloglucan in cell walls is through its contribution to cell wall integrity, cellulose patterning, loadbearing and cell wall mechanics. Xyloglucan maintains the integrity of the cell wall matrix through covalent bonds with pectins, hydrogen bonding with the hydrophilic surfaces of cellulose and interactions with proteins, such as expansins (Popper and Fry, 2008; Pauly et al., 2013). Xyloglucan effects the synthesis and distribution of cellulose, as in its absence CESAs move slower with a lower rate of production and cellulose has abnormal patterning in primary cell walls (Xiao et al., 2016). One of the main functions of xyloglucan was thought to be the binding and spacing of cellulose microfibrils as a tether, which maintains the porosity and strength of the cell wall (McCann et al., 1990). The sugars on the side chains, particularly fucose, stabilise xyloglucan in a conformation which can efficiently bind cellulose microfibrils (Levy et al., 1991). This is the tethered network model, as mention in section 1.1.2 (Figure 1.2), in which the cellulose xyloglucan network is the dominant load-bearing structure in growing cell walls (Pauly et al., 1999). However, more recent work suggests that the interactions between cellulose and xyloglucan are weaker and less abundant than previously thought (Dick-Pérez et al., 2011), whereas, there are more pectin-cellulose interactions (Wang et al., 2015). This new data implies that cellulose, hemicellulose and pectins all have a role in the load-bearing capacity of the cell wall. Additionally, measurements taken of xyloglucan-digested cell wall suggest that xyloglucan has a limited load-bearing

capacity and only has a minor role in cell wall mechanics (Park and Cosgrove, 2012b). The role of xyloglucan in cell wall mechanics, particularly wall loosening, could be mediated at biomechanical hotspots where tight cellulose-cellulose junctions form (Cosgrove, 2014). Xyloglucan is essential for expansin-mediated wall loosening, a process important for normal plant growth and development (Park and Cosgrove, 2012a).

1.1.3.2 Xylan

Xylan is the most prevalent non-cellulosic polysaccharide on Earth (Chiniquy et al., 2013), constituting 25-35% of the woody biomass of dicots (Ebringerová and Heinze, 2000). The xylan backbone consists of β-1,4-linked xylose residues, attached to which are various side chains. The xylose residues of the backbone can be substituted with arabinose, glucuronic acid and/or methyl-glucuronic acid to create distinct classes of xylan, such as glucuronoarabinoxylan and arabinoxylan (Scheller and Ulvskov, 2010). Furthermore, the backbone residues can also be highly modified by O-acetyl groups on the O2 and O3 position with a degree of acetylation of up to 50% (Gille and Pauly, 2012; Xiong et al., 2013). Several glycosyltransferases are involved in xylan synthesis, for example, IRREGULAR XYLEM9, 10 & 14 (IRX9, 10 & 14) are glycosyltransferases that elongate the xylan backbone and GLUCORONIC ACID SUBSTITUTION OF XYLAN (GUX) glycosyltransferases add glucuronic acid and methyl-glucuronic acid branches to the xylan backbone (Mortimer et al., 2010; Pauly et al., 2013). Other enzymes are involved in xylan synthesis, such as TBL29 is an O-acetyltransferase which is responsible for the O-acetylation of xylan (Xiong et al., 2013).

Xylan has load-bearing capacity and its abundance is essential to the mechanical strength of secondary cell walls; when IRX9 is overexpressed, the plant stem strength is increased by 124% (Chiniquy et al., 2013). Furthermore, O-acetylation of xylan is also important to the load-bearing capacity of xylan; the *tbl29* mutant, which has a 60% reduction in xylan O-acetylation, has a severe collapsed xylem phenotype, which occurs when weak xylem fail to withstand the high pressure generated by transpirational pull. The lack of xylan O-acetylation in *tbl29* is implicated as a cause of the weak secondary cell walls that result in cell collapse under the negative pressure of water transport (Pauly et al., 2013; Xiong et al., 2013). The O-acetylation of xylan is also important to the growth and development of the plant, as *rwa* mutants which have decreased acetylation of xylan have severe growth phenotypes (Manabe et al., 2013). Additionally, xylan maintains the integrity of the cell wall by interacting with other cell wall polysaccharides. Xylan contorts into a two-fold helical screw conformation, which forms a close interaction with cellulose microfibrils in secondary cell walls via hydrogen bonds with the hydrophilic surfaces of cellulose. The tight interaction influences cellulose interaction with other cell wall components, such as lignin (Simmons et al., 2016). The correct patterning of xylan O-acetylation is essential to the interaction with cellulose, as abnormal O-acetylation can alter microfibril orientation (Zhang et al., 2019a). Xylan also interacts with pectins via an arabinogalactan protein named ARABINOXYLAN PECTIN ARABINOGALACTAN PROTEIN1 (APAP1; Tan et al., 2013). Finally, xylan, particularly arabinoxylan, is abundant in seeds as a storage polymer (Naran et al., 2008).

1.1.4 Lignin

Lignin is a large component of secondary cell walls, composing approximately 30% of the dry weight of woody plants, which varies between and within species (Campbell and Sederoff, 1996). The term lignin covers a diverse range of complex aromatic polymers resulting from the oxidative coupling of 4-hydroxyphenylpropanoids and other phenols derived from amino acids (Varner and Lin, 1989; Delmer, 1999) Lignin synthesis is induced by developmental programming and by various stresses (Vanholme et al., 2010). Lignin is deposited prior to the terminal differentiation of cells (Campbell and Sederoff, 1996). As lignin is predominantly incorporated into the secondary cell walls of cells that need structural support, lignin provides mechanical support by hardening and stiffening walls. The addition of lignin to secondary cell walls thickens them and protects cell wall polysaccharides from microbial degradation (Vanholme et al., 2010). A 20-40% reduction in lignin content increases the vulnerability to xylem embolism, which disrupts the transpiration stream with a resultant decrease in plant survival (Voelker et al., 2011). With this maintenance of plant transpiration, increased lignin accumulation can also aid drought tolerance and enhance stomatal closure under drought (Vanholme et al., 2010).

1.1.5 Cell Wall Proteins

Proteins of diverse structure and function are present in the cell wall, composing 5-10% of cell walls and including enzymatic, receptor, transport, structural and signalling proteins (McNeil et al., 1984; Fry, 1988). As previously mentioned, some of the enzymes present in the cell wall are the synthases and transferases involved in the synthesis of the cell wall polysaccharides, such as cellulose synthases (Doblin et al., 2002) and RG-I:rhamnosyltransferases (Takenaka et al., 2018). As well as, enzymes that modify the cell wall polysaccharides by the addition or removal of methyl-ester and O-acetyl-ester groups, the addition or removal of sugar residues and branches, for example, PMEs (Pelloux et al., 2007), RWA O-acetyltransferases (Manabe et al., 2011) and RG-II specific xylosyltransferase (Voragen et al., 2009). Additionally transport proteins are important for importing and exporting materials required for polysaccharide synthesis, for example BOR2 is a boron transporter essential to the uptake of boron into cell walls for the formation of dimeric RG-II (Miwa et al., 2013). Other proteins of note due to their functional importance in the cell wall are extensins, arabinogalactan proteins and expansins. Extensins are basic, hydroxyproline-rich glycoproteins with a protein moiety content of 50% and a small polysaccharide chain of 1-4 residues of D-arabinose and D-galactose (Stuart and Varner, 1980). Extensins are major structural proteins that covalently interact with other cell wall components, especially cellulose. The cellulose-extensin network increases the mechanical strength of the cell wall (Iraki et al., 1989). Arabinogalactan proteins are another type of hydroxyproline-rich glycoproteins that consist of up to 95% carbohydrate and have several functional roles from involvement in cell development and growth, to regulating plant defence and maintaining cell wall integrity through covalently linking xylans and pectins (Seifert and Roberts, 2007; Tan et al., 2013). Expansins are a diverse group of proteins classified based on their involvement in cell wall-loosening through targeting microfibrils at tight cellulose-cellulose junctions (Wang et al., 2013a; Cosgrove, 2015, 2016a). Expansins also have roles in modulating cellulose-xyloglucan interaction and drought tolerance (Harb et al., 2010; Lü et al., 2013; Cosgrove, 2014).

1.1.6 Cell Wall Fucosylation

Fucosylation is the process by which fucose sugar residues are incorporated into a molecule by fucosyltransferases. In plant cell walls, some components are fucosylated including, pectins (section 1.1.2.2 and 1.1.2.3), hemicellulose (section 1.1.3.1) and proteins (section 1.2.1) by a range of specific fucosyltransferases (Liang et al., 2013; Pauly and Keegstra, 2016; Ndeh et al., 2017; Zentella et al., 2017). Fucose can be extracted from soil or synthesised in plants (Reiter et al., 1993).

1.2   Cell Wall Mutants: *sfr8* and *mur1*

1.2.1   *mur1*: The First Identified Cell Wall Mutant

Cell wall polysaccharides are so fundamental to plant function, growth and development that any deviation from proper polysaccharide distribution and composition tends to be lethal (Zablackis et al., 1996a). Accordingly, before 1993, no cell wall polysaccharide mutants had been identified. Through a mutant screen of over 5000 plants analysing cell wall composition, the first mutants of cell wall polysaccharide composition were discovered, including *MURUS1* (*mur1*; Reiter et al., 1993). *MUR1* encodes the enzyme GDP-D-mannose-4,6-dehydratase, which is involved in the first of three steps in the de novo synthesis of the sugar GDP-L-fucose (Bonin et al., 1997). *mur1* is a heritable, recessive point mutation that results in an amino acid substitution of serine for phenylalanine, changing the chemical properties and knocking out the function of GDP-D-mannose-4,6-dehydratase (Reiter et al., 1993). As a result of this loss-of-function mutation, *mur1* has significantly reduced abundance of L-fucose, by 98% in the aerial parts of the plant and 40% in the roots (Reiter et al., 1993). L-fucose is incorporated into many cell wall components: the pectic domains RG-I and RG-II (McNeil et al., 1984; Ndeh et al., 2017), the hemicellulose xyloglucan (Pauly and Keegstra, 2016), and cell wall proteins, such as arabinogalactan proteins (Van Hengel and Roberts, 2002), glycoproteins (Faye et al., 1989) and DELLA proteins (Zentella et al., 2017).

The cell wall polysaccharides and proteins in *mur1* have altered composition with missing L-fucose residues or the replacement of L-fucose by another sugar. For example, the root arabinogalactan proteins of *mur1* have altered sugar composition with changes to galactose, arabinose, rhamnose and xylose abundance with a notable 38% reduction in fucose content and a doubling of glucose concentration (Van Hengel and Roberts, 2002). Additionally, while 5% of the glycoproteins in *mur1* use L-galactose in the place of L-fucose, the remaining glycoproteins do not replace the missing L-fucose residue with another monosaccharide (Rayon et al., 1999). The L-fucose and 2-O-methyl L-fucose residues of RG-II are replaced by L-galactose and 2-O-methyl galactose in *mur1,* which truncates side chain A (O'Neill et al., 2001; Sechet et al., 2018). The truncation of *mur1* side chain A in RG-II reduces the stability of the borate diol-ester between the adipose residues of adjacent RG-II side chains, which results in only 50% of RG-II being present as a dimer in *mur1* compared to 95% in wildtype (O'Neill et al., 2001; Sechet et al., 2018). Therefore, not only is protein composition effected, but pectin crosslinking is reduced too. Moreover, the terminal α-L-fucopyranosyl residue of *mur1* xyloglucan is replaced by an α-L-galactosyl residue (Zablackis et al., 1996a). The incorporation of fucose potentially stabilises xyloglucan in a conformation that can

efficiently bind cellulose microfibrils (Levy et al., 1991). Consequently, the lack of fucose in the xyloglucan of *mur1* may effect hemicellulose-cellulose interactions.

The changes to cell wall composition and crosslinking in *mur1* has huge consequences on the functional properties of the cell wall. In some cases, *mur1* is dwarfed with shorter petioles, internodes and height due to reduced growth (Figure 1.4; Reiter et al., 1993; O'Neill et al., 2001). However, the dwarf phenotype is not observed under some growth conditions (Panter et al., 2019). Supplementation of *mur1* with borate restores the growth rate of dwarfed *mur1* to wildtype levels and increases the proportion of RG-II that is dimerised from 50% to 78% (O'Neill et al., 2001). The rescue of growth and increase in dimeric RG-II upon supplementation with borate suggests that it is the reduction in borate-diol ester formation and RG-II dimerisation that causes the dwarf phenotype (O'Neill et al., 2001). Furthermore, the addition of exogenously applied fucose also restores the growth and development of *mur1* to a phenotype indistinguishable from wildtype and increases the proportion of dimeric RG-II in *mur1* to wildtype levels, this further implicates RG-II dimerisation as the cause of *mur1* dwarfing (O'Neill et al., 2001). *mur1* is also significantly weaker than wildtype with twofold less force required to remove inflorescences than wildtype (Reiter et al., 1993). The mechanical strength of cell wall could also be restored when L-fucose was supplemented to *mur1* plants (Reiter et al., 1993). Similarly, the tensile strength of *mur1* could be restored to within 99% of wildtype by the addition of borate (Ryden et al., 2003). Therefore, as tensile strength was restored when RG-II dimerisation is increased, this suggests that the lack of dimeric RG-II in *mur1* causes the reduction in wall strength as well as growth (O'Neill et al., 2001; Ryden et al., 2003). Moreover, fucose also has a role in development, as the CUP-SHAPED COTYLEDON2 (CUC2) transcription factor has reduced expression in *mur1* leaves leading to improper developmental boundary establishment and rounder leaves of *mur1* (Gonçalves et al., 2017).
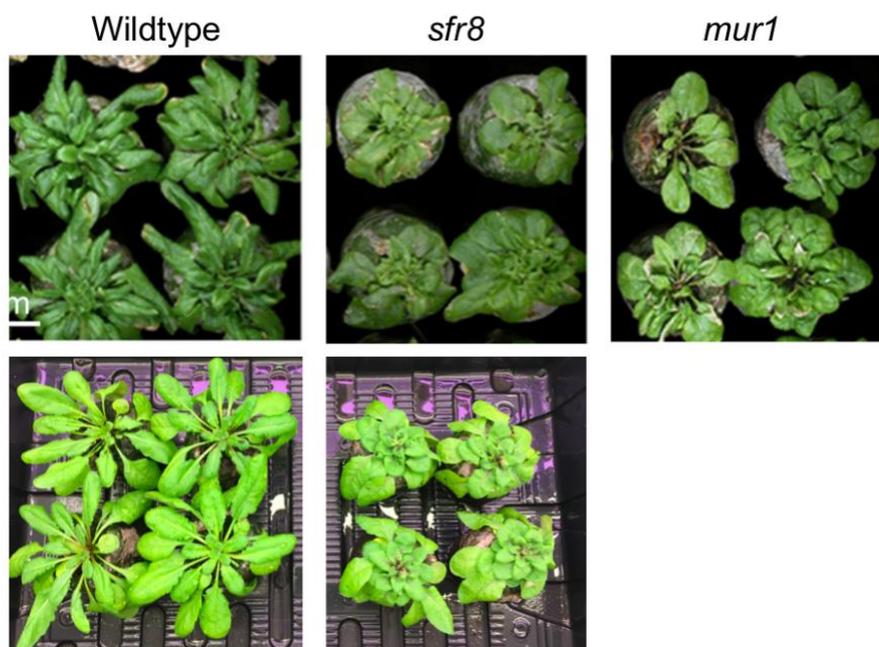
Figure 1.4: The phenotypic differences between wildtype, *sfr8* and *mur1*. Top panel: adapted from Panter et al., 2019. Bottom panel: wildtype and *sfr8* plants used in the project.

1.2.2 *sfr8*: An Allelic Variant of *mur1*

SENSITIVE TO FREEZING8 (*sfr8*) is another cell wall mutant that was first identified in a forward genetic screen searching for cold acclimation mutants (Panter et al., 2019). *SFR8* was mapped to a locus on chromosome 3 and identified as a single nucleotide polymorphism in the *MUR1* gene (Thorlby et al., 1999; Panter et al., 2019). The wildtype glycine amino acid is exchanged for glutamate which alters the protein chemical properties and knocks out the function of GDP-D-mannose-4,6-dehydratase (Panter et al., 2019). As a result, *sfr8* has phenotypic similarity to *mur1* with shorter petioles and rounder leaves, as well as reduced abundance of cell wall GDP-L-fucose and RG-II dimerisation (Figure 1.4; Gonçalves et al., 2017; Panter et al., 2019). Additionally, like *mur1*, the dwarfism depends on the growth conditions and is not present under all growth regimes utilised in this project (Gonçalves et al., 2017; Panter et al., 2019). Wildtype levels of fucose and dimeric RG-II can be restored in *sfr8* by introducing functional *MUR1* gene, confirming *mur1* and *sfr8* are allelic (Panter et al., 2019).

1.2.3 Stress Tolerance of Cell Wall Mutants Lacking MUR1

As well as the impacts on growth, development and cell wall strength, plants lacking functional MUR1 have defects in defence against plant pathogens. *mur1* has significantly less resistance than wildtype to fungal infection by powdery mildew species, *Blumeria graminis f. sp. Hordei* (Assaad et al., 2004). The powdery mildew species, like most fungi, begin their attack on plant tissue by penetrating the plant cell wall. Therefore, any disruption to the integrity of cell wall will result in higher fungal infection, which is what is seen in the *mur1* mutants that have reduced pectin crosslinking and wall integrity (Assaad et al., 2004). Moreover, *mur1* has increased susceptibility to bacterial infection and has increased severity of disease symptoms compared to wildtype (Zhang et al., 2019b). Typically, foliar bacterial pathogens enter the plant through wounds or natural openings on the surface of leaf epidermis, such as the stomata, the microscopic pores in leaf surface (Melotto et al., 2008). Correspondingly, *mur1* plants had stomata with a greater degree of opening than wildtype, which provided an entry point for more bacteria and *mur1* had higher bacterial populations than wildtype (Zhang et al., 2019b). This research suggests that as *sfr8* has a mutation in the same gene as *mur1*, it is likely *sfr8* also has a stomatal defect.

On top of the increased susceptibility to pathogen attack, *mur1* and *sfr8* have altered abiotic stress tolerance, including salinity, freezing and desiccation stress. *mur1* has decreased salinity stress tolerance as significantly more *mur1* root cells burst under salinity stress than wildtype root cells (Feng et al., 2018). When supplemented with boron, the number of *mur1* cells that burst is statistically the same as wildtype, implicating a role of dimeric RG-II in salt stress tolerance as the only cell wall component depending on the presence of boron is dimeric RG-II (Feng et al., 2018). Moreover, both *mur1* and *sfr8* exhibit freezing sensitivity, where wildtype showed signs of recovery 1 week after a 24-hour freezing period, *mur1* and *sfr8* exhibit almost complete chlorosis and had failed to grow (Panter et al., 2019). Freezing tolerance could be restored to wildtype levels when *sfr8* and *mur1* were sprayed with supplementary fucose, linking the lack of fucose with the freezing sensitivity in these mutants (Panter et al., 2019). Similarly, *sfr8* and *mur1* plants supplemented with boron had wildtype levels of freezing damage and had significantly

greater freezing tolerance than non-supplemented mutant plants (Panter et al., 2019). This implicates the role of RG-II dimerisation in plant freezing tolerance and suggests that the freezing sensitivity of *sfr8* and *mur1* is due to reduced RG-II dimerisation (Panter et al., 2019). Additionally, both *mur1* and *sfr8* have increased sensitivity to water loss stress than wildtype. When leaves were excised and left to dry, inflicting a desiccation stress, *sfr8* and *mur1* had a higher rate of water loss than wildtype (Panter, 2018). Initially during leaf water loss, transpiration occurs through the stomata and later through the cuticle once the stomata have closed (Hall and Jones, 1961). Accordingly, *mur1* has been found to have stomata that are more open, which could explain the higher water loss rate (Zhang et al., 2019b). The abiotic stress tolerance defects of *mur1* and *sfr8* also suggest that *sfr8* has a stomatal defect.

1.3   Stomata, Guard Cell Walls and Desiccation

The rate at which water is lost from the plant is mainly controlled by the guard cells, which restrict the movement of gas, including water vapour, into and out of leaves. Guard cells must balance CO_2 intake for photosynthesis and increasing biomass, with the large efflux of water (Lawson and Blatt, 2014). Limiting water loss is crucial to plant survival as water is essential to plant development, structural integrity, biochemical reactions, nutrient transport and thermoregulation (Riederer and Schreiber, 2001; Zlatev and Lidon, 2012). Furthermore, guard cell control of transpiration is especially important in agricultural systems and will become even more important while climate change limits the water availability to crops and a growing population necessitating an increase in food production (Dai, 2011; Dumas et al., 2019). One way in which guard cell function can be optimised for maximising photosynthesis and minimising water use is through manipulating the guard cell walls. Guard cells walls have a specialised structure and function, which can provide drought tolerance by maintaining strength and flexibility of cell wall and optimising the hydration status of the matrix (Shope et al., 2003; Gribaa et al., 2013; Le Gall et al., 2015; Hunt et al., 2017; Novaković et al., 2018).

1.3.1   Stomata and Plant Water Loss

Stomata are microscopic pores on the surface of leaf epidermis that allow gas exchange between the plant and the external environment. The openness, also known as aperture, of the stomatal pore can change in response to both internal and external environmental stimuli, a phenomenon first observed over 120 years ago (Darwin, 1898). The purpose of changing the stomatal aperture is to adjust the rate of gas exchange in a way that maximises the intake of CO_2 for optimal photosynthesis, while minimising the efflux of water through transpiration (Lawson and Blatt, 2014). Low stomatal aperture and slow changes in stomatal aperture limit photosynthesis by up to 20%, resulting in reductions in productivity and crop yield (Lawson and Blatt, 2014; McAusland et al., 2016). In contrast, large stomatal aperture is correlated with increased photosynthetic rate and yield; by increasing stomatal conductance by 63%, photosynthesis can increase by 23%, incurring a 27% increase in yield (Fischer et al., 1998). The change in stomatal aperture is precisely controlled by a pair of identical guard cells, which surround the stoma. Guard cells have a huge capacity to alter their shape; their surface area can fluctuate by as much as 40% (Shope et al., 2003). This ability to change shape and volume drives the adjustments to stomatal aperture. The

change in guard cell shape is regulated by the water content of the guard cells with higher water content increasing turgor pressure and volume which opens the stomata. The water content of guard cells is controlled by the concentration of solutes in the cell and the consequent water uptake or efflux by osmosis. Guard cell solute concentration is regulated by light intensity, cellular CO_2 concentration, the plant phytohormone abscisic acid (ABA) and plant water status (Kriedemann et al., 1972; Assmann et al., 1985; Roelfsema et al., 2002; Hanstein and Felle, 2002; Hsu et al., 2021).

Detecting plant water status and minimising plant water loss is of particular importance because water is the crucial factor that determines the existence of plant life (Riederer and Schreiber, 2001). Water is fundamental to plant growth and development, as well as maintaining cellular integrity and being a reagent in a multitude of essential reactions that keep the plant alive (Zlatev and Lidon, 2012). On top of this, water buffers temperature changes and provides thermal regulation that limits the effects of heat stress on plants (Kramer and Boyer, 1995). Moreover, water movement through the xylem, from root to leaves, provides the pressure necessary to transport essential nutrients throughout the plant (Kramer and Boyer, 1995). Consequently, significant plant water loss, where water is transpired at a rate that cannot be replaced, results in malfunction of plant growth, development and integrity, essential biochemical reactions, temperature regulation and the transport of nutrients. When water deficit is severe enough or occurs for an extended period of time, the plant will die (Kramer and Boyer, 1995). Therefore, plants utilise many structural features to minimise water loss, such as the waterproof cuticle, adapted plant surface area and leaf hairs (Ehleringer and Mooney, 1978; Holloway, 1994). However, initially during leaf water loss, a colossal amount of water is transpired through the stomata, which needs to be controlled (Hetherington and Woodward, 2003). The stomata are closed to prioritise preventing water loss over photosynthesis to better preserve the water currently available, stalling the negative consequences of severe water loss and restricting water loss to through the cuticle (Hall and Jones, 1961).

1.3.1.1 How Stomatal Aperture is Regulated During Water Loss

Water deficit stress occurs when there is an imbalance between soil water availability and evaporative demand (Zlatev and Lidon, 2012). Water deficit stress can be detected in dehydrated roots and communicated to leaves via a hydraulic change, which stimulates the production of plant hormone, abscisic acid (ABA; Christmann et al., 2007). Water deficit stress can also be detected in the leaves as leaf water potential through either liquid or vapour diffusion (Buckley, 2019). Leaf water potential is influenced by environmental changes in humidity and soil moisture, and internal changes to plant water transport (Buckley, 2019). Water vapour transport through the leaf airspaces can be driven by small temperature gradients and the factors that affect temperature gradients, including light absorption, leaf thickness and amount of airspace (Buckley et al., 2017). Responses to perturbations in water potential are not unique to individual stomata (Mott and Buckley, 2000). Instead small groups of stomata share the same responses to changes in water potential, even when individuals within that group are not experiencing a change in water potential (Mott et al., 1997).

An essential component of stomatal closure is ABA. As well as regulating root and stomatal development (Tanaka et al., 2013a; Chater et al., 2014; Rosales et al., 2019), ABA induces stomatal closure in response to water stress (Hsu et al., 2021). Under ambient conditions, guard cells contain levels of ABA higher than that of adjacent mesophyll cells and it is the basal level of ABA in guard cells that maintains steady-state stomatal conductance (Lahr and Raschke, 1988; Hsu et al., 2018; Zhang et al., 2020). However, under drought conditions, the ABA concentration within guard cells increases as ABA production is stimulated by water deficit stress (Christmann et al., 2007). ABA can be synthesised near to the stomatal pore in guard cells and mesophyll cells, or in other distant plant tissues, like phloem companion cells and root cells, then transported to leaves through xylem sap (Zhang and Davies, 1991; Endo et al., 2008; Bauer et al., 2013; McAdam and Brodribb, 2018). The majority of water-deficit induced ABA synthesis occurs in the mesophyll cells (McAdam and Brodribb, 2018). Synthesis can be increased by upregulating ABA synthetic enzymes, such as NCED, which is strongly induced by water stress and leads to vast increases in ABA concentration (McAdam et al., 2016). ABA initiates stomatal closure through a signalling cascade, starting with the binding of ABA to the PYR/PYL/RCAR family of receptors (Park et al., 2009). The binding changes the conformation of PYR/PYL/RCAR proteins so that they can bind and inhibit protein phosphatases type 2C (PP2Cs) (Umezawa et al., 2009). In the absence of dephosphorylation by PP2Cs, SNF-related kinases (SnRKs), the target of PP2Cs, are free to phosphorylate and activate S-type anion channels, which mediate anion efflux from guard cells (Schroeder and Hagiwara, 1989; Geiger et al., 2009). The resulting depolarisation of the plasma membrane activates K+ efflux channels (Hsu et al., 2021). The water potential of the cell increases causing an osmotic efflux. As water leaves the cell, the cell turgor is reduced and the volume of the cell decreases, closing the stomata (Hsu et al., 2021).

DELLA proteins are involved in ABA biosynthesis, ABA-signalling and ABA-induced stomatal closure (Piskurewicz et al., 2008; Lim et al., 2013; Nir et al., 2017). DELLAs, so named after a highly conserved D-E-L-L-A amino acid sequence in their N-terminal region, are nuclear proteins that are the target of the plant signalling hormone, gibberellin (GA; Sun and Gubler, 2004; Locascio et al., 2013). GA is involved in many processes of plant development and is a key regulator of plant growth (Yamaguchi, 2008). In the absence of GA, DELLA proteins are involved in regulating gene expression through interacting with DNA-binding transcription factors to upregulate or downregulate the expression of a target gene (Locascio et al., 2013). However, when GA accumulates and binds with its receptor, GIBERELLIN INSENSITIVE DWARF1 (GID1), the activated GID1 interacts with a DELLA protein and an E3 polyubiquitin ligase (Harberd et al., 2009). DELLA is polyubiquitinated and targeted for degradation by the 26S proteasome, inhibiting DELLA regulation of transcription (Harberd et al., 2009). In seeds, the DELLA protein, RGA-LIKE2 (RGL2), is involved in the synthesis of ABA and is essential to seed germination as RGL2 elevates the ABA concentration (Piskurewicz et al., 2008). Moreover, it was also found in seeds that DELLA proteins interact with two transcription factors that are essential parts of the ABA-signalling pathway. The interaction with the transcription factors and the involvement of DELLA in the ABA-signalling pathway was a necessary requirement for the expression of the target gene, *SOMNUS* and to achieve seed germination at high temperature (Lim et al., 2013). In mature plants, increased DELLA activity reduces the whole plant transpiration rate, stomatal aperture and stomatal conductance. Conversely, decreased DELLA activity

significantly increases stomatal aperture and conductance compared to wildtype (Nir et al., 2017). Despite having the same ABA concentration, the stomatal responses to water deficit stress depended on whether the plant was a loss-of-function DELLA mutant or a DELLA-overexpression line, with increased DELLA activity promoting earlier stomatal closure and decreased DELLA activity giving worse drought tolerance (Nir et al., 2017). Based on these results, it was suggested that DELLAs enhance the sensitivity of guard cells to ABA (Nir et al., 2017).

1.3.1.2 Why Minimising Water Loss Through the Stomata is Important

Transpiration through the stomata is the main source of plant water loss as such a huge volume passes through. Approximately 60% of the water that falls on Earth passes through all the stomata on the planet (Hetherington and Woodward, 2003). This immense water loss can be problematic for plant survival, especially when soil water availability and atmospheric humidity are low, such as during periods of drought. Drought is characterised by a temporary reduction in precipitation below the normal level for that region (Dai, 2011). A dry period of any length inflicts a water deficit stress on plants and induces a range of molecular, biochemical and physiological responses; including reduced growth, membrane stability and photosynthesis (Pandey and Shukla, 2015), as well as impacting stomatal closure through reducing turgor, osmotic adjustment and leaf water potential (Shao et al., 2008). The severity of these drought-induced effects depends on the plant developmental stage and the duration and severity of the drought period (Ahmad et al., 2009; Nadeem et al., 2019). Ultimately, despite the stomatal-closure response to drought stress, the biochemical and physiological impacts of drought stress result in a reduction in plant growth, which has negative impacts on natural systems, as well as agricultural crop yields (Heffernan, 2013; Pandey and Shukla, 2015).

By 2050, the global population is expected to exceed at least 9 billion, and to feed this growing population, the total global crop production of 2019 needs to be increased by 50% (Dumas et al., 2019). As increasing stomatal conductance increases carbon fixation and plant yield, one solution for meeting the predicted food demand may be to breed agricultural crops for greater stomatal conductance (Fischer et al., 1998; Tanaka et al., 2013b). However, with the expanding population and increased pressure on agricultural systems, fresh-water usage is predicted to triple by 2050, despite fresh water being a finite resource (Chen et al., 2017). Plants will be required to grow with less water and so plants with lower stomatal conductance may be selected for because their water use efficiency, the ratio of assimilated carbon to water uptake, will be higher, meaning more biomass is produced per unit of water (Ehleringer et al., 1993; Dunn et al., 2019). Moreover, the occurrence of drought is expected to increase globally in areas that experience drought periods currently and areas which currently do not (Dai, 2011). Key determinants of drought tolerance are stomatal characteristics including, conductance and density (Xiong et al., 2002; Hughes et al., 2017). Therefore, stomatal traits will need to be optimised in order to maximise yields, while minimising water use and conferring drought tolerance.

1.3.2 Guard Cell Walls and Drought Stress

One stomatal trait which has potential to be optimised and is the focus of this thesis, is guard cell walls. Guard cell walls have a unique composition and abundance of cellulose, pectin and hemicellulose, as well as rare polysaccharides not found in other cell types (Fujita and Wasteneys, 2014; Giannoutsou et al., 2016; Amsbury et al., 2016; Carter et al., 2017). Moreover, the physical structure of guard cell walls is different to other cell types, with different thickness and the outer cuticular ledges (Zeiger, 1983; Hunt et al., 2017). The specialised structure of guard cell walls provides the flexibility and strength necessary for proper control of stomatal aperture in response to a range of opening and closure signals (Shope et al., 2003; Hunt et al., 2017). On top of allowing guard cells to adapt stomatal aperture, guard cell walls can be adapted in response to abiotic and biotic stresses, such as drought stress (Novaković et al., 2018). The abundance of cellulose, lignin, xyloglucan, pectin and the cell wall protein expansin influence drought tolerance, while the modification of xyloglucan and pectin maintains the hydration status of the matrix during water deficit stress (Gribaa et al., 2013; Le Gall et al., 2015; Novaković et al., 2018).

1.3.2.1 The Structure and Function of Guard Cell Walls

Guard cell walls are adapted to have the flexibility to mediate the large fluctuations in guard cell shape (Hunt et al., 2017), while also maintaining the cell wall strength needed to withstand high turgor pressure (Shope et al., 2003). As guard cell walls have a specialised function, guard cell walls have a composition and structure different to other cell types. The inner radial guard cell wall, the wall adjacent to the pore, is thickened, whereas, the outer walls, that are connected to epidermal cells, is thinner (Zeiger, 1983). With the extra thickness, the inner radial wall also has an extended ledge, known as the outer cuticular ledge, that seals the stomata shut to prevent water loss (Hunt et al., 2017). In addition to altered structure, the polysaccharide composition of guard cell wall differs to other cells. Cellulose is abundant in guard cell walls to a similar degree to other cell types, but the microfibrils are arranged radially relative to the pore, unlike other cells (Fujita and Wasteneys, 2014). The hemicellulose xyloglucan is more abundant in guard cells compared to neighbouring epidermal cells (Amsbury et al., 2016). While xyloglucan has an even distribution, pectins are highly localised within guard cell walls (Amsbury et al., 2016; Carter et al., 2017). The outer cuticular ledges are abundant in highly methy-esterified HG, whereas the rest of guard cell walls are rich in unesterified HG (Amsbury et al., 2016). Furthermore, an unusual arabinan polysaccharide, 1,5-α-L-arabinan, is found in guard cells but not in neighbouring cells (Giannoutsou et al., 2016).

Cellulose is an important polysaccharide in guard cell walls, contributing wall strength (Rui et al., 2018). Moreover, cellulose is also important in enabling the cell wall to change in shape. The cellulose is reorganised from an even distribution when stomata are open to a more bundled and fibrillar arrangement when stomata are closed (Rui and Anderson, 2016). The presence of sufficient xyloglucan is essential for proper regulation of stomatal aperture (Rui and Anderson, 2016). Similarly, de-methyl-esterification of pectin is required for normal stomatal aperture response to stomatal closure signals, such as high CO_2 concentration and plant water loss, as well as normal response to stomatal opening signals, like low CO_2 concentration (Amsbury et al., 2016). Furthermore, the unique pectin constitution at the

stomatal poles provides the cell wall polar stiffening required to close the stomata (Carter et al., 2017). Pectic arabinan has been found to be particularly important in maintaining guard cell wall flexibility across species. When arabinose is degraded due to exogenous application of arabinanase, stomatal movement is eliminated (Jones et al., 2003). The opening and closing stomata can be restored by degradation of HG, suggesting that HG Ca^{2+} crosslinks limit cell wall flexibility and that arabinan enables guard cell flexibility by preventing HG forming too tight Ca^{2+} crosslinks (Jones et al., 2003). Moreover, the specific structure of guard cell walls is as important to its function as composition is. The additional thickness of the inner radial wall provides the strength and stiffness necessary to changing guard cell shape (Zeiger, 1983). The outer cuticular ledge is important in pathogen resistance; mutants, including *susceptibility to COR-deficient Pst* DC3000 (*scord6*) and *mur1*, that have greatly reduced cuticular ledges also have compromised stomatal and apoplastic defences to bacterial pathogens (Zhang et al., 2019b). Additionally, the outer cuticular ledge allows changes to stomatal aperture (Hunt et al., 2017). The formation of the outer cuticular ledge is dependent on the putative glycoprotein, *FUSED OUTER CUTICULAR LEDGE1 (FOC1)*. As the name suggests *foc1* mutants lack the outer cuticular ledge and as a result *foc1* have a much reduced ability to control stomatal aperture and transpiration rate (Hunt et al., 2017).

1.3.2.2 Drought Stress Tolerance and Plant Cell Walls

Cell wall structure is a determinant of tolerance to abiotic stresses, including drought stress (Balsamo et al., 2015). Drought tolerance is associated with mutants that have higher abundances of some cell wall sugars, including galactose and arabinose, both constituents of pectin and arabinogalactan proteins (Balsamo et al., 2015). Resurrection plants, which can fully recover from a dehydrated state, have pectic side chains and hemicellulosic xylan enriched with arabinose-abundant polymers and along with increased arabinogalactan proteins, this helps prevent water loss during desiccation (Moore et al., 2013). Additionally, xyloglucan synthesis increases during drought stress. Under drought conditions, desiccation tolerant plants synthesise xylose, a sugar highly abundant in hemicellulose and a small constituent of pectic side chains (Balsamo et al., 2015). Similarly, rice (*Oryza sativa*) subjected to water deficit upregulated the expression of xyloglucan synthesis-related and xylose synthesis-related genes in the elongation zone of root hypocotyls. The location of the enhanced xyloglucan synthesis suggests that xyloglucan is necessary for root growth during drought stress (Yang et al., 2006).

Moreover, cell wall can be actively remodelled in response to abiotic stresses (Novaković et al., 2018). Drought stress and other osmotic stresses, through loss of cellular water, change the mechanical properties of the cell wall which can be detected with cell wall integrity sensors (Novaković et al., 2018). The integrity sensors activate a signalling cascade that results in the remodelling of cell wall to enhance mechanical strength (Novaković et al., 2018). One way to increase wall strength is to increase the synthesis of cellulose. For example, under drought stress, wild wheat (*Triticum boeoticum*) plants increase the expression of CESA3 (Placido et al., 2013), cotton plants (*Gossypium hirsutum*) increases the expression of sucrose synthase and UDP-glucose pyrophosphorylase genes, and tomato plants (*Solanum lycopersicum*) upregulate the expression of cellulose synthase-like genes 50-fold, all of which are involved

in cellulose synthesis (Placido et al., 2013; Ricardi et al., 2014; Zheng et al., 2014). Another effective way to protect the cell from damage during long exposure to water deficit stress is to increase the incorporation of lignin into primary cell walls (Moura et al., 2010). Across species exposed to drought stress, the expression of lignin biosynthetic genes is upregulated. For example, in wild wheat, brassinosteroid signalling genes, which regulate the synthesis of lignin precursors, are upregulated (Placido et al., 2013). Additionally, in rice, the expression of phenylalanine ammonia lyase, a key intermediate between the phenolics and lignin synthesis pathways, is increased (Pandey et al., 2010). Finally, in cotton, phenylcoumaran benzylic ether reductases, which are mainly involved in lignin synthesis, are upregulated (Zheng et al., 2014).

Alongside maintaining cell wall strength through synthesising cellulose and lignin, under drought stress, cell wall plasticity also needs to be maintained to allow root growth (Le Gall et al., 2015). Xyloglucan is important for maintaining plasticity as well as strength following drought stress. Xyloglucan modifying enzymes, such as xyloglucan endotransglucosylases/hydrolases, are highly upregulated during drought stress and are associated with drought tolerance (Rose et al., 2002; Choi et al., 2011; Dong et al., 2011). The xyloglucan modifying enzymes alter the configuration of xyloglucan so that there are fewer tight associations across the cell wall, enabling cell wall loosening for growth. Another set of cell wall enzymes with a similar function are expansins that are involved in cell wall loosening and confer drought tolerance. When the rose (*Rosa hybrida*) expansin A4 is overexpressed in Arabidopsis, plant survival following a 16-day-drought period is increased compared to wildtype (Lü et al., 2013). Equally, the tobacco (*Nicotiana tabacum)* transgenic plant line overexpressing wheat *EXP23* has higher drought tolerance than wildtype tobacco plants (Li et al., 2013). Furthermore, various expansin genes across species are induced by drought, such as *EXPB2* in soybean (Guo et al., 2011) and EXP1, EXP5, EXPB6, and EXPB8 in maize (*Zea mays;* Wu et al., 2001). Expansins regulate cellulose-cellulose and cellulose-xyloglucan interactions to allow cell wall loosening for plasticity and growth (Wang et al., 2013a; Cosgrove, 2016b).

Furthermore, as an element that is important in regulating the hydration status of the cell wall matrix, pectin is important for drought tolerance (Leucci et al., 2008). More pectin is present in the cell walls of drought tolerant wheat cultivars than drought sensitive wheat cultivars (Piro et al., 2003). Similarly, during drought stress, pectin degrading enzymes are down-regulated in Arabidopsis, enhancing the pectin content (Bray, 2004). In wheat, the amount of RG-I and RG-II side chains is increased during water deficit stress and this confers better drought tolerance (Leucci et al., 2008). Pectin modification also effects drought tolerance; methylesterification of pectin is reduced during water deficit stress (Gribaa et al., 2013). Moreover, xyloglucan is also important for maintaining the hydration status of the matrix through its modification with methyl- and O-acetyl-esters. For example, when water deficit stress is applied to date palm plants (*Phoenix dactylifera)*, the O-acetylation of xyloglucan decreases compared to the well-watered condition (Gribaa et al., 2013). Methyl-esters and O-acetyl groups are hydrophobic and so their reduction during drought stress allows the cell wall to retain more water (Gribaa et al., 2013).

1.4 Aims

There is evidence that cell wall defects have an impact on stomatal dynamics in response to bacterial infection and salinity stress, especially in the Arabidopsis cell wall mutant, *mur1* and allelic mutant *sfr8* (Melotto et al., 2008; Feng et al., 2018; Isayenkov and Maathuis, 2019; Zhang et al., 2019b). Moreover, there is preliminary evidence that *mur1* and *sfr8* may also have a transpiration defect, which could be due to faulty stomatal characteristics (Panter, 2018). The main purpose of this project is to confirm that *sfr8* has a transpirational defect and to investigate why this is. *sfr8* has perturbations in many aspects of cell wall, including, general fucosylation, pectin, xyloglucan and protein composition, pectin crosslinking and mechanical strength.

To accommodate all of these *sfr8* defects, there are five hypotheses for why *sfr8* may have a transpiration defect:

1. The reduction in general fucosylation of *sfr8* increases leaf transpiration.
2. Decreased abundance of pectin causes increased leaf transpiration.
3. Reduced pectin modification and the resultant reduction in pectin crosslinking increases leaf transpiration.
4. A perturbation to the hemicellulose xyloglucan increases leaf transpiration.
5. The reduced mechanical strength of *sfr8* cell walls increases leaf transpiration.

The investigation into the link between cell wall structure and increased transpiration in *sfr8* may reveal stomatal defects and a broader understanding of how guard cell walls effect stomatal opening and closure. Optimising stomatal aperture is important in agricultural crops to maximise photosynthesis while minimising water loss and stomatal closure in response to dehydration is particularly important in drought tolerance (Xiong et al., 2002; Lawson and Blatt, 2014). Therefore, optimising guard cell walls for efficient stomatal dynamics can be useful for crop productivity and drought tolerance.

Chapter 2: Materials and Methods

2.1 Plant Materials and Growth Conditions

2.1.1 Seed Material

All *Arabidopsis thaliana* plants used were Columbia-0 (Col-0) background. Lab seed stocks of *agp8, cgl1, fut4, msr1, mur2, pme34, pmr5, prc1, qul1, rwa2, sfr8,* and *xxt1 xxt2* were used (Table 2.1). *gaut5, gaut6-1* and *gaut6-2* were obtained from the Nottingham Arabidopsis stock centre (NASC, arabidopsis.info).

Table 2.1: The mutant name, gene name and AGI code and of the mutants under investigation.

Mutant name (Stock ID)	Name(s) of gene(s)	AGI Code	Reference
agp8 (SALK_141852C)	*AGP8 (ARABINOGALACTAN PROTEIN 8)* or *FLA8 (FASCICLIN-LIKE ARABINOGALACTAN PROTEIN 8)*	At2g45470	(MacMillan et al., 2010)
cgl1	*CGL1 (COMPLEX GLYCAN LESS 1)*	At4g38240	(Frank et al., 2008)
fut4	*FUT4 (FUCOSYLTRANSFERASE 4)*	At2g15390	(Liang et al., 2013)
gaut5 (SALK_050186C)	*GAUT5 (GALACTURONOSYLTRANSFERASE 5)*	At2g30575	(Lund et al., 2020)
gaut6-1 (SALK_073484C) *gaut6-2* (SALK_056646C)	*GAUT6 (GALACTURONOSYLTRANSFERASE 6)*	At1g06780	(Lund et al., 2020)
msr1-2 (SALK_075245C)	*MSR1 (MANNAN SYNTHESIS RELATED 1)*	At3g21190	(Wang et al., 2013b)
mur2 (N8565)	*MUR2 (MURUS 2)* or *FUT1 (FUCOSYLTRANSFERASE 1)*	At2g03220	(Ryden et al., 2003)
pme34 (SALK_098874C)	*PME34 (PECTIN METHYLESTERASE 34)*	At3g49220	(Huang et al., 2017)
pmr5 (N6579)	*PMR5 (POWDERY MILDEW RESISTANT 5)*	At5g58600	(Chiniquy et al., 2019)
prc1 (N6203)	*CESA6 (CELLULOSE SYNTHASE 6)* or *IXR1 (ISOZABEN RESISTANT 2)* or *PRC1 (PROCUSTE 1)*	At5g64740	(Hu et al., 2018)
qul1 (SALK_094635C)	*QUL1 (QUASIMODO2 LIKE 1)*	At1g13860	(Fuentes et al., 2010)
rwa2	*RWA2 (REDUCED WALL ACETYLATION 2)*	At3g06550	(Nafisi et al., 2015)
sfr8	*MUR1 (MURUS 1)* or *SFR8 (SENSITIVE TO FREEZING 8)*	At3g51160	(Reiter et al., 1993)
xxt1 xxt2	*XXT1 (XYLOGLUCAN XYLOSYLTRANSFERASE 1)*	At3g62720	(Cavalier et al., 2008)
	XXT2 (UDP-XYLOSYLTRANSFERASE 2)	At4g02500	

2.1.2   Initial Growth on Agar

Seeds were surface sterilised by shaking with 0.5 ml of 70% ethanol in a 1.5-ml microcentrifuge tube for approximately 5 minutes. Seeds were then pipetted onto sterile filter paper and allowed to dry in a microflow horizontal laminar flow hood (Bioquell, Andover, UK). Once the ethanol had evaporated, seeds were transferred to 9 cm circular petri dishes containing 0.8% plant tissue grade agar (Sigma-Aldrich, Missouri, USA) supplemented with ½ x Murashige and Skoog (MS) media (Murashige and Skoog, 1962; Duchefa Biochemie, The Netherlands). The agar had been sterilised earlier by autoclaving at 120°C for 20 minutes and had pH adjusted to 5.8 by the addition of 0.1 M KOH.

Plated seeds were stored for 2-4 days in the dark at 4°C to aid uniform germination. Once stratification was complete, agar plates were transferred to Percival CU36L5 growth chamber (Percival Scientific Inc., Perry, USA) with conditions set to a 16-hour light, 8-hour dark cycle with a light intensity of 150 μmol m^{-2} s^{-1} and a temperature of 20°C (±1°C).

2.1.3 Growth in Peat Plugs

After 8-12 days in the Percival, seedlings were transferred to 44 mm Jiffy pellets (Jiffy Products International, The Netherlands) and then placed in trays in a walk-in growth chamber. Trays were covered with clingfilm for 2-4 days to provide a 100% humid environment. Holes were then made in the clingfilm to gradually change the humidity and allow the seedlings to acclimatise. After another 1-2 days the clingfilm was removed. The growth chamber was set to short-day conditions of 12-hour light, 12-hour dark cycles at a light intensity of 150 μmol m^{-2} s^{-1} to promote vegetative growth. The growth chamber also maintained temperature at 20°C (±2°C) and humidity at a maximum of 70%. Mature plants were used in experiments at 5-9 weeks old.

2.1.4   Growth in Pots

Alternatively, for some of the plants used in the thermal imaging and all the plants used in the drought assessment experiments, seedlings were transferred to 5.5 cm x 5 cm round pots (Kuma, Waardenburg, Netherlands) filled with equal amounts of compost (J. Arthur Bower's John Innes No.2, County Tyrone, Northern Island). Trays were covered with sealed propagator lids for 2-4 days to achieve a 100% humid environment. The humidity was gradually decreased by opening the propagator lids, allowing the seedlings to acclimatise. After 1-2 days the propagator lids were removed. Plants were grown in short-day growth conditions as stated above. Mature plants were used in experiments at 5-6 weeks old.

2.2 Leaf Drying Assay

The plants in these experiments were grown in peat plugs as previously described and used at 5-8 weeks old. The day before the experiment, the plants were well-watered and sealed in a plastic bag to create 100% humidity. Six plants were used per genotype and leaves were selected based on size to be approximately uniform. One rosette leaf was removed from each plant, blotted and weighed immediately.

The detached leaf was then placed in a weighing boat abaxial side up and left to dry in conditions of approximately 20°C after being removed from the plant. The final measurement was taken at 7 days and is assumed to be the dry weight of the leaf. Each measurement was expressed as a percentage of the original weight. The experiment was repeated three times per group of genotypes.

2.3 Infra-Red Thermal Imaging

2.3.1 Imaging in Peat Plugs

The plants in these experiments were grown in peat plugs as previously described and used at 5-8 weeks old. The day before the experiment, the plants were well-watered and sealed in a plastic bag to create 100% humidity. The whole plants were removed from the tray and placed on a matte white surface in the pattern depicted in Figure 2.1. The plants were imaged immediately, every hour for 8 hours after the first image and then every day until all plants were desiccated. In between images plants were stored in trays without water in the same room as the images were taken and the plants were grown in. The plants were imaged using a Flir E50 Thermal Imaging camera (Teledyne Flir, Oregon, USA) at a distance of approximately 1 m. Emissivity was set at 1 m. The conditions were constant with light levels at 150 μmol $m^{-2} s^{-1}$, humidity at a maximum of 70% and temperature at 20°C (±2°C).
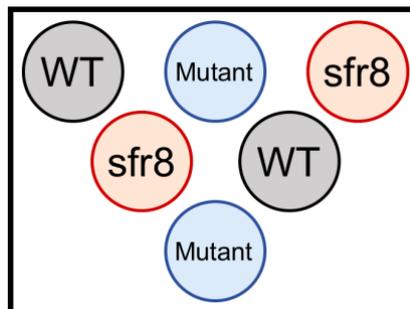
Figure 2.1: The arrangement of plants for thermal imaging, where mutant can be agp8, pmr5, prc1 or rwa2 depending on which mutant is being tested. Wildtype and sfr8 were included in every experiment as controls to which the temperature of the mutant can be compared.

2.3.2 Imaging in Pots

The plants in later experiments were grown in pots as previously described and used at 5-6 weeks old. The plants were imaged exactly as previously described.

2.4 Stomatal conductance

The plants in these experiments were grown in peat plugs as previously described. At the start of the experiment, plants were 5-6 weeks old and by the end of the experiment, they were 7-8 weeks old. The stomatal conductance was measured using a LI-6400XT Portable Photosynthesis System with attached 6400-15 Extended Reach 1 cm Chamber (LI-COR Biosciences, Nebraska, USA). One leaf was placed into the chamber and allowed to acclimatise to the initial CO_2 concentration of 400 ppm for 30 minutes. After

which the CO_2 concentration was changed to 50 ppm for 1 hour and then changed again to 1000 ppm for 1 hour. A decrease in CO_2 concentration should increase stomatal conductance and an increase in CO_2 concentration should decrease stomatal conductance. A measurement was recorded every minute and taken as an average over 15 seconds. Flow rate was constant at 300 µmol s^{-1} and the CO_2 value was matched after every change in CO_2 concentration. The measurements were carried out on six plants per genotype, three of which were started in the morning (before 12pm) and three of which were started in the afternoon (after 12pm) to limit the effect of circadian rhythms or diurnal factors on stomatal conductance. The experiment was carried out three times for a total of 18 repeats per genotype.

2.5   Stomatal Density and Size Measurements

2.5.1   Leaf Impressions

The plants in this experiment were grown in peat plugs as previously described and used at 8-9 weeks old. 28 plants from each genotype were used and one leaf per plant was removed. Leaves were selected to be of roughly the same size to limit leaf area effects. The excised leaf was blotted dry and any dirt was removed. Dental putty (President The Original Light Body, Coltene, Altstätten, Switzerland) was applied to the leaf using a dispensing gun (Dental Impression Mixing Dispenser, Walfront) and left to dry for at least 30 minutes. After which the leaf was removed. A thin layer of clear nail varnish (Ultra Shine Top Coat, Rimmel London) was applied to the putty and left to dry for at least 30 minutes and then the impression was removed. The impression captured the outline of the cells covering the leaf surface. The length and width of the leaf impression was measured to give an approximation of leaf area, calculated as length x width.

2.5.2   Stomatal Density Measurements

The impressions were viewed under a Leica DM 2500 optical microscope (Leica Microsystems, Wetzlar, Germany) at 10x magnification. A Panasonic 3CCD 1080p HD Colour camera (Panasonic, Osaka, Japan) was attached to the microscope and linked to a PC, which allowed pictures of the impressions to be taken. A 1 mm graticule was visualised with this microscope and camera. The length of the graticule was analysed using the image analysis software, Fiji (ImageJ, Schindelin et al., 2012) and was as a reference used to convert number of pixels into the corresponding length. From this the area of the camera's field of view was calculated. The number of stomata were counted per camera's field as view and stomatal density was calculated as number of stomata per unit area. Stomatal density was calculated for six sections across each leaf impression per genotype, giving a total of 168 areas for which stomatal density had been calculated per genotype. A picture was taken at each area where stomatal density was calculated.

2.5.3   Stomatal Size Measurements

The images taken of the leaf impressions as described above were analysed using Fiji. The length of stomatal complex is taken as the line running through the centre of the pore starting and finishing where the two guard cells meet at either end. The width of the stomatal complex is shown by the line running

perpendicular to the length at the halfway point of the pore (Figure 2.2). The length and width of stomata were measured by using the graticule as size reference as described above. Three stomata were measured per image, of which there were 168 images per genotype, giving a total of 504 stomata measured per genotype.
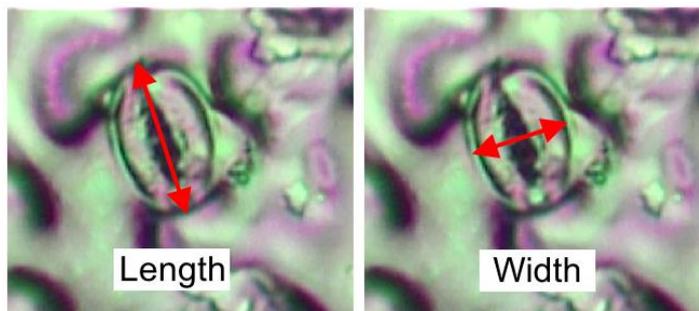
Figure 2.2: The length and width of stomatal complexes.

2.3.4 Stomatal aperture

Stomatal aperture was calculated based on the stomatal length and width measurements taken from leaf impressions as described previously. Stomatal aperture = width/length. A total of 504 stomatal apertures were calculated per genotype.

2.6   Drought Tolerance Assay

2.6.1 17-day Drought Period

The plants in this experiment were grown in pots as previously described and were well watered twice a week until their use at 5 weeks old. At this age the plants were transferred to a tray without water and photographed. The rosette size was measured, and the number of green leaves was recorded. Water was withheld for 17 days after which the plants were rewatered and photographed. A note was made of plants that had wilted. After another 10 days of regular watering, the plants were photographed a final time. The rosette size and number of green leaves was remeasured and used to calculate growth during the drought period and aftermath. The number of green leaves and dead leaves was recorded and used to assess survival; plants which had a greater number of green leaves than dead leaves had survived, whereas, plants which had fewer green leaves than dead leaves had died. Three plants were used per genotype.

2.6.2 19-day Drought Period

The experiment was repeated exactly as before but with a more severe drought period of 19-days. At least 15 plants were used per genotype.

2.7   Root Length Assay

Seedlings were grown on 0.8% agar plates supplemented with ½ x MS as previously described. At 7 days old, seedlings were transferred to 9 cm circular petri dishes containing 1.2% plant tissue grade agar (Sigma-Aldrich, Missouri, USA) supplemented with ½ x Murashige and Skoog (MS) media (Murashige and Skoog, 1962; Duchefa Biochemie, The Netherlands). The agar had been sterilised by autoclaving at 120°C for 20 minutes and had pH adjusted to 5.8 by the addition of 0.1 M KOH. The seedlings were carefully placed with their rosettes aligned with each other. Six wildtype and six mutant seedlings were used per plate, separated by a line marked on the back of the plate. The root length at 7 days old was marked on the back of the plate. The seedlings were placed vertically in the Percival growth chamber and left to grow for a further 5 days. After which photographs were taken and the images were analysed with Fiji using the marked lines of known length to convert pixels into the corresponding length. The root length at 7 and 12 days old was measured and growth was calculated. Seedlings which did not grow between 7 and 12 days old were excluded from the data analysis. The experiment was performed twice with 5-7 plates used per mutant genotype, giving at least 50 repeats per genotype.

2.8   Molecular Biology Techniques

2.8.1   DNA Extraction

DNA extraction was performed using a modified version of the method outlined by Edwards (Edwards et al., 1991). Mature plants grown in peat plugs as previously described were used in this experiment. A leaf was extracted from one plant and placed into a 1.5-ml microcentrifuge tube, which was frozen in liquid nitrogen. The sample was removed from the liquid nitrogen and ground with an electronic micropestle. 400 μL of Edward's extraction buffer (200 nM Tris-HCl, pH 7.5/ 250 mM NaCl/ 25 mM EDTA, pH 8.0/ 0.5% SDS) was added and homogenised with the micropestle. Samples were briefly vortexed and then centrifuged for 1 min at 13,300 g in a Pico 17 Centrifuge (Thermo Fisher Scientific, Massachusetts, USA). 300 μL of the resulting supernatant was extracted and transferred to a fresh 1.5-ml microcentrifuge tube. 300 μL of isopropanol was added to the supernatant, which was then mixed and incubated at room temperature for 2 minutes. The sample was centrifuged again at 13,300 g for 5 minutes. After which as much supernatant was removed as possible. Then the sample was centrifuged a final time at the same speed for another minute and again as much supernatant was removed as possible. The sample was dried in a drying centrifuge (Eppendorf Concentrator 5301, Eppendorf Ltd., Stevenage, UK) for approximately 1 hour to remove all supernatant. The pellet was resuspended in 50 μL of TE buffer (10 mM Tris, pH 8.0/ 1 mM EDTA) and left to incubate for 3 days at 5°C to allow DNA to dissolve into the solution. This was repeated for each genotype as required and performed alongside wildtype as a control.

2.8.2   Primers

The three mutants genotyped were all T-DNA insertion lines. Two gene-specific primers were designed per mutant using the online SIGnAL primer design tool provided by the SALK Institute Genomic Analysis Laboratory (T-DNA Express: Arabidopsis Gene Mapping Tool (signal.salk.edu)). One primer mapped

upstream of the T-DNA insertion site (forward primer) and the other mapped to a locus downstream of the insertion site (reverse primer). Confirmation that the insert was present in the desired gene was obtained by PCR reaction using one gene-specific primer and a T-DNA left border-specific primer, LBb1.3 was used as recommended by SIGnAL (Figure 2.3). An alternative primer of an older design, called SALK LBb1.3, was used for some of the genotyping were LBb1.3 failed to produce a product. All primers were synthesised by Integrated DNA Technologies (IDT, Inc., Iowa, USA).
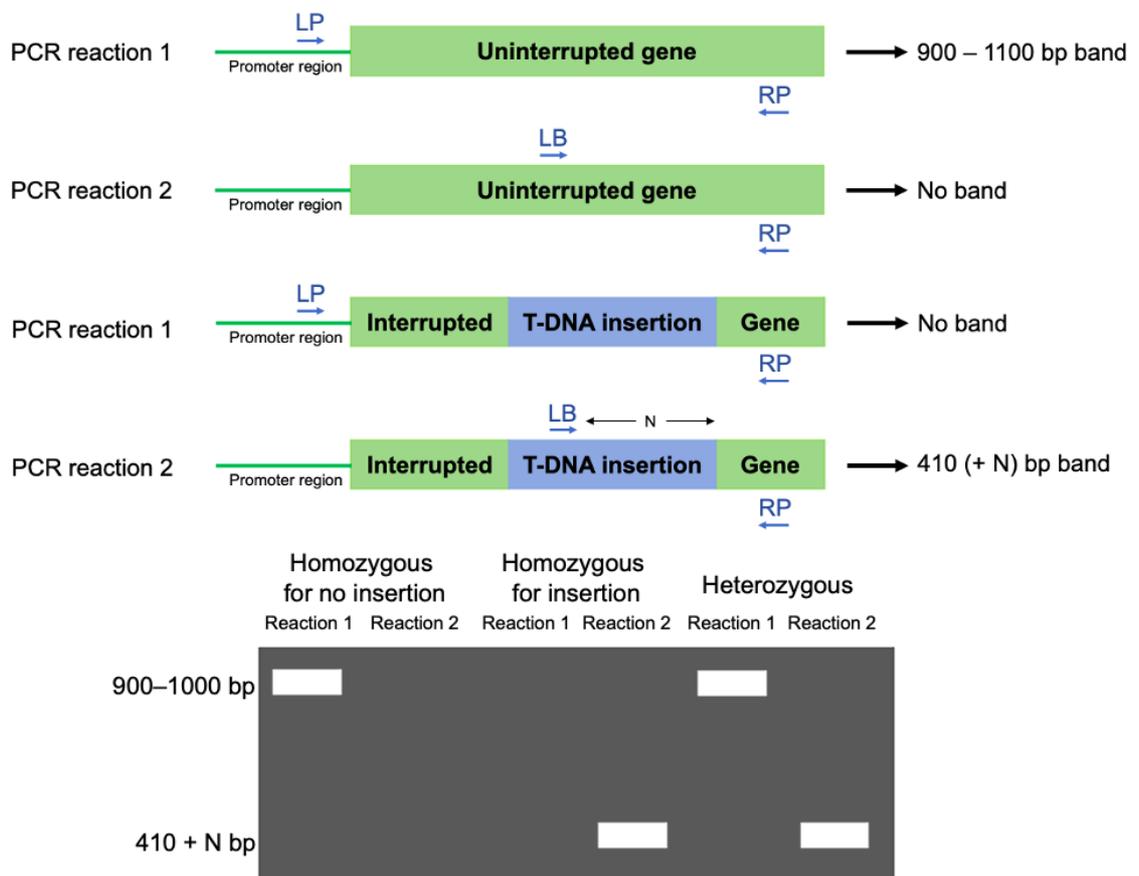
Figure 2.3: Representation of the location of the primers and the bands produced by PCR reaction. LP = left genomic primer/forward primer. RP = right genomic primer/reverse primer. LB = left border T-DNA primer/T-DNA primer/alternative T-DNA primer. N = difference between actual insertion site and flanking sequence position, usually 0-300 bp. Adapted from SIGnAL primer design tool (signal.salk.edu).

2.8.3   Polymerase Chain Reaction (PCR)

For genotyping wildtype and T-DNA insertion lines, two PCR reactions were set up per sample to reveal the presence of the T-DNA insert in one or both copies of the genomic sequence, indicating homozygous or heterozygous lines respectively (Figure 2.3). Reactions were set up in a 0.5-ml microcentrifuge tube. Reaction mixture contained 25 µL of MyTaq red mix (Meridian Bioscience, Ohio, USA), 22 µL of nuclease free water, 1 µL each of two primers used, as depicted in Table 2.2, and 1 µL of wildtype or *gaut* DNA. A 50-µL no template control (NTC) reaction was also set up per sample containing MyTaq red mix and nuclease free water as before, but also containing three primers (Table 2.2) and no DNA. The five 50 µL reaction mixtures were placed in a PCR express thermal cycler (Thermo Hybaid, Thermo Fisher Scientific,

Massachusetts, USA) and run on the following programme: 95°C, 2 min x 1; (95°C, 30 s; Ta, 30 s; 72°C, 1 min) x 35; 72°C, 5 min x 1. The annealing temperature (Ta) was chosen to be 50°C, which was 3-5°C below the melting temperature of all the primers. The PCR products were analysed using gel electrophoresis.

Table 2.2: Primers used in the first PCR experiments performed on all *gaut* mutants and the alternative PCR experiment performed on *gaut5* only. NTC = no template control.

	First experiment			Alternative experiment		
	Reaction 1	Reaction 2	NTC	Reaction 1	Reaction 2	NTC
Reverse primer	✓	✓	✓	✓	✓	✓
Forward primer	✓		✓	✓		✓
T-DNA primer		✓	✓			
Alternative T-DNA primer					✓	✓

2.8.4 Gel Electrophoresis

DNA was separated by size using gel electrophoresis. 0.5 g of molecular biology grade agarose (Bioline, London, UK) was melted in 50 ml of 0.5 x TBE buffer (1.1 M Tris, 900 mM borate, 25 mM EDTA, pH 8) forming a 0.8% gel. 2 µL of Midori green advance DNA stain (Geneflow Ltd., Staffordshire, UK) was added before the gel was set. 10 µL of each PCR product was loaded into a well, alongside 6 µL of 1 kB hyperladder (Bioline, London, UK) for size comparison. Gels were run at 35 mA for 1 hour then imaged under UV light using an uvidoc transilluminator (Uvitec Ltd., Cambridge, UK).

2.9 Statistical Analysis

All data analysis was performed using SPSS Statistics (IBM SPSS Statistics for Macintosh, Version 26). The quantitative data involving more than two means, including the extracted leaf drying data, the extracted stomatal conductance data, stomatal measurements and drought tolerance data, were tested for normality using a Shapiro-Wilk test. For data in which all categories were normally distributed ($p>0.005$), a One-Way ANOVA was used, followed by a Tukey's post-hoc test for pairwise comparisons. For data in which at least on category was not normally distributed ($p<0.005$), a Kruskal Wallis test was performed. Following this, if there was a significant difference between categories ($p<0.005$), then Mann-Whitney U-tests were performed for each pairwise comparison.

The quantitative data involving only two means, namely the root length assay, were tested for normality using a Shapiro-Wilk test. None of the data were normally distributed ($p<0.005$), therefore, a Mann-Whitney U-test were performed to test for significance between means.

Chapter 3: Results

3.1 Leaf Drying Assay

Leaf excision can be used to investigate transpiration as following excision leaves lose water. This is the principle of the leaf drying assay; leaves are excised from healthy plants and left to dry in ambient environment during which they are weighed at regular intervals to measure their transpiration rate (Lösch, 1979). Leaf excision can also indirectly show differences in stomatal responses as leaf excision induces changes in stomatal aperture. First the stomata open transiently, then close completely, this is often called the Iwanoff effect (Iwanoff, 1928). The rate at which stomatal aperture changes during the period following leaf excision can be inferred from transpiration rate. Several Arabidopsis cell wall mutants were compared to wildtype and *sfr8* in leaf drying assays. Leaves that lose water more quickly or slowly than wildtype after removal have a transpiration defect and may have different stomatal dynamics that will be worth investigating further to elucidate which component/components of Arabidopsis cell wall influence stomatal function. The initial mass and dry mass (taken to be the leaf mass 1 week after excision) of the leaves are included in the statistical analysis to highlight any differences in leaf area and leaf water content, which would cause a difference in leaf water loss rate, other than due to difference in genotype. The gradient of water loss in the first hour, during hour 1-4 and hour 4-8 are also extracted from the leaf drying assay data to statistically analyse and test for significance between the genotypes for their water loss rate.

3.1.1 Fucosylation Mutants

sfr8 has a point mutation in the gene, *MUR1*, which causes an amino acid change in the encoded protein, GDP-D-mannose-4,6-dehydratase, an enzyme involved in the synthesis of the cell wall sugar fucose (Zablackis et al., 1996b; Panter et al., 2019). The substitution of glycine for glutamate in *sfr8* GDP-D-mannose-4,6-dehydratase renders the enzyme significantly less effective, and therefore *sfr8* has reduced fucose content (Panter et al., 2019). As a result, there is less fucosylation of cell wall components, including RG-I, RG-II, xyloglucan and cell wall proteins (Zablackis et al., 1996b; Rayon et al., 1999; O'Neill et al., 2001; Van Hengel and Roberts, 2002; Sechet et al., 2018). One of the hypotheses for why *sfr8* has a water loss defect is that reduced fucosylation of cell wall components facilitates a water loss rate faster than wildtype. To test the hypothesis, Arabidopsis cell wall mutants with reduced cell wall fucosylation were chosen. *mur2* has a mutation in the fucosyltransferase, FUT1, which is specific to the fucosylation of xyloglucan and as a consequence has less than 2% the wildtype amount of fucosylated xyloglucan (Vanzin et al., 2002). The *fut4* mutant has a T-DNA insertion mutation in the fucosyltransferase, FUT4, which is specific to the fucosylation of arabinogalactan proteins located in the cell wall of leaf and root cells (Liang et al., 2013; Tryfona et al., 2014). The T-DNA insertion causes a loss of function mutation in FUT4 reducing the fucose content of root arabinogalactan proteins and eliminating all leaf arabinogalactan protein fucose residues (Liang et al., 2013). *msr1* has a mutation in an O-fucosyltransferase, which is highly expressed in the guard cells and is important for the synthesis of mannose, a sugar incorporated into

many cell wall components, such as mannans, galactosmannans and glucomannans. The lack of this O-fucosyltransferase means that *msr1* has a 40% reduction of mannosyl residues and a 50% reduction of glucomannan by 50% (Wang et al., 2013b). *cgl1* lacks the ability to process N-linked glycans, a cell wall component that is fucosylated, therefore, *cgl1* lacks fucosylated glycoproteins (Frank et al., 2008). *cgl1* has previously been used in comparison with fucosyltransferases and has compromised apoplastic and stomatal defences when infected with *Pseudomonas syringae pv*. tomato DC3118, which indicates a stomatal aperture defect (Zhang et al., 2019b). Each of the mutants lacks or has a reduction in a fucosylated component of cell wall, *mur2* has reduced fucosylated xyloglucan, *fut4* has a reduction in fucosylated arabinogalactan proteins, *msr1* lacks fucosylation involved in the synthesis of mannose and *cgl1* lacks fucosylated N-glycans. Therefore, together these mutants and cell wall defects test the hypothesis that the lack of general fucosylation is what causes the water loss defect in *sfr8*.
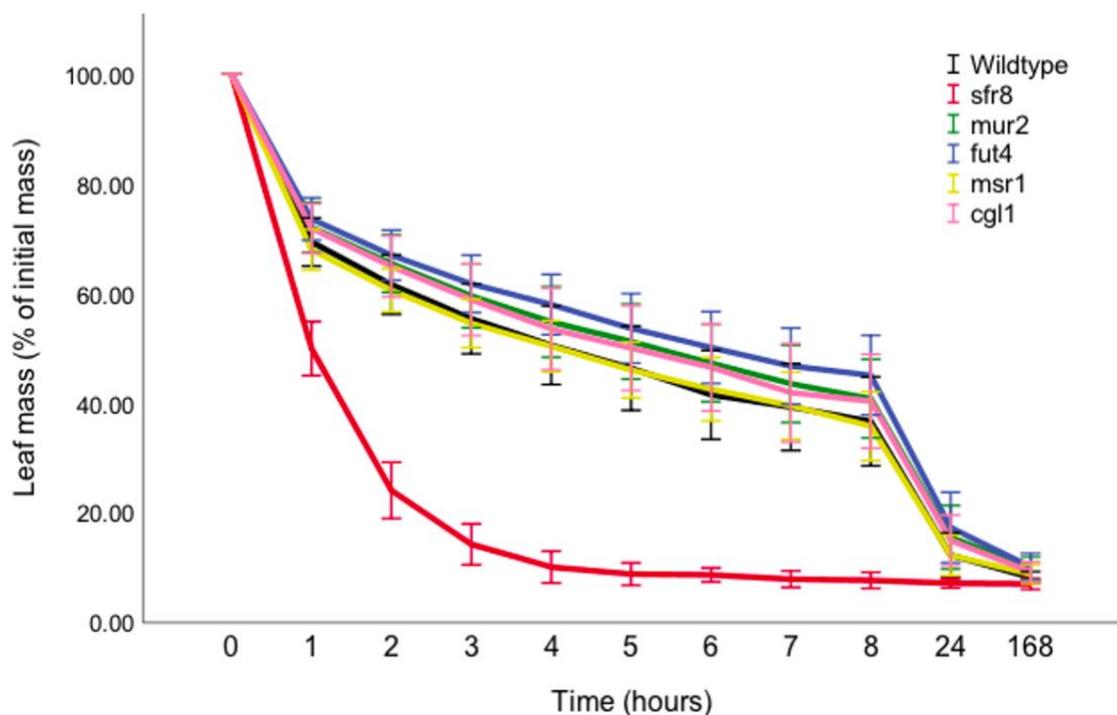
Figure 3.1.1: Water loss in excised leaves of fucosylation mutants: % of original leaf mass immediately after removal from the rosette. Wildtype (black), *sfr8* (red), *mur2* (green), *fut4* (blue), *msr1* (yellow) and *cgl1* (pink). The rate at which leaf mass is loss is taken to be the rate of water loss. Error bars show ±1 standard error. n=18 per genotype.

Wildtype had a reduction in mass to a mean of 69.45% (± 2.20) the original mass (Figure 3.1.1). The mass decreased over the next 7 hours to a mean of 36.72% (±4.05). By 24 hours, mass had decreased to a mean of 12.31% (±2.04) of the original mass. The mass after 1 week was taken to be the dry weight, which for wildtype was 8.28% (±0.52) of the original mass.

Out of the fucosylation mutants being compared, *mur2*, *fut4* and *cgl1* mutants maintained a mean mass higher than wildtype throughout the experiment (Figure 3.1.1). During the first hour after excision, *mur2* reached a mean mass of 72.14% (±2.29), *fut4* reached a mean mass of 73.64% (±1.93), *cgl1* reached a mean mass of 71.90% (±2.26). By 8 hours following excision, *mur2, fut4* and *cgl1* had reached a % of original mass of 40.88% (±3.59), 45.14% (±3.63) and 40.40% (±4.29) respectively, with a dry mass after 1

week of 9.92% (±1.03), 10.15% (±1.24) and 9.26% (±0.90), respectively. The water loss of the mutants was entirely dissimilar to the water loss of *sfr8*. The other fucosylation mutant being compared, *msr1*, maintained a mean mass slightly larger than wildtype throughout the assay. *msr1* had a mean mass of 68.01% (±1.85) after 1 hour, 35.85% (±3.14) at 8 hours and 8.85% (±0.87) after 1 week. The water loss was comparable to wildtype and the other fucosylation mutants, which was highly dissimilar to *sfr8*, like the other fucosylation mutants.

sfr8 showed a different pattern of water loss to wildtype and the fucosylation mutants (Figure 3.1.1). Within the first hour after excision, *sfr8* leaf mass had a steeper decline than wildtype, reaching a mean mass of 49.99% (±2.46) the original. The sharp decline of leaf mass continued during the second, third and fourth hour and by 5 hours after excision the leaves had almost reached their dry weight (7.06% (±0.49)), with a mean mass of 8.86% (±1.02).
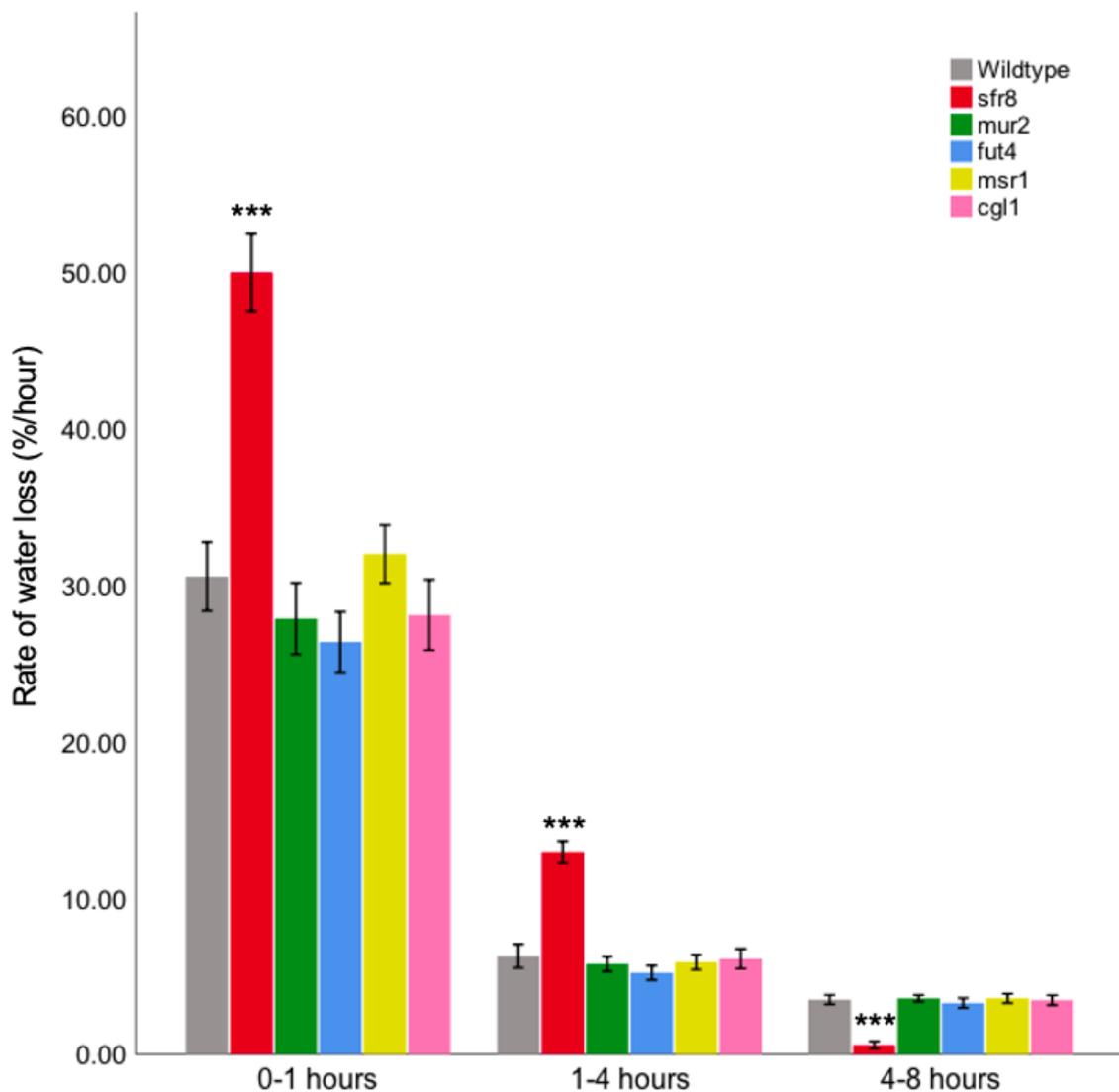
Figure 3.1.2: Rate at which excised leaves of fucosylation mutants lost water (% of leaf mass) per hour during the first hour (0-1 hours), the following 3 hours (1-4 hours) and the following 4 hours (4-8 hours). Wildtype (grey), *sfr8* (red), *mur2* (green), *fut4* (blue), *msr1* (yellow) and *cgl1* (pink). Error bars show ±1 standard error. n=18 per genotype. *** = p<0.001.

During the first hour, there was a significant difference between the genotypes for water loss rate (Kruskal Wallis, X^2_5=37.508, p<0.001). The transpiration rate of *sfr8* was the highest of all genotypes with an average gradient of 50.01 (±2.46; Figure 3.1.2), which was significantly faster than all other genotypes (Mann Whitney U-test; *mur2* – U=20.5, p<0.001; *fut4* – U=10.5, p<0.001; *msr1* – U=25.0, p<0.001; *cgl1* – U=18.0, p<0.001; wildtype – U=27.0, p<0.001). Wildtype, *mur2, fut4, cgl1* and msr1 had statistically similar water loss rates during the first hour, with gradients of 27.86 (±2.29), 26.36 (±1.93), 28.10 (±2.26) and 31.99 (±1.85) respectively (Mann Whitney U-test; *mur2* – U=138.0, p=0.462; *fut4* – U=115.0, p=0.143; *msr1* – U=145.0, p=0.606; *cgl1* – U=141.0, p=0.521).

The water loss rate for all genotypes decreased over the next 3 hours compared to their respective rate in the first hour (Figure 3.1.2). During hours 1-4, there was a significant difference between the genotypes for gradients of water loss (Kruskal Wallis, X^2_5=39.731, p<0.001). *sfr8* still had the highest water loss rate during this period, with a gradient of 12.94 (±0.68), which was significantly faster than the other genotypes (Mann Whitney U-test; *mur2* – U=6.5, p<0.001; *fut4* – U=3.0, p<0.001; *msr1* – U=6.5, p<0.001; *cgl1* – U=15.5, p<0.001; wildtype – U=23.0, p<0.001). Wildtype had a water loss rate of 6.28 (±0.76), which was a quicker rate than all fucosylation mutants: *mur2, fut4, cgl1* and *msr1* had gradients of 5.78 (±0.48), 5.21 (±0.46), 6.10 (±0.63) and *msr1* had a gradient of 5.88 (±0.48). Despite having a slightly quicker water loss rate, wildtype had statistically the same water loss as the fucosylation mutants between hours 1 – 4 (Mann Whitney U-test; *mur2* – U=161.0, p=0.988 , *fut4* – U=136.0, p=0.424; *msr1* – U=161.5, p=0.988; *cgl1* – U=162.0, p=1.000).

Again, the water loss rate for all genotypes decreased over the next 4 hours compared to their previous rate (Figure 3.1.4). There was a significant difference between the genotypes for rate of water loss during hours 4-8 (Kruskal Wallis, X^2_5=38.252, p<0.001). *sfr8* no longer had the fastest water loss rate, instead *sfr8* was significantly slower than the other genotypes (Mann Whitney U-test; *mur2* – U=9.0, p<0.001; *fut4*– U=19.0, p<0.001; *msr1* – U=11.0, p<0.001; *cgl1* – U=13.0, p<0.001; wildtype – U=15.0, p<0.001). The remaining genotypes had a statistically similar water loss rate; wildtype, *mur2, fut4, cgl1* and *msr1* had gradients of 3.49 (±0.29), 3.57 (±0.21), 3.27 (±0.31), 3.45 (±0.32) and 3.57 (±0.30), respectively (Mann Whitney U-test; *mur2*– U=157.0, p=0.888 , *fut4* – U=144.5, p=0.584; *msr1* – U=154.5, p=0.815; *cgl1* – U=156.0, p=0.864).

Table 3.1: Mean leaf initial and dry mass of fucosylation mutants. n=18 per genotype.

Mutants	Initial mass (mg) (±1 SE)	Dry mass (mg) (±1 SE)
Wildtype	39.8 (±1.9)	3.3 (±0.2)
sfr8	38.1 (±3.3)	2.7 (±0.3)
mur2	36.8 (±2.3)	3.5 (±0.3)
fut4	38.7 (±1.8)	3.9 (±0.5)
msr1	39.9 (±2.2)	3.4 (±0.3)
cgl1	40.8 (±2.4)	3.8 (±0.4)

All genotypes had a similar leaf initial and dry mass (Table 3.1). There is no statistically significant difference between the genotypes for initial leaf mass (One-way ANOVA; $F_{5,\ 101}$=0.389, p=0.855), nor leaf dry mass (Kruskal Wallis, X^2_5=5.176, p=0.395), meaning differences in leaf water loss rate are not due to leaf size or water content, and are likely be caused by the different genotypes.

In summary, fucosylation mutants, *mur2*, *fut4, msr1* and *cgl1* maintained a similar mean mass and water loss rate to wildtype throughout the assay. In contrast, the fucosylation mutants maintained a higher mean mass than *sfr8* up until 1 week after excision, and had a significantly different water loss rate to *sfr8.* Therefore, *mur2*, *fut4, msr1* and *cgl1* do not have a water loss defect like *sfr8* and have a water loss rate similar to wildtype.

3.1.2 Pectin Abundance Mutants

Pectin is a component of cell walls that is fucosylated, particularly two of the main pectic domains, rhamnogalacturonan I and rhamnogalacturonan II (McNeil et al., 1984; Ndeh et al., 2017). *sfr8* cell wall has reduced pectin fucosylation, which has functional consequences (O'Neill et al., 2001; Sechet et al., 2018). Therefore, the reduction in fucosylated pectin could be the cause of the water loss defect in *sfr8*. To test this hypothesis, Arabidopsis cell wall mutants with a general reduction or general increase in pectin content were compared to *sfr8* and wildtype in a water loss assay.

The pectin abundance mutants were subjected to the leaf drying assay on different occasions due to the *gaut* mutants arriving from the NASC stock centre later in the project and the other mutants being lab stocks, so could be used immediately. Therefore, the results for these experiments are presented separately because the rate of water loss depends on temperature, air flow and humidity, conditions which fluctuate day-to-day and cannot be perfectly replicated. The water loss rates cannot be directly compared between experimental conditions and so it was necessary for the data to be presented and analysed independently.

3.1.2.1 *gaut* Mutants

The *gaut* mutants, *gaut5*, *gaut6-1* and *gaut6-2*, were chosen for inclusion in this experiment because both GAUT5 and GAUT6 are essential in the synthesis of HG (Lund et al., 2020). They localise the galacturonosyltransferase responsible for HG synthesis, GAUT1, to the golgi, where HG synthesis occurs (Lund et al., 2020). *gaut5* has a T-DNA insertion in the *GAUT5* gene which knocks out its function. *gaut6-1* and *gaut6-2* have T-DNA insertions in the *GAUT6* gene, which knocks out its function. In their absence, the amount of HG in the cell walls of *gaut5, gaut6-1* and *gaut6*-2, is severely reduced and so the mutants test the hypothesis that reduced amount of pectin leads to a faster leaf water loss rate (Lund et al., 2020).

The *gaut* mutants were later genotyped using PCR to confirm whether or not they are T-DNA insert knock-out mutants in the genes stated by NASC (Section 3.1.2.2).
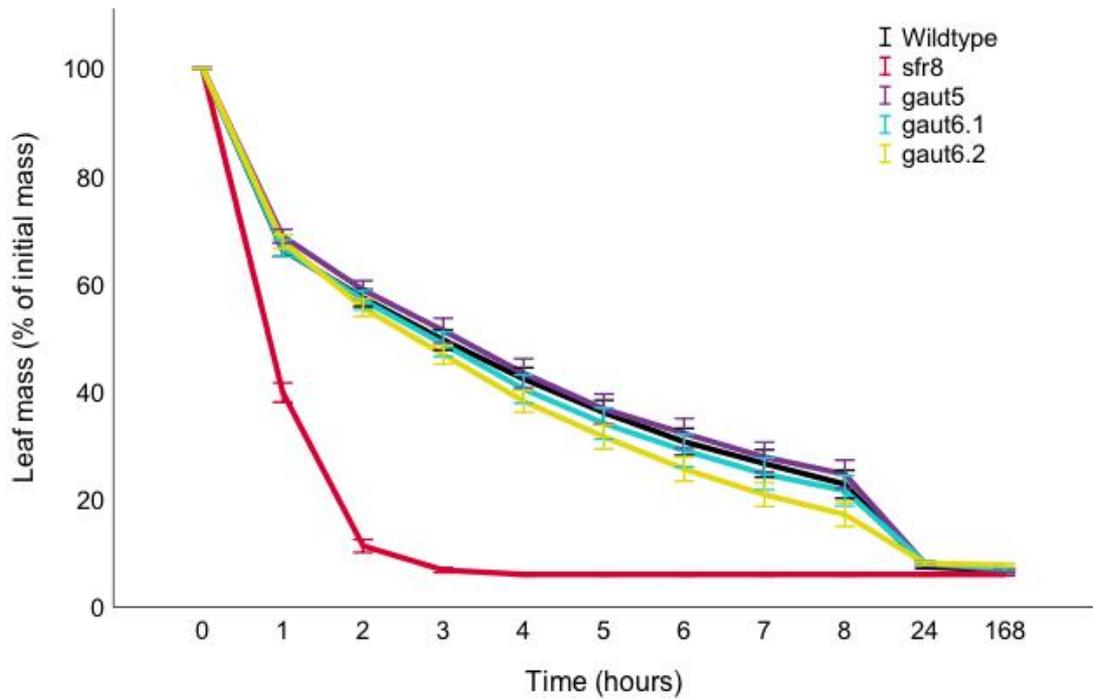
Figure 3.2.1: Water loss in excised leaves of gaut mutants: % of original leaf mass immediately after removal from the rosette. Wildtype (black), *sfr8* (red), *gaut5* (purple), *gaut6-1* (cyan), and *gaut6-2* (yellow). The rate at which leaf mass is loss is taken to be the rate of water loss. Error bars show ±1 standard error. n=18 per genotype.

Following excision, wildtype leaves had a decrease in mass to a mean of 66.30% (±1.28) the original mass (Figure 3.2.1). By 8, 24 and 168 hours after excision, wildtype leaves had reached an average mass of 22.78% (±2.60), 7.44% (±0.31) and 6.79% (±0.26) of initial weight. Similar to the *sfr8* pattern of water loss shown previously, *sfr8* lost the most mass of all genotypes during the first hour, reaching 39.80% (±1.80). By hour 4, *sfr8* had reached its average dry weight of 6.06% (±0.28).

The *gaut* mutants had a similar % mass to wildtype throughout the assay. After 1 hour, *gaut5, gaut6-1* and *gaut6-2* reached mean masses of 68.79% (±1.29), 66.54% (±1.57) and 67.78% (±1.29) respectively. By 8 hours after excision, *gaut5, gaut6-1* and *gaut6-2* reached mean masses of 24.64% (±2.63), 21.58% (±2.82) and 17.16% (±2.23) respectively. By 24 hours, *gaut5*, *gaut6-1* and *gaut6-2* had almost reached their dry masses (6.78% (±0.40), 7.15% (±0.28) *1* and 7.79% (±0.31), respectively), with mean masses of 8.02% (±0.46), 8.16% (±0.29) and 8.10% (±0.31), respectively.

During the first hour, there was a significant difference between the genotypes for water loss rate (One-way ANOVA, $F_{4,85}$=71.537, $p<0.001$). *sfr8* had by far the fastest water loss rate during the first hour with a gradient of 60.20 (±1.80) (Figure 3.2.2) and had a significantly faster transpiration rate than the other genotypes (Tukey's post-hoc test, $p<0.001$). Wildtype, *gaut5, gaut6-1* and *gaut6-2* had statistically similar water loss rates with gradients of 34.39 (±1.53), 31.21 (±1.29), 31.96 (±1.39) and 32.22 (±1.29), respectively (Tukey's post-hoc test; *gaut5* – p=0.549; *gaut6-1* – p=0.769; *gaut6-2* – p=0.835).
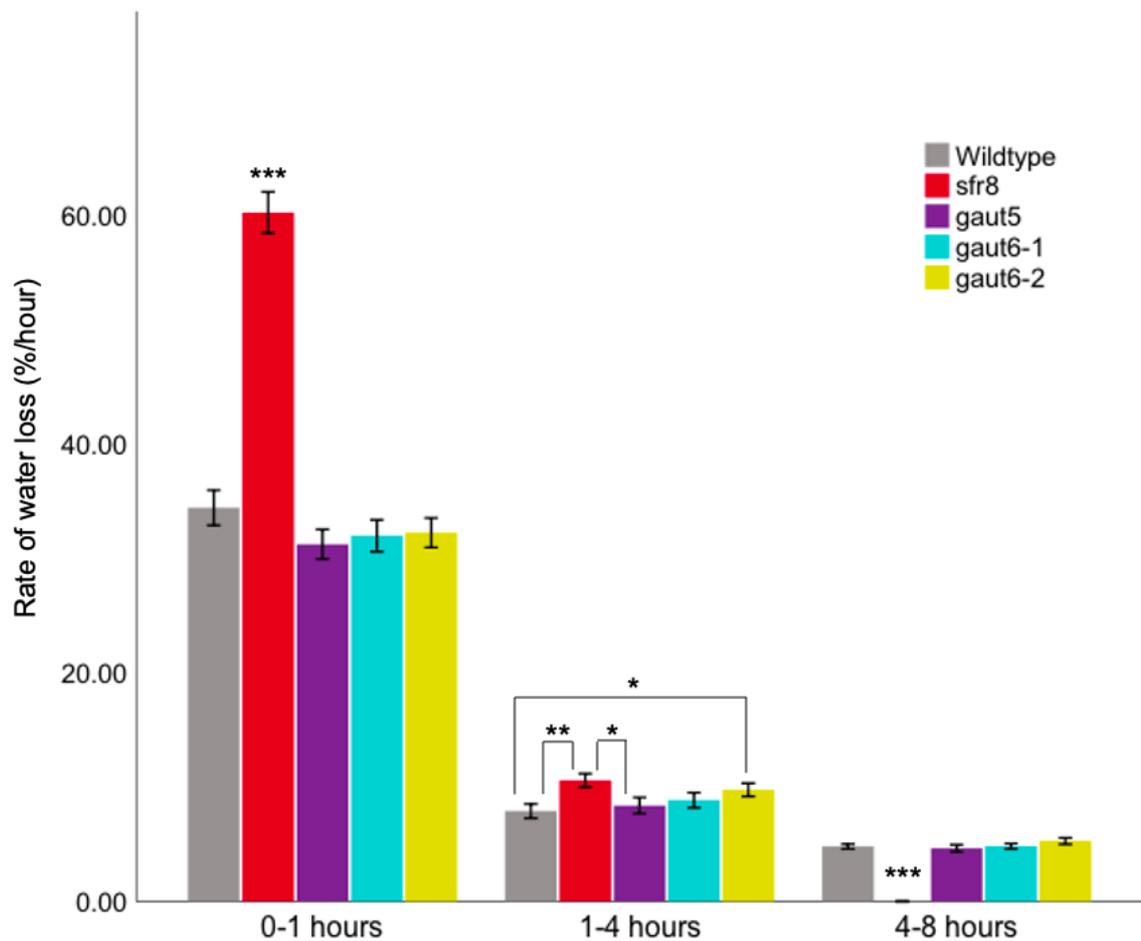
Figure 3.2.2: Rate at which excised leaves of gaut mutants lost water (% of leaf mass) per hour during the first hour (0-1 hours), the following 3 hours (1-4 hours) and the following 4 hours (4-8 hours). Wildtype (grey), sfr8 (red), gaut5 (purple), gaut6-1 (cyan) and gaut6-2 (yellow). Error bars show ±1 standard error. n=18 per genotype. * means p<0.05; ** means p<0.01; *** means p<0.001.

The water loss rate for all genotypes decreased over the next 3 hours compared to their respective rate in the first hour (Figure 3.2.2). There was a significant difference between the genotypes for water loss rate in hours 1-4 (Kruskal Wallis, X^2_4=12.666, p=0.013). *sfr8* had the highest water loss rate during this period with a gradient of 10.57 (±0.58), which was significantly faster than wildtype and *gaut5*, but not *gaut6-1* and *gaut6-2* (Mann Whitney U-test; U=70.0, p=0.003; U=83.0, p=0.012; U=100.5, p=0.051; U=128.5, p=0.293, respectively). Wildtype had the slowest water loss during this period with a gradient of 7.89 (±0.62), whereas, *gaut5* had a water loss rate of 8.38 (±0.70), *gaut6-1* had a water loss rate of 8.84 (±0.66) and *gaut6-2* had a water loss rate of 9.75 (±0.58). *gaut5* and *gaut6-1* had statistically the same water loss as wildtype during this period (Mann Whitney U-test; U=138.5, p=0.462; U=130.0, p=0.323, respectively), but *gaut6-2* did not (Mann Whitney U-test, U=94.0, p=0.031).

The water loss rate decreased again over the next 4 hours for all genotypes (Figure 3.2.4). There was a statistically significant difference between the water loss rates of the genotypes (One-way ANOVA, $F_{4,85}$=87.158, p<0.001). *sfr8* had significantly slower water loss rate than all other genotypes with a gradient of 0 (±0; Tukey's post-hoc test, p<0.001). *gaut5, gaut6-1* and *gaut6-2* had statistically similar

water loss rates to wildtype (4.80 (±0.21)), with gradients of 4.64 (±0.31), 4.82 (±0.24) and 5.28 (±0.28), respectively (Tukey's post-hoc test; *gaut5* – p=0.989; *gaut6-1* – p=1.000; *gaut6-2* – p=0.607).
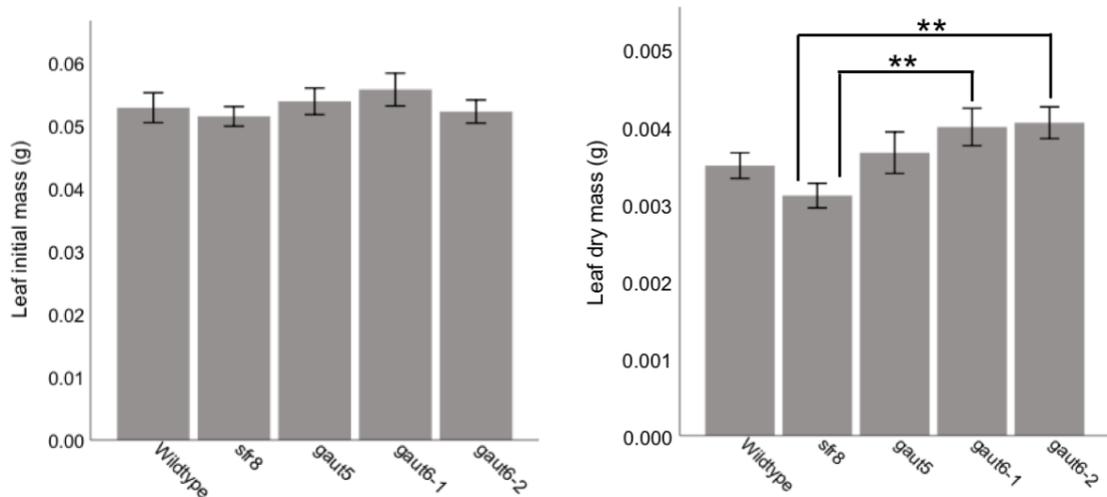
Figure 3.2.3: Mean leaf initial and dry mass of gaut mutants. Error bars show ±1 standard error. n=18 per genotype. ** means p<0.01.

Wildtype, *sfr8*, *gaut5*, *gaut6-1* and *gaut6-2* all had statistically similar mean initial masses at 52.8 mg (±2.4), 51.4 mg (±1.6), 53.8 mg (±2.1), 55.7 mg (±2.6) and 52.2 mg (±18.3; Figure 3.2.2), respectively (One-way ANOVA, $F_{4,85}$=0.601, p=0.663). Leaf area can be taken to be statistically the same, meaning leaf area had no effect on water loss rate. However, there was a statistically significant difference between dry weights (Kruskal Wallis, X^2_4=12.649, p=0.013). *sfr8* had a significantly smaller dry mass than *gaut6-1* and *gaut6-2* at 3.1 mg (±0.2) compared with 4.0 mg (±0.2) and 4.1 mg (±0.2), respectively (Mann Whitney U-test; U=78.0, p=0.007; U=70.0, p=0.003). *sfr8* may have significantly more water content than *gaut6-1* and *gaut6-2*, which could affect water loss rate. Wildtype weighed on average 3.5mg (±0.2) and *gaut5* weighed 3.7 mg (±0.3). All other pairwise combinations of genotypes had statistically the same dry weight, therefore, water content did not have an effect on water loss rate for the remaining genotypes.

In summary, throughout the leaf drying assay, the *gaut* mutants maintained mean leaf mass similar to wildtype, which was much larger than *sfr8.* The *gaut* mutants had similar water loss rates to wildtype during the first hour and between hours 4-8. The *gaut6* mutants had the same water loss gradient as *sfr8* during hours 1-4, however this does not reflect the overall patterns of water loss, which were different between the *gaut6* mutants and *sfr8.* Leaf area is disregarded as a factor that could influence the water loss rate and although *gaut6* mutants had a slightly greater water content than *sfr8,* the huge differences in water loss rate cannot be attributed to water content alone and implicate some role of genotype. Therefore, the *gaut* mutants have a water loss pattern similar to wildtype, which is dissimilar to *sfr8*.

3.1.2.2 PCR Genotyping of *gaut* Mutants

The *gaut* mutants all had T-DNA insertions (Figure 3.2.4) and were obtained from NASC, therefore, it was necessary to confirm their genotype with PCR before making any conclusions about their effect on cell

wall and the result upon leaf water loss rate. The seed stock sent could have been heterozygous, which would explain the water loss rate equal to wildtype of the putative *gaut* mutants.
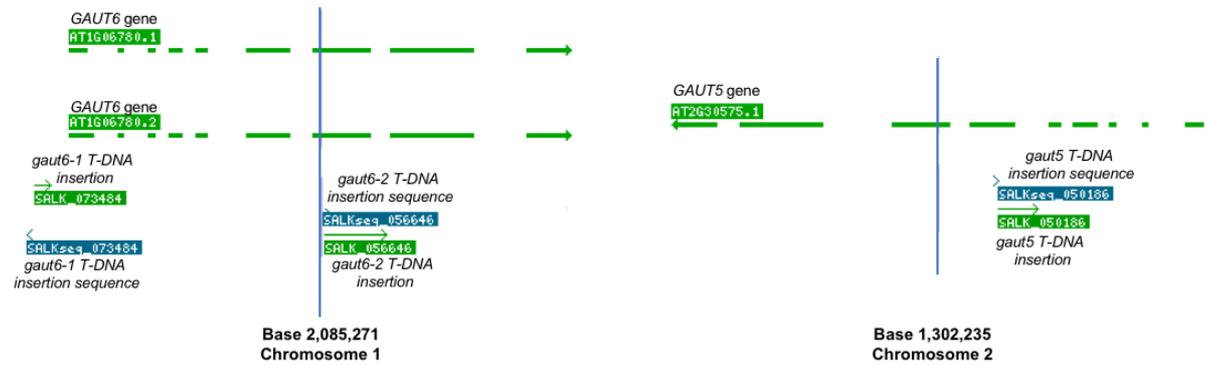
Figure 3.2.4: The locations of the T-DNA insertions in gaut6-1, gaut6-2 and gaut5. Adapted from SIGnAL T-DNA Express: Arabidopsis Gene Mapping Tool (signal.salk.edu)

A PCR reaction with GAUT6-1 forward and reverse gene-specific primers revealed that wildtype genomic DNA contained an uninterrupted copy of the *GAUT6* gene, as a band of the expected size, approximately 1000 bp, can be seen in lane 2 of the gel (Figure 3.2.6.A). Therefore, the primers and PCR reaction work for the *GAUT6* gene and can produce a DNA product. The lack of PCR product in Lane 3 of the gel shows that PCR reaction of wildtype DNA with T-DNA and reverse GAUT6-1 primer shows that wildtype does not contain a T-DNA insertion in the *GAUT6* gene. The PCR reaction of *gaut6-1* DNA with GAUT6-1 primers did not yield a DNA product, as there is no band in lane 4. However, the PCR reaction of *gaut6-1* DNA with GAUT6-1 reverse and T-DNA primers yielded a large quantity of PCR product, as shown by the bright band of the expected size in the region of 400-700 bp. Taken together, lane 4 and 5 confirm *gaut6-1* is homozygous for the T-DNA insert in the GAUT6-1 gene, which is as ordered from NASC. Finally, the NTC lane of the gel (lane 6) produced no PCR product, therefore, the bands present in other lanes are not due to the primers but are genomic DNA products.

The PCR products of wildtype DNA reacted with *GAUT6-2* forward and reverse gene-specific primers form a bright band in lane 2 between 1000 and 1500 bp, which is the expected size of the *GAUT6* gene (Figure 3.2.6.B). Therefore, wildtype contains an uninterrupted copy of the *GAUT6* gene and the PCR reaction using these primers works. In contrast, when reacted with *GAUT6-2* reverse and T-DNA primer, no bands can be seen in lane 3 of the resultant gel, which shows wildtype does not contain a T-DNA insertion in the *GAUT6* gene. A faint band of approximate size 200 bp can be seen in lane 4 of the gel, which contains the PCR products of *gaut6-2* genomic DNA reacted with *gaut6-2* forward and reverse primers. The band is most likely caused by the primers present in this reaction, as the band is faint and at a size expected of the primers, which is less than 200 bp. In lane 5, which contains the PCR products of *gaut6-2* DNA reacted with *GAUT6-2* reverse and T-DNA primer, there is a bright band of size 1000 bp, the expected size for the *GAUT6* gene interrupted by the GAUT6-2 T-DNA insertion. The bright band in lane 5 and lack of a bright band of expected size in lane 4 imply that *gaut6-2* is homozygous for the T-DNA knockout of the *GAUT6*

gene. The NTC shows that bands are due to plant genomic DNA and not contaminants or primer DNA as there is no band in lane 6, apart from a very faint band of size lower than 200 bp that is also present in lanes 2-5 and is due to the primers.
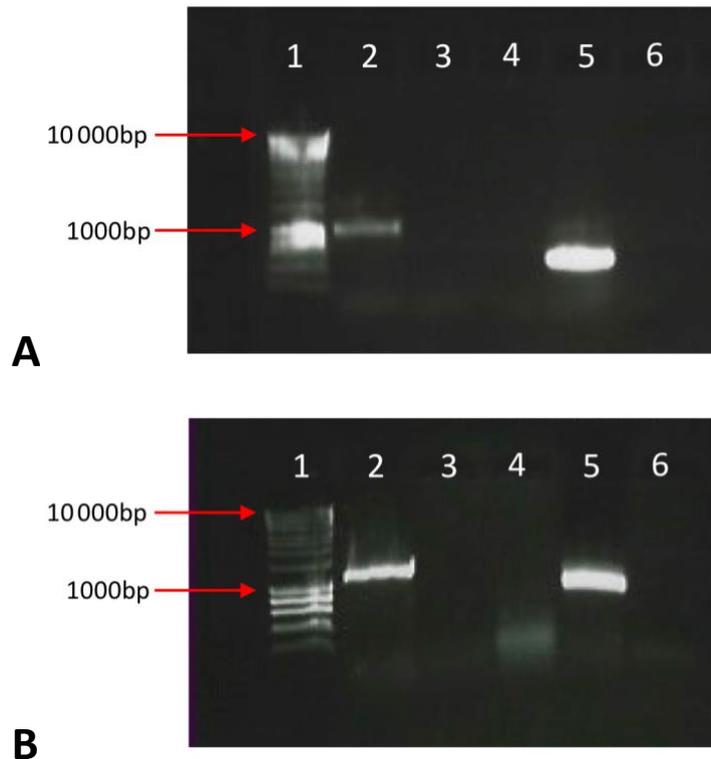
Figure 3.2.5: Genotyping of putative *gaut6* mutant plants. **A:** *gaut6-1.* **B:** *gaut6-2.* An agarose gel stained with MIDORI[GREEN] and visualised under UV revealing gene-specific and T-DNA-specific PCR products in wildtype (lanes 2-3) and putative *gaut6* mutants (lanes 4-5). Lane 1 = 1kb Hyperladder; Lanes 2 and 4 = forward and reverse gene-specific primer; Lanes 3 and 5= gene-specific reverse and T-DNA primer; Lane 6 = No Template Control (NTC), using all three primers without DNA.

Neither lanes (4&5) containing the PCR products of *gaut5* DNA have a bright band of the expected size for either the *GAUT5* uninterrupted gene or the *GAUT5* gene interrupted by the T-DNA insert (Figure 3.2.7.A). There are faint bands of size about 600 bp in lane 4 and 800 bp in lane 5, but as they are so faint compared to the bright wildtype band in lane 2 and the hyperladder in lane 1, nothing can be concluded based on them. The PCR reaction and gel electrophoresis were repeated twice, producing the same pattern and brightness of bands. The lack of bright *GAUT5* bands in both gels suggests that the PCR reaction has failed to work. Therefore, the PCR reaction was repeated using the alternative T-DNA primer.

When PCR was performed using the alternative T-DNA primer instead of the newer version, a bright band of expected size 700 bp can be seen in one of the *gaut5* lanes, lane 5 which contains the PCR product of the reaction with *GAUT5* reverse and alternative T-DNA primer (Figure 3.2.7.B). This band shows that *gaut5* contains a copy of the *GAUT5* gene which is interrupted by the T-DNA insert. When reacted with *GAUT5* forward and reverse primers, *gaut5* DNA does not yield a PCR product that is visualised on the gel, which provides good evidence that the *gaut5* seed stock obtained from NASC is homozygous for the T-DNA insert in the *GAUT5* gene, as expected. The wildtype band of approximately 1100 bp in lane 2 shows

that the *GAUT5* forward and reverse primers can yield a PCR product and therefore, the lack of band in lane 4 is due to the absence of an uninterrupted copy of the *GAUT5*, and not due to faulty primers. The lack of bands of any size in the NTC lane (lane 6) shows that the bands present are due to plant genomic DNA and not due to primers or contaminants.
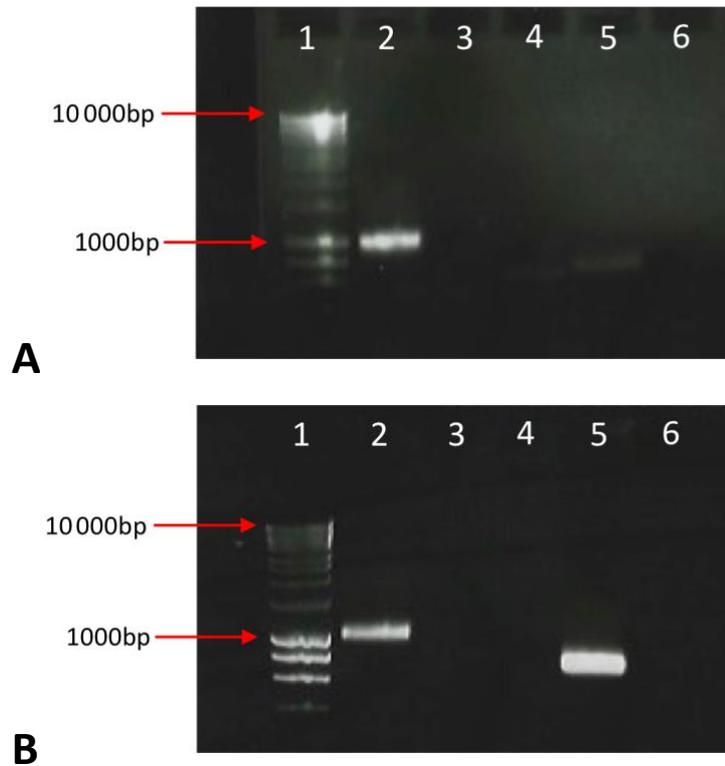
Figure 3.2.6: Genotyping of putative *gaut5* mutant plants. **A:** Using T-DNA primer. **B:** Using alternative T-DNA primer. An agarose gel stained with MIDORI[GREEN] and visualised under UV revealing gene-specific and T-DNA-specific PCR products in wildtype (lanes 2-3) and putative *gaut5* mutants (lanes 4-5). Lane 1 = 1kb Hyperladder; Lanes 2 and 4 = forward and reverse gene-specific primer; Lanes 3 and 5= gene-specific reverse and T-DNA primer (A) or alternative T-DNA primer; Lane 6 = No Template Control (NTC), using all three primers without DNA.

All seed stocks obtained from NASC were as expected; homozygous for the T-DNA insert in the gene stated. Therefore, any divergence from normal of these genes, was due to the lack of their respective *gaut* gene and the resultant effect on pectin abundance. The results of the leaf drying assay (Section 3.1.2.1) for these mutants showed that their leaf water loss rate was equivalent to water, so based on the experiments performed on these mutants, a decrease in pectin abundance in the cell wall does not affect water rate from leaves.

3.1.2.3 *pmr5* and *qul1* Pectin Abundance Mutants

QUASIMODO2 LIKE1 (QUL1) is a member of the QUASIMODO2 (QUA2) clade, which have a role in vascular development and synthesis of HG (Fuentes et al., 2010). Therefore, *qul1* mutants have a reduction in pectin content, like the *gaut* mutants. *POWDERY MILDEW RESISTANT5 (pmr5)* is a dwarf mutant that has increased resistance to fungal, but not bacterial, infection like other *pmr* mutants. *pmr5* offers an interesting comparison to *sfr8, gaut* and *qul1* mutants, as this cell wall mutant has increased pectin

abundance in comparison to wildtype (Vogel et al., 2004). The pectin reduction phenotype will help to uncover whether pectin abundance has an effect on water loss or not.

Wildtype and *qul1* had similar mean % masses throughout (Figure 3.3.1). After 1 hour, wildtype reached 71.42% (±1.91) and *qul1* had reached 69.26% (±1.81) its original weight. By 8 hours, wildtype and *qul1* had reached 33.69% (±4.88) and 35.02% (±4.03) respectively and by 24 hours, they had almost reached their dry weight (10.61% (±0.54) and 8.90% (±0.47), respectively), with mean masses of 14.73% (±1.62) and 13.72% (±1.64), respectively. *pmr5* had lost more % mass than wildtype in the first hour, with a mean mass of 61.12% (±1.13). Similarly, by 8 and 24 hours, *pmr5* % mass was lower than wildtype at 27.04% (±2.94) and 11.62% (±0.88), respectively. *sfr8* had the lowest % mass throughout, with mean masses of 44.08% (±3.20) after 1 hour, 20.80% (±3.07) after 2 hours, and 9.25% (±0.45) by 6 hours, which is almost the dry weight of 9.13% (±0.43).
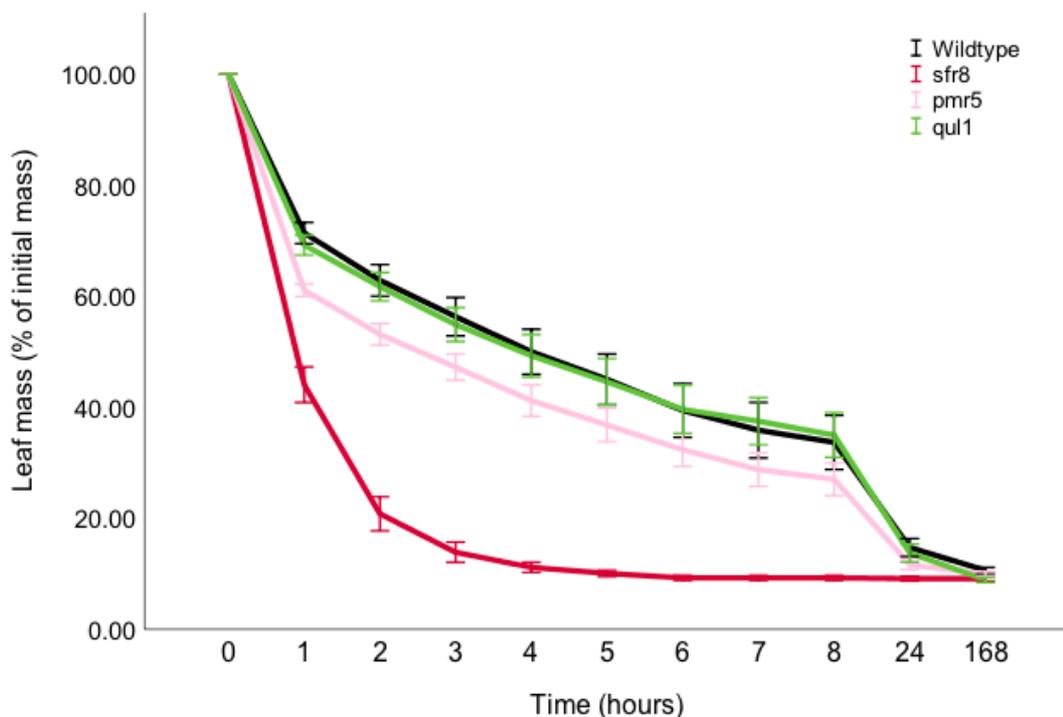
Figure 3.3.1: Water loss in excised leaves of pectin abundance mutants: % of original leaf mass immediately after removal from the rosette. Wildtype (black), *sfr8* (red), *pmr5* (pink) and *qul1* (green). The rate at which leaf mass is loss is taken to be the rate of water loss. Error bars show ±1 standard error. n=18 per genotype.

During the first hour, there was statistically significant difference between the genotypes for rate of water loss (Figure 3.3.2; One-way ANOVA, $F_{3,68}=33.456$, $p<0.001$). *sfr8* had significantly faster water loss rate than the other genotypes with a gradient of 55.92 (±3.20; Tukey's post-hoc test; $p<0.001$). *pmr5* had the second fastest water loss rate of 38.88 (±1.13), which was significantly faster than wildtype and *qul1* (Tukey's post-hoc test; $p=0.006$, $p=0.044$). Wildtype and *qul1* had statistically similar water loss rates of 28.58 (±1.91) and 30.74 (±1.81) respectively (Tukey's post-hoc test, $p=0.893$).

There is statistically significant difference between the genotypes for rate water loss during hours 1-4 (Kruskal Wallis, X^2_3=12.012, p=0.007). *sfr8* maintained a significantly faster water loss rate for the next 3 hours with a gradient of 10.57 (±0.94; Mann Whitney U-test; U=85.0, p=0.014; U=66.5, p=0.002; U=69.5, p=0.003, respectively). *pmr5* and *qul1* had a statistically similar water loss rate as wildtype (7.07 (±0.81)), with gradients of 6.56 (±0.63) and 6.67 (±0.76) respectively (Mann Whitney U-test; U=154.0, p=0.815; U=155.0, p=0.839, respectively).

During hours 4-8, , there was a significant difference between the genotypes (Kruskal Wallis, X^2_3=40.729, p<0.001).). *sfr8* had a significantly slower water loss rate than the other genotypes with a gradient of 0.46 (±0.19; Mann Whitney U-test; wildtype – U=1.0, p<0.001; *pmr5* – U=4.0, p<0.001; *qul1* – U=4.5, p<0.001). *pmr5* and *qul1* had a statistically similar water loss rate as wildtype (4.18 (±0.26)) during this period with gradients of 3.64 (±0.25) and 3.57 (±0.26; Mann Whitney U-test; U=117.5, p=0.161; U=106.0, p=0.079, respectively).
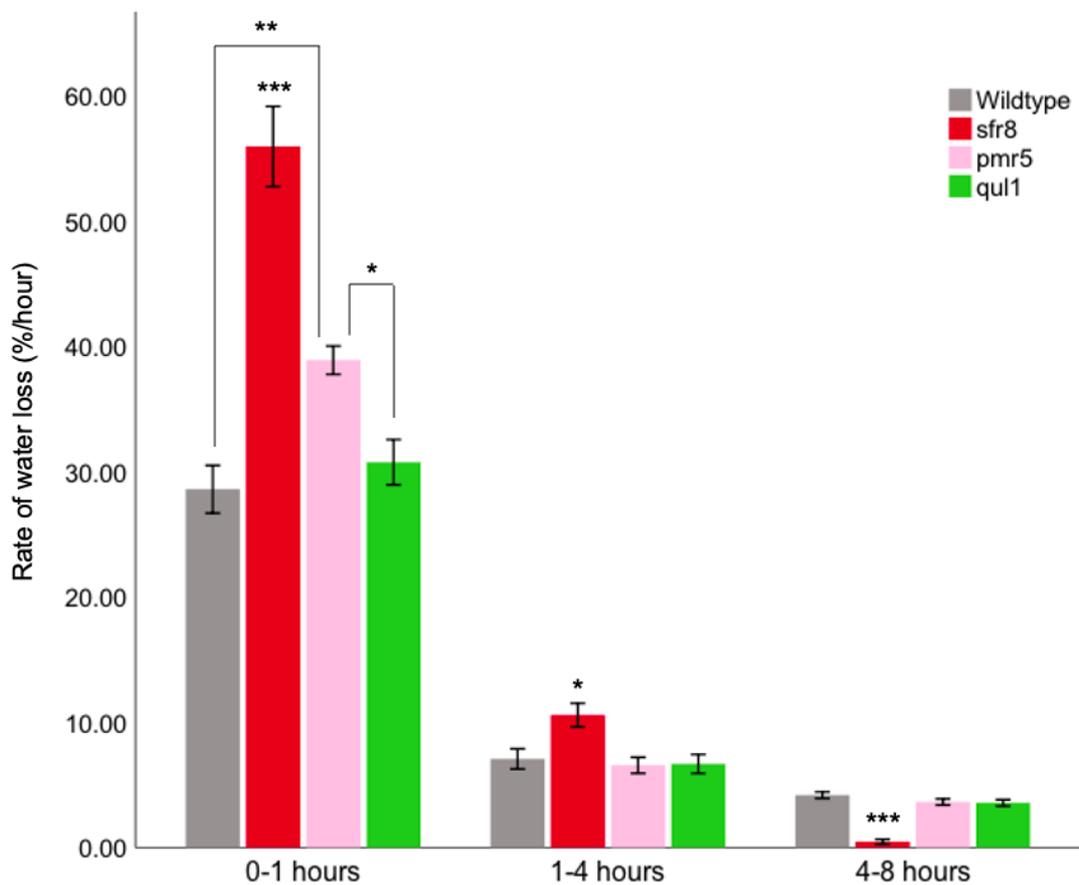
Figure 3.3.2: Rate at which excised leaves of pectin abundance mutants lost water (% of leaf mass) per hour during the first hour (0-1 hours), the following 3 hours (1-4 hours) and the following 4 hours (4-8 hours). Wildtype (grey), *sfr8* (red), *pmr5* (pink) and *qul1* (green). Error bars show ±1 standard error. n=18 per genotype. * means p<0.05; ** means p<0.01; *** means p<0.001.

There is a significant difference between the genotypes for initial mass (Figure 3.3.3; One-way ANOVA, $F_{3,68}$=4.796, p=0.004). The initial mass of *pmr5* is the smallest of all genotypes at 29.1 mg (±1.8) and *qul1* had the largest initial mass of all genotypes at 35.1 mg (±2.1) (Figure 3.3.3). Wildtype and *sfr8* had a similar initial leaf mass at 32.2 mg (±1.7) and 3.13 mg (±1.9) respectively. A Tukey's post-hoc test revealed that

pmr5 is significantly smaller in leaf initial mass than *qul1* (p=0.003). All other pairwise comparisons were not significant, and the leaf area can also be taken to be statistically the same. As the only difference in initial masses is found between two test mutants and not the comparison genotypes, wildtype and *sfr8*, there is not much importance to the result. Wildtype, *sfr8*, *pmr5* and *qul1* all had statistically similar dry masses with mean dry masses of 3.0 mg (±0.2), 2.4 mg (±0.1), 2.7 mg (±0.2) and 2.7 mg (±0.1), respectively (Kruskal Wallis, X^2_3=4.405, p=0.221). Therefore, there is no statistically significant difference between leaf area and leaf water content, eliminating these as factors that could affect the leaf water loss rate.
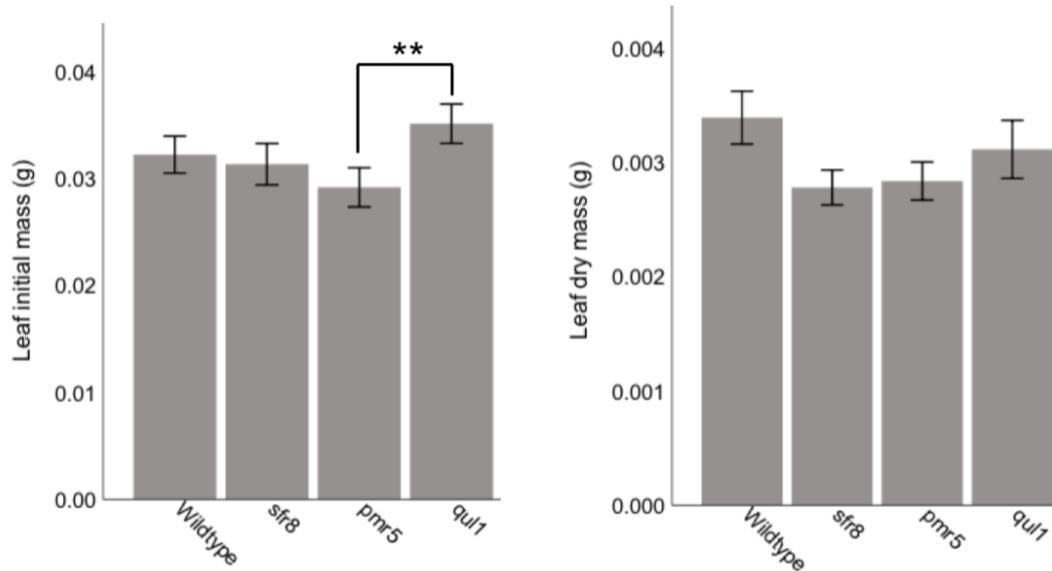
Figure 3.3.3: Mean leaf initial and dry mass of pectin abundance mutants. Error bars show ±1 standard error. n=18 per genotype. ** means p<0.010

In summary, throughout the leaf drying assay, *qul1* leaves maintained a % mass highly similar to wildtype and much higher than *sfr8*. Additionally, *qul1* maintained a gradient of water loss statistically the same as wildtype for all time periods, which was statistically different to *sfr8*. On the contrary, *pmr5* leaves had a water loss rate in the first hour which was significantly higher than wildtype and maintained a mass lower than wildtype throughout the drying experiment. *pmr5* leaves were worse at preventing initial water loss than wildtype, a defect similar, though not as severe, as *sfr8*. The initial decline in mass of *pmr5* leaves also implicates a slow stomatal response, therefore, *pmr5* plants were chosen for further analysis of stomatal function.

3.1.3 Pectin Modification Mutants

In *sfr8* mutants, which lack of fucose, galactose residues replace fucose on side chain A of pectic RG-II, which truncates the side chain and reduces the formation of dimeric RG-II from 98% in wildtype to 50% (O'Neill et al., 2001; Sechet et al., 2018). Dimeric RG-II is important to cell wall function as it maintains the integrity (Sechet et al., 2018); tensile strength (Ryden et al., 2003); thickness (Ishii et al., 2001); and pore size (Fleischer et al., 1999) of the cell wall. As a result of losing dimeric RG-II, mutants lacking MUR1 have demonstrated reduced growth and abnormal development (O'Neill et al., 2001), however this has not been shown under all the growth conditions used in these experiments. Furthermore, due to the defects in cell wall resulting from decreased RG-II dimerisation, mutants lacking MUR1 have increased

susceptibility to salinity (Feng et al., 2018) and freezing stress (Panter et al., 2019). Therefore, other cell wall mutants with defects in pectin crosslinking were subjected to the leaf drying assay to determine whether it is the integrity of the pectin network which gives the water loss defect in *sfr8.* HG pectin forms Ca^{2+} crosslinks between adjacent HG chains if at least 10 consecutive residues are de-esterified (Levesque-Tremblay et al., 2015). By consequence, mutants in enzymes involved in methyl- or O-acetyl-esterification of homogalacturonan, such as pectin methylesterases and pectin acetylesterases, may have pectin crosslinking defects (Pelloux et al., 2007; Philippe et al., 2017). Three pectin esterification mutants were included in the project. First, *PECTIN METHYLESTERASE34* (*PME34)* is involved in the de-esterification of homogalacturonan and is highly expressed in guard cells (Huang et al., 2017). It has been suggested PME34 may have a role in crosslinking pectic domains to regulate guard cell wall flexibility and stomatal aperture (Huang et al., 2017; Wu et al., 2018). *pme34* has increased HG methyl-esterification and so less pectin crosslinking occurs, a phenotype similar to that of *sfr8.* The second esterification mutant used is *REDUCED WALL ACETYLATION2* (*RWA2*)*,* which has reduced O-acetylation of pectins, with total wall acetyl content decreased 15% to 30% that of wildtype (Manabe et al., 2011). *rwa2* mutants have increased susceptibility to pathogens, abnormal growth and development and potentially have abnormal pectin crosslinking (Manabe et al., 2011; Nafisi et al., 2015). The remaining pectin esterification mutant, *pmr5*, has already been discussed in section 3.1.2.3 as a pectin abundance mutant. *pmr5* is also a pectin esterification mutant because it is a member of the TRICHOME BIREFINGENCE-LIKE (TBL) family of pectin acetyltransferase and has decreased pectin esterification or O-acetylation of cell walls (Vogel et al., 2004; Chiniquy et al., 2019). The change to pectin esterification in *pmr5* may result in abnormal pectin crosslinking, like the defect in *sfr8.*
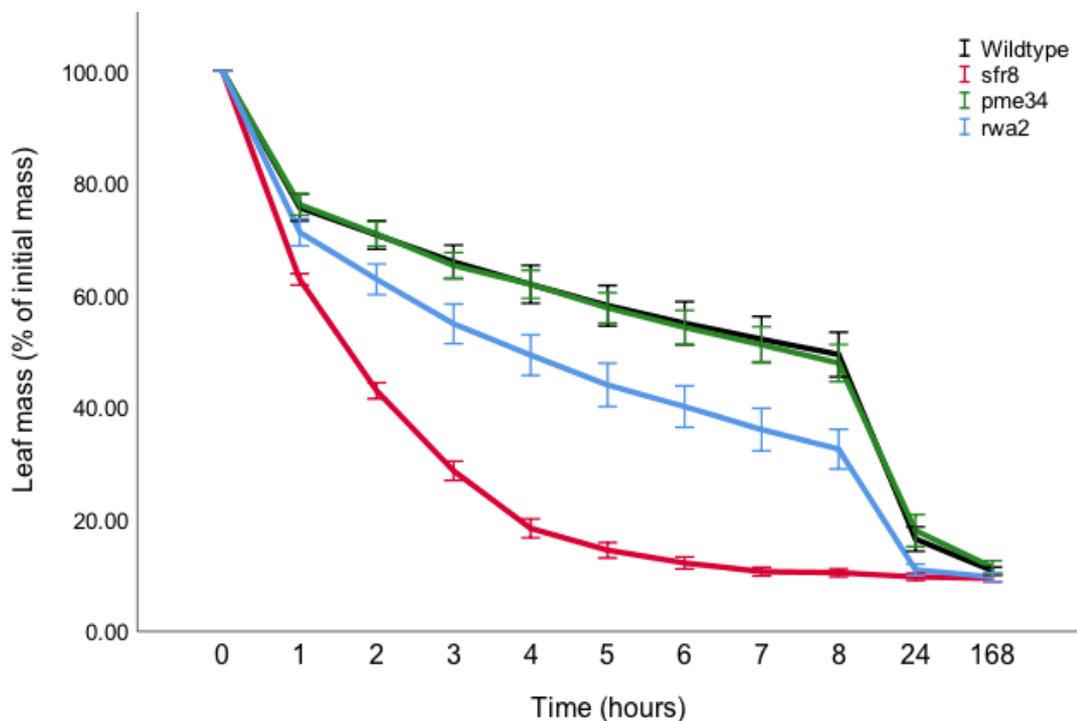
Figure 3.4.1: Water loss in excised leaves of pectin modification mutants: % of original leaf mass immediately after removal from the rosette. Wildtype (black), *sfr8* (red), *pme34* (green) and *rwa2* (blue). The rate at which leaf mass is loss is taken to be the rate of water loss. Error bars show ±1 standard error. n=18 per genotype.

Wildtype and *pme34* had a similar leaf mass after the first hour at 75.70% (±2.39) and 76.23% (±1.90) respectively and maintained a similar mass throughout the experiment (Figure 3.4.1). After 4 hours, wildtype and *pme34* leaves had reached a mass of 61.98% (±3.37) and 61.99% (±2.51) respectively and by 8 hours, they had masses of 49.44% (±3.98) and 47.93% (±3.30) respectively. 24 hours after the excision wildtype weighed 16.51% (±2.17) of its initial mass and *pme34* had a larger mass of 18.02% (±2.87), similar to their leaf masses of 10.84% (±0.65) and 11.44% (±1.20) respectively. *sfr8* had the lowest mass after 1 hour, with a mass of 62.87% (±1.03). By 4, 8 and 24 hours after excision, *sfr8* had reached a mass of 18.42% (±1.68), 10.49% (±0.71) and of 9.76% (±0.64), respectively a dry weight of 9.47% (±0.57). *rwa2* had the second smallest mass after 1 hour, with a mass of 71.27% (±2.42) and maintained a mass lower than wildtype and *pme34* throughout the experiment. By 4, 8 and 24 hours, *rwa2* had a mean mass of 49.35% (±3.62) 32.56% (±3.56) and 10.99% (±1.03) of their initial mass, respectively, with a dry weight of 9.74% (±0.81).
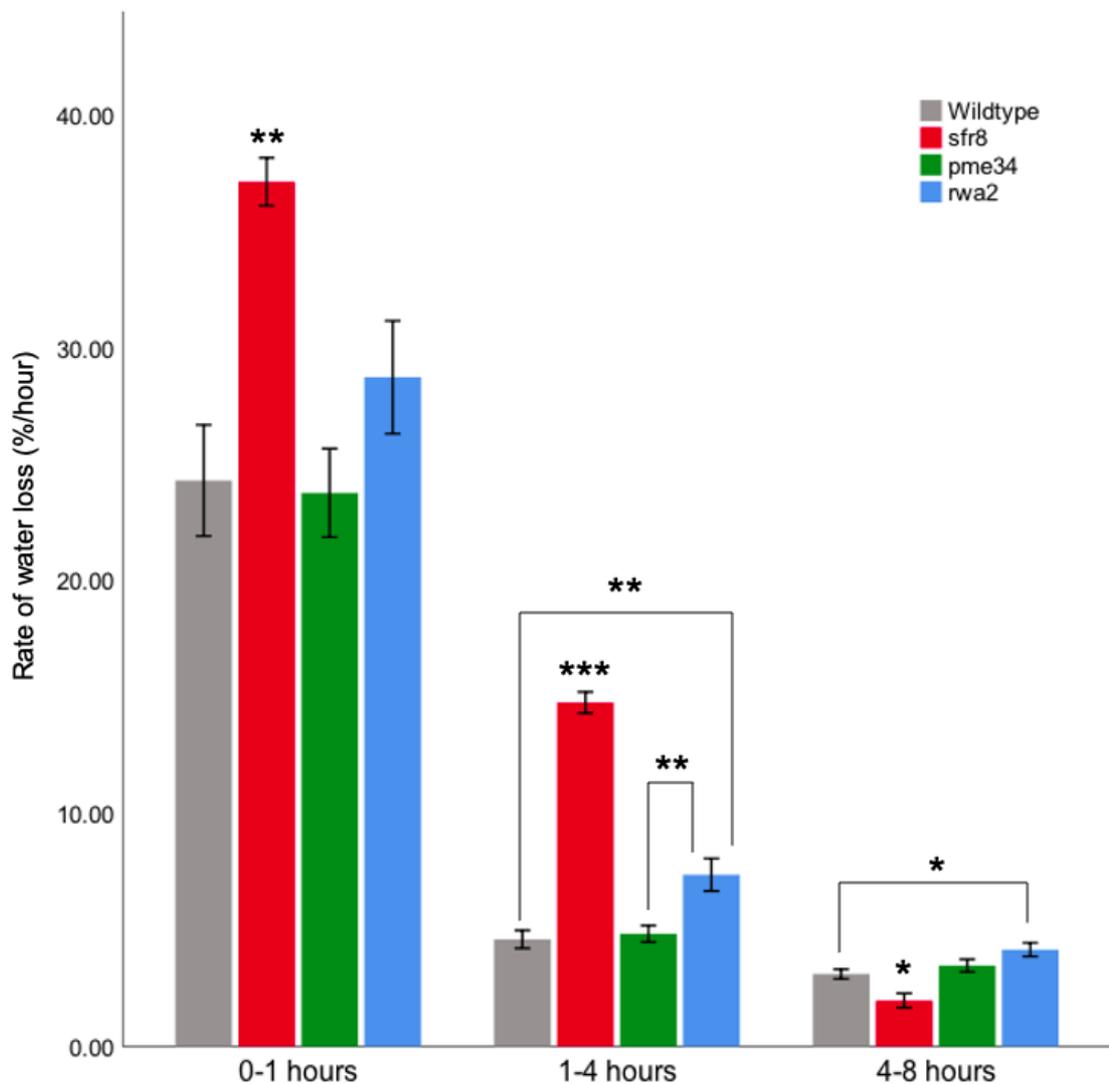
Figure 3.4.2: Rate at which excised leaves of pectin modification mutants lost water (% of leaf mass) per hour during the first hour (0-1 hours), the following 3 hours (1-4 hours) and the following 4 hours (4-8 hours). Wildtype (grey), *sfr8* (red), *pme34* (green) and *rwa2* (blue). Error bars show ±1 standard error. n=18 per genotype. * means $p<0.05$; ** means $p<0.01$; *** means $p<0.001$.

During the first hour, there was a significant difference between the genotypes for the water loss rate (Figure 3.4.2; Kruskal Wallis, X^2_3=20.971, p<0.001). *sfr8* had a significantly faster water loss rate than wildtype, *pme34* and *rwa2* with a gradient of 37.13 (±1.03; Mann Whitney U-test; U=57.0, p=0.001; U=30.0, p<0.001; U=75.5, p=0.005, respectively). *pme34* and *rwa2* had a statistically similar faster water loss rate as wildtype (24.30 (±2.39) with a gradients of 23.77 (±1.90) and 28.74 (±2.42; Mann Whitney U-test; U=145.5, p=0.606; U=104.5, p=0.068).

During hours 1-4, there was a significant difference between the genotypes for the water loss rate between hours 1 and 4 (One-way ANOVA, $F_{3, 68}$=92.564, p<0.001). *sfr8* had a faster water loss rate than wildtype, *pme34* and *rwa2*, with a gradient of 14.77 (±0.46; Tukey's post-hoc test, p<0.001, respectively). *rwa2* had a significantly faster water loss rate than wildtype and *pm34*, with a gradient of 7.37 (±0.70; Tukey's post-hoc test, p=0.001, p=0.003, respectively). Wildtype and *pme34* maintained a statistically similar water loss rate in this period with gradients of 4.60 (±0.38) and 4.84 (±0.36), respectively (Tukey's post-hoc test, p=0.986).

Between hours 4 and 8, there was a significant difference between the genotypes for the water loss rate (One-way ANOVA, $F_{3, 68}$=11.442, p<0.001). *sfr8* had a water loss rate significantly slower than wildtype, *pme34* and *rwa2* (Tukey's post-hoc test, p=0.020, p=0.001, p<0.001, respectively) with a gradient of 1.97 (±0.31). *rwa2* had significantly faster water loss rate than wildtype with a gradient of 4.15 (±0.29; Tukey's post-hoc test; p=0.038,). *pme34* had a water loss rate statistically the same as wildtype (3.11 (±0.21)) and *rwa2* (Tukey's post-hoc test, p=0.775, p=0.289, respectively) with a gradient of 3.47 (±0.27).

Table 3.2: Mean leaf initial and dry mass of pectin modification mutants. n=18 per genotype.

Mutants	Initial mass (mg) (±1 SE)	Dry mass (mg) (±1 SE)
Wildtype	47.9 (±5.5)	5.5 (±0.8)
sfr8	51.7 (±5.7)	5.1 (±0.7)
pme34	43.9 (±4.4)	5.4 (±0.8)
rwa2	42.8 (±5.4)	4.7 (±0.9).

All genotypes had a similar leaf initial and dry mass (Table 3.2). There is no statistically significant difference between the genotypes for initial leaf mass (One-way ANOVA; $F_{3, 68}$ =0.590, p=0.624), nor leaf dry mass (Kruskal Wallis; X^2_3=1.095, p=0.778). Therefore, any differences in leaf water loss rate are due to the different genotypes, not due to size.

In summary, *pme34* leaves maintained a % mass highly similar to wildtype throughout the leaf drying assay and maintained a rate of water loss statistically the same as wildtype for all time periods. Therefore, *pme34* has a water loss phenotype similar to wild type and does not have the water loss defect *sfr8* has, so was not chosen for further investigation of stomatal defects. In contrast, *rwa2* leaves had a lower % mass than wildtype throughout the leaf drying assay up until one week after excision. In agreement, *rwa2*

had a significantly larger water loss rate than wildtype after the first hour. Hence, *rwa2* leaves had a water loss defect compared to wildtype and so *rwa2* mutants were chosen for additional analysis into stomatal function. Additionally, *pmr5* has abnormal pectin esterification and as discussed in section 3.1.2.2, has a water loss defect when compared to wildtype, so was also included in following experiments of stomatal function.

3.1.4 Xyloglucan Mutants

Fucose is a sugar incorporated into the hemicellulose xyloglucan and may stabilise xyloglucan in a conformation which is most efficient for binding cellulose microfibrils (Levy et al., 1991; Pauly and Keegstra, 2016). Xyloglucan maintains the integrity of the cell wall through hydrogen bonding with the hydrophilic surfaces of cellulose microfibrils, as well as throuhg covalent bonds with pectins and interactions with cell wall proteins (Popper and Fry, 2008; Pauly et al., 2013). Additionally, through its interaction with cellulose and expansin, xyloglucan can mediate wall loosening at biochemical hotspots, an important process for normal growth and development (Park and Cosgrove, 2012a; Cosgrove, 2014). In *sfr8*, fucose is lacking so the terminal α -L-fucose residue of xyloglucan is replaced with a stereochemically similar α-L-galactose residue, which changes the chemical and physical properties of xyloglucan (Zablackis et al., 1996b). The lack of fucosylated xyloglucan may mean xyloglucan-cellulose interactions are weaker with consequences on wall mechanics for normal growth and development (Levy et al., 1991; Reiter et al., 1993; Cosgrove, 2014). Furthermore, the defective xyloglucan may also cause the water loss defect present in *sfr8.* With that in mind, other mutants with defective xyloglucan were chosen for comparison in the leaf drying assay with wildtype and *sfr8*. *XYLOGLUCAN XYLOSYLTRANSFERASE1 XYLOGLUCAN XYLOSYLTRANSFERASE2* (*xxt1 xxt2*) double mutants lack two xylosyltransferases involved in the synthesis of xyloglucan and as a result lack detectable xyloglucan in their cell walls (Cavalier et al., 2008). Despite lacking an abundant cell wall component, *xxt1 xxt2* mutant plants had normal development but did have reduced size compared to wildtype (Cavalier et al., 2008). Previous work has implicated that *xxt1 xxt2* stomata have a significantly smaller aperture than wildtype in response to both stomatal opening and closing signals (Rui and Anderson, 2016), making *xxt1 xxt2* an interesting mutant to compare to *sfr8* in the leaf drying assay. Furthermore, two mutants previously discussed also have xyloglucan defects. MUR2, as discussed in section 3.1.1, is a xyloglucan-specific fucosyltransferase and so *mur2* mutants have less than 2% the fucosylated xyloglucan that wildtype has (Vanzin et al., 2002). Therefore, *mur2* has a very similar xyloglucan defect to *sfr8* and offers an interesting comparison to *sfr8* in the leaf drying assays. Finally, RWA2 is an acetyltransferase, which, as well as being invovled in the O-acetylation of pectins, as discussed in 3.1.3, is also involved in the O-acetylation of xyloglucan (Manabe et al., 2011). *rwa2* mutants have decreased acetylation of cell wall polymers by about 20% and have increased suspectibility to biotic stresses, on top of plant growth and development issues (Manabe et al., 2011; Nafisi et al., 2015).

After 1 hour since leaf excision, *sfr8* had the lowest mean mass at 44.08% (±3.20; Figure 3.5.1). By 4 hours, *sfr8* leaf mass had reached 11.15% (±0.90) and by 6 hours, the mean mass was 9.25% (±0.45), which is

almost the dry mass. The actual average dry mass of 9.13% (±0.43) was reached by 24 hours. By 1 hour, *xxt1 xxt2* and wildtype had a similar weight, with masses of 68.97% (±1.39) and 71.42 (±1.91) respectively. By 8 hours, wildtype had reached a mass of 33.69% (±4.88) and *xxt1 xxt2* had reached a mass of 25.07% (±3.37). After 24 hours, wildtype reached a mass of 14.73% (±1.62), whereas, *xxt1 xxt2* had almost reach dry weight at a mass of 8.56% (±0.58). The dry mass of *xxt1 xxt2* was 7.60% (±0.39), the lowest of all genotypes, and the dry mass of wildtype was higher at 10.61% (±0.54).
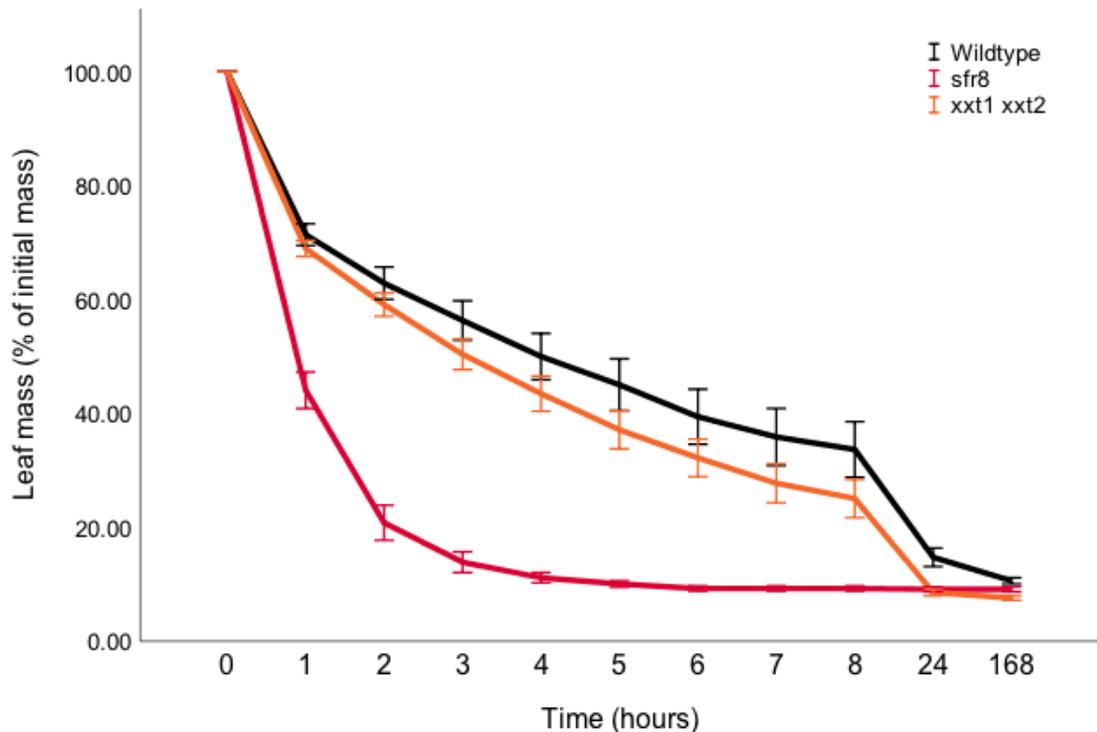
Figure 3.5.1: Water loss in excised leaves of xyloglucan mutants: % of original leaf mass immediately after removal from the rosette. Wildtype (black), *sfr8* (red) and *xxt1 xxt2* (orange). The rate at which leaf mass is loss is taken to be the rate of water loss. Error bars show ±1 standard error. n=18 per genotype.

All genotypes had their highest water loss rate during the first hour (Figure 3.5.2). A One-way ANOVA showed that there was a statistical difference between the genotypes for water loss rate during the first hour ($F_{2, 51}$=43.418, p<0.001), which was due to *sfr8* having a water loss rate significantly faster than wildtype and *xxt1 xxt2* (Tukey's post hoc test; p<0.001, p<0.001, respectively) with a gradient of 55.92 (±3.20). Wildtype and *xxt1 xxt2* had statistically similar water loss rates in the first hour, with gradients of 28.58 (±1.91) and 31.03 (±1.39; Tukey's post hoc test, p=0.733).

The water loss rate for all genotypes decreased during hours 1-4 compared to the first hour (Figure 3.5.4). Again, *sfr8* had the highest water loss rate during this period with a gradient of 10.57 (±0.94). Wildtype had the lowest water loss rate during hours 1-4 with a gradient of 7.07 (±0.81) and *xxt1 xxt2* was intermediate with a gradient of water loss of 8.52 (±0.64). There was a significant difference between the genotypes for water loss rate in this period (One-way ANOVA, $F_{2, 51}$=4.760, p=0.013), which was due to wildtype having a significantly lower water loss rate than *sfr8* (Tukey's post hoc test, p=0.009). *xxt1 xxt2* leaves had statistically the same water loss rate as wildtype and *sfr8* (Tukey's post hoc test, p=0.420, p=0.179, respectively).

Similarly, the water loss rate for all genotypes decreased during hours 4-8 compared to the previous period (Figure 3.5.4). There is a significant difference between the genotypes for the water loss rate during this period (Kruskal Wallis, X^2_2=36.359, p<0.001). During hours 4-8, *sfr8* had significantly slower water loss rate than wildtype and *xxt1 xxt2* with a gradient of 0.46 (±0.19; Mann Whitney U-test; U=1.0, p<0.001; U=0.0, p<0.001, respectively). *xxt1 xxt2* had the largest water loss gradient of 4.62 (±0.23), which was statistically similar to the water loss rate of wildtype with a gradient of 4.18 (±0.26; Mann Whitney U-test; U=122.5, p=0.214).
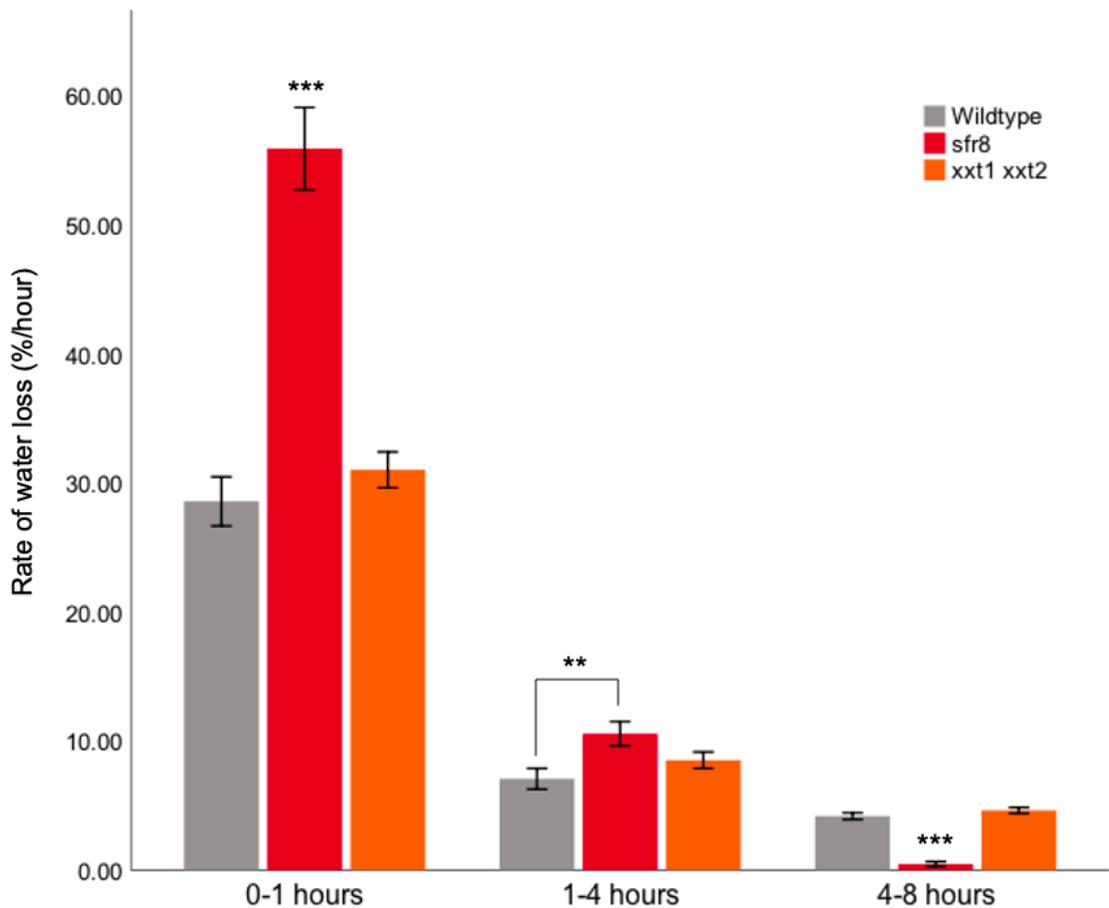
Figure 3.5.2: Rate at which excised leaves of xyloglucan mutants lost water (% of leaf mass) per hour during the first hour (0-1 hours), the following 3 hours (1-4 hours) and the following 4 hours (4-8 hours). Wildtype (grey), *sfr8* (red) and *xxt1 xxt2* (orange). Error bars show ±1 standard error. n=18 per genotype. ** means p<0.01; *** means p<0.001.

The initial masses of the wildtype, *sfr8* and *xxt1 xxt2* leaves were similar at 32.2 mg (±1.7), 31.3 mg (±1.9) and 32.9 mg (±21.2) respectively (Figure 3.5.3). A Kruskal Wallis test confirmed there was no statistically significant difference between the genotypes for initial mass (X^2_2=0.322, p=0.851). Therefore, despite *xxt1 xxt2* being a dwarf mutant, all the genotypes had the same initial mass so it can be assumed leaf area was the same and leaf area had no effect on the rate of water loss. However, there was a statistically significant difference between the genotypes for dry mass (Kruskal Wallis, X^2_2=9.847, p=0.007). Wildtype had the largest dry mass of all genotypes at 3.4 mg (±0.2) and *xxt1 xxt2* has the smallest at 2.4 mg (±0.2). *sfr8* was

intermediate with a dry mass of 2.8 mg (±0.2) and was statistically the same as both wildtype and *xxt1 xxt2* (Mann Whitney U-test; U=102.0, p=0.059; U=123.0, p=0.226, respectively). Wildtype had a significantly larger dry mass than *xxt1 xxt2* (Mann Whitney U-test, U=74.5, p=0.005) and so *xxt1 xxt2* had a larger water content than wildtype, which may result in a difference in water loss rates between the two.
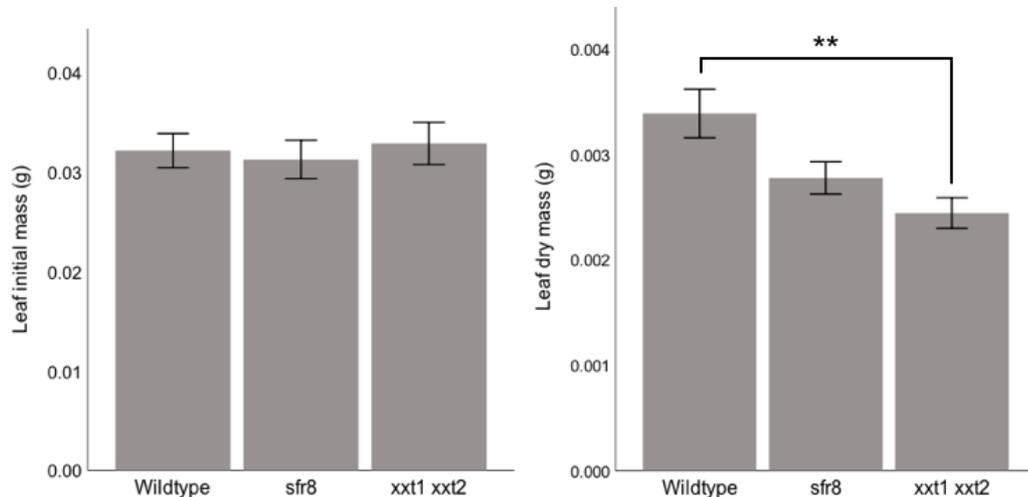
Figure 3.5.3: Mean leaf initial and dry mass of xyloglucan mutants. Error bars show ±1 standard error. n=18 per genotype. ** means p<0.01.

In summary, *xxt1 xxt2* leaves maintained a % mass similar to wildtype for the first two hours after which *xxt1 xxt2* had a lower % mass than wildtype up until one week after excision. Despite this difference, *xxt1 xxt2* had statistically the same water loss rate as wildtype for all time periods. Therefore, *xxt1 xxt2* had the same water loss phenotype as wildtype, which was significantly different to *sfr8.* Consequently, *xxt1 xxt2* was not chosen for further measurements of stomatal function. Confirming the little impact xyloglucan defects have on water loss rate is *mur2,* this mutant had the most similar xyloglucan defect to *sfr8* of all mutants used and as shown in section 3.1.1, maintained a % mass greater than wildtype throughout the experiment and had statistically the same water loss rate as wildtype. Finally, the remaining xyloglucan mutant, *rwa2*, did have a water loss defect statistically different to wild type and so was chosen for further experiments of stomatal function, as discussed in section 3.1.3.

3.1.5 Mechanical Strength Mutants

Due to the defects in many components of cell wall, mutants lacking *MUR1* have reduced mechanical strength (Reiter et al., 1993; Ryden et al., 2003). Strength of cell walls is particularly important in guard cells to enable the cells to withstand the high turgor pressure that opens and closes the stomata (Rui et al., 2018). As a feature of cell walls that impacts stomatal dynamics, mechanical strength may cause the water loss defect in *sfr8*, so it is worth investigating the water loss rate of mechanical strength mutants by using them in a leaf drying assay. Three mechanical strength mutants were chosen for inclusion in the leaf drying assays. First, *arabinogalactan protein8* (*agp8*) lacks a fasciclin-like arabinogalactan protein and is significantly weaker than wildtype with decreased wall stiffness and only 70% the tensile strength of wildtype (MacMillan et al., 2010). Moreover, *prosecute1* (*prc1*) is a mechanical strength mutant with

slight deficiencies in cellulose synthesis, cell elongation and seedling growth (Hu et al., 2018). Lastly, the previously discussed (section 3.1.4) *xxt1 xxt2* mutant, as well as completely lacking xyloglucan, also has hypocotyl cell walls that are 20-50% weaker than wildtype (Cavalier et al., 2008).
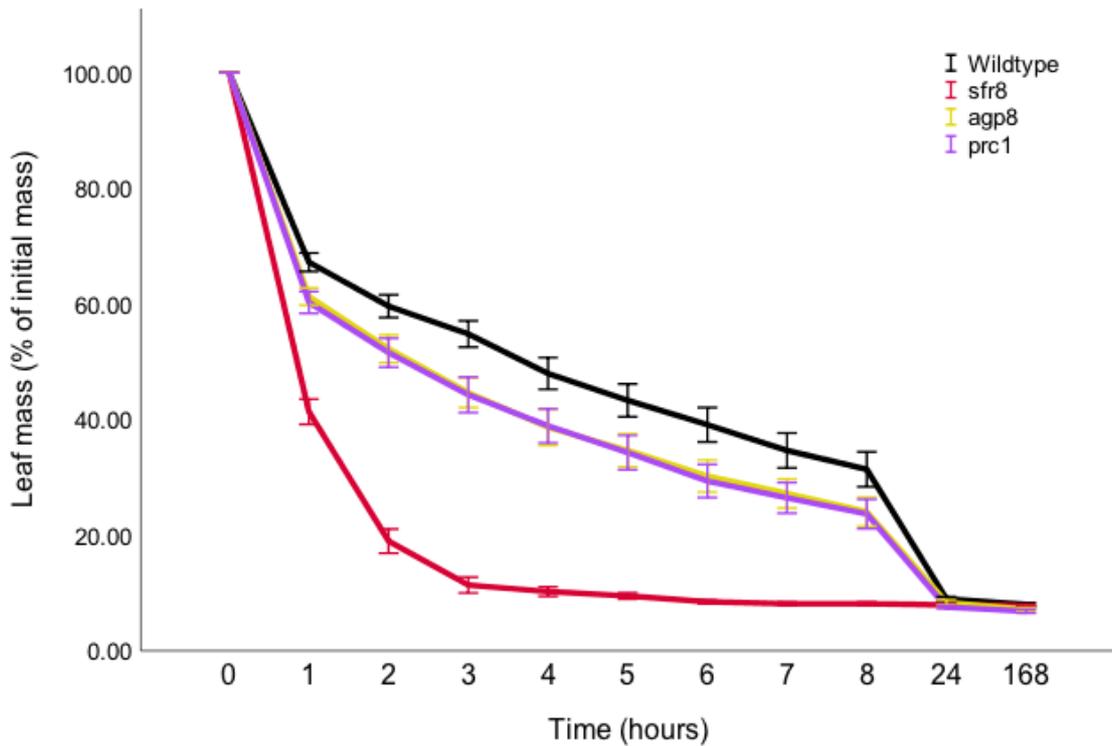
Figure 3.6.1: Water loss in excised leaves of mechanical strength mutants: % of original leaf mass immediately after removal from the rosette. Wildtype (black), *sfr8* (red), *agp8* (yellow) and *prc1* (purple). The rate at which leaf mass is loss is taken to be the rate of water loss. Error bars show ±1 standard error. n=18 per genotype.

The largest reduction in mass occurred during the first hour for all genotypes (Figure 3.6.1). Wildtype had the largest mass after 1 hour at 67.23% (±1.60) the original mass, whereas, *sfr8* had the smallest mass after 1 hour at 41.38% (±2.19). *agp8* and *prc1* had similar masses after 1 hour at 61.28% (±1.48) and 60.27% (±1.89), respectively. Wildtype mass steadily decreased over the next 7 hours to reach a mass of 31.40% (±3.01). Similarly, the mass of *agp8* and *prc1* also steadily decreased over the next 7 hours, but maintained masses lower than that of wildtype at 24.07% (±2.49) and 23.69% (±2.54), respectively. By 24 hours, all genotypes had a similar mass; wildtype weighed 8.97% (±0.39), *sfr8* weighed 7.95% (±0.22), *agp8* weighed 8.38% (±0.44) and *prc1* weighed 7.56% (±0.27). The masses of the genotypes at 24 hours were similar to the dry masses of the genotypes after 1 week; wildtype weighed 8.03% (±0.31), *sfr8* weighed 7.83% (±0.22), *agp8* weighed 7.16% (±0.32) and *prc1* weighed 6.85% (±0.32).

For all genotypes, water loss gradient was highest during the first hour (Figure 3.6.2). There was a significant difference between the genotypes for water loss rate in the first hour (Kruskal Wallis, X^2_3=38.574, p<0.001). *sfr8* had a significantly faster water loss rate than wildtype, *agp8* and *prc1* with a gradient of 58.62 (±2.19; Mann Whitney U-test; U=82.0, p=0.011; U=87.0, p=0.017, respectively). *agp8* and *prc1* had statistically similar water loss gradients in this period, at 38.72 (±1.48) and 39.73 (±1.89)

respectively (Mann Whitney U-test, U=154.0, p=0.815). Wildtype was significantly faster water loss rates than wildtype with a gradient of 32.77 (±1.60). *agp8* and *prc1* had a significantly slower water loss rate than wildtype (Mann Whitney U-test; U=82.0, p=0.011; U=87.0, p=0.017, respectively).
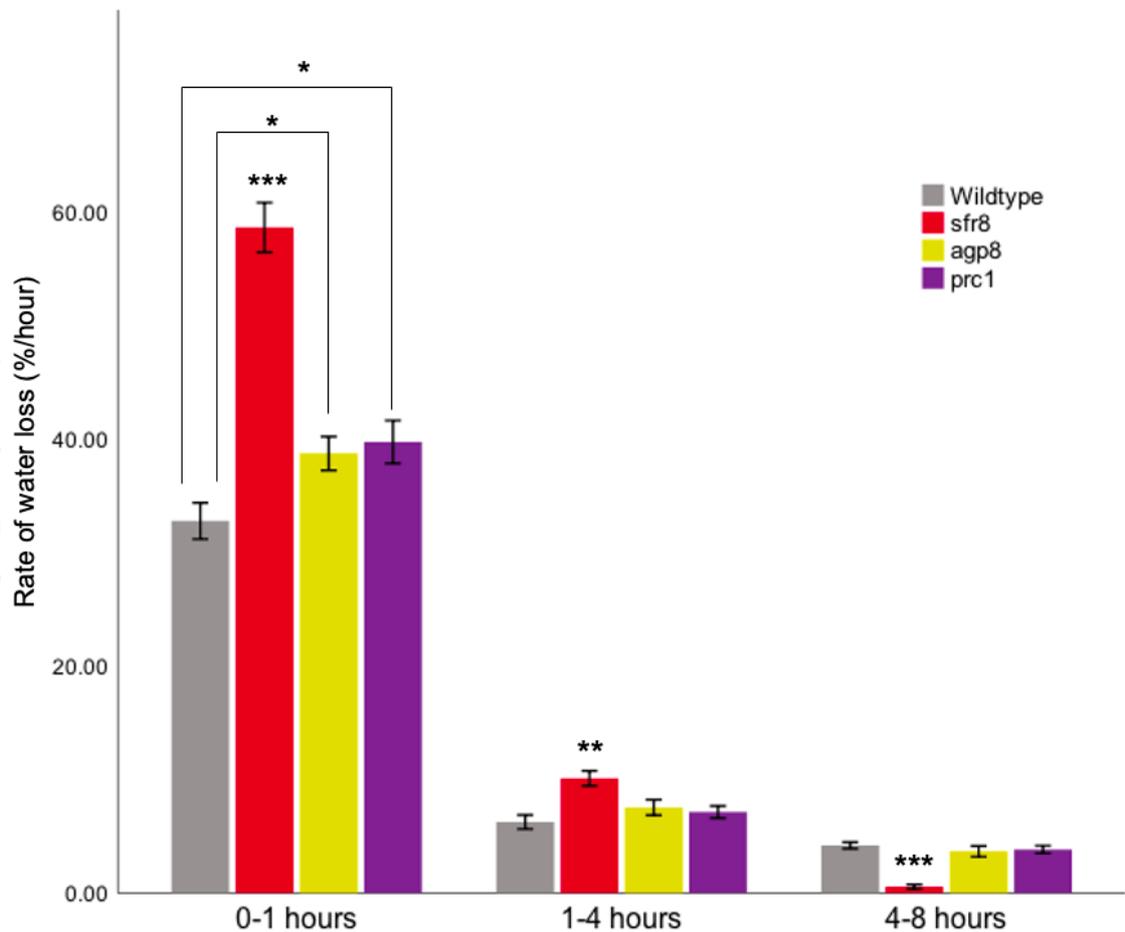
Figure 3.6.2: Rate at which excised leaves of mechanical strength mutants lost water (% of leaf mass) per hour during the first hour (0-1 hours), the following 3 hours (1-4 hours) and the following 4 hours (4-8 hours). Wildtype (grey), *sfr8* (red) *agp8* (yellow) and *prc1* (purple). Error bars show ±1 standard error. n=18 per genotype. * means p<0.05; ** means p<0.01; *** means p<0.001.

During hours 1-4, there was a significant difference between the genotypes for water loss rate (Kruskal Wallis, X^2_3=16.905, p=0.001). *sfr8* maintained a significantly highest water loss rate than wildtype, *agp8* and *prc1* genotypes with a gradient of 10.10 (±0.66; Mann Whitney U-test; U=54.0, p<0.001; U=73.0, p=0.004; U=64.0, p=0.001, respectively).Wildtype, *agp8* and *prc1* had statistically similar water loss rate in this period, with gradients of 6.25 (±0.62), 7.54 (±0.69) and 7.13 (±0.54), respectively (Mann Whitney U-test; wildtype & *agp8* -U=107.5, p=0.085; wildtype & *prc1* - U=122.5, p=0.214; *agp8* & *prc1* - U=150.5, p=0.719).

During hours 4-8, there was a significant difference between the genotypes for water loss rate between hours 4-8 (Kruskal Wallis, X^2_3=34.131, p<0.001). Wildtype, *agp8* and *prc1* maintained statistically similar water loss rates which were slower than previous time periods, with gradients of 4.18 (±0.29), 3.66 (±0.47) and 3.83 (±0.34), respectively (Mann Whitney U-test; wildtype & *agp8* - U=131.5, p=0.339; wildtype &

prc1 - U=157.0, p=0.888; *agp8* & *prc1* -U=144.0, p=0.584) *sfr8*, in contrast to period time periods, had the slowest water loss rate between hours 4-8, with a gradient of 0.55 (±0.20), which was significantly slower water loss rate than wildtype, *agp8* and *prc1* (Mann Whitney U-test; U=2.5, p<0.001; U=28.5, p<0.001; U=15.5, p<0.001, respectively).

Table 3.3: Mean leaf initial and dry mass of pectin modification mutants. n=18 per genotype.

Mutants	Initial mass (mg) (±1 SE)	Dry mass (mg) (±1 SE)
Wildtype	28.1 (±2.08)	2.2 (±0.17)
sfr8	29.1 (±1.94)	2.3 (±0.16)
agp8	29.1 (±2.11)	2.1 (±0.15)
prc1	27.7 (±2.21)	1.9 (±0.18)

All genotypes had a similar leaf initial and dry mass (Table 3.3). There is no statistically significant difference between the genotypes for initial leaf mass (One-way ANOVA; $F_{3, 68}$=0.112, p=0.953), nor leaf dry mass (Kruskal Wallis; X^2_3=3.195, p=0.363). Therefore, any differences in leaf water loss rate are due to the different genotypes, not due to size.

In summary, the mechanical strength mutants, *agp8* and *prc1* maintained % masses lower than wildtype throughout the leaf drying assay up until 24 hours after excision (Figure 3.6.1). However, their water loss rate during the first hour was significantly faster than wildtype (Figure 3.6.2), which implies a slow stomatal closing response or a stomatal closing response that is slow to initiate. Therefore, *agp8* and *prc1* have a water loss rate different to wildtype, particularly in the first hour, and so these mutants were chosen for further experiments of stomatal function. *xxt1 xxt2* is also a mechanical strength mutant but, as discussed in section 3.1.4, did not display a water loss rate different to wildtype so was not included in following experiments.

3.1.6 Results Summary of the Leaf Drying Assays

To conclude this section, all of the fucosylation mutants, *mur2, fut4, msr1* and *cgl1*, had a water loss rate similar to wildtype and so were not pursued in the following experiments (Table 3.4). Out of the remaining cell wall mutants, *gaut5, gaut6-1, gaut6-2, qul1, pme34* and *xxt1 xxt2*, did not show a significant difference in leaf water loss from wildtype and so were not included in the measurements of stomatal function. On the other hand, the following mutants did show a significant difference in water loss during the leaf drying assay from wildtype and so are used in the following experiments of stomatal function. These mutants include: *pmr5*, a pectin abundance and pectin crosslinking mutant; *rwa2*, a pectin crosslinking and xyloglucan mutant; *agp8*, a mechanical strength mutant; and *prc1*, a mechanical strength mutant. Although these mutants did have a different water loss rate to wildtype, none of the mutants showed a water loss defect as severe as *sfr8.*

Table 3.4: Summary of the mutant phenotypes and result of the leaf drying assays of the mutants used. ✓ means this cell wall mutant differs from wildtype by the phenotype stated. Blank cell means this cell wall mutant is the same as wildtype in the phenotype stated. ↑ means an increase in this component in comparison to wildtype. ↓ means a decrease in this component in comparison to wildtype.

Mutant	Reduced general fucosylation	Altered pectin abundance	Altered pectin crosslinking	Altered xyloglucan	Reduced mechanical strength	Water loss different to wildtype
mur2	✓			✓		
fut4	✓					
msr1	✓					
cgl1	✓					
gaut5		↓				
gaut6-1		↓				
gaut6-2		↓				
pmr5		↑	✓			✓
qul1		↓				
pme34			✓			
rwa2			✓	✓		✓
xxt1 xxt2				✓	✓	
agp8					✓	✓
prc1					✓	✓

3.2 Infra-Red Thermal Imaging

Thermal imaging is a useful tool for measuring differences in stomatal conductance between genotypes under controlled conditions (Prashar and Jones, 2014), such as those in the walk-in growth chamber used in this experiment. Stomatal conductance is a measure of the gas that passes through the stomata, either the CO_2 entering the leaf through the stomata or the water vapour exiting the leaf through the stomata. Stomatal conductance is primarily regulated by the stomatal aperture (size of the stomatal pore), which is controlled by the guard cells, although stomatal density and the water transport capacity of the guard cells do have an effect on stomatal conductance (Zhu et al., 2018). Thermal imaging can measure whole

plant stomatal conductance because the leaf temperatures differ depending on the stomatal conductance. When stomatal pores are open, evaporative cooling occurs; water exits the stomata and evaporates on the leaf surface, cooling the leaf. Therefore, plants with cooler leaves can be identified with thermal imaging and used to indicate a higher stomatal conductance. Conversely, plants with closed stomata will not have evaporative cooling occurring, so will appear warmer on thermal imaging, which indicates a lower stomatal conductance.

When plants were grown in peat plugs and water was withheld, the roots of drying plants are almost directly exposed to air, leading to high susceptibility to subtle variations in environmental conditions within the growth chamber and variability in the severity of drought inflicted. Furthermore, plant drying in this manner is not reflective of drying in a natural environment. Therefore, growth and imaging conditions were altered so that plants were better protected from environmental conditions and had more uniform water content. This was achieved by growing the plants in small plastic pots. When water was withheld from plants in pots, the plants took longer to fully desiccated than plants in peat plugs. The desiccation experiment was repeated three times in total, once with plants in peat plugs and twice with plants in pots. Only the repeat of plants in pots with the most observable difference in temperature is shown in the figures.

3.2.1 *pmr5*

When grown and imaged in peat plugs in a preliminary experiment, *sfr8* maintained a leaf temperature lower than wildtype, indicating a higher stomatal conductance than wildtype throughout the drying period (Figure 3.7.A). One *pmr5* plant tended to display a leaf temperature cooler than wildtype so also had a higher stomatal conductance. At 10 days of desiccation, this *pmr5* plant was the coolest and had the highest stomatal conductance of all plants. However, the other *pmr5* plant tended to maintain a temperature similar to wildtype and so had a similar stomatal conductance, only once displaying a lower temperature than wildtype at 3 days. By day 14 all plants showed visible signs of desiccation, *sfr8* plants had wilted and so had one wildtype plant. By day 17 all plants were fully desiccated.

When grown in pots, all plants maintained a similar temperature and stomatal conductance throughout the drying experiments (Figure 3.7.B). The plants grown in pots took 27 days to dry out, which is 10 days longer than plants grown in peat plugs. This is possibly due to the protection the pots provide from the air, larger soil content of pots and/or different constitution of growth medium.
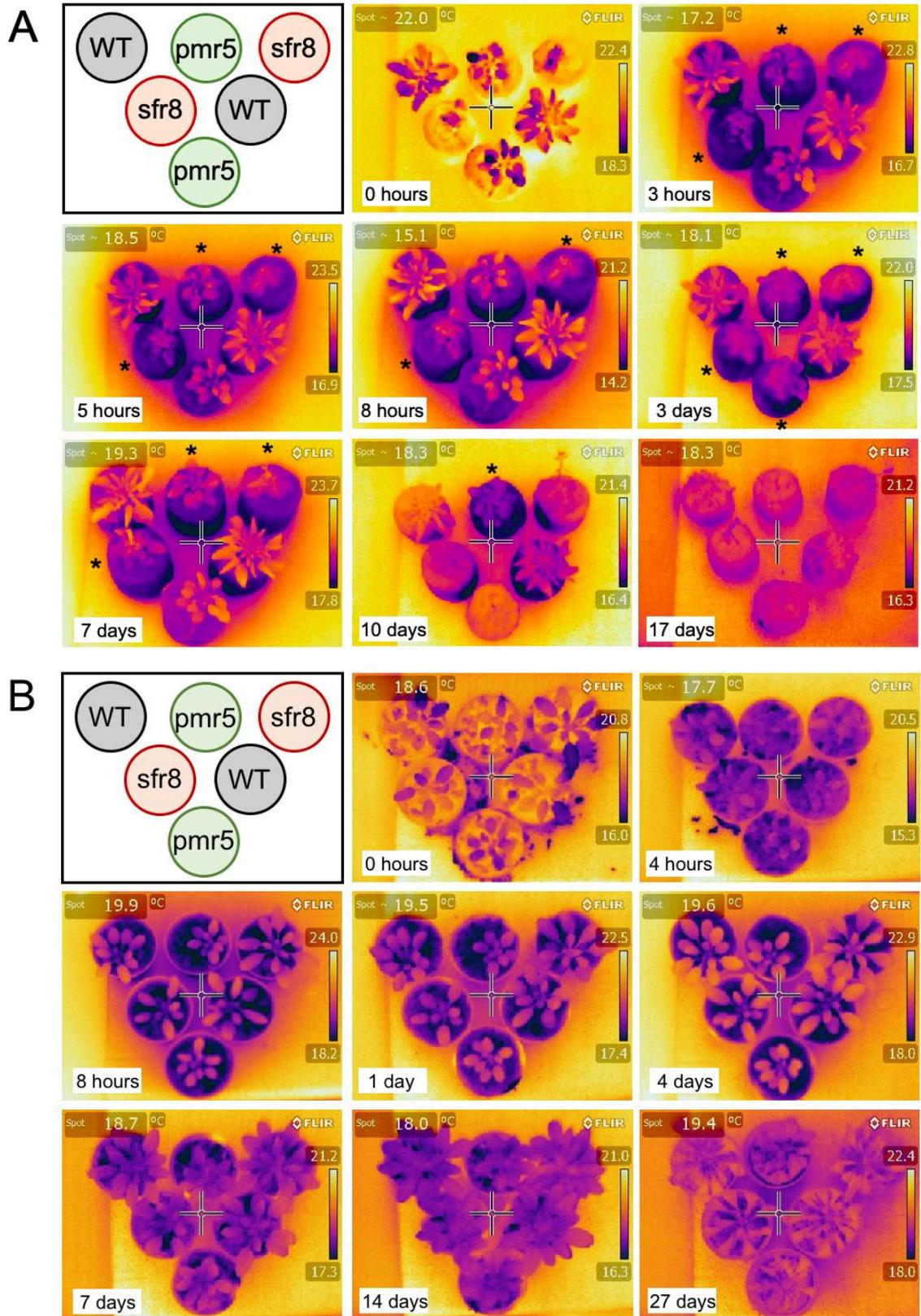
Figure 3.7: Images of wildtype, *sfr8* and *pmr5* taken using an infra-red thermal imaging camera as the plants dry out over time. A: Wildtype, *sfr8* and *pmr5* grown and imaged in peat plugs. B: Wildtype, *sfr8* and *pmr5* grown and imaged in pots, representing two biological replicates. Temperature scale on right of each image, ranging from hottest (shown in yellow) to coolest temperatures (shown in purple). Bottom right indicates what stage of drying out the images were taken. * indicates plants which were cooler than wildtype.
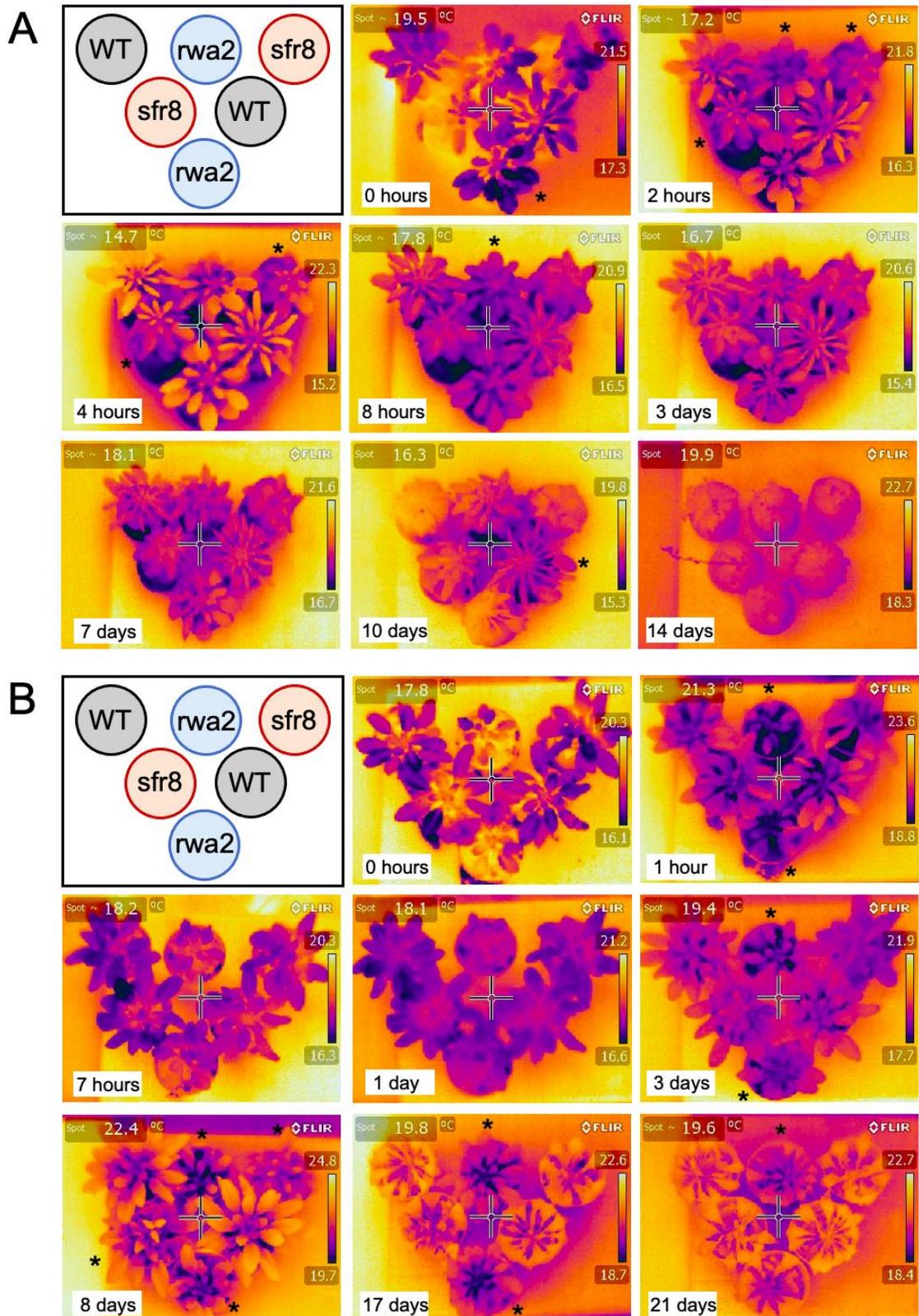
Figure 3.8: Images of wildtype, *sfr8* and *rwa2* taken using an infra-red thermal imaging camera as the plants dry out over time. A: Wildtype, *sfr8* and *pmr5* grown and imaged in peat plugs. B: Wildtype, *sfr8* and *pmr5* grown and imaged in pots, representing two biological replicates. Temperature scale on right of each image, ranging from hottest (shown in yellow) to coolest temperatures (shown in purple). Bottom right indicates what stage of drying out the images were taken. * indicates plants which were cooler than wildtype.

When grown and imaged in peat plugs, *sfr8* maintained a temperature similar to or lower than wildtype throughout the drying period and so had a similar or higher stomatal conductance (Figure 3.8.A). Occasionally, *rwa2* plants had the coolest leaves and the highest stomatal conductance, for example, at the start of the experiment, at 2 hours and at 8 hours. Equally, at some points rwa2 had temperature similar to wildtype, for example at 4 hours. At 3 days and 7 days, all plants were the same temperature and had the same stomatal conductance. By 10 days, the one wildtype and one *rwa2* plant showed signs of desiccation. The inner plants were cooler than the outer, more-exposed plants, with wildtype being the coolest plant. By 14 days, all the plants were fully desiccated.

For plants grown in pots, *sfr8* maintained a similar temperature to wildtype throughout the drying period and at 8 days, *sfr8* plants were cooler than wildtype (Figure 3.8.B). For some of the drying period, at 7 hours and 1 day, *rwa2* maintained a similar temperature to wildtype and *sfr8.* However, for the majority of the time (1 hour, 3 days, 8 days, 17 days and 21 days), *rwa2* plants were the coolest plants and had the highest stomatal conductance. After 17 days of drying out, wildtype and *sfr8* showed signs of desiccation whereas *rwa2* was not desiccated. By 21 days, all plants had fully desiccated, which took 7 days longer than plants grown in peat plugs.

3.2.3 *agp8*

Once again, *sfr8* consistently had a lower temperature than wildtype throughout the drying experiment done in peat plugs (Figure 3.9.A). *agp8* was consistently warmer and had a lower stomatal conductance than *sfr8* throughout the experiment. *agp8* maintained a similar temperature and stomatal conductance to wildtype throughout and at times the top *agp8* plant was warmer than wildtype, for example, at 3 hours, 1 day and 5 days. *sfr8* plants were the coolest throughout. All the plants had desiccated by 12 days.

The differences in temperature were less distinct when grown and imaged in pots (Figure 3.9.B). Most of the time, *sfr8* was slightly cooler and had a slightly higher stomatal conductance than wildtype and *agp8,* except at 4 days when all plants had the same temperature. *agp8* maintained a temperature and stomatal conductance similar to wildtype throughout and at times, was warmer than wildtype and had a lower stomatal conductance, for example at 7 hours and 13 days. The plants took 27 days to fully desiccate, 15 days longer than when grown in peat plugs.
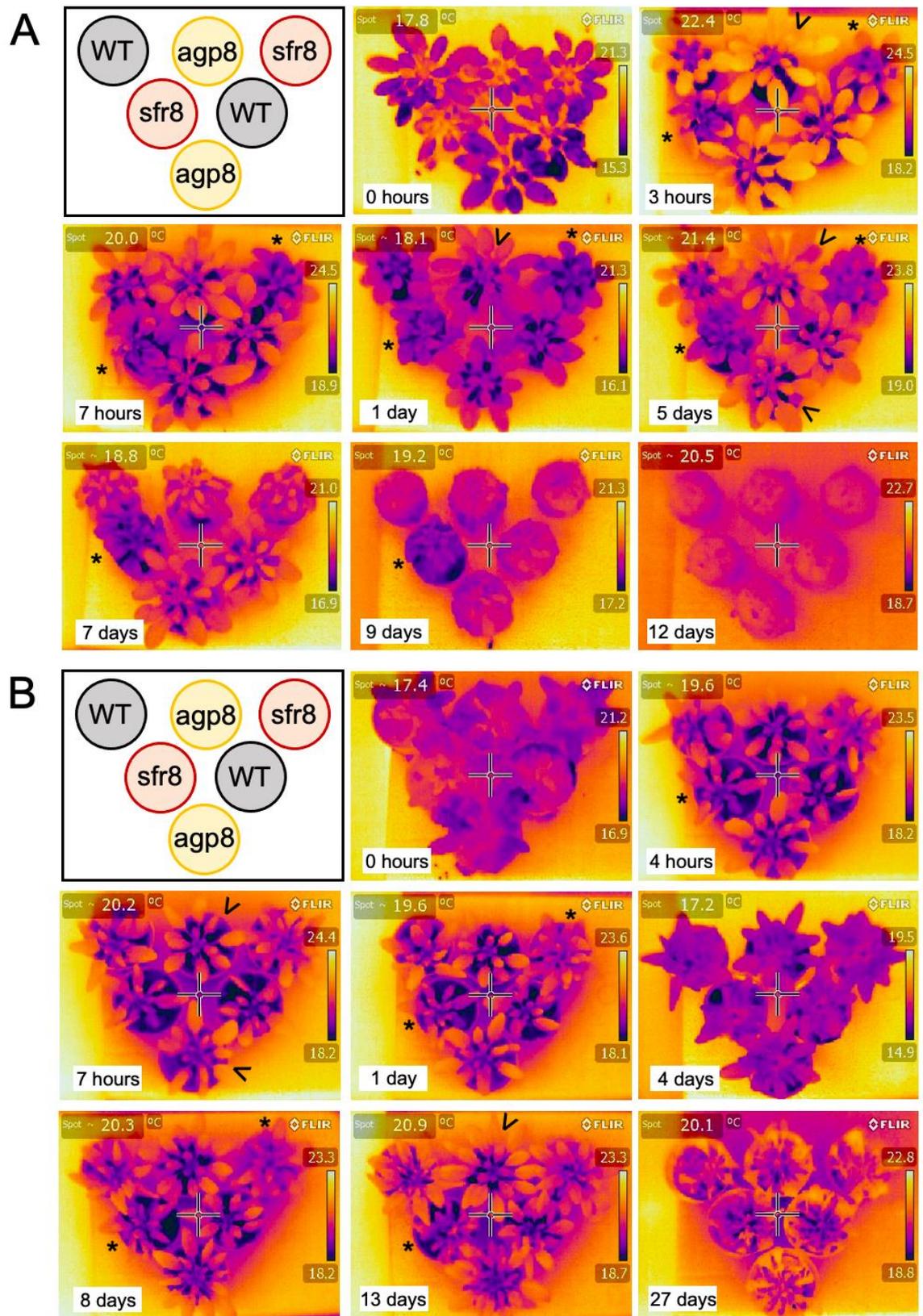
Figure 3.9: Images of wildtype, *sfr8* and *agp8* taken using an infra-red thermal imaging camera as the plants dry out over time. A: Wildtype, *sfr8* and *pmr5* grown and imaged in peat plugs. B: Wildtype, *sfr8* and *pmr5* grown and imaged in pots, representing two biological replicates. Temperature scale on right of each image, ranging from hottest (shown in yellow) to coolest temperatures (shown in purple). Bottom right indicates what stage of drying out the images were taken. * indicates plants which were cooler than wildtype. > indicates plants which were warmer than wildtype.

3.2.4 *prc1*

Figure 3.10: Images of wildtype, *sfr8* and *prc1* taken using an infra-red thermal imaging camera as the plants dry out over time. A: Wildtype, *sfr8* and *pmr5* grown and imaged in peat plugs. B and C: Two replicates of wildtype, *sfr8* and *pmr5* grown and imaged in pots, representing two biological replicates. Temperature scale on right of each image, ranging from hottest (shown in yellow) to coolest temperatures (shown in purple). Bottom right indicates what stage of drying out the images were taken. * indicates plants which were cooler than wildtype.

Like the other thermal imaging experiments, *sfr8* maintained a temperature lower than wildtype when grown in peat plugs for the first 8 hours (Figure 3.10.A). *prc1* maintained a temperature and stomatal conductance similar to wildtype throughout the experiment, which tended to be warmer and have a lower stomatal conductance than *sfr8*. At days 2 and 6, the plants all had a similar temperature and stomatal conductance. The coolest plants on day 9 were *sfr8* and *prc1*. By day 12, all plants had desiccated. In contrast, when grown in pots all plants had a similar temperature and stomatal conductance throughout the experiment (Figure 3.10.B). The plant took 27 days to desiccate, 15 days longer than when grown in peat plugs.

Overall, *sfr8* plants tended to have a stomatal conductance similar to or higher than wildtype. One *pmr5* plant grown in peat plugs had a stomatal conductance similar to *sfr8* and was occasionally the plant with the highest stomatal conductance. However, the other *pmr5* plant grown in peat plugs had a lower stomatal conductance than *sfr8* and had a similar stomatal conductance to wildtype. When grown in pots, wildtype, *sfr8* and *pmr5* all had similar stomatal conductance. Therefore, as the majority of *pmr5* plants did not show a difference in stomatal conductance with wildtype, on top of an only slight difference in the rate of water loss to wild type, as shown in section 3.1.2.2, *pmr5* was not included in further experiments. Furthermore, agp8 and *prc1* plants tended to have a lower stomatal conductance than *sfr8* and a similar stomatal conductance to wildtype regardless of growth conditions. This implies that *agp8* and *prc1* do not exhibit a stomatal closure defect similar to *sfr8* so were not included in the remainder of the project. Finally, *rwa2* plants grown in peat plugs and pots occasionally had a similar stomatal conductance to wildtype, however, some of the time, *rwa2* had a higher stomatal conductance than wildtype and had a similar to or higher stomatal conductance than *sfr8*. This taken with the significant water loss rate of *rwa2*, which was the most severe water loss defect of all mutants tested other than *sfr8*, as shown in section 3.1.3, is why *rwa2* was chosen for inclusion in the remainder of the project.

3.3 Infra-Red Gas Analyser (IRGA) Measurements

A more accurate measure of stomatal conductance than the qualitative measure taken using the thermal imaging camera was taken using an infra-red gas analyser (IRGA). It is widely considered that the IRGA is the most accurate measure of leaf stomatal conductance available (Toro et al., 2019). The IRGA measures the diffusion of CO_2 and water vapour through the stomata and uses this to calculate stomatal conductance by Ohm's law analogy (Toro et al., 2019). The leaf drying assay data for *sfr8* (Section 3.1) suggest that the water loss defect of *sfr8* may be due to a slow stomatal closing response or a permanent large stomatal aperture. Therefore, it is important to measure the stomatal conductance when a closing or opening signal is applied. In this experiment, the opening signal used is decreased CO_2 concentration and the closing signal is increased CO_2 concentration. In response to changing CO_2 concentration, the stomatal aperture and conductance will change to maintain an optimal photosynthesis rate while limiting water loss rate. As CO_2 concentration decreases outside of the leaf, the photosynthesis rate will be limited as CO_2 availability is reduced. To maintain an optimal photosynthesis rate, the guard cells will increase the stomatal aperture to allow more CO_2 to enter the intercellular space, which increases stomatal

conductance. Conversely, as CO_2 concentration increases outside the leaf, there is abundant CO_2 inside the leaf for an optimal photosynthesis rate, therefore, the guard cells will decrease the stomatal aperture to limit water loss through the stomata, which decreases stomatal conductance.

Additional data were extracted from that taken by the IRGA. The mean stomatal conductance of each genotype was calculated for the different CO_2 concentrations, which shows the overall stomatal conductance for each phase of the experiment. The mean change in stomatal conductance between 400ppm – 50ppm CO_2 concentration and 50ppm – 1000ppm CO_2 concentration was calculated to highlight the capacity of the stomata to respond to opening and closing signals for the different genotypes. The time taken to reach maximum and minimum conductance values and the gradient of conductance change during the first 15 minutes after a change in CO_2 concentration was used to show the speed of stomatal conductance changes.

3.3.1 Stomatal Conductance Change Over Time
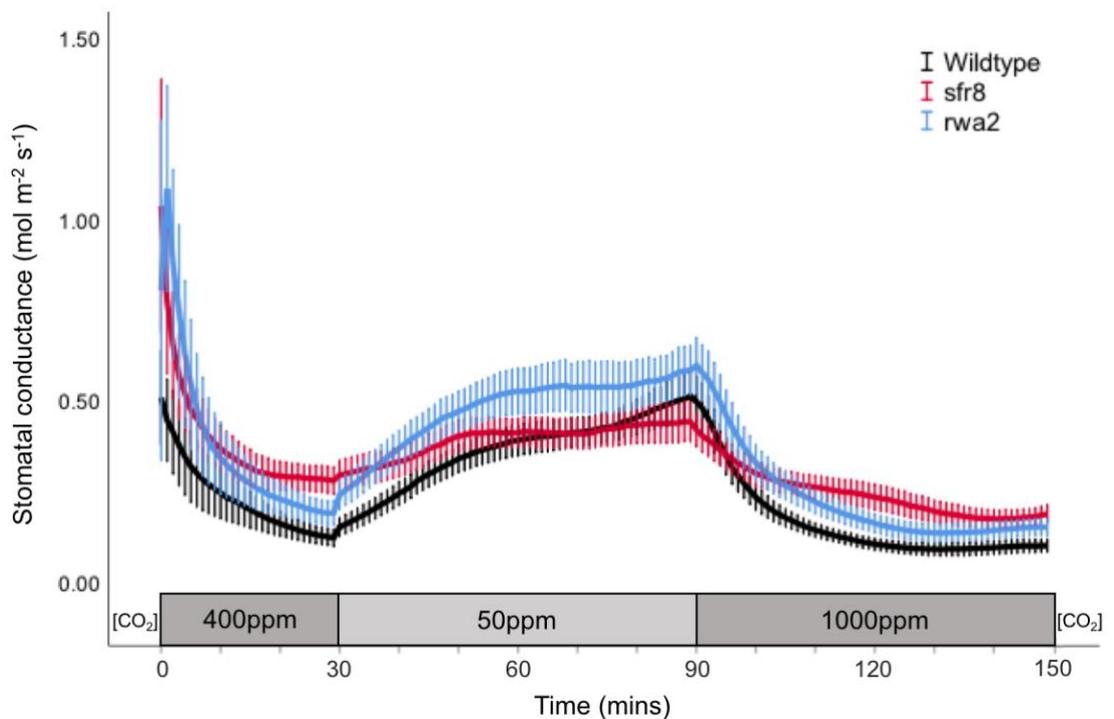
Figure 3.11.1: Stomatal conductance of wildtype (black), *sfr8* (red) and *rwa2* (blue) over time when subjected to changes in CO_2 concentration. Conductance measured over a $1cm^2$ area of leaf. At 0-30mins, $[CO_2]$ = 400ppm; at 31-90mins, $[CO_2]$ = 50ppm; at 91-150 mins, $[CO_2]$ = 1000ppm. Error bars show ±1 standard error. n=18 per genotype.

When subjected to a decrease in CO_2 concentration from ambient conditions, 400ppm, to an extreme low of 50ppm, the stomata should open and stomatal conductance should change. The stomatal conductance of wildtype leaves increased from a mean end value of 0.123 mol $m^{-2} s^{-1}$ (±0.023) to a mean end value of 0.514 mol $m^{-2} s^{-1}$ (±0.0.068), which is as expected (Figure 3.11.1). When subjected to an increase in CO_2 concentration from 50ppm to 1000ppm, the stomata should close and stomatal conductance should

decrease. Also as predicted, wildtype stomatal conductance decreased from 0.514 mol m^{-2} s^{-1} (±0.0.068) to a mean end value of 0.101 mol m^{-2} s^{-1} (±0.017) during this stomatal closing signal.

The stomatal conductance of *sfr8* followed a similar pattern of increase and decrease corresponding to changes in CO_2 concentration to that of wildtype. The decrease in CO_2 concentration, the stomatal opening signal, resulted in a stomatal conductance increase from a mean end value of 0.281 mol m^{-2} s^{-1} (±0.038) to a mean end value of 0.442 mol m^{-2} s^{-1} (±0.055). The following increase in CO_2 concentration, the stomatal closing signal, decreased stomatal conductance from 0.442 mol m^{-2} s^{-1} (±0.055) to an average end value of 0.254 mol m^{-2} s^{-1} (±0.043).

Similarly, the stomatal conductance of *rwa2* paralleled the pattern of increase and decrease like wildtype and *sfr8*. When CO_2 concentration was decreased, *rwa2* stomatal conductance increased from a mean end value of 0.192 mol m^{-2} s^{-1} (±0.034) to a mean end value of 0.586 mol m^{-2} s^{-1} (±0.068) Following this, as CO_2 concentration decreased, *rwa2* stomatal conductance decreased to an average end value of 0.151 mol m^{-2} s^{-1} (±0.023). The genotypes all responded to the CO_2 induced stomatal opening and closing signals, however, the absolute conductance values and magnitude of conductance change was different between genotypes. Therefore, further analysis was done.

3.3.2 Mean Stomatal Conductance per CO_2 Concentration
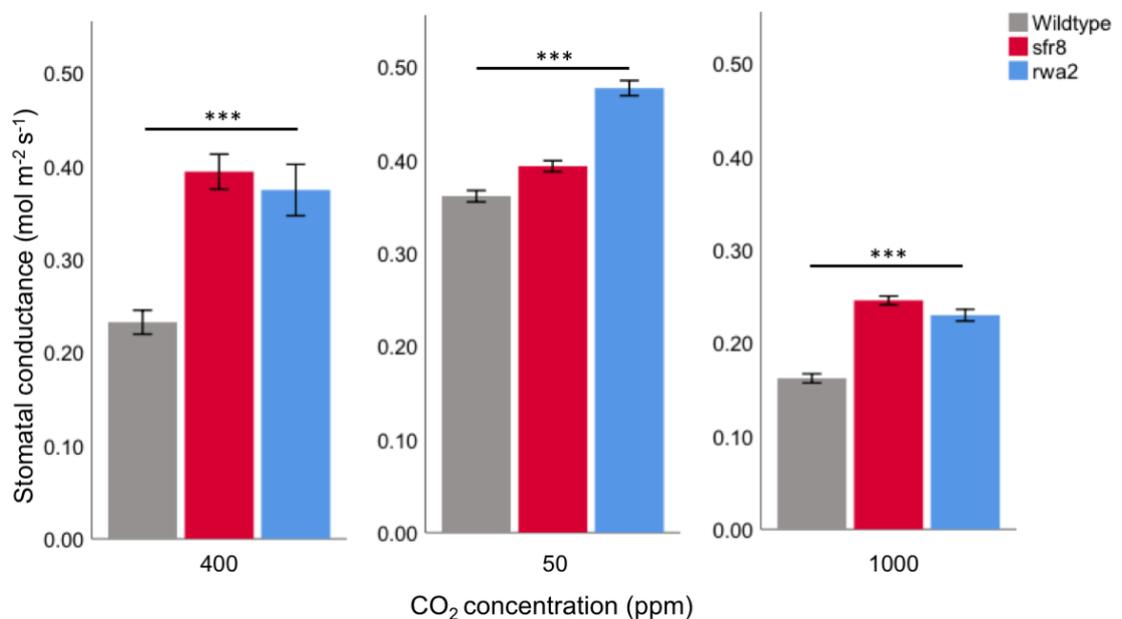
Figure 3.11.2: The mean stomatal conductance of wildtype (grey), *sfr8* (red) and *rwa2* (blue) at different CO_2 concentrations of 400, 50 and 1000ppm. Error bars show ±1 standard error. *** means p<0.001 for all pairwise combinations.

Wildtype had the lowest mean stomatal conductance for all CO_2 concentrations at 0.233 mol m^{-2} s^{-1} (±0.013) at 400ppm, 0.361 mol m^{-2} s^{-1} (±0.006) at 50ppm and 0.162 mol m^{-2} s^{-1} (±0.005) at 1000ppm (Figure 3.11.2). The mean stomatal conductance of *sfr8* started at 0.394 mol m^{-2} s^{-1} (±0.019) at 400ppm, then unlike wildtype and *rwa2* maintained a similar mean stomatal conductance of 0.393 mol m^{-2} s^{-1} (±0.006)

at 50ppm and finally decreased to 0.246 mol m^{-2} s^{-1} (±0.005) at 1000ppm. At 400ppm, rwa2 had a mean stomatal conductance of 0.310 mol m^{-2} s^{-1} (±0.071) which increased to 0.477 mol m^{-2} s^{-1} (±0.008) at 50ppm and decreased to 0.230 mol m^{-2} s^{-1} (±0.006) at 1000ppm. There was a highly significant difference between the genotypes for mean stomatal conductance for all CO_2 concentrations (Kruskal Wallis; 400ppm - X^2_2=185.649, p<0.001; 50ppm - X^2_2=117.090, p<0.001; 1000ppm - X^2_2=242.439, p<0.001) and in fact all pairwise combinations of mean stomatal conductance were significantly different from each other. The mean stomatal conductance of *sfr8* was significantly higher than wildtype at all CO_2 concentrations (Mann Whitney U-test; 400ppm - U=77429.0, p<0.001; 50ppm – U=521516.0, p<0.001; 1000ppm - U=355882.0, p<0.001) and higher than *rwa2* at 400ppm and 1000ppm (Mann Whitney U-test; U=109961.0, p<0.001; U=496854.0, p<0.001, respectively). The mean stomatal conductance of *rwa2* significantly was higher than wildtype at all CO_2 concentrations (Mann Whitney U-test; 400ppm - U=108921.0, p<0.001; 50ppm - U=433022.0, p<0.001; 1000ppm - U=451763.0, p<0.001) and was higher than sfr8 at 50ppm (Mann Whitney U-test; U=480255.0, p<0.001).

3.3.3 Mean Change in Stomatal Conductance
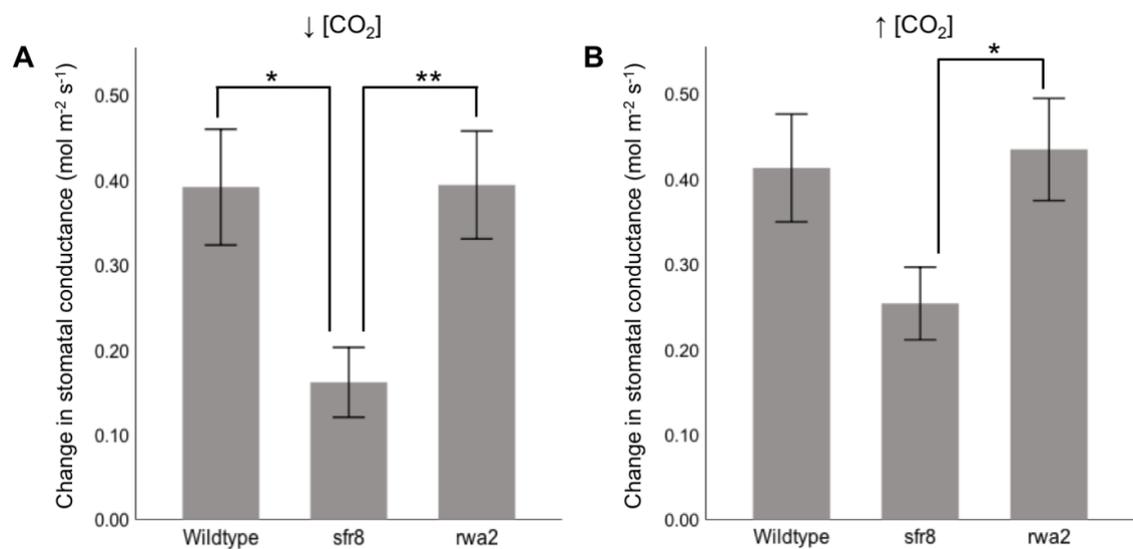
Figure 3.11.3: The change in stomatal conductance of wildtype, *sfr8* and *rwa2* when CO_2 concentration was changed. **A**: CO_2 concentration increased from 400ppm to 50ppm. **B:** CO_2 concentration decreased from 50ppm to 1000ppm. Values calculated by subtracting the conductance values at the end of each CO_2 concentration period. Error bars show ±1 standard error. * means p<0.05, ** means p<0.01.

Wildtype showed a mean change in conductance of 0.391 mol m^{-2} s^{-1} (±0.068) when CO_2 concentration was increased and 0.413 (±0.063) when CO_2 concentration was decreased (Figure 3.11.3). *rwa2* had a similar change in stomatal conductance to wildtype; when CO_2 concentration was decreased, the stomatal opening signal, the stomatal conductance of *rwa2* changed by 0.393 mol m^{-2} s^{-1} (±0.064) and when CO_2 concentration was decreased, the stomatal closing signal, conductance changed by 0.435 mol m^{-2} s^{-1} (±0.060). *sfr8* exhibited smaller changes in stomatal conductance than wildtype and *rwa2;* when CO_2 concentration was decreased and increased, the stomatal conductance values changed by 0.161 mol m^{-2} s^{-1} (±0.041) and 0.254 mol m^{-2} s^{-1} (±0.043) respectively. There is a significant difference between the genotypes for stomatal conductance change (Kruskal Wallis; decreased [CO_2] – X^2_2=10.848, p=0.004;

increased [CO_2] – X^2_2=6.817, p=0.033). Wildtype and *rwa2* have statistically the same stomatal conductance changes (Mann Whitney U-test; decreased [CO_2] – U=154.0, p=0.815; increased [CO_2] – U=148.0, p=0.673). During the stomatal opening signal, the stomatal conductance change of wildtype and *rwa2* was significantly larger than *sfr8* (Mann Whitney U-test; U=76.0, p=0.006; U=69.0, p=0.003, respectively). During the stomatal closure signal, only the stomatal conductance change of rwa2 was significantly larger than *sfr8* (Mann Whitney U-test, U=84.0, p=0.013), and wildtype had statistically the same stomatal conductance change as *sfr8* (Mann Whitney U-test, U=100.0, p=0.051).

3.3.4 Time Taken to Reach Maximum and Minimum Stomatal Conductance Values

Wildtype took an average of 50.83 mins (±2.84) and 42.61 mins (±2.54) to maximally change stomatal conductance during the 50ppm CO_2 concentration period and the 1000ppm CO_2 concentration period respectively (Figure 3.11.4). *sfr8* took slightly less time than wildtype to reach the maximum stomatal conductance during the 50ppm period, taking an average of 38.83 mins (±3.97) and took slightly longer than wildtype to reach the minimum stomatal conductance during the 1000ppm period, taking an average of 49.11 mins (±2.10). *rwa2* took 47.44 mins (±3.13) for the 50ppm CO_2 concentration period and 46.00 mins (±1.96) for the 1000ppm period. All genotypes took statistically the same amount of time to maximally change stomatal conductance during the 50ppm period (Kruskal Wallis, X^2_2=5.364, p=0.068) and during the 1000ppm period (One-way ANOVA, $F_{2,51}$=2.160, p=0.126; Kruskal Wallis, X^2_2=3.550, p=0.169).
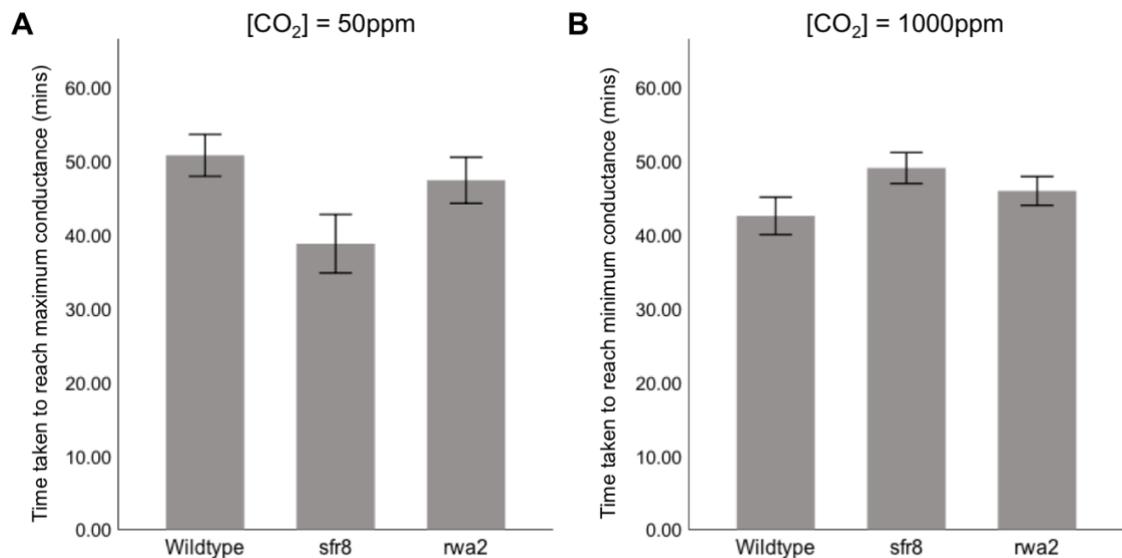
Figure 3.11.4: Time taken for wildtype, *sfr8* and *rwa2* to maximally change stomatal conductance. **A:** During the 50ppm CO_2 concentration period. **B:** During the 1000ppm CO_2 concentration period. Error bars show ±1 standard error.

3.3.5 Gradient of Stomatal Conductance Change

For the first 15 mins after changing CO_2 concentration to 50ppm, the stomatal conductance of wildtype was increasing with an average gradient of 0.0117 (±0.0020; Figure 3.11.5). *sfr8* stomatal conductance was increasing but at a less steep gradient, which was on average 0.0042 (±0.0011). The increase in the

stomatal conductance of *rwa2* had an average gradient of 0.0127 (±0.0016), which is slightly larger than wildtype. Although the gradient of wildtype and *rwa2* stomatal conductance was statistically the same (Mann Whitney U-test, U=131.0, p=0.339), there was a highly significant difference between the gradient of the genotypes (Kruskal Wallis, X^2_2=18.504, p<0.001). Both wildtype and *rwa2* had a stomatal conductance gradient that was larger than *rwa2* (Mann Whitney U-test; U=57.5, p=0.001; U=37.0, p<0.001, respectively).
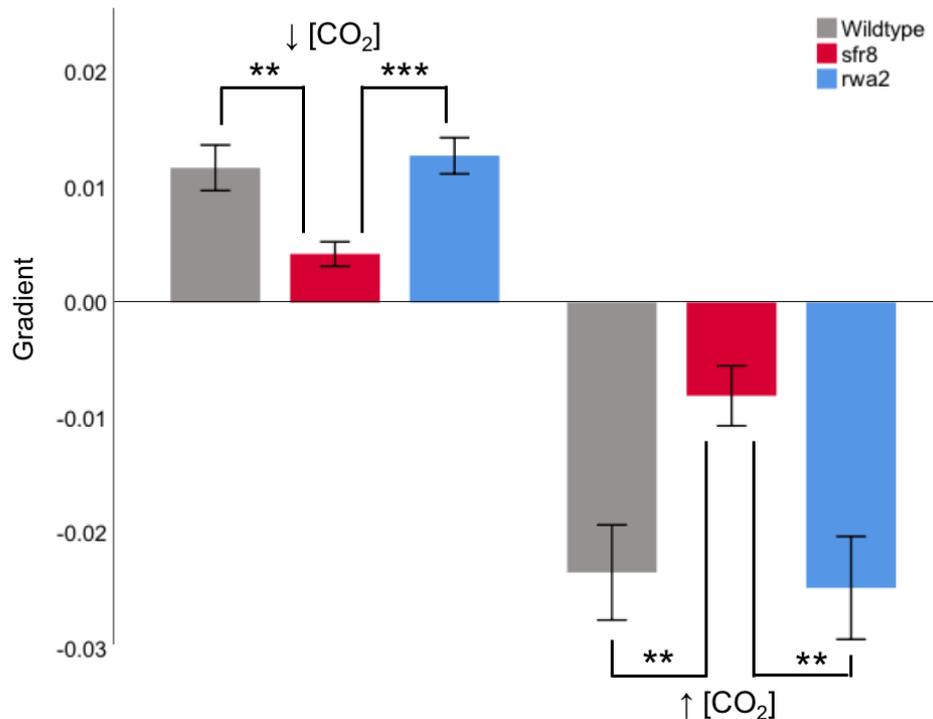
Figure 3.11.5: Gradient of a linear fit to the first 15 stomatal conductance values taken after a decrease in CO_2 concentration from 400ppm to 50ppm ($\downarrow$ [CO_2]) and after an increase in CO_2 concentration from 50ppm to 1000ppm ($\uparrow$[CO_2]). Error bars show ±1 standard error. ** means p<0.005, *** means p<0.001.

Furthermore, for the first 15 mins after changing CO_2 concentration from 50ppm to 1000ppm, wildtype stomatal conductance decreased at a mean gradient of -0.0235 (±0.0041). Again, *sfr8* had a less steep gradient than wildtype with a mean gradient of -0.0081 (±0.0026) and *rwa2* had a similar stomatal conductance decrease to wildtype with a mean gradient of -0.0248 (±0.0045). There was a significant difference between genotypes for the gradient of stomatal conductance decrease (Kruskal Wallis, X^2_2=12.136, p=0.002). There was not a significant difference between wildtype and *rwa2* (Mann Whitney U-test, U=152.0, p=0.7670), but both wildtype and *rwa2* had a significantly larger gradient of stomatal conductance decrease than *sfr8* (Mann Whitney U-test; U=73.0, p=0.004; U=62.0, p=0.001, respectively).

In summary, all genotypes had the correct pattern of opening and closing following stomatal opening and closing signals with changing CO_2 concentration. *sfr8* and *rwa2* had significantly higher mean stomatal conductance values than wildtype regardless of the CO_2 concentration. *sfr8* had significantly higher mean stomatal conductance values than *rwa2* when CO_2 concentration was 400ppm and 1000ppm, however, *rwa2* had a significantly higher mean stomatal conductance value than *sfr8* at 50ppm. *sfr8* had a significantly less change in stomatal conductance than wildtype and *rwa2* when CO_2 concentration was

changed from 400ppm to 50ppm and a significantly less change than *rwa2* when CO_2 concentration was changed from 50ppm to 1000ppm. Similarly, *sfr8* had a significantly slower rate of change than wild type and *rwa2* during both changes in CO_2 concentration, although, the plants took statistically the same amount of time to maximally change their CO_2 values.

3.4 Stomatal measurements

Stomatal conductance is affected by stomatal density, as leaves with more stomatal pores will have a higher stomatal conductance value without having a difference in stomatal dynamics and conversely, leaves with fewer stomatal pores will have lower stomatal conductance values without having a difference in stomatal dynamics (Zhu et al., 2018). Therefore, stomatal density was measured using impressions taken of the leaf surface using dental putty and clear nail varnish and imaged under a light microscope. In the process of measuring the density, it was noticeable that the genotypes had different sized stomata and so stomatal size was also measured. Furthermore, as stomatal aperture is an important factor of stomatal function, it was calculated from the stomatal size data as stomatal length x stomatal width. Finally, to show that the differences in stomatal measurements were not due to leaf size, the mean area of the leaf impressions was included in the analysis.

3.4.1 Size of Impressions

The mean approximate leaf area for wildtype, *sfr8* and *rwa2* were 358.61 (±27.31), 354.61 (±28.87) and 323.61 (±26.58) mm^2 respectively (Figure 3.12.1). There was no statistically significant difference between the genotypes for approximate leaf area (Kruskal Wallis, X^2_2=1.093, p=0.579). Therefore, any difference in stomatal density, size or aperture should be due to the difference in genotype, not a difference in leaf area.
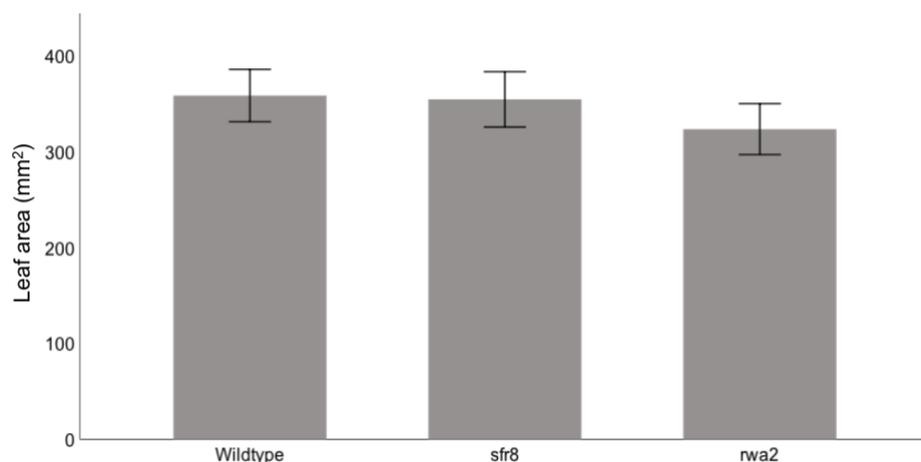
Figure 3.12.1: Mean approximate leaf area of the impressions for each genotype. Error bars show ±1 standard error. n=28 per genotype

3.4.2 Stomatal Density

sfr8 had the smallest stomatal density as shown in the examples (Figure 3.12.2) and the smallest overall stomatal density with a mean of 91.16 stomatal per mm^2 and a range of 49.96 – 154.23 stomata per mm^2

(Figure 3.12.3). Wildtype and *rwa2* had similar stomatal densities in the example and overall with means of 133.55 (± 6.63) and 124.55 (±2.88) stomata per mm^2 respectively. Wildtype had a range of 57.56 – 219.40 stomata per mm^2 and *rwa2* had a range of 76.03 – 187.90 stomata per mm^2. There was a statistically significant difference between the mean stomatal density of the different genotypes (Kruskal Wallis, X^2_2=93.746, p<0.001). The stomatal density of *sfr8* was significantly lower than both wildtype and *rwa2* (Mann Whitney U-test, U=6502.5, p<0.001; U=6964.0, p<0.001, respectively). This result predicts that *sfr8* leaves should have a lower stomatal conductance value (Zhu et al., 2018), which is in contrast to the higher stomatal conductance found in sections 3.1.2 and 3.1.3. Wildtype and *rwa2* had statistically the same stomatal density (Mann Whitney U-test, U=12529.5, p=0.075), which predicts that they should have the same stomatal conductance. However, the data in sections 3.1.2 and 3.1.3 show that *rwa2* has a higher stomatal conductance than wildtype.
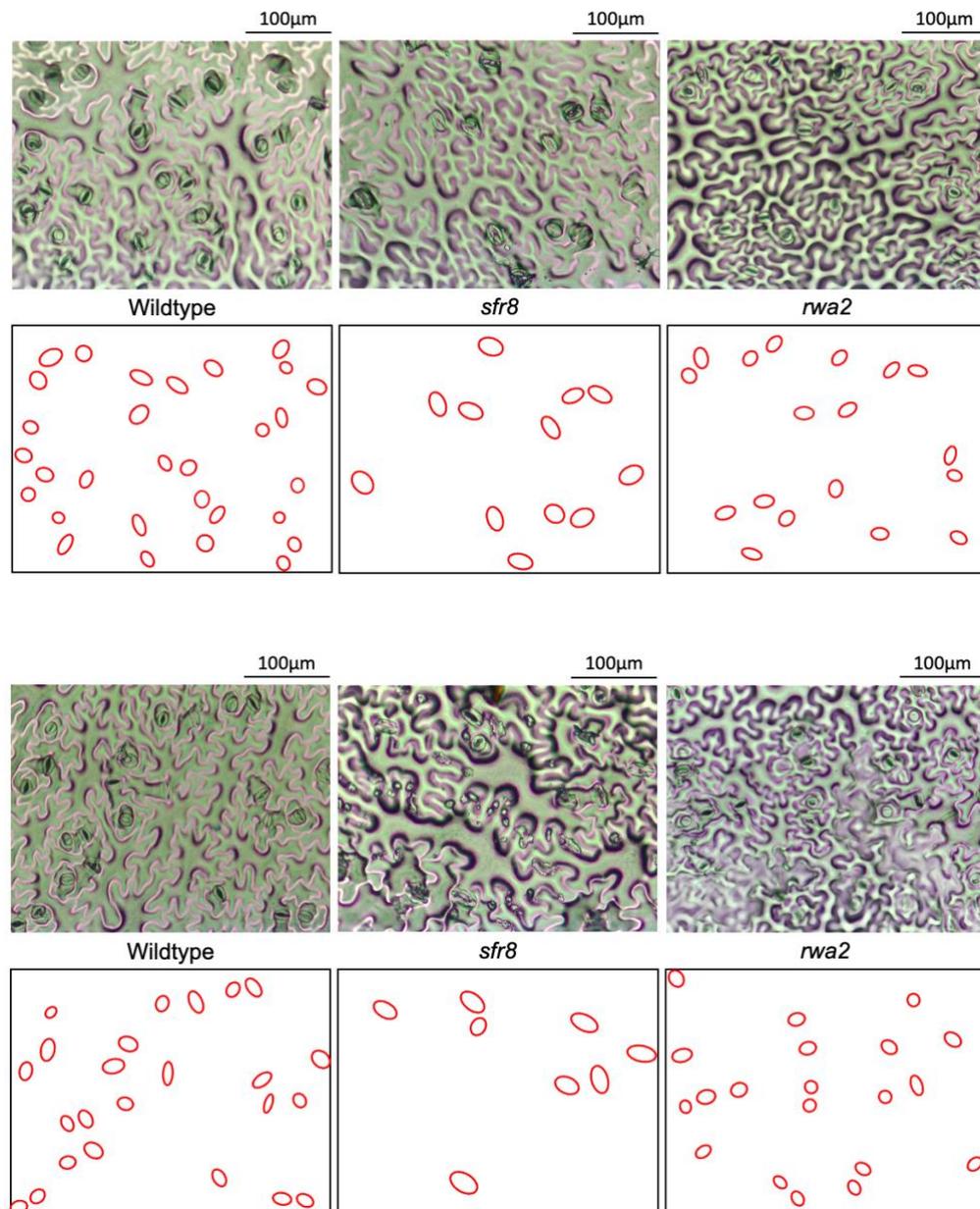
Figure 3.12.2: Examples of the impressions as viewed under the microscope (top) and a copy of the images showing just the outlines of stomatal complexes as red circles (bottom).
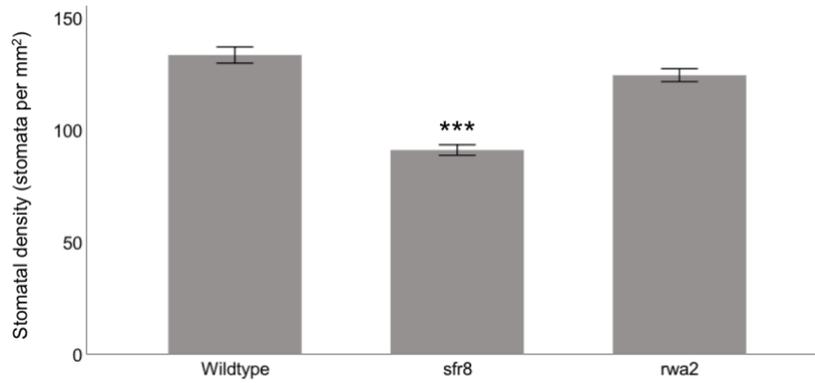
Figure 3.12.3: Stomatal density of wildtype, *sfr8* and *rwa2*. Error bars show ±1 standard error. n=168 per genotype. *** means p<0.001.

3.4.3 Stomatal Size

sfr8 had the largest stomatal complexes as shown in the example impressions (Figure 3.12.2) and had the largest mean stomatal size, with a mean length of 24.01 μm (±0.14) and a mean width 15.66 μm (±0.09) (Figure 3.12.5). Although there was no observable difference in stomatal size between wildtype and *rwa2* in the example impressions, wildtype had the smallest stomatal size of all genotypes, with mean length of 18.79 μm (±0.12) and mean width of 13.13 μm (±0.06). *rwa2* had a similar complex size to wildtype, with mean length of 19.65 μm (±0.12) and mean width of 13.49 μm (±0.07). There was a significant difference between the genotypes for stomatal complex length (One-Way ANOVA, $F_{2, 1508}$=482.888, p<0.001). The stomatal length of wildtype was significantly smaller than *sfr8* and *rwa2* (Tukey's post-hoc test, p<0.001, p<0.001, respectively). The stomatal length of *sfr8* was significantly larger than *rwa2* (Tukey's post-hoc test, p<0.001). Similarly, there was a significant difference between the genotypes for stomatal complex width (One-Way ANOVA, $F_{2, 1508}$=318.238, p<0.001). The stomatal width of wildtype was significantly smaller than *sfr8* and *rwa2* (Tukey's post-hoc test, p<0.001, p=0.002, respectively). The stomatal width of *sfr8* was significantly larger than *rwa2* (Tukey's post-hoc test, p<0.001).
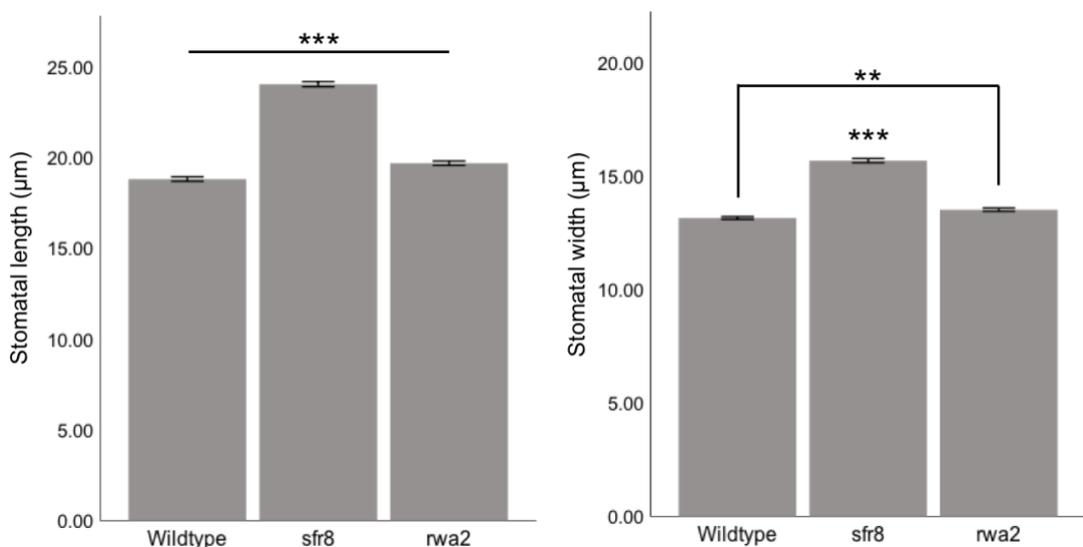
Figure 3.12.4: Stomatal complex length and width of wildtype, *sfr8* and *rwa2*. Error bars show ±1 standard error. n=504 per genotype. ** means p<0.01, *** means p<0.001, *** means p<0.001 for all pairwise combinations.

3.4.4 Stomatal Aperture

Under steady-state conditions, wildtype had the largest stomatal aperture of all genotypes at 0.711 μm (±0.005) (Figure 3.12.7). Closely following is *rwa2* with a stomatal aperture of 0.697 μm (±0.005). *sfr8* had the smallest stomatal aperture at 0.659μm (±0.004). There is a significant difference between the genotypes for stomatal aperture (Kruskal Wallis, X^2_2=55.437, p<0.001). *sfr8* had a significantly smaller stomatal aperture than wildtype and *rwa2* (Mann Whitney U-test; U=93809.5, p<0.001; U=102498.0, p<0.001, respectively). There was also a slightly significant difference between wildtype and *rwa2* for stomatal aperture (Mann Whitney U-test, U=117678.0, p=0.049).
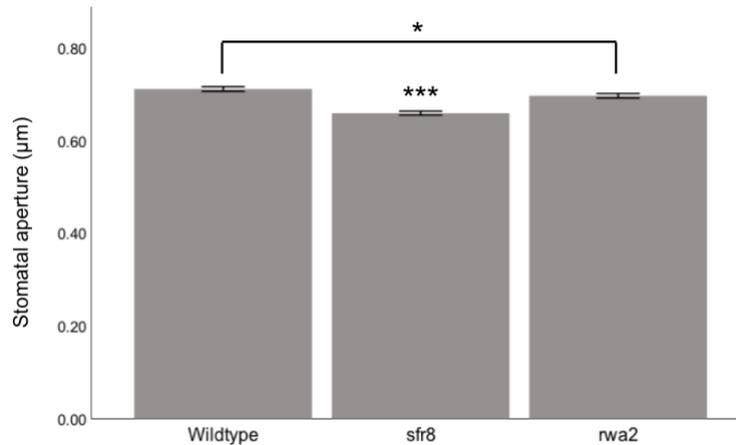
Figure 3.12.5: Stomatal aperture of wildtype, *sfr8* and *rwa2*. Error bars show ±1 standard error. n=504 per genotype. * means p<0.05, *** means p<0.001.

In summary, *sfr8* had a significantly lower stomatal density, a significantly larger stomatal size and a significantly lower aperture than wildtype and *rwa2*. *rwa2* had a significantly larger stomatal size and a significantly lower aperture than wildtype. As the size of leaves selected was statistically the same, the difference in stomatal measurements is not due to leaf area.

3.5 Drought Tolerance Assay

Wildtype, *sfr8* and *rwa2* plants were exposed to a drought stress to investigate the drought tolerance of the genotypes.

3.5.1 17-day Drought Period

Plants were all healthy and well-watered prior to the drought period (Figure 3.13.1). *rwa2* plants were smaller than wildtype and *sfr8* plants; *rwa2* plants had an initial mean rosette area of 1580mm^2, less than half the mean rosette area of wildtype and *sfr8* at 3888mm^2 and 3601mm^2 respectively. *rwa2* plants also had fewer leaves, having only 12-13 leaves, whereas wildtype and *sfr8* had 14-18 leaves. After the drought period of 17 days, all plants apart from one *rwa2* plant (the one in the centre) had wilted. After 10 days of rewatering, one wildtype plant had died (the one on the left), having no green leaves. The remaining living wildtype plants had more dead leaves than *sfr8* and *rwa2* plants; wildtype had 15-20 dead leaves, whereas *sfr8* had 5-7 dead leaves and *rwa2* had 0-4 dead leaves.

Wildtype plants grew the least during the drought period, both in terms of rosette area, which actually decreased by 25.60% (±54.86) and leaf number which also decreased by 39.31% (±32.96; Figure 3.13.2). *rwa2* plants grew the most during the drought period, with an increase in rosette area of 426.02% (±76.89) and an increase in leaf number of 173.93% (±38.06). During the drought period, *sfr8* plants did not change very much in rosette area, growing by only 2.43% (±9.70), but did largely increase in leaf numbers by 128.99% (±20.26). There was no significant difference between the genotypes for neither rosette growth nor increase in leaf number (Kruskal Wallis; X^2_2=5.956, p=0.051; X^2_2=5.600, p=0.061, respectively).
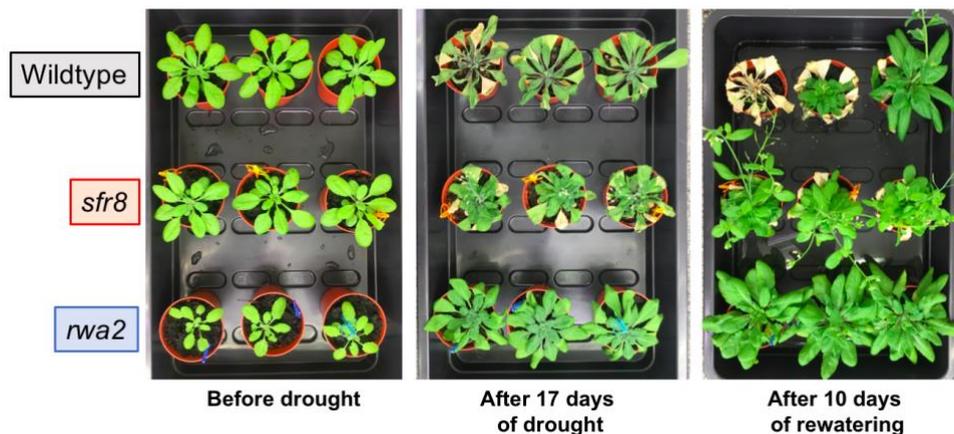
Figure 3.13.1: Plants throughout the preliminary drought tolerance assay. Top row is wildtype, middle row is *sfr8* and bottom row is *rwa2*. Plants are pictured immediately before drought period (left), after the drought period (middle) and after rewatering for 10 days (right). Plants were arranged randomly for the drought and rewatering period and organised by genotype for photographing.
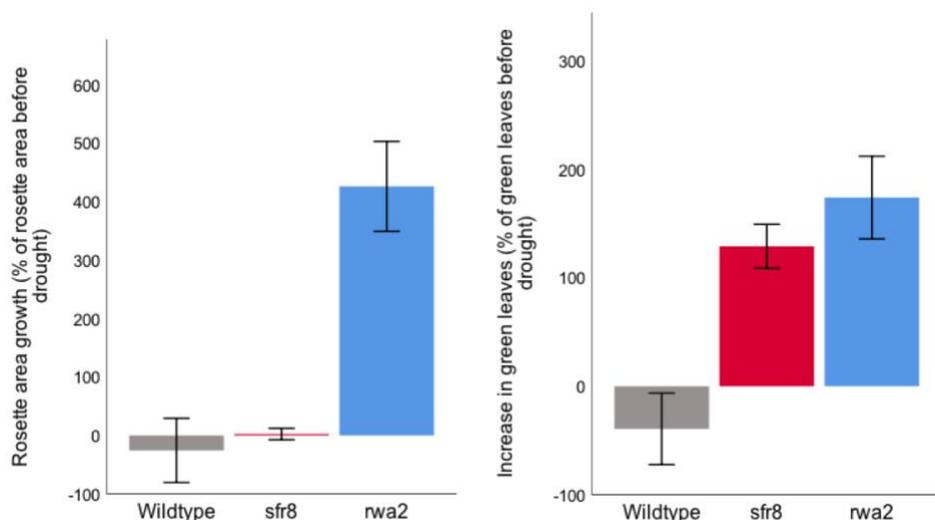
Figure 3.13.2: Plant growth of wildtype (grey), *sfr8* (red) and *rwa2* (blue) during the drought period in the preliminary experiment. Error bars mean ±1 standard error. n=3.

Therefore, *rwa2* plants had the best survival rate after the 17-day drought period; the only plant to not wilt during the drought was *rwa2* genotype and the *rwa2* plants grew the most of all genotypes both in terms of rosette area and leaf number. Wildtype plants had the worst survival rate and the plants did not grow in rosette area or leaf number during the 17-day drought period. *sfr8* plants had intermediate

survival; all *sfr8* plants survived but had all wilted by the end of the period and did not grow in rosette area.

3.5.2 19-day Drought Period

The drought tolerance assay was repeated with a longer drought period, as not all plants had wilted by the end of the drought period, so the drought stress was made more severe.

All plants started out healthy before the drought period started, albeit there were some size differences amongst the plants (Figure 3.13.3). Wildtype plants had the largest rosette area on average at 1456.47 mm^2 (±144.76). *sfr8* plants had the smallest rosette area before the drought period, almost half that of wildtype at 758.30 mm^2 (±97.47) and *rwa2* had a rosette area of 1179.13 mm^2 (±162.96). There is a statistically significant difference between the genotypes for the rosette area before the drought period (Kruskal Wallis, X^2_2=10.524, p=0.005). *sfr8* had a significantly smaller rosette area before the drought than wildtype and *rwa2* (Mann Whitney U-test; U=56.0, p=0.002; U=91.0, p=0.049). Whereas, wildtype and *rwa2* had statistically the same rosette area (Mann Whitney U-test; U=126.0, p=0.074). Despite size differences, the plants were all that the same developmental stage as they all had statistically the same number of leaves (Kruskal Wallis, X^2_2=3.838, p=0.147).
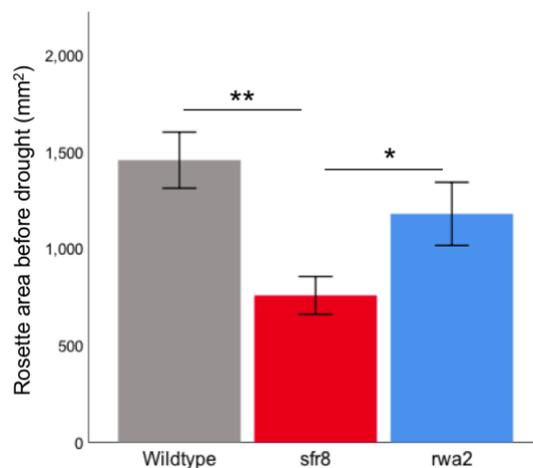
Figure 3.13.3: Mean rosette area of wildtype (grey, n=19), *sfr8* (red, n=15) and *rwa2* (blue, n=20) before the drought period. Error bars show ±1 standard error. * indicates p<0.05; ** indicates p<0.01.
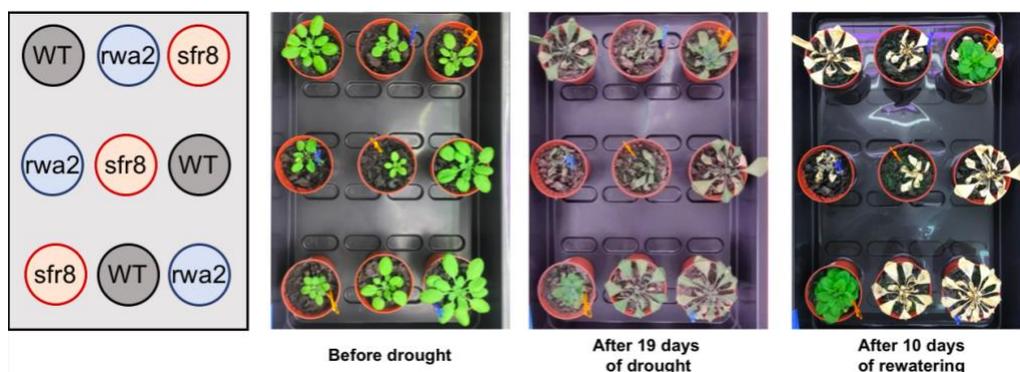
Figure 3.13.4: Example of a tray including 3 wildtype plants, 3 *sfr8* plants and 3 *rwa2* plants throughout the drought tolerance assay.

Figure 3.13.5: Wildtype (left), *sfr8* (middle) and *rwa2* (right) after the 19-day drought period. Plants were rearranged at the end of the experiment to present all plants of the same genotype together, with the surviving plants placed at the bottom of the image together. During the experiment the genotypes were placed in a random arrangement like shown in Figure 3.13.4 and arranged by genotype for photographing.

After the 19-day drought period, all wildtype and *rwa2* plants had wilted, but 13.33% (2 out of 15) of *sfr8* had not wilted. One of these *sfr8* plants which did not wilt is shown in Figure 3.13.4 in the bottom left corner. After 10-days of rewatering, one wildtype plant had survived, six *sfr8* plants survived and two *rwa2* plants survived, giving respective survival rates of 5.26%, 40% and 10% respectively (Figure 3.13.5).

Wildtype also had the least growth during the 19-day drought period; rosette area on average decreased by 87.34% (±12.66) and leaf number on average decreased by 91.50% (±5.67) (Figure 3.13.6). *sfr8* was the genotype which grew the most during the 19-day drought period; rosette area on average increased by 34.71% (±76.53), but leaf number actually decreased by 14.02% (±26.58). *rwa2* had intermediate growth, decreasing 40.13% (±48.76) in rosette area and 50.55% (±33.35) in leaf number. There was a statistically significant difference between the genotypes for rosette area growth and change in leaf number (Kruskal Wallis; X^2_2=7.426, p=0.024; X^2_2=8.850, p=0.012). *rwa2* had statistically the same growth as wildtype (Mann Whitney U-test; rosette area growth – U=181.0, p=0.813; change in leaf number - U=169.5, p=0.569) and *sfr8* (Mann Whitney U-test; rosette area growth – U=108.0, p=0.169; change in leaf number - U=98.0, p=0.086). *sfr8* grew more than wildtype in terms of leaf number (Mann Whitney U-test; U=72.0, p=0.014), but had statistically the same rosette area growth as wildtype (Mann Whitney U-test, U=94.0, p=0.096).

However, when including only plants that survived, *rwa2* had the greatest growth, increasing in rosette area by 498.66% (±359.38) and leaf number by 328.57% (±221.43) (Figure 3.13.6). *sfr8* rosette growth was less than half that of *rwa2* at 236.77% (±165.50) and *sfr8* increase in leaf number was less than a third that of *rwa2* at 98.21% (±25.88). Wildtype growth was much less than *sfr8* and *rwa2*, increasing in rosette area only 140.56% and not increasing in leaf number at all. A Kruskal Wallis test did not find a significant

difference between the genotypes for growth if surviving after the drought period (rosette area growth – $X^2_2=1.089$, p=0.580; change in leaf number – $X^2_2=3.854$, p=0.146).
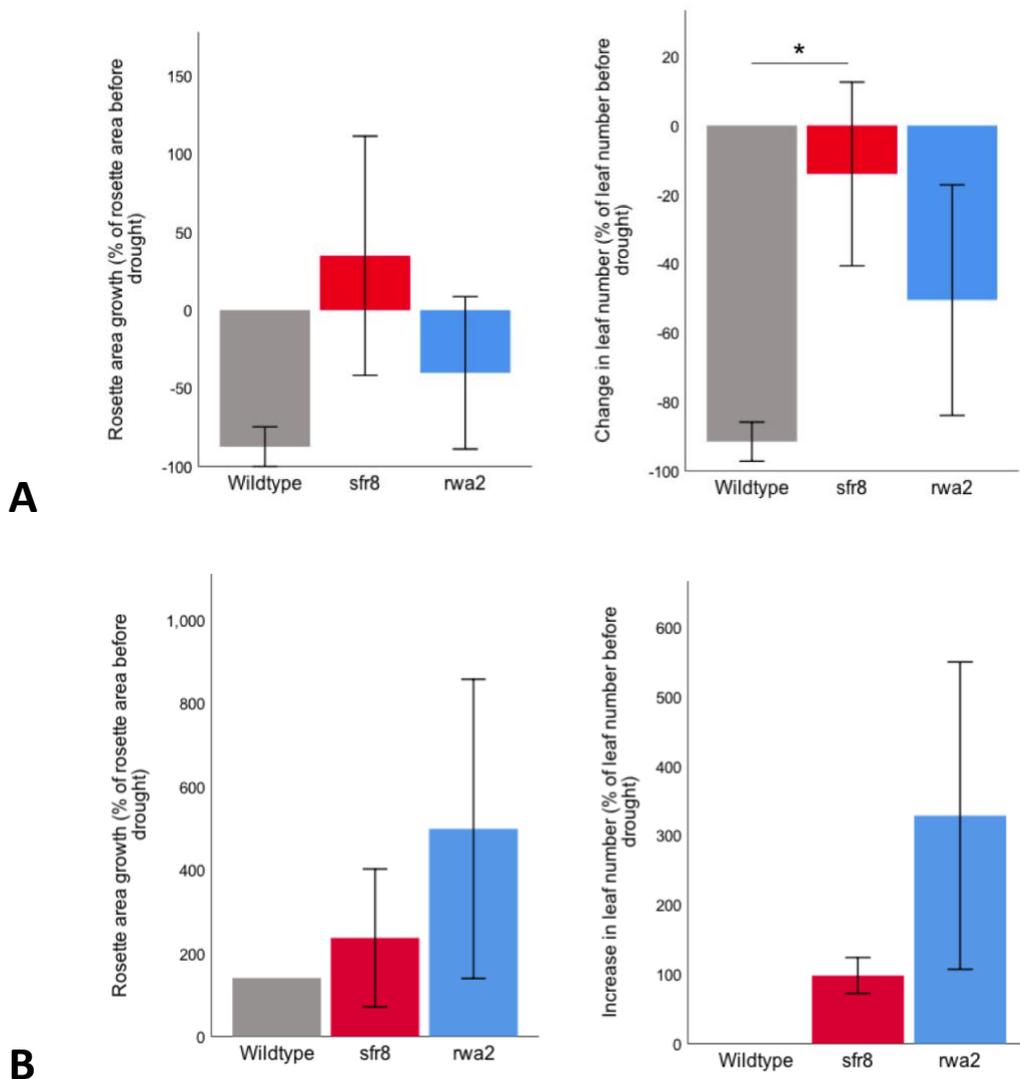
Figure 3.13.6: Plant growth during the 19-day drought period. **A:** Overall mean growth of rosette area and leaf number. Wildtype (grey, n=19), *sfr8* (red, n=15) and *rwa2* (blue, n=20). **B:** Mean growth excluding plants that did not survive the drought period. Wildtype (grey, n=1), *sfr8* (red, n=6) and *rwa2* (blue, n=2). Error bars mean ±1 standard error. * indicates p<0.05.

In summary, *sfr8* had the best drought tolerance during the 19-day drought period, as 40% of *sfr8* plants survived. Wildtype had the worst drought tolerance, like the 17-day drought period, as only 5.26% of wildtype plants survived. Unlike the 17-day drought period, *rwa2* had a worse survival rate than *sfr8*, but maintained a higher survival rate than wildtype. When the *rwa2* plants survived, they grew much more than *sfr8* plants in both rosette area and leaf number. Therefore, *sfr8* and *rwa2* have drought tolerance above wildtype levels under different severities of drought stress.

3.6 Root Length Assay

The root length of the genotypes was measured because the roots are involved in sensing and responding to drought stress, especially soil drying drought stress (Buckley, 2019), the type inflicted on mature plants in the thermal imaging and drought tolerance assay (Section 3.5). Therefore, if the genotypes have

differences in root length, it could explain the survival and growth differences between the genotypes seen in the drought tolerance assay.
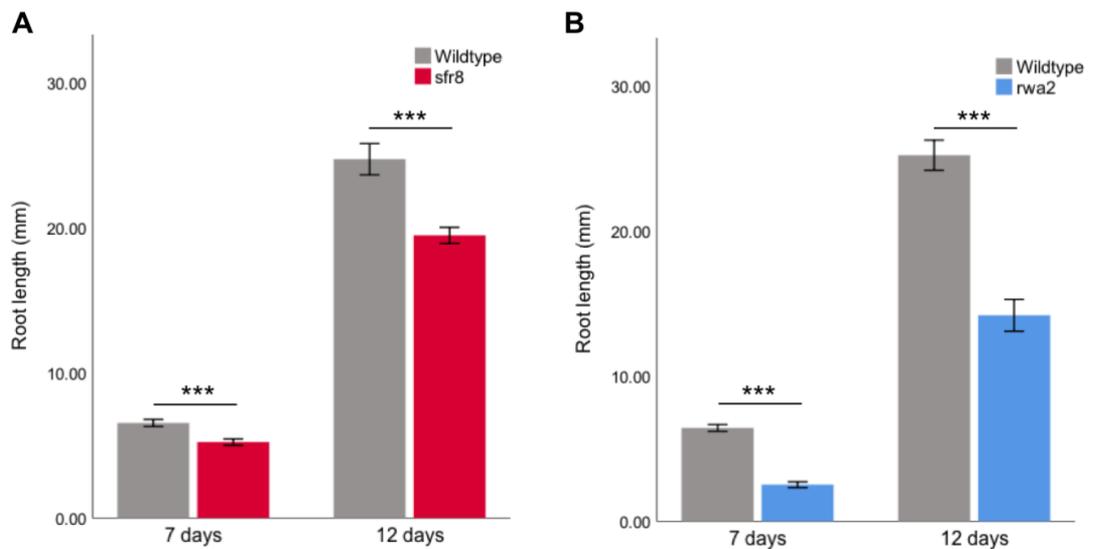
Figure 3.14.1: Mean root length of seedlings 7 and 12 days old. **A:** Wildtype (n=61) and *sfr8* (n=67) seedlings. **B:** Wildtype (n=61) and *rwa2* (n=50) seedlings. Error bars show ±1 standard error. *** means p<0.001.

When grown with *sfr8* seedlings, wildtype seedlings had a root length of 6.55mm (±0.24) at 7 days old and 24.74mm (±1.09) at 12 days old (Figure 3.14.1.A). *sfr8* seedlings had smaller root lengths at both ages, which were 5.23mm (±0.21) at 7 days old and 19.49mm (±0.56) at 12 days old. The root length of wildtype seedlings is significantly longer than that of *sfr8* seedlings at both ages (Mann Whitney U-test; 7 days – U=1219.5, p<0.001; 12 days – U=1181.5, p<0.001). When grown with *rwa2* seedlings, wildtype seedlings had a root length of 6.43mm (±0.23) at 7 days old and 25.24mm (±1.04) at 12 days old, which was similar to the root length of wildtype seedlings when grown with *sfr8* (Figure 13.14.1.B). Like *sfr8*, *rwa2* seedlings had a root length smaller than wildtype at both ages, with a length of 2.52mm (±0.20) at 7 days old and 14.20mm (±1.10) at 12 days old. Wildtype seedlings have a root length which is significantly longer than *rwa2* seedlings at both ages (Mann Whitney U-test; 7 days - U=157.0, p<0.001; 12 days – U=539.5, p<0.001).

Wildtype and *sfr8* had very similar root growth when grown on the same plate; wildtype root length increased by 309.45% (±22.83) and *sfr8* root length increased by 309.67% (±18.83) (Figure 3.14.2). There is no statistically significant difference between wildtype and *sfr8* for root growth between 7 and 12 days old (Mann Whitney U-test, U=2017.0, p=0.899). When grown with *rwa2* seedlings, wildtype roots grew in length by 316.41% (±21.80), which is similar to wildtype root growth when grown with *sfr8* seedlings. However, *rwa2* had much higher root growth between 7 and 12 days old at 528.64% (±43.30) and this difference in root growth between wildtype and *rwa2* was statistically significant (Mann Whitney U-test, U=837.0, p<0.001).
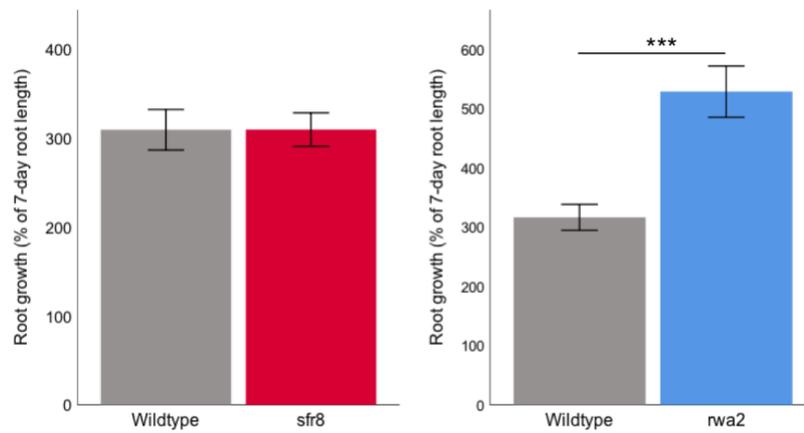
Figure 3.14.2: Mean seedling root growth between 7 and 12 days old. **A:** Wildtype (n=61) and *sfr8* (n=67) seedlings. **B:** Wildtype (n=61) and *rwa2* (n=50) seedlings. Error bars show ±1 standard error. *** means p<0.001.

In summary, *sfr8* had smaller roots than wildtype as seedlings and reduced root growth, implicating decreased root size in mature plants. Similarly, *rwa2* had smaller roots than wildtype but had much higher growth between 7 and 12 days old, suggesting root size may reach wildtype size in mature plants.

3.7 Results Summary

To conclude, no other cell wall mutant tested had a water loss defect similar to *sfr8*. Excluding *sfr8,* out of the remaining cell wall mutants tested in the leaf drying assays, only four mutants had a significantly different water loss rate than wildtype, these were: *pmr5*, a pectin abundance and pectin crosslinking mutant; *rwa2*, a pectin crosslinking and xyloglucan mutant; *agp8*, a mechanical strength mutant; and *prc1*, a mechanical strength mutant. *rwa2* had the most noticeable difference in water loss rate to wildtype of the mutants. In the thermal imaging experiment, *rwa2* plants were the only mutants that consistently had a similar stomatal conductance to *sfr8*, and a higher stomatal conductance than wildtype, suggesting that *rwa2* plants may have a stomatal function defect similar to *sfr8*. In the IRGA experiment, *sfr8* and *rwa2* had significantly higher mean stomatal conductance values than wildtype regardless of the CO_2 concentration. *sfr8* had a significantly smaller and significantly slower changes in stomatal conductance than wildtype and *rwa2*. Based on the leaf impressions, *sfr8* had larger stomatal size, lower stomatal density and lower aperture than wildtype and *rwa2*. While, *rwa2* had a significantly larger stomatal size and a significantly lower aperture than wildtype. Both *sfr8* and *rwa2* mutant plants had better drought tolerance than wildtype; *rwa2* plants wilted the least and grew the most during the 17-day drought period, and *sfr8* plants had the best survival during the 19-day drought period. On top of the morphological differences with the stomata, *sfr8* and *rwa2* also have shorter roots than wildtype as both 7- and 12-day-old seedlings. However, between days 7 and 12 *rwa2* roots had approximately two-thirds more growth than wildtype did, so there is potential for *rwa2* roots to equal wildtype in mature plants.

Chapter 4: Discussion

4.1 Which component of *sfr8* cell wall causes the higher transpiration rate?

Preliminary research indicated *sfr8* had a water loss defect, which was attributed to transpiration through the stomata due to the volume of water lost and as stomata are the primary route of leaf water loss (Panter, 2018). The first part of the project intended to discover which defective component of *sfr8* cell wall causes the higher transpiration rate. The proposed hypotheses were that the defect of *sfr8* in general fucosylation (hypothesis 1), pectin abundance (hypotheses 2), pectin modification (hypothesis 3), xyloglucan (hypothesis 4) or mechanical strength (hypothesis 5) causes the higher transpiration rate through the stomata when measured with a leaf drying assay. It is concluded that pectin modification is the only tested factor which causes a higher transpiration rate in its mutants and therefore, it is likely pectin crosslinking, a factor dependent on pectin modification, causes the water loss defect in *sfr8.*

4.1.1 Does fucosylation of single or multiple cell wall components affect leaf water loss?

sfr8 lacks GDP-D-mannose-4,6-dehydratase, which is involved in the synthesis of GDP-L-fucose, and as a consequence, lacks fucosylation of several cell wall components (Panter et al., 2019). To identify whether the transpiration defect of *sfr8* is due to lack of fucosylation of specific cell wall components or due to the general lack of fucosylation across cell wall components, four mutants lacking fucosylation across specific cell wall components were tested. The mutants, *mur2, fut4, msr1* and *cgl1*, did not lose water more quickly than wildtype in leaf drying assays (Section 3.1.1). Through the absence of a fucosyltransferase, *mur2* lacks fucosylated xyloglucan (Vanzin et al., 2002) and *fut4* lacks fucosylated arabinogalactans (Tryfona et al., 2014) Additionally, *msr1* lacks an O-fucosyltransferase involved in the synthesis of cell wall components that incorporate the sugar mannose, including mannans, galactomannans and glucomananns (Wang et al., 2013b). Moreover, *cgl1* has an inability to process N-linked glycans, a fucosylated component of cell wall, and therefore, like *fut4,* lacks fucosylated glycoproteins (Frank et al., 2008). Based on the mutant phenotypes and the leaf drying assay data, general fucosylation of xyloglucan and glycoproteins, as well as the synthesis of mannose, are not contributing factors of the water loss defect observed in *sfr8*. Therefore, hypothesis 1, that general fucosylation causes the water loss defect in *sfr8*, is rejected.

mur2, fut4 and *cgl1* have been used in a previous study investigating the effect of fucosylation on plant immunity (Zhang et al., 2019b). The mutants were inoculated with *Pseudomonas syringae* (DC3118), a foliar bacterial plant pathogen that enters the plant primarily through the stomata and other natural openings, and also produces coronatine, a virulence factor that actively opens the stomata (Melotto et al., 2008). When inoculated with *P. syringae*, *mur2* and *fut4* had wildtype levels of bacterial growth, indicating normal apoplastic and stomatal defences (Zhang et al., 2019b). The wildtype water loss rate

found in this thesis corroborates the normal stomatal closure response of Zhang (2019) and suggests *mur2* and *fut4* do not have a problem with their transpiration rate nor stomatal dynamics. However, Zhang et al. (2019b) also found that a *cgl1* mutant had compromised stomatal defences to *P. syringae* infection; despite having equivalent stomatal apertures before infection, the stomatal aperture of *cgl1* was significantly higher than wildtype after inoculation with *P. syringae*, which indicates a compromised stomatal closure response. The transpiration rate, and inferred stomatal closure response, of *cgl1* observed in Section 3.1.1 is highly similar to wildtype, which contradicts the findings of Zhang *et al.* (2019). The differences between the experimental results of *cgl1* may be because although *P. syringae* infection and leaf excision both involve stomatal closure responses, they are different stresses that involve different sensing, signalling and stomatal response pathways. Therefore, *cgl1* may have an issue dealing with biotic stress, but has normal stomatal responses to water deficit stress.

Although there are no other experiments investigating any stomata-related phenotype of *msr1*, there is evidence that mannose is involved in a stomatal closure response (Zang et al., 2019). Mannan oligosaccharides that incorporate mannose are a danger-associated molecular pattern and can trigger stomatal closure when exogenously applied (Zang et al., 2019). The reverse of this observed phenotype would mean that the lack of the sugar mannose, like in *msr1*, could cause stomatal aperture to be larger than wildtype during closure signals, particularly closure signals associated with damage, such as herbivorous pathogens. However, there is no direct evidence of reduced mannose content effecting stomatal closure response to pathogens nor is there any evidence to suggest that the lack of mannose in *msr1* would affect stomatal closure in response to plant dehydration signals like leaf excision, which is consistent with the data in Section 3.1.1.

Overall, the supporting evidence upholds the conclusion that general fucosylation is not a factor that affects stomatal closure response nor the rate at which water is transpired through the stomata. *fut4* and *mur2* have a wildtype level of infection to a foliar bacterial plant pathogen that primarily enters through the stomata. *cgl1* had compromised stomatal defences in response to the same pathogen, indicating *cgl1* is defective in its response to pathogen-related closure signals specifically, which leaves the possibility that *cgl1* has wildtype response to desiccation-related stomatal closure signals as seen in the leaf drying assay. Finally, there is no report measuring the leaf transpiration rate or stomatal dynamics of *msr1* for comparison to the data present in this thesis. Therefore, based on the available evidence, it can be concluded that mutations in a range of cell wall fucosylation events do not result in the water loss defect observed in *sfr8* and therefore, the lack of general fucosylation events in *sfr8* are unlikely to affect transpiration through the stomata or stomatal dynamics.

4.1.2 Altered fucosylated pectin abundance is unlikely to cause *sfr8* water loss

sfr8 has a reduction in fucosylated pectin, which could cause the transpirational defect (O'Neill et al., 2001; Sechet et al., 2018). No pectin-specific transferase has been found as yet (Zhang et al., 2019b), therefore, the effect of reduced fucosylated pectin needs to be investigated in an indirect way. To test if

reduced fucosylated pectin can cause a water loss defect, mutants with altered pectin abundance were tested in a leaf drying assay. All mutants that had decreased pectin abundance, *gaut5, gaut6-1, gaut6-2* and *qul1,* had water loss rates similar to wildtype in the leaf drying assay (Section 3.1.2). GAUT5, GAUT6 and QUL1 are crucial for the synthesis of HG, the most abundant cell wall pectin, therefore, their respective mutants have reduced HG (Mohnen, 2008; Fuentes et al., 2010; Lund et al., 2020). The wildtype stomatal closure response of these pectin abundance mutants does not support hypothesis 2, that altered fucosylated pectin abundance results in a water loss defect, and the data suggests that it is not the reduction in fucosylated pectin abundance in *sfr8* that causes the water loss defect.

HG is not the domain of pectin that is fucosylated, RG-I and RG-II are instead (McNeil et al., 1984; Pabst et al., 2013). Thus, for testing this hypothesis, mutants in RG-I or RG-II abundance should be included in the leaf drying assay for comparison with *sfr8.* Such mutants include, RG-I:rhamnosyltransferases involved in RG-I synthesis (Takenaka et al., 2018), or RG-II SPECIFIC XYLOSYLTRANSFERASEs and GLUCURONYLTRANSFERASE 1, which are involved in RG-II synthesis (Iwai et al., 2002; Voragen et al., 2009). Furthermore, there is some evidence that *gaut* mutants, as well as reducing HG abundance, also decrease RG-I and RG-II abundance too. *gaut11, gaut13* and *gaut14* mutants have reduced abundance of xylose and rhamnose, which are sugars highly incorporated into RG-I, implicating reduced RG-I content (Caffall et al., 2009). On the other hand, there is also evidence that suggests *gaut* mutants increase the proportion of other pectins. *gaut6* mutants have higher xylose and rhamnose content compared to wildtype, suggesting the proportion of RG-I is increased to compensate a reduction in HG (Caffall et al., 2009). Two of the mutants tested, *gaut6-1* and *gaut6-2,* potentially have increased RG-I content and no difference in water loss with wildtype, suggesting altered abundance of other pectic domains does not affect transpiration either, but this is speculative. Moreover, arabinan side chains on RG-I are known to be associated with drought tolerance and maintaining cell wall flexibility, an important component for stomatal opening and closure (Moore et al., 2013). Therefore, an additional set of mutants could also have been included in the leaf drying assay that have reduced arabinan side chains, such as the arabinosyltransferases, ARABINAN DEFICIENT1 and 2 (ARAD1 and ARAD2), involved in arabinan synthesis (Harholt et al., 2012). *arad1* mutants have already been included in a similar leaf drying assay; an *arad1* leaf was excised and weighed a similar amount to wildtype over time as they were left to dry (Harholt et al., 2006). Additional measurements of stomatal dynamics of *arad1* using microscopy showed no divergence from wildtype behaviour (Harholt et al., 2006). Therefore, the alteration to the abundance of arabinan side chains is unlikely to cause the water loss and stomatal defects of *sfr8.* The hypothesis of pectin abundance effecting transpiration could have been more rigorously tested with better chosen mutants, however, with the time constraints of the project it was not possible to test so many mutants.

Despite HG not being a pectic domain that is fucosylated, there is evidence HG is involved in normal stomatal dynamics. The wildtype level water loss rate of the reduced pectin mutants is in contrast to another mutant of reduced pectin content, *quasimodo1* (*qua1*). In a similar leaf drying assay to the one used in this project, *qua1* and wildtype leaves were excised from one-month old Arabidopsis plants

(Wassilewskija, Ws ecotype) and left to dry in ambient conditions. *qua1* leaves declined in mass much quicker than wildtype, which indicates a severe water loss defect in *qua1* mutants (Bouton et al., 2002). The rapid dehydration of *qua1* leaves implicates that reduced pectin abundance may cause a water loss defect, such as the one in *sfr8*, therefore, this is an avenue that needs to be explored more thoroughly.

The remaining mutant of altered pectin abundance, *pmr5*, is different from the other mutants as it has increased pectin content compared to wildtype (Vogel et al., 2004) and had an initial water loss rate significantly quicker than wildtype (Figure 3.3.4). Together, the data suggests that increased pectin content may have an impact on the speed of stomatal closure or the detection of stomatal closure signals. However, once viewed under an infra-red thermal-imaging camera, there was no noticeable difference between *pmr5* and wildtype in temperature and so there was no difference in evaporative cooling nor stomatal conductance. Therefore, confirming that hypothesis 2, that altered pectin abundance is a contributing factor to the water loss rate of *sfr8*, is unlikely to be correct, as already shown with the decreased pectin content mutants. This conclusion is confirmed by another experiment measuring the stomatal conductance of *pmr5* and a similar powdery mildew-resistant mutant *pmr6* which also has an increase in pectin content (Vogel et al., 2002; Woolfenden et al., 2017). Both *pmr5* and *pmr6* had statistically equivalent stomatal conductance to wildtype before and after the application of fusicoccin, a fungal toxin that triggers stomatal opening (Turner and Graniti, 1969; Woolfenden et al., 2017).

To summarise, increased pectin abundance can be confidently ruled out as a cause of increased transpiration through the stomata because of the leaf drying and stomatal conductance data of *pmr5* in this project, but also because of the complimentary stomatal conductance data of *pmr5* and *pmr6* from Woolfenden et al. (2017). Similarly, decreased pectin abundance is unlikely to have an impact on transpiration rate through the stomata, indicating pectin abundance has little to no correlation with transpiration. Moreover, even though *qua1* has a higher transpiration rate than wildtype, the pectin abundance mutation of *qua1* is not specific to the pectic domains that are fucosylated, RG-I and RG-II, which would be affected in *sfr8* (Bouton et al., 2002). Therefore, the higher transpiration rate of *qua1* is likely to be caused by a factor unrelated to *sfr8*.

4.1.3 Some xyloglucan mutants have little similarity to *sfr8*

Xyloglucan is a cell wall component that is fucosylated and has a different structure in *sfr8*, suggesting lack of fucosylated xyloglucan may cause the water loss defect in *sfr8* (Zablackis et al., 1996a). However, the xyloglucan-deficient mutant, *xxt1 xxt2*, lost water at an equivalent rate to wildtype (Section 3.1.4). Additionally, the xyloglucan-specific fucosyltransferase-mutant, *mur2*, has a wildtype rate of transpiration (Section 3.1.1). *mur2* offers a great comparison to *sfr8* as the lack of fucosylation in *mur2* is limited to xyloglucan and no other cell wall components, therefore, the effect of xyloglucan fucosylation on water loss can be observed directly. The water loss phenotype of these xyloglucan-defective mutants implicates that a perturbation to xyloglucan is highly unlikely to have an impact on transpiration through the

stomata. Thus, it is unlikely that the defects in xyloglucan fucosylation causes quicker loss of water from the leaf in *sfr8*.

The data published in this thesis, that xyloglucan defects are unlikely to cause transpiration defects similar to *sfr8*, may be in agreement with the published literature. *xxt1 xxt2* has smaller stomatal aperture than wildtype immediately before and up to 2.5 hours after fusicoccin-induced stomatal opening and ABA-induced stomatal closure (Rui and Anderson, 2016). Stomatal aperture is a main determinant of stomatal conductance, with a reduced stomatal aperture causing a decrease in stomatal conductance (Fanourakis et al., 2015). Therefore, the smaller aperture indicates *xxt1 xxt2* may have reduced stomatal conductance compared to wildtype in both open and closed states, which implies after leaf excision, a closing signal, *xxt1 xxt2* may have lower stomatal conductance and lose water slower than wildtype. Additionally, stomatal size of *xxt1 xxt2* was found to be smaller than wildtype, which was not found to cause the smaller stomatal aperture (Rui and Anderson, 2016). Instead the authors attributed the smaller aperture size to the role of xyloglucan in allowing longitudinal expansion during stomatal movement (Rui and Anderson, 2016). Similarly, *xxt1 xxt2* has been found to have smaller stomatal pore widths than wildtype in both open and closed states and proposed that the loss of xyloglucan causes anisotropic effect on wall stiffening (Yi et al., 2018). Sufficient xyloglucan is necessary for wildtype stomatal aperture, and the lack of xyloglucan possibly results in reduced stomatal conductance compared to wildtype, a phenotype opposite to *sfr8*. Therefore, it is unlikely the defects in xyloglucan that *sfr8* has causes the water loss defect.

In the leaf drying assays in this thesis, *xxt1 xxt2* has a statistically equivalent water loss rate to wildtype and so most likely have similar transpiration and stomatal conductance as wildtype, which contradicts the reduced stomatal conductance implicated by the results of Rui and Anderson (2016) and Yi et al. (2018). The positive correlation between stomatal aperture and stomatal conductance is only true if the other factors that affect stomatal conductance, such as stomatal density, stomatal pore depth and diffusion coefficient, stay the same as stomatal aperture changes (Fanourakis et al., 2015). Therefore, in the leaf drying assay, *xxt1 xxt2* may have the same water loss rate as wildtype despite a smaller aperture due to an increased stomatal density, increased diffusion coefficient or decreased pore depth. The growth and experimental conditions used in this thesis may result in alterations to these factors, which means the smaller stomatal aperture of *xxt1 xxt2* did not result in a reduction of stomatal conductance. Although *xxt1 xxt2* has been observed to have the same stomatal density as wildtype in some conditions (Rui and Anderson, 2016), this may not be the case under the growth conditions used in this thesis. The stomatal density and aperture of *xxt1 xxt2* used in this thesis could be measured by leaf surface impressions as in Section 2.5.1, to confirm if there is a difference to wildtype or not.

As previously discussed in Section 4.1, *mur2* has wildtype water loss rate during the leaf drying assay, indicating that *mur2* has wildtype stomatal dynamics. This is in agreement with published data that *mur2* has wildtype stomatal dynamics and responds normally to pathogen infection (Zhang et al., 2019b), a stomatal closure signal like leaf excision is. *mur2* and *sfr8* show high similarity in their xyloglucan mutation,

both lack fucosylation of xyloglucan. However, the two differ in that *mur2* has wildtype water loss rate following leaf excision, whereas *sfr8* has a significantly quicker water loss. Therefore, as with comparison to *xxt1 xxt2*, it is unlikely the lack of fucosylated xyloglucan in *sfr8* causes the water loss defect.

In summary, there is strong evidence from the leaf drying assays of *mur2* and *xxt1 xxt2* and the supporting literature that aberrant xyloglucan causes increased transpiration through the stomata. However, another mutant with a defect in xyloglucan, *rwa2*, did have a water loss defect dissimilar to wildtype. *rwa2* also has a defect in another cell wall component, which will be discussed later. The strong evidence of wildtype stomatal dynamics in *mur2*, a mutant that has a similar effect on xyloglucan fucosylation to *sfr8*, can be used to conclude it is not the different modification of xyloglucan in *rwa2* that causes the water loss difference, instead potentially the other component causes this.

4.1.4 Mechanical strength is unlikely to affect transpiration through the stomata

Mechanical strength is important for guard cell walls to withstand the turgor pressure needed to open and close the stomata (Shope et al., 2003). Mechanical strength is reduced in mutants lacking *MUR1* (Reiter et al., 1993; Ryden et al., 2003), therefore, a reduction in the strength of guard cell walls could cause aberrant stomatal dynamics and result in higher transpiration through the stomata in *sfr8*. In the leaf drying assay, two cell wall mutants with reduced mechanical strength, *agp8* and *prc1,* had significantly faster water loss than wildtype in the first hour after excision, while also having significantly slower water loss than *sfr8* (Figure 3.6.2). The thermal imaging data showed that the stomatal conductance of *agp8* and *prc1* tended to be lower than *sfr8* and was similar to wildtype (Figure 3.9 and 3.10). The data suggests that mechanical strength is not a causal factor of the increased transpiration of *sfr8.* Furthermore, another mutant with reduced mechanical strength was used in the leaf drying assays, *xxt1 xxt2*. As previously discussed, *xxt1 xxt2* had water loss rate so similar to wildtype and different to *sfr8* that it was not used in any further measure of stomatal dynamics, which adds more support to the argument that the water loss rate of *sfr8* is not due to its reduced mechanical strength.

There is little supporting literature about *agp8* mutants and even less specifically about *agp8* stomatal dynamics or related measurements, such as water loss rate or infection susceptibility. Thus, a confident conclusion about the transpiration rate and stomatal conductance of *agp8* observed in this experiment cannot be achieved. However, there is supporting evidence for *prc1* and *xxt1 xxt2*. Further substantiating the wildtype stomatal conductance of mechanical strength mutants*,* in another experiment on Arabidopsis plants, *prc1,* a mechanical strength mutant defective in cellulose synthesis, had statistically equivalent stomatal aperture as wildtype (Col-0) following light treatment, a stomatal opening signal (Rui and Anderson, 2016). Therefore, despite mechanical strength being an important trait for guard cells in withstanding high turgor pressure and allowing reversible stomatal movements (Hunt et al., 2017; Rui et al., 2018), the evidence suggests that mutants whose cell walls are weaker than wildtype display similar stomatal dynamics to wildtype regardless. In the same study, *xxt1 xxt2* was found to have smaller stomatal aperture than wildtype in both open and closed states (Rui and Anderson, 2016), which as previously

discussed implicates a slower transpiration rate than wildtype and suggests that mechanical strength is not a causal factor of *sfr8* transpiration rate. There is the possibility that by coincidence all the mechanical strength mutants chosen in this project do not show altered stomatal dynamics similar to *sfr8*, where other mechanical strength mutants would. As the mechanical strength mutants chosen are affected in different aspects of cell wall composition, xyloglucan, cellulose and arabinogalactan protein abundance, yet they all share weaker mechanical strength and similarity to wildtype in water loss rate or stomatal conductance, this suggests that mechanical strength is not a contributing factor to the faster water loss of *sfr8*. Therefore, hypothesis 5, that reduced mechanical strength causes the higher water loss rate of *sfr8*, is unlikely to be true.

4.1.5 Pectin modification may cause a water loss defect

sfr8 has a reduction in RG-II dimerisation, a type of pectin crosslinking that is formed of a borate-diol ester (O'Neill et al., 2001; Sechet et al., 2018). Other pectin crosslinking mutants include pectin modification mutants with aberrant methyl-esterification and O-acetylation of HG, as altered esterification effects the formation of HG Ca^{2+} crosslinks (Levesque-Tremblay et al., 2015). Pectin modification mutants were used to test the hypothesis that the reduction in pectin crosslinking of *sfr8* causes the transpirational defect. There is some variation amongst the pectin modification mutants in the leaf drying assay. *pme34*, a mutant in pectin methyl-esterification, had a water loss rate similar to wildtype, whereas, *rwa2*, a mutant in pectin and xyloglucan O-acetylation, had a water loss rate significantly greater than wildtype (Figure 3.4.2). Furthermore, *pmr5*, a mutant in both pectin modification and pectin abundance, has an initial water loss rate significantly greater than wildtype (Figure 3.3.2), as discussed in Section 4.1.2. The data from the leaf drying assay suggests that some specific pectin modifications do have an impact on leaf transpiration, which may occur through the stomata.

The results of *pme34* in the leaf drying assay are contradicted by a similar published measure of transpiration rate in which excised *pme34* leaves had lost significantly more %mass than wildtype (Col-0) at both 1 and 2 hours after excision (Huang et al., 2017). However, with heat treatments of 37°C for 1 hour and 44°C for 30 mins, *pme34* had a slower transpiration rate from excised leaves than wildtype (Huang et al., 2017), suggesting that the results of the leaf drying assay depend upon the prior growth conditions. The results in this project may differ to those in Huang's (2017) work because of different temperatures for growth and different ambient conditions during the leaf drying assay. Moreover, Huang (2017) also found that the stomatal aperture of *pme34* was larger than that of wildtype from 0-40 mins after a heat stress treatment and significantly larger 1 hour after the heat stress treatment, which correlates with higher transpiration rate after the same heat shock treatments. It was concluded that PME34 regulates stomatal movements downstream of ABA during heat stress to limit stomatal opening (Huang et al., 2017). Therefore, a transpiration phenotype dissimilar to wildtype was not observed in this thesis because the stomatal closure signal was desiccation-related rather than heat stress.

Moreover, a similar guard cell-localised pectin methylesterase, PME6, is involved in limiting water loss from detached leaves. A leaf drying assay was performed on *stomatal carpenter1, scap1*, a loss-of-function mutant with a transposon inserted into PME6. *scap1* lost over 40% of its leaf fresh weight within an hour of excision from the plant, a value more than double the water loss of wildtype in the same period (Negi et al., 2013). The water loss rate of *scap1* is highly similar to the leaves of *sfr8*, which lost 40-60% of their fresh weight within the first hour following removal from the plant (Section 3.1). The water loss rate of *scap1* is also greater in the first hour than *rwa2*, which only lost less than 30% of its fresh weight (Figure 3.4.1). However, it is difficult to compare values between leaf drying assays as the results depend heavily on environmental conditions of the experimental location, hence the large range of water loss that *sfr8* displays. Furthermore, in a similar experiment to the thermal imaging using the infra-red camera, *pme6* had a lower temperature than wildtype after a water-withheld period of 29 days, indicating more evaporative cooling is occurring, so the degree of stomatal openness is larger than wildtype (Amsbury et al., 2016). This is a phenotype similar to *rwa2* and *sfr8*, which were cooler than wildtype at several points during the water-withheld period lasting 14 - 23 days. Similarly under water stress from incubation in a high concentration of mannitol, an osmoticum which exerts osmotic pressure on plants, the stomatal pore area of *pme6* is significantly higher than wildtype, suggesting impaired stomatal dynamics in response to osmotic stress (Amsbury et al., 2016). Therefore, mutants lacking *PME6* behave similarly to *sfr8* in both their water loss rate and stomatal aperture as detected from thermal imaging, as well as having aberrant stomatal dynamics under water stress (Negi et al., 2013; Amsbury et al., 2016). As a result, pectin methyl-esterification cannot be completely disregarded as a cause of *sfr8* water loss rate and aberrant stomatal dynamics due to the leaf drying assay results of *pme34*.

Moving on from pectin methyl-esterification, defective pectin acetylation also possibly causes a transpirational defect. In a similar leaf drying experiment by Nafisi et al. (2015), *rwa2* had a water loss rate higher to wildtype (Col-0) and the water loss pattern of *rwa2* is consistent with that observed in Figure 3.4.1. Additionally, transpiration rate of *rwa2* following leaf excision is significantly higher than wildtype after 1-4 hours and 4-8 hours since leaf removal (Nafisi et al., 2015). Similarly, *rwa2* has a significantly higher transpiration rate than wildtype when measured by gas exchange analysis (Nafisi et al., 2015). Therefore, the results of the leaf drying assay of *rwa2* are supported by published literature, which in turn supports the idea that plants with defective pectin acetylation have higher water loss. Based on leaf drying assay data of *pme6* and *rwa2*, there is an indication pectin modification by methyl- and O-acetyl-esters and thus pectin crosslinking has an impact on the transpiration rate of excised leaves. Therefore, *sfr8*, with its reduced pectin crosslinking, may have a higher transpiration rate than wildtype may be due to this reduced pectin crosslinking.

Despite the supporting evidence of *rwa2*, the other mutant in pectin modification, *pmr5*, did not have a difference in stomatal conductance to wildtype when observed with an infra-red thermal imaging camera (Figure 3.7) and lacks support from published literature. The stomatal conductance of *pmr5* and related mutant *pmr6* is statistically the same as wildtype in ambient conditions and following application of fusicoccin (Woolfenden et al., 2017). Both *pmr5* and *pmr6* have decreased pectin methyl-esterification

and O-acetylation, the opposite phenotype to *pme6* and *pme34*, which have increased pectin methyl-esterification (Vogel et al., 2004; Amsbury et al., 2016; Huang et al., 2017). Furthermore, as pectin crosslinking between HG domains depends on the de-esterification, loss of methyl- and O-acetyl-esters, of HG, *pmr5* has at least wildtype levels of pectin crosslinking, if not greater, whereas, *sfr8* has decreased pectin crosslinking (O'Neill et al., 2001; Levesque-Tremblay et al., 2015). Therefore, although both *sfr8* and *pmr5* have defects in pectin composition, only *sfr8* has reduced pectin crosslinking. The wildtype stomatal conductance of *pmr5*, in comparison to the higher stomatal conductance of *sfr8* in Figure 3.7, is in agreement that mutants with reduced pectin crosslinking have higher stomatal conductance compared to mutants with greater crosslinking. Additionally, the transpiration rate of *sfr8* is significantly different to *pmr5* at all times throughout the leaf drying assay, indicating that mutants with reduced pectin crosslinking have higher transpiration rates. Therefore, the transpiration and stomatal conductance of *pmr5* supports the conclusion that the water loss defect of *sfr8* could be due to pectin crosslinking, rather than a general effect of pectin modification.

In summary, pectin modification and pectin crosslinking contribute to the higher transpiration rate of *sfr8*. *pme34* does not show a higher transpiration rate following leaf excision, but does exhibit altered stomatal dynamics in response to heat stress (Huang et al., 2017). The author's suggested that the larger stomatal aperture than wildtype under heat stress is due to the reduction in pectin crosslinking weakening the mechanical strength of guard cell walls, which results in cell walls to withstand the turgor pressure necessary to close the stomata (Huang et al., 2017). Therefore, de-esterification of pectin can affect stomatal dynamics under heat stress. Moreover, *pme6* with reduced de-methyl-esterification of guard cell wall pectin has a similar water loss rate following leaf excision and temperature as measured with thermal imaging to *sfr8*, which further implicates pectin de-methyl-esterification in the higher transpiration rate of *sfr8* (Negi et al., 2013; Amsbury et al., 2016). Additionally, *rwa2* has reduced O-acetylation of pectin and has significantly higher water loss rate than wildtype following leaf excision and when measured with a gas exchange analyser, highlighting that O-acetylation of pectin is just as important as methylesterification in pectin crosslinking and its effect on transpiration rate (Nafisi et al., 2015). Finally, *pmr5*, a mutant with decreased esterification of pectin and an increase in pectin crosslinking, did exhibit a higher transpiration rate than wildtype, but had wildtype stomatal conductance (Woolfenden et al., 2017). Therefore, not all pectin modification mutants have a defect in transpiration, only specific mutants with a reduction in pectin crosslinking exhibit an altered water loss rate.

Based on the results of the leaf drying assay and supporting literature, it is unlikely the higher transpiration of *sfr8* is caused by a defect in general fucosylation, pectin abundance, xyloglucan or mechanical strength. The results of the leaf drying assay of *rwa2* and similar experiments performed on *pme34, rwa2*, *pme6* and *pmr5*, indicate that the higher transpiration rate of *sfr8* may be caused by a reduction in pectin crosslinking.

4.2 *sfr8* differs from wildtype in stomatal conductance, size, density and aperture

Following the results of the leaf drying assay, various parameters of stomata were measured for wildtype, *sfr8* and *rwa2*, including, stomatal conductance, density, size and aperture. *sfr8* significantly differed from wildtype in all these stomatal measurements, indicating that some component as a result of the lack of fucose in *sfr8*, potentially reduced pectin crosslinking, causes limited stomatal dynamics as well as altered stomatal development. *rwa2* did not differ from wildtype in stomatal development or aperture, but did have significantly higher stomatal conductance values, which may not be due to a stomatal defect, instead a cell wall integrity phenotype may be the cause.

4.2.1 A possible connection between pectin crosslinking and stomatal dynamics

rwa2 has different stomatal conductance values to wildtype (Figure 3.11.1). At all concentrations of CO_2 tested, *rwa2* had significantly higher stomatal conductance than wildtype (Figure 3.11.2). However, the rate at which stomatal conductance changed and the average difference in stomatal conductance change when CO_2 concentration was increased or decreased was statistically the same as wildtype (Figure 3.11.3 & 3.11.5). This means that *rwa2* has the same capacity to change stomatal conductance and as quickly as wildtype but maintained a higher stomatal conductance than wildtype at all time points. Therefore, the IRGA data confirms the thermal imaging data that *rwa2* has higher stomatal conductance than wildtype and identifies that the higher transpiration rate of *rwa2* in the leaf drying is due to higher stomatal conductance. The higher stomatal conductance is confirmed by another study. Under ambient conditions of 400ppm CO_2, gas exchange analysis measured *rwa2* stomatal conductance to be 1.5 times bigger than wildtype, a significant difference (Nafisi et al., 2015). The results from the IRGA are highly similar; at 400ppm CO_2, *rwa2* stomatal conductance is 1.33 times bigger than wildtype, a highly significantly difference (Figure 3.11.2). However, the authors did not attribute the higher stomatal conductance and transpiration rate of *rwa2* to altered stomatal dynamics, instead, the damaged leaf cuticle was implicated. The reduced acetylation of pectin results in excess hydroxyl groups which were suggested to form atypical crosslinks with cutins, causing abnormal cuticle assembly (Nafisi et al., 2015). The impairment of leaf cuticle integrity meant 30% *rwa2* trichomes were collapsed, with many of the remaining trichomes being fragile (Nafisi et al., 2015).

sfr8 also has stomatal conductance values that are different to wildtype (Figure 3.11.1). Like *rwa2*, *sfr8* had an average stomatal conductance rate that was significantly higher than wildtype at all CO_2 concentrations (Figure 3.11.2). However, the stomatal conductance of *sfr8* and *rwa2* were significantly different from each other and vary depending on the CO_2 concentration. At the higher CO_2 concentrations of 400 and 1000ppm, *sfr8* stomatal conductance was significantly higher than *rwa2*, whereas at 50ppm of CO_2, the stomatal conductance of *rwa2* was much higher (Figure 3.11.2). The reason for this is because the stomatal conductance of *sfr8* does not change as much as *rwa2* nor as quickly, both the speed and amount of stomatal conductance change is significantly lower for *sfr8* (Figure 3.11.3 & 3.11.5). Similarly,

in comparison to wildtype, *sfr8* changes stomatal conductance significantly less and significantly more slowly when CO_2 concentration is changed (Figure 3.11.3 & 3.11.5). This suggests that *sfr8* has slow or limited stomatal dynamics, meaning the stomatal aperture of *sfr8* can reach wildtype levels but takes a much longer time than wildtype to do so or the stomatal aperture has a much more limited range. It is more likely that the latter is true, that *sfr8* has limited stomatal dynamics, because, the data from the IRGA is collected over a period of 2.5 hours in which the stomatal conductance values of *sfr8* reach a steady state by the end of each CO_2 concentration period. On the other hand, the stomatal conductance values of wildtype and *rwa2* are still changing every minute by the end of the 400ppm and 50ppm CO_2 concentration period (Figure 3.11.1). Therefore, *sfr8* reaches a steady state of stomatal conductance quicker than wildtype and *rwa2*, which implies that *sfr8* does not have slow stomatal dynamics, *sfr8* instead has limited stomatal dynamics because of a limited range of stomatal apertures. To ensure that *sfr8* does have limited stomatal dynamics rather than slow stomatal dynamics, the different CO_2 concentration periods could be run for longer until all genotypes have reached steady state stomatal conductance. Moreover, under steady state conditions, *sfr8* has a significantly smaller stomatal aperture than wildtype and *rwa2* (Figure 3.12.7), indicating the stomatal pore is less open under ambient conditions, which would be due to limited stomatal dynamics rather than slow stomatal dynamics. Limited stomatal dynamics would cause a higher transpiration rate; under closing signals due to leaf water loss, *sfr8* stomata would close less than wildtype stomata and so lose more water through the more open pore. This is shown in Figure 3.11.1, at ambient conditions (400ppm [CO_2]), like those in the leaf drying assay and thermal imaging, *sfr8* has a higher stomatal conductance than wildtype and so is exchanging more gas, including water vapour with the environment, meaning a higher transpiration rate.

sfr8 and *rwa2* both have higher stomatal conductance and transpiration; which adds to the conclusion that pectin crosslinking contributes to higher leaf water loss. However, the two differ from wildtype in different ways; *rwa2* has higher stomatal conductance regardless of CO_2 concentration due to abnormal cuticle development and *sfr8* has limited stomatal dynamics due to having a more limited range of stomatal apertures. Therefore, it could be by coincidence that two pectin crosslinking mutants share higher transpiration rates without the problem being caused by pectin crosslinking. There is further evidence from another pectin crosslinking mutant, *pme6*, which also has differences in stomatal conductance (Amsbury et al., 2016). Under changing CO_2 levels, the stomatal conductance of *pme6* had a small range of values compared to wildtype (Amsbury et al., 2016). This result is confirmed by other work in which *scap1*, which lacks functional PME6, had a much reduced range of stomatal conductance during periods of changing CO_2 concentration (Negi et al., 2013). Therefore, *sfr8, pme6* and *scap1* show limited stomatal dynamics and are all pectin crosslinking mutants, adding more evidence to the conclusion that pectin crosslinking has an impact on stomatal dynamics in response to CO_2. Furthermore, *scap1* not only exhibits altered stomatal conductance to CO_2 concentration, but also has a reduced range of stomatal conductance values compared to wildtype in response to light intensity (Negi et al., 2013). Therefore, pectin crosslinking may impact stomatal dynamics in response to environmental factors other than CO_2, such as light intensity or water loss.

To summarise, the stomatal conductance values of *sfr8, pme6* and *scap1* under stomatal closing and opening signals demonstrate that it is likely that pectin crosslinking has an effect on stomatal dynamics, in particular the range of stomatal conductance values that can be reached (Negi et al., 2013; Amsbury et al., 2016). This contributes to the conclusion that pectin crosslinking is a cause of the higher transpiration rate of *sfr8* in the leaf drying assay; *sfr8* has higher stomatal conductance and so transpiration rate under ambient conditions. Furthermore, *sfr8* and *rwa2* exhibit different stomatal conductance defects, whereas *sfr8* has limited dynamics, *rwa2* has higher stomatal conductance due to damaged trichomes causing a highly permeable leaf surface (Nafisi et al., 2015).

4.2.2 *sfr8* may have atypical stomatal development

Stomatal conductance is effected by many factors, including stomatal size and stomatal density. There is a negative correlation between stomatal size and stomatal density found across plant species (Hetherington and Woodward, 2003; Franks and Beerling, 2009). In this thesis, *sfr8* with the largest stomata is expected to have the lowest stomatal density, as it does, and accordingly, wildtype have the smallest stomata and the highest stomatal density (Figure 3.12.3 & 3.12.4). The correlation between stomatal size and density is due to the limited number of stomata of a given size that can fit within a unit area of leaf (Franks and Beerling, 2009). There is a theoretical upper limit of the stomatal density to size ratio, but all species have a density to size ratio well below the maximum due to the requirement of stomatal spacing (Franks and Beerling, 2009). Both stomatal size and density are regulated by many environmental factors, such as CO_2 concentration, light intensity and water restriction (Casson and Gray, 2008; Doheny-Adams et al., 2012). Moreover, genetic factors, including transcription factors, plant hormones and other signalling components, influence stomatal development and determine stomatal size and density (Casson and Gray, 2008).

sfr8 was observed to have significantly lower stomatal density than wildtype in this thesis (Figure 3.12.3). However, this is not replicated in the published literature; another study found *sfr8* to have statistically equivalent stomatal density to wildtype (Panter, 2018) and another mutant lacking functional MUR1, *susceptible-to-coronatine-deficient Pst DC300* (*scord6*) has a stomatal density equivalent to wildtype (Zeng et al., 2011). The difference in stomatal density may be due to environmental factors (Casson and Gray, 2008; Doheny-Adams et al., 2012). Under some growth conditions, stomatal density is different to wildtype, like in this thesis, and under different conditions, no difference to wildtype is observed like in Panter (2018) and Zeng et al. (2011). Alternatively, stomatal density may have been underestimated in this thesis due to abnormal stomatal morphology. Mutants lacking functional MUR1, *mur1* and *scrod6*, have been observed to have collapsed outer cuticle ledges (Zhang et al., 2019b), which implies *sfr8* may have collapsed outer cuticle ledges also. An atypical stomatal morphology may make detection by light microscopy more difficult and therefore, more stomata could have been present on the leaf surface than were counted on the leaf impressions. This is unlikely as the stomatal density as measured by Panter (2018) and Zeng (2011) was also visualised using a light microscope. The method of collecting an impression of the leaf surface may have caused the difference in stomatal density and size; Panter (2018)

and Zeng (2011) used epidermal peels, whereas, dental putty and nail varnish were used in this thesis. The difference in method may mean in the work of Panter (2018) and Zeng et al. (2011), the stomatal density was overestimated possibly due to introduced artefacts or in this study, stomatal density was underestimated due to a lack of detail preserved from the impression, exacerbated by abnormal stomatal morphology.

sfr8 leaves have significantly larger stomata than wildtype in both length and width (Figure 3.12.4). The larger size of *sfr8* stomata is also observed in *scord6* mutants (Zeng et al., 2011). Therefore, unlike stomatal density, the difference in size is present under two different growth conditions and must be due to altered stomatal development. The atypical stomatal development of *sfr8* must be caused by a lack of fucosylation of some plant cell component. One component that could influence *sfr8* stomatal development are DELLA proteins, which may be defective in *sfr8*. DELLA proteins must be fucosylated by a fucosyltransferase, SPINDLY (SPY), to become active (Zentella et al., 2017). Therefore, the lack of fucose in *sfr8* may mean that DELLAs are inactive in *sfr8*. A plant line overexpressing a guard cell-specific DELLA, PROCERA (PRO), had significantly higher stomatal density than wildtype with significantly smaller stomatal length (Nir et al., 2017). Conversely, *pro* mutants had significantly larger stomatal length than wildtype (Nir et al., 2017). Therefore, *sfr8* has an opposite phenotype to the overactive DELLA line and a similar phenotype to the mutant, *pro*, which lacks active DELLA proteins, indicating the stomatal developmental defect of *sfr8* could be due to inactive DELLAs. This could be tested by measuring the stomatal size and density of DELLA protein-specific O-fucosyltransferase deficient mutant, *spy*, or by measuring the level of DELLA activity, potentially the guard cell-specific PRO activity, in *sfr8* compared to wildtype.

Stomatal density is a known factor that influences stomatal conductance. Across species, plant lines overexpressing EPF1, which have reduced stomatal density, also have reduced stomatal conductance (Hughes et al., 2017; Caine et al., 2019; Dunn et al., 2019). Therefore, the reduced stomatal density of *sfr8* may explain the lower stomatal conductance than wildtype for the latter half of continuous exposure to the stomatal opening signal, reduced CO_2 concentration (Figure 3.11.1). Overall, however, *sfr8* does not behave like other reduced stomatal density mutants, as during ambient conditions and stomatal closure signals, the conductance of *sfr8* is significantly higher than that of wildtype (Figure 3.11.1 & 3.11.2). Additionally, reductions in stomatal density can be compensated by larger stomatal apertures to maintain normal stomatal conductance. For example, *STOMATAL DENSITY AND DISTRIBUTION1 (SDD1)* overexpression lines have a 40% reduction in stomatal density and have a compensatory increase in stomatal aperture to provide wildtype stomatal conductance (Büssis et al., 2006). However, in *sfr8*, there is no compensatory increase in stomatal aperture despite the 32% reduction in stomatal density compared to wildtype (Figure 3.12.3). Instead, *sfr8* stomatal aperture is decreased compared to wildtype (Figure 3.12.7), and so *sfr8* does not have stomatal aperture like other reduced stomatal density mutants. The comparison to similar low stomatal density (EPF1OE and SDD1OE) plant lines implies that although stomatal density does influence conductance, for *sfr8*, it is not a factor which causes the limited stomatal dynamics. Moreover, *pme6*, the pectin-crosslinking mutant with similar limited stomatal conductance

range to *sfr8*, had the same stomatal density as wildtype (Amsbury et al., 2016). Therefore, limited stomatal dynamics is not caused by aberrant stomatal density in another mutant, further suggesting *sfr8* stomatal dynamics are not influenced by stomatal density. Furthermore, Panter's (2018) research that found *sfr8* stomatal density to be equivalent to wildtype, also found *sfr8* to lose water much quicker than wildtype. High transpiration rate is an indicator of high stomatal conductance rate, which compliments the conclusion that stomatal density is not a determining factor of *sfr8* stomatal conductance.

Stomatal size determines stomatal pore area, the other main determinant of stomatal conductance in addition to stomatal density. Thus, the larger stomatal size of *sfr8* may have an influence of the stomatal conductance. An increase in stomatal size tends to correspond with an increase in stomatal conductance due to the increase in stomatal pore area (Franks and Beerling, 2009). For example, within the same species of wheat, plants that developed with smaller stomatal size, due to elevated CO_2 growth conditions, had reduced stomatal conductance compared to plants that developed with normal stomatal size under ambient CO_2 conditions (Zhu et al., 2018). Similarly, wheat plants that developed with larger stomatal size, due to inoculation with a pathogenic fungus, had higher stomatal conductance values than the non-infected plants with normal-sized stomata (Zhu et al., 2018). Therefore, like other large-stomata plants, *sfr8* tends to have higher stomatal conductance than wildtype, although during opening signals, *sfr8* stomatal conductance can be lower than wildtype, which is more similar to small-stomata plants (Figure 3.11.1). This indicates that the stomatal size of *sfr8* cannot cause the limited stomatal dynamics of *sfr8.* Additionally, *pme6* had the same stomatal size as wildtype, confirming that the limited stomatal dynamics in *pme6* is also not caused by stomatal size (Amsbury et al., 2016). Moreover, stomatal size is negatively correlated with speed of stomatal opening (Kardiman and Ræbild, 2018). Following this pattern, *sfr8* with larger stomata should have slower stomatal opening than wildtype, however, this is not observed in the data of this thesis. Under the both opening and closure signals of changed CO_2 concentration, *sfr8* took statistically the same amount of time as wildtype to maximally change CO_2 values (Figure 3.11.4). Therefore, the larger stomatal size of *sfr8* is unlikely to contribute to the stomatal dynamics observed.

While *sfr8* differed from wildtype in stomatal density, *rwa2* did not (Figure 3.12.3), which corroborates a previously published study, in which *rwa2* had statistically equivalent stomatal density to wildtype (Nafisi et al., 2015). The stomata of wildtype and *rwa2* differed in length by less than 1 μm and in width by less than 0.5 μm, despite this, *rwa2* stomata are significantly larger in size than wildtype stomata (Figure 3.12.4). Larger stomata would give higher stomatal conductance due to larger pore area (Franks and Beerling, 2009; Zhu et al., 2018). Therefore, *rwa2* could have significantly higher stomatal conductance at all CO_2 concentrations due to having significantly larger stomata (Figure 3.11.2). However, there are no other published data confirming the significant difference in size between *rwa2* and wildtype and the difference in size is comparatively small; the difference in size between *sfr8 and* wildtype is five times larger than the difference in size between *rwa2* and wildtype. Additionally, the negative correlation between stomatal size and speed of opening would predict that *rwa2* would have slower stomatal dynamics than wildtype (Kardiman and Ræbild, 2018). Instead, wildtype and *rwa2* have statistically the

same gradient of change in stomatal conductance following changes in CO_2 concentration and take the same amount of time to maximally change stomatal conductance (Figure 3.11.4 & 3.11.5), indicating equivalent speed of opening. Therefore, it is probably a factor other than a difference in stomatal size that causes the difference in stomatal conductance between *rwa2* and wildtype, such as stomatal aperture. Under steady-state conditions, there was a slightly significant difference in stomatal aperture between wildtype and *rwa2*, despite *rwa2* being only 0.014 µm larger than wildtype (Figure 3.12.5). Another study did not find a significant difference between the stomatal aperture of wildtype and *rwa2* (Nafisi et al., 2015)*. Taken together, the similar stomatal parameters of wildtype and *rwa2* found in this thesis and Nafisi's 2015 work imply the high transpiration rate is not due to stomatal factors at all. Nafisi's research group attributed the higher gas flow from *rwa2* leaves to a more permeable leaf surface, which was mainly caused by a reduction in cuticle integrity as a result of decreased cell wall O-acetylation (Nafisi et al., 2015).

In summary, *sfr8* has a stomatal development defect, which leads to larger stomata and lower stomatal density. The developmental defect could be caused by a combination of a fucosylation defect, such as inactive DELLA proteins, and environmental conditions, such as humidity. Both stomatal density and size are determining factors of stomatal conductance, however, the data from this thesis and published literature indicate that the stomatal conductance of s*fr8* is not solely due to a difference in stomatal density or size (Büssis et al., 2006; Amsbury et al., 2016; Panter, 2018; Dunn et al., 2019). The larger size may contribute to slower stomatal dynamics in *sfr8* (Kardiman and Ræbild, 2018), but this is not observed in the data. Focusing on *rwa2*, the stomatal size, density and aperture is all highly similar to wildtype in this thesis and in published literature, which indicates the increased stomatal conductance of *rwa2* is due to a factor other than stomata, which is hypothesised to be a damaged cuticle (Nafisi et al., 2015).

4.3 *sfr8* and *rwa2* may be more drought tolerant than wildtype

There is evidence *sfr8* may have higher drought tolerance than wildtype. Exactly half of *sfr8* plants survived a drought period of 17-19 days, whereas, only 3 out of 22 wildtype plants did. Moreover, *sfr8* tended to have higher growth than wildtype following the drought period (Section 3.5). The sample size was small, however, only 18 *sfr8* and 22 wildtype plants were used and so this is treated as preliminary data from which limited conclusions can be drawn. *sfr8* has not been tested for drought tolerance before so direct comparisons between results cannot be made.

sfr8 shares a similar phenotype with other mutants with reduced stomatal density. Across plant species, loss-of-function mutants or overexpression lines with lower stomatal density have reduced water use and are more drought tolerant (Hepworth et al., 2015; Hughes et al., 2017; Caine et al., 2019; Dunn et al., 2019; Xiang et al., 2021). For example, *EPIDERMAL PATTERNING FACTOR1 (EPF1)* overexpression lines in barley have reduced stomatal density by approximately 50% and when exposed to a water-withheld period of 12 days, the yield of *HvEPF1OE* plants was around 1.5 times larger than wildtype, demonstrating superior drought tolerance (Hughes et al., 2017). Similarly, the overexpression of transcription factor

NAC49 in rice significantly reduces stomatal density and following an 8-day drought period and 3-day recovery period, 56% of *ZmNAC49OE* plants had survived compared to only 29% of wildtype plants (Xiang et al., 2021). Moreover, the association between stomatal density and drought tolerance is also true in Arabidopsis. Arabidopsis plants that were manipulated to overexpress *EPF2* had a significant reduction in stomatal density compared to wildtype and were more drought tolerant; *AtEPF2OE* had higher soil water content than wildtype throughout a 6-day drought period, and survived and continued to grow when wildtype did not during a 10-day drought period (Hepworth et al., 2015). Therefore, Arabidopsis *sfr8* mutants with a significant reduction in stomatal density is likely to be more drought tolerant due to the higher water use efficiency of having fewer stomata. However, this is not the observed result in the leaf drying assays, *sfr8* is consistently poor at retaining water following leaf excision (Section 3.1), so there is a discrepancy in the behaviour of *sfr8* during leaf drying assays and drought tolerance assays.

There is a compensatory effect between stomatal size and stomatal density found across plant species, with smaller stomata being compensated with higher density and lower stomatal density being compensated with larger size (Hetherington and Woodward, 2003; Franks and Beerling, 2009). Manipulated plants with lower stomatal density do not always have a compensatory increase in stomatal size. The guard cell length of *HvEPF2OE* drought tolerant plants is significantly smaller than wildtype, alongside a significant reduction in stomatal density (Hughes et al., 2017). This would suggest that the increase in drought tolerance in *HvEPF2OE* is unrelated to the increase in drought tolerance of *sfr8* as the total stomatal area is different. However, *AtEPF2OE* plants, which have reduced stomatal density and increased drought tolerance, also have larger stomatal size, like *sfr8* (Franks et al., 2015). Therefore, the drought tolerance of *sfr8* is possibly due to the increased stomatal size and decreased stomatal density. Although, the reduced stomatal size of drought tolerant *HvEPF1OE* indicates that stomatal density is the main determinant of drought tolerance not stomatal size.

Furthermore, plants with reduced stomatal conductance can have higher drought tolerance (Bertolino et al., 2019). *AtEPF2OE* plants had reduced maximum potential stomatal conductance compared to wildtype, regardless of CO_2 concentration and soil water content (Doheny-Adams et al., 2012). The reduction in stomatal conductance meant the plants had a slower transpiration rate, conserving more water and were adversely affected by drought (Doheny-Adams et al., 2012; Hepworth et al., 2015). Additionally, other manipulated plant lines with higher drought tolerance have reduced stomatal conductance, for example, *ZmNAC49OE* (Xiang et al., 2021), *OsEPF1OE* (Caine et al., 2019), *TaEPF1OE* (Dunn et al., 2019) and *HvEPF1OE* (Hughes et al., 2017). *sfr8* is in contradiction with this published data; despite having better drought tolerance than wildtype, for the majority of the time measured the stomatal conductance of *sfr8* was higher than wildtype, and *sfr8* had significantly higher mean stomatal conductance for all CO_2 concentrations (Figure 3.11.1 & 3.11.2). Additionally, *sfr8* has higher transpiration rate than wildtype in the leaf drying assays (Section 3.1), which would indicate an inability to conserve water during drought. Therefore, there is a contradiction between *sfr8* transpiration and drought tolerance that must be caused by something else.

One possible cause for the contradiction in the results of the leaf drying assay, stomatal conductance measurements and drought tolerance assay of *sfr8* is that the treatments inflicted in these experiments are detected and responded to as different stresses. The stomatal conductance of *sfr8* was measured when responding to changes in CO_2 concentration, which is detected as a nutrient deficiency stress (under low [CO_2]) and as air pollutant stress (under high [CO_2]; Le Gall et al., 2015). CO_2-related stresses are sensed differently to osmotic stresses, such as those induced by leaf excision or drought, and involve different signalling components (Le Gall et al., 2015). Moreover, leaf excision and drought are detected as different stresses, as the former involves air drying and the latter involves soil drying (Bray, 2004). Very few genes are expressed during both air drying treatments and soil drying treatments, indicating different stress response to similar osmotic stresses (Bray, 2004). Moreover, drought responsive traits and drought tolerance are not associated with the transpiration rate from the leaf surface (Ferguson et al., 2018). Removing a leaf from its water source is a different stress to gradually reducing the soil water content of an intact plant. Therefore, the results of this thesis seem to contradict each other as different stresses have been inflicted and *sfr8* does not behave them same between stresses.

Another possible cause of the discrepancy amongst the results of this thesis is the root length of *sfr8*. Root length is a factor that effects the drought tolerance of a plant. In some cases, smaller roots provide greater drought tolerance; for example, short, horizontally distributed roots are beneficial to Arabidopsis under drought conditions when water is present in the surface layer of soil for a brief period of time (Ogura et al., 2019). On the other hand, longer, vertically-distributed roots are beneficial under drought conditions in which water is contained in deeper soil layers (Uga et al., 2013). The conditions of the drought tolerance assay used in this thesis favour shorter roots. The plants are grown in small pots which contain the same amount of soil and water. Roots that are longer will have access to and be able to extract all soil water content in the small pots immediately, whereas, shorter roots will only be able to access water in the top layers of the soil so will take longer to extract soil water. Therefore, plants with longer roots will run out of water quicker than shorter roots. The roots of *sfr8* seedlings are significantly smaller than wildtype at 7 and 12 days old (Figure 3.14.1). Thus, *sfr8* is more drought tolerant in this assay because *sfr8* has significantly shorter roots than wildtype. However, this may not be true in other drought tolerance assays, such as if the water deficit was equal by using larger pots, by planting genotypes in the same soil or by performing the assay in the field (Feng et al., 2017; Schulz et al., 2021).

Moreover, rosette size affects plant water usage. For example, Arabidopsis plants that had larger rosette areas used more water; their relative soil water content reached 20% more quickly than Arabidopsis plants with smaller rosette areas (Ferguson et al., 2018). The average rosette area of *sfr8* was significantly smaller than wildtype before the 19-day drought period (Figure 3.13.3). Therefore, *sfr8* would have less water usage than wildtype during the drought period. The soil water content for *sfr8* would have been used up slower than wildtype, meaning the drought inflicted on *sfr8* was not as severe as wildtype. To make sure the drought stress is the same regardless of size, the method could be changed to only include plants that are of a similar size, or regularly weighing the pots to measure water loss and adding water to plants with reduced soil water content to ensure a similar drought stress is inflicted (Earl, 2003).

Similar to *sfr8*, there is evidence that *rwa2* also has higher drought tolerance than wildtype; *rwa2* survival rate and growth rate was higher than wildtype following both the 17-day and 19-day drought period (Section 3.5). The sample size was small with only 22 wildtype and 23 *rwa2* plants used and so this is treated as preliminary data. *rwa2* has stomatal density statistically equal to wildtype and only a slight difference in stomatal size (Figure 3.12.3 & Figure 3.12.4). Therefore, the increased drought tolerance of *rwa2* cannot be associated with differences in stomatal size or density. Moreover, plants with higher stomatal conductance than wildtype tend to have reduced drought tolerance (Bertolino et al., 2019). *rwa2* has significantly higher stomatal conductance and faster transpiration rate than wildtype (Figure 3.11.2 and Figure 3.4.2), and if following the trend, that means *rwa2* should have reduced drought tolerance, which is not the case. Therefore, a factor or factors other than stomatal size, density and conductance must explain the higher drought tolerance of *rwa2* in this assay. Additionally, the water retention of *rwa2* differs between the leaf drying assay, stomatal conductance data and the drought tolerance assay. *rwa2* has higher transpiration rate so should have higher water use and be more susceptible to drought, but the opposite is found. Thus, another factor or factors must influence this discrepancy.

Like *sfr8*, *rwa2* may behave differently to CO_2 concentration-related stress (stomatal conductance data), air-drying stress (leaf excision) and soil-drying stress (drought tolerance assay) as they are detected and responded to as different stresses (Bray, 2004; Le Gall et al., 2015). Alternatively, *rwa2* has significantly shorter roots than wildtype at 7 and 12 days old. As previously mentioned, the drought conditions inflicted in this thesis are likely to favour plants with smaller roots as there are no deep-water sources and water is present briefly at the surface level (Uga et al., 2013; Ogura et al., 2019). Plants with longer roots are likely to extract the available water quicker and experience a drought stress quicker in this drought tolerance assay. Therefore, *rwa2*, with its shorter roots, might experience a less severe drought stress and appears to be more drought tolerant. With a change to experimental design, as discussed earlier, the plants could be exposed to identical drought stresses and the drought tolerance of each genotype could be compared on a more equal basis. However, as *rwa2* has significantly faster root growth than wildtype between 7 and 12 days old, the root length of *rwa2* could catch up to that of wildtype by the time the plants reach maturity at 5 weeks old, when the drought experiments were performed so root length may not have an effect on drought tolerance in this case. To confirm this, root length of mature plants would need to be measured. Given that root length of *rwa2* may equal wildtype at 5 weeks old, another factor may cause *rwa2* to have higher drought tolerance in this assay, which could be rosette size. From visual inspection the rosette area of *rwa2* plants appeared smaller than wildtype at the start of the 19-day drought period and the average rosette area size of *rwa2* at the start of the 17-day drought period was less than half that of wildtype (Figure 3.13.1 & 3.13.3). Arabidopsis plants with smaller rosette area use less water than larger plants (Ferguson et al., 2018). Therefore, *rwa2* may have used the available water slower than wildtype and experienced a less severe drought stress, which meant *rwa2* appeared to be more drought tolerant. The experimental method would need to be changed, as mentioned earlier, to ensure plants experience the same drought stress regardless of size.

In summary, *sfr8* has increased drought tolerance, which could be due to its lower stomatal density and larger stomatal size. Although a more likely an explanation is that the experimental design could inflict different severities of drought stress on plants depending on their root length or rosette size. Therefore, *sfr8* with its smaller roots and smaller rosette size experience a less severe drought stress than wildtype and appear to be more drought tolerant when that may not be the case under different experimental design. Similarly, *rwa2* most likely has higher drought tolerance than wildtype in this assay because *rwa2* has smaller rosette area and shorter roots. Correcting the method would involve using larger pots, planting all genotypes in the same soil, repeating in the field, measuring and correcting soil water content throughout the drought period or selecting plants on the basis of size (Earl, 2003; Feng et al., 2017; Schulz et al., 2021). Another explanation for this disparity between the leaf drying assay and drought survival data is that the inflicted treatment involves different stresses as leaf excision is an air-drying stress and water withdrawal treatment is a soil drying stress, which can be responded to differently by the plant (Bray, 2004; Le Gall et al., 2015).

4.4 The water loss and stomatal defects of *sfr8* are probably due to a combination of factors

None of the mutants tested in the leaf drying assay had a water loss rate as high as *sfr8*. Under further measures of stomatal function, the pectin modification mutant, *rwa2*, which had the water loss rate most similar to *sfr8* of all tested mutants, had dissimilar stomatal conductance and stomatal dynamics to *sfr8*, as well as significantly different stomatal size and density to *sfr8*. Furthermore, *pme6,* with similar transpiration rate and stomatal conductance to *sfr8*, did not have a stomatal development defect like *sfr8* did. Therefore, although pectin modification and crosslinking probably does have an impact on transpiration and stomatal function, it is unlikely to be the only cause of the water loss defect observed in *sfr8*. There may be a synergistic effect between pectin modification and one or more components that were not tested in this project that when present together in a mutant result in a higher transpiration rate.

4.4.1 DELLA proteins

One possible untested factor that could cause the higher transpiration of *sfr8* is the fucosylation of DELLA proteins. Fucose is incorporated into DELLA proteins (Zentella et al., 2017), and therefore, *sfr8,* lacking the ability to synthesise fucose, also lacks fucosylated DELLA proteins. DELLA proteins are involved in stomatal closure by activating the synthesis of ABA, a plant hormone that triggers stomatal closure in response to osmotic stress (Piskurewicz et al., 2008; Nir et al., 2017; Hsu et al., 2021). As well as needing the absence of the plant signalling hormone GA, DELLAs also require fucosylation to be active and interact with DNA-binding transcription factors and regulate the expression of target genes (Locascio et al., 2013; Zentella et al., 2017). *sfr8*, due to the lack of fucose, may have reduced DELLA activity. Decreased DELLA activity has been associated with significant increases stomatal aperture and conductance compared to wildtype, implicating that DELLA enhances the sensitivity of guard cells to ABA (Nir et al., 2017). Moreover,

DELLAs are fucosylated by SPINDLY (SPY) O-fucosyltransferases and *spy* mutants lack wildtype expression of DELLA-regulated genes with significantly higher transcript levels of growth-related genes that are commonly downregulated by DELLAs (Zentella et al., 2017). It is possible for inactive DELLA lacking fucosylation could misregulate the expression of other DELLA-regulated genes, such as ABA (Piskurewicz et al., 2008). Decreased expression of ABA would result in reduced stomatal closure following a dehydration stress and could cause a higher transpiration rate (Park et al., 2009; Hsu et al., 2021). Therefore, the very high transpiration rate of *sfr8* mutants compared to other cell wall mutants could be because as well as having a defect in pectin modification, *sfr8* has a defect in osmotic stress signalling, specifically DELLA-ABA signalling. Furthermore, the altered stomatal size and density could be due to lack of fucosylated DELLAs, as previously discussed in section 4.2.2. *pro* mutants lacking a specific DELLA protein have significantly larger stomatal length than wildtype and when *PRO* is overexpressed and DELLA activity is increased, stomatal size decreases and stomatal density increases (Nir et al., 2017). Thus, *sfr8* has similarity in stomatal development with a mutant lacking active DELLA proteins.

To test the hypothesis that the lack of fucosylated DELLA proteins contributes to the higher transpiration rate in *sfr8*, *spy* mutants could be compared to *sfr8* and wildtype in a leaf drying assay and measures of stomatal features. *spy* mutants have already been found to have compromised stomatal defences in response to pathogen infection, therefore, there is potential for lack of stomatal closure in response to leaf excision (Zhang et al., 2019b). Alternatively, this hypothesis could also be tested by measuring the activity level of DELLA proteins in *sfr8* in comparison to wildtype. However, as the project is investigating the effect of cell wall composition on transpiration and stomatal dynamics, pursuing a mutant in plant signalling is beyond the scope of this project. Nevertheless, *spy* mutants and the fucosylation of DELLAs in *sfr8* would be an interesting avenue to pursue in future projects for their possible effects on stomatal dynamics.

4.4.2 Cell adhesion

Pectins of the cell wall are particularly important in cell adhesion; the middle lamella, which forms a continuous matrix between neighbouring cells, is rich in pectins (Voragen et al., 2009; Cosgrove, 2016b). Pectin crosslinking provides the adhesive properties to the middle lamella, sticking cells together and keeping them adjoined throughout the life cycle (Seymour et al., 2004). Therefore, mutations in pectin and pectin crosslinking impact cell adhesion with physiological consequences. For example, during pollen development, cell adhesion needs to be loosened to allow cell separation and pollen dispersal. *quartet* mutants have reduced pectin degradation and as a result have strong cell adhesion, producing pollen that fails to separate appropriately (Rhee et al., 2003). Alternatively, too weak cell adhesion is also problematic. The *qua1* mutant is deficient in HG due to inhibited synthesis and have reduced cell adhesion in the hypocotyl and root with SEM showing relatively large gaps between cells (Bouton et al., 2002). With the cell adhesion phenotype, *qua1* also has higher leaf water loss than wildtype; one hour after leaves were detached from 1-month old plants and left to dry, *qua1* leaves weighed only 20% of their initial weight, whereas wildtype weighed 70% (Bouton et al., 2002). This is a similar water loss pattern to *sfr8* in

the leaf drying assays, suggesting *sfr8* could have a cell adhesion defect. *mur1* and *sfr8* have reduced pectin crosslinking due to the reduction in RG-II dimerisation (Reiter et al., 1993; Panter et al., 2019). Therefore, it is reasonable to suspect that *sfr8* may have weaker cell adhesion due to a less adhesive middle lamella. However, other mutants with similar levels of HG deficiency to *qua1*, such as *irx8* and *pme3*, do not have a cell adhesion phenotype (Persson et al., 2007; Guénin et al., 2011; Verger et al., 2016). Consequently, it cannot be confidently concluded that *sfr8* has a cell adhesion defect that causes higher leaf transpiration purely based on the fact that *sfr8* has a defect in pectin crosslinking. A direct measure of cell adhesion of *sfr8* is needed to confirm this hypothesis that disruption to cell adhesion causes the higher water loss rate.

Some O-fucosyltransferases have been identified that effect cell adhesion. *FRIABLE1 (FRB1)* encodes a putative O-fucosyltransferase that when functionally knocked-out results in cell dissociation giving mechanical weakness and occasionally killing the seedlings, as well as cell adhesion phenotypes resulting in fused hypocotyl and/or cotyledons (Neumetzler et al., 2012). *FRB1* is essential to maintaining appropriate levels of adhesion that is not too weak or too strong, without manipulating pectin content (Neumetzler et al., 2012). Another putative O-fucosyltransferase, ESMERALDA1 (ESMD1), has been identified that is also involved in maintaining appropriate cell adhesion (Verger et al., 2016). Single mutants of *frb1* and *qua1* were transformed with the functional knockout of *ESMD1* by insertion of *pESMD1*::*uidA* gene construct into plant lines. The double mutants *esmd1 frb1* and *esmd1 qua1* had wildtype cell adhesion phenotype, rescuing the mutant phenotype of *frb1* and *qua1* single mutants (Verger et al., 2016). *ESMD1* and *FRB1* are two putative O-fucosytransferases that have opposite effects on cell adhesion (Verger et al., 2016). The involvement of fucosyltransferases in cell adhesion identifies how *sfr8* may have a cell adhesion phenotype other than through effecting pectin crosslinking; a reduction in fucose content will mean a reduction in the fucosylation of targets of *ESMD1* and *FRB1*, which may give a cell adhesion phenotype. To test this hypothesis, the *frb1* mutant and an *ESMD1* overexpression line could be used in the leaf drying assay to determine the effect of reduced cell adhesion, resulting directly from fucosylation events, on leaf water loss.

4.4.3 Cuticle damage

As previously mentioned, Nafisi *et al.* 2015 concluded that the higher stomatal conductance of *rwa2* plants is probably due to damaged trichomes as a result of a reduction in cuticle integrity, which increases leaf surface permeability and gas exchange. Therefore, it is possible that *sfr8* water loss rate is also caused by cuticle damage. The cuticle is the main barrier to preventing plant water loss, other than the stomatal closure (Pollard et al., 2008), thus, damage to the cuticle would result in severe water loss. However, as *sfr8* loses such a vast amount of water so quickly, much quicker than *rwa2* (Figure 3.4.1), it is unlikely that this volume could be lost at that rate through damaged cuticle alone. Moreover, *sfr8* has limited stomatal dynamics (Figure 3.11.1), which means *sfr8* must have a defect in its stomata. *sfr8* is unlikely to solely lose water through a damaged cuticle, but this does not rule out the possibility that *sfr8* has both a stomatal defect and a defective cuticle and that the huge volume of *sfr8* water loss is due to a combination of these

two phenotypes. The cuticle is composed of fatty acids and does not contain fucose (Pollard et al., 2008). Therefore, it is unlikely the cuticle will be effected by the lack of GDP-L-fucose synthesis in *sfr8* and so cuticle damage is an unlikely cause of the high transpiration rates of *sfr8.* Furthermore, *rwa2* cuticle defect results from reduced wall esterification causing an excess of hydroxyl groups that may crosslink with cutins (Nafisi et al., 2015). *sfr8* does not affect pectin esterification, meaning *sfr8* cannot cause increased crosslinking with cutins and *sfr8* probably does not impair cuticle assembly. Overall, the evidence suggests *sfr8* does not have a damaged cuticle, which would cause higher transpiration.

4.4.4 Pectin water holding

Pectin has a high water-holding capacity, with the ability to contain 56.2g of water per gram (Stephen and Cummings, 1979). Pectins are essential to maintaining the hydration status of the cell wall matrix and providing high water absorption speed (Einhorn-Stoll et al., 2012; Boanares et al., 2018). Moreover pectin modification and the resulting crosslinking influences the water holding capacity, for example, a reduction in pectin methylesterification increases the water holding capacity of pectin by increasing pectin crosslinking (Willats et al., 2001b). It has also been suggested that as well as HG crosslinks, RG-II dimerisation could increase the water-holding capacity of the cell wall (Forand et al., 2022). Therefore, it is feasible that *sfr8*, with a significant reduction in RG-II dimerisation, could have a reduction in the water-holding capacity of pectin, which would contribute to the faster water loss rate. However, this is only speculative, the water-holding capacity of *sfr8* would need to be measured directly to confirm.

4.4.5 Plant size

Plant size, particularly the size of leaves, effects plant transpiration rate, with larger leaves losing water at a faster rate (Parkhurst and Loucks, 1972). Therefore, dwarfed plants may have a water loss rate slower than plants that are normal sized. *sfr8* is reported to be dwarfed in some studies, depending on growth conditions (Reiter et al., 1993; O'Neill et al., 2001; Gonçalves et al., 2017). All wildtype and *sfr8* leaves used in the leaf drying assay, stomatal conductance measurements, stomatal density and size measurements were of the same size in this thesis (Section 3.1 and Figure 3.12.1). There is some evidence of dwarfing in the *sfr8* plants used in the 19-day drought period, as they are significantly smaller than wildtype. However, there is no occurrence of *sfr8* growing larger than wildtype in this thesis or in published literature, therefore, it is highly unlikely that the faster transpiration rate of *sfr8* is due to its leaf size, in fact the opposite may be true that the dwarfism of *sfr8* compensates for its faster water loss rate to some extent.

In summary, the high transpiration rate and stomatal defects of *sfr8* are most likely due to a combination of factors, which may include: the reduced pectin crosslinking, inactive DELLA proteins and/or defective cell adhesion. A reduction to the water-holding capacity may also have an effect on *sfr8* transpiration but this is an area that requires more research. The transpiration rate of *sfr8* is unlikely to be affected by cuticle damage or its size. The hypotheses that DELLA proteins, cell adhesion and pectin water-holding

effect transpiration rate can be tested by utilising *spy*, *frb1* and *ESMD1OE* mutants and measuring the cell adhesion and pectin water-holding properties of *sfr8.*

4.5 Conclusion

sfr8 has a higher transpiration rate than wildtype and out of all tested mutants cell wall acetylation mutant, *rwa2,* had the most similarity to *sfr8* in both the leaf drying assay and the infra-red thermal imaging. The result of these experiments and the similar experiments performed on an pectin modification mutant, *pme6* (Negi et al., 2013; Amsbury et al., 2016), indicated that defects in pectin crosslinking, such as lack of pectin acetylation, methylesterification or reduced RG-II dimerisation, increases transpiration rate and stomatal conductance measured by thermal imaging.

However, the similarities between *sfr8* and *rwa2* extend no further. *rwa2* stomata are the same density and size as wildtype, whereas *sfr8* stomata are not. *rwa2* has significantly higher stomatal conductance than wildtype when measured using an IRGA, whereas *sfr8* has limited stomatal dynamics. The higher stomatal conductance of *rwa2* is attributed to a damaged cuticle, which makes the leaf surface more permeable. Additionally, with a different drought tolerance assay, one that selected plants on the basis of size or applied equal drought stress to each plant, *rwa2* probably would not have higher drought tolerance than wildtype, whereas *sfr8* might.

sfr8 has limited stomatal dynamics, which can be attributed to reduced pectin crosslinking as a similar stomatal conductance pattern is observed in *pme6* (Negi et al., 2013; Amsbury et al., 2016). Moreover, *sfr8* have significantly larger stomata and significantly reduced stomatal density compared to wildtype due to a combination of genetic and environmental factors. The change to stomatal development may give *sfr8* greater drought tolerance.

sfr8 is a mutation that affects many plant components and processes, therefore, the *sfr8* phenotype of limited stomatal dynamics and altered stomatal development could be caused by a combination of factors. Moreover, as no other tested mutant has a transpiration rate anything like *sfr8*, the mutant phenotype of *sfr8* could be due to a combination of factors, including reduced pectin modification and the untested factors, which could be inactive DELLA proteins, defective cell adhesion and/or potentially reduced pectin water-holding capacity.

Identifying components that effect drought tolerance, such as stomatal conductance, stomatal density and stomatal size, is important for future agricultural crop growth. The occurrence and severity of drought is predicted to increase under future climate models (Dai, 2011), therefore, identifying genes that impact stomatal conductance, density or size will be necessary for breeding or engineering plants for improved drought tolerance. As a gene that effects stomatal conductance, density and size, *sfr8* may be important in future crop growth under drought.

References

Ahmad, S., R. Ahmad, M.Y. Ashraf, M. Ashraf, and E.A. Waraich. 2009. Sunflower (Helianthus annuus L.) response to drought stress at germination and seedling growth stages. *Pakistan J. Bot.* 41.

Alberts, B., A. Johnson, J. Lewis, M. Raff, K. Roberts, and P. Walter. 2007. Molecular Biology of the Cell.

Amsbury, S., L. Hunt, N. Elhaddad, A. Baillie, M. Lundgren, Y. Verhertbruggen, H. V. Scheller, J.P. Knox, A.J. Fleming, and J.E. Gray. 2016. Stomatal Function Requires Pectin De-methyl-esterification of the Guard Cell Wall. *Curr. Biol.* 26:2899–2906. doi:10.1016/j.cub.2016.08.021.

Assaad, F.F., J.L. Qiu, H. Youngs, D. Ehrhardt, L. Zimmerli, M. Kalde, G. Wanner, S.C. Peck, H. Edwards, K. Ramonell, C.R. Somerville, and H. Thordal-Christensen. 2004. The PEN1 syntaxin defines a novel cellular compartment upon fungal attack and is required for the timely assembly of papillae. *Mol. Biol. Cell*. 15. doi:10.1091/mbc.E04-02-0140.

Assmann, S.M., L. Simoncini, and J.I. Schroeder. 1985. Blue light activates electrogenic ion pumping in guard cell protoplasts of Vicia faba. *Nature*. 318. doi:10.1038/318285a0.

Baldwin, L., J.M. Domon, J.F. Klimek, F. Fournet, H. Sellier, F. Gillet, J. Pelloux, I. Lejeune-Hénaut, N.C. Carpita, and C. Rayon. 2014. Structural alteration of cell wall pectins accompanies pea development in response to cold. *Phytochemistry*. 104. doi:10.1016/j.phytochem.2014.04.011.

Balsamo, R., M. Boak, K. Nagle, B. Peethambaran, and B. Layton. 2015. Leaf biomechanical properties in Arabidopsis thaliana polysaccharide mutants affect drought survival. *J. Biomech.* 48:4124–4129. doi:10.1016/j.jbiomech.2015.10.016.

Bauer, H., P. Ache, S. Lautner, J. Fromm, W. Hartung, K.A.S. Al-Rasheid, S. Sonnewald, U. Sonnewald, S. Kneitz, N. Lachmann, R.R. Mendel, F. Bittner, A.M. Hetherington, and R. Hedrich. 2013. The stomatal response to reduced relative humidity requires guard cell-autonomous ABA synthesis. *Curr. Biol.* 23. doi:10.1016/j.cub.2012.11.022.

Bertolino, L.T., R.S. Caine, and J.E. Gray. 2019. Impact of stomatal density and morphology on water-use efficiency in a changing world. *Front. Plant Sci.* 10. doi:10.3389/fpls.2019.00225.

Boanares, D., B.G. Ferreira, A.R. Kozovits, H.C. Sousa, R.M.S. Isaias, and M.G.C. França. 2018. Pectin and cellulose cell wall composition enables different strategies to leaf water uptake in plants from tropical fog mountain. *Plant Physiol. Biochem.* 122. doi:10.1016/j.plaphy.2017.11.005.

Bonin, C.P., I. Potter, G.F. Vanzin, and W.D. Reiter. 1997. The MUR1 gene of Arabidopsis thaliana encodes an isoform of GDP-D-mannose-4,6-dehydratase, catalyzing the first step in the de novo synthesis of GDP-L-fucose. *Proc. Natl. Acad. Sci. U. S. A.* 94:2085–2090. doi:10.1073/pnas.94.5.2085.

Bouton, S., E. Leboeuf, G. Mouille, M.T. Leydecker, J. Talbotec, F. Granier, M. Lahaye, H. Höfte, and H.N. Truong. 2002. Quasimodo1 encodes a putative membrane-bound glycosyltransferase required for normal pectin synthesis and cell adhesion in Arabidopsis. *Plant Cell*. 14:2577–2590. doi:10.1105/tpc.004259.

Bray, E.A. 2004. Genes commonly regulated by water-deficit stress in Arabidopsis thaliana. *J. Exp. Bot.* 55:2331–2341. doi:10.1093/jxb/erh270.

Buckley, T.N. 2019. How do stomata respond to water status? *New Phytol.* 224. doi:10.1111/nph.15899.

Buckley, T.N., G.P. John, C. Scoffoni, and L. Sack. 2017. The sites of evaporation within leaves. *Plant Physiol.* 173. doi:10.1104/pp.16.01605.

Büssis, D., U. Von Groll, J. Fisahn, and T. Altmann. 2006. Stomatal aperture can compensate altered stomatal density in Arabidopsis thaliana at growth light conditions. *Funct. Plant Biol.* 33. doi:10.1071/FP06078.

Caffall, K.H., and D. Mohnen. 2009. The structure, function, and biosynthesis of plant cell wall pectic polysaccharides. *Carbohydr. Res.* 344:1879–1900. doi:10.1016/j.carres.2009.05.021.

Caffall, K.H., S. Pattathil, S.E. Phillips, M.G. Hahn, and D. Mohnen. 2009. Arabidopsis thaliana T-DNA mutants implicate GAUT genes in the biosynthesis of pectin and xylan in cell walls and seed testa. *Mol. Plant*. 2. doi:10.1093/mp/ssp062.

Caine, R.S., X. Yin, J. Sloan, E.L. Harrison, U. Mohammed, T. Fulton, A.K. Biswal, J. Dionora, C.C. Chater, R.A. Coe, A. Bandyopadhyay, E.H. Murchie, R. Swarup, W.P. Quick, and J.E. Gray. 2019. Rice with reduced stomatal density conserves water and has improved drought tolerance under future climate conditions. *New Phytol.* 221. doi:10.1111/nph.15344.

Campbell, M.M., and R.R. Sederoff. 1996. Variation in lignin content and composition: Mechanisms of control and implications for the genetic improvement of plants. *Plant Physiol.* 110:3–13. doi:10.1104/pp.110.1.3.

Carter, R., H. Woolfenden, A. Baillie, S. Amsbury, S. Carroll, E. Healicon, S. Sovatzoglou, S. Braybrook, J.E.

Gray, J. Hobbs, R.J. Morris, and A.J. Fleming. 2017. Stomatal Opening Involves Polar, Not Radial, Stiffening Of Guard Cells. *Curr. Biol.* 27:2974–2983. doi:10.1016/j.cub.2017.08.006.

Casson, S., and J.E. Gray. 2008. Influence of environmental factors on stomatal development. *New Phytol.* 178. doi:10.1111/j.1469-8137.2007.02351.x.

Cavalier, D.M., O. Lerouxel, L. Neumetzler, K. Yamauchi, A. Reinecke, G. Freshour, O.A. Zabotina, M.G. Hahn, I. Burgert, M. Pauly, N. V. Raikhel, and K. Keegstra. 2008. Disrupting two Arabidopsis thaliana xylosyltransferase genes results in plants deficient in xyloglucan, a major primary cell wall component. *Plant Cell*. 20. doi:10.1105/tpc.108.059873.

Chater, C.C.C., J. Oliver, S. Casson, and J.E. Gray. 2014. Putting the brakes on: Abscisic acid as a central environmental regulator of stomatal development. *New Phytol.* 202. doi:10.1111/nph.12713.

Chen, Z.H., G. Chen, F. Dai, Y. Wang, A. Hills, Y.L. Ruan, G. Zhang, P.J. Franks, E. Nevo, and M.R. Blatt. 2017. Molecular Evolution of Grass Stomata. *Trends Plant Sci.* 22:124–139. doi:10.1016/j.tplants.2016.09.005.

Chiniquy, D., W. Underwood, J. Corwin, A. Ryan, H. Szemenyei, C.C. Lim, S.H. Stonebloom, D.S. Birdseye, J. Vogel, D. Kliebenstein, H. V. Scheller, and S. Somerville. 2019. PMR5, an acetylation protein at the intersection of pectin biosynthesis and defense against fungal pathogens. *Plant J.* 100. doi:10.1111/tpj.14497.

Chiniquy, D., P. Varanasi, T. Oh, J. Harholt, J. Katnelson, S. Singh, M. Auer, B. Simmons, P.D. Adams, H. V. Scheller, and P.C. Ronald. 2013. Three novel rice genes closely related to the Arabidopsis IRX9, IRX9L, and IRX14 genes and their roles in xylan biosynthesis. *Front. Plant Sci.* 4. doi:10.3389/fpls.2013.00083.

Choi, J.Y., Y.S. Seo, S.J. Kim, W.T. Kim, and J.S. Shin. 2011. Constitutive expression of CaXTH3, a hot pepper xyloglucan endotransglucosylase/hydrolase, enhanced tolerance to salt and drought stresses without phenotypic defects in tomato plants (Solanum lycopersicum cv. Dotaerang). *Plant Cell Rep.* 30. doi:10.1007/s00299-010-0989-3.

Chormova, D., D.J. Messenger, and S.C. Fry. 2014. Rhamnogalacturonan-II cross-linking of plant pectins via boron bridges occurs during polysaccharide synthesis and/or secretion. *Plant Signal. Behav.* 9. doi:10.4161/psb.28169.

Christmann, A., E.W. Weiler, E. Steudle, and E. Grill. 2007. A hydraulic signal in root-to-shoot signalling of water shortage. *Plant J.* 52:167–174. doi:10.1111/j.1365-313X.2007.03234.x.

Cosgrove, D.J. 2005. Growth of the plant cell wall. *Nat. Rev. Mol. Cell Biol.* 6:850–861. doi:10.1038/nrm1746.

Cosgrove, D.J. 2014. Re-constructing our models of cellulose and primary cell wall assembly. *Curr. Opin. Plant Biol.* 22. doi:10.1016/j.pbi.2014.11.001.

Cosgrove, D.J. 2015. Plant expansins: Diversity and interactions with plant cell walls. *Curr. Opin. Plant Biol.* 25:162–172. doi:10.1016/j.pbi.2015.05.014.

Cosgrove, D.J. 2016a. Catalysts of plant cell wall loosening. *F1000Research*. 5. doi:10.12688/f1000research.7180.1.

Cosgrove, D.J. 2016b. Plant cell wall extensibility: Connecting plant cell growth with cell wall structure, mechanics, and the action of wall-modifying enzymes. *J. Exp. Bot.* 67. doi:10.1093/jxb/erv511.

Cosgrove, D.J. 2018. Diffuse growth of plant cell walls. *Plant Physiol.* 176:16–27. doi:10.1104/pp.17.01541.

Cosgrove, D.J., and M.C. Jarvis. 2012. Comparative structure and biomechanics of plant primary and secondary cell walls. *Front. Plant Sci.* 3. doi:10.3389/fpls.2012.00204.

Dai, A. 2011. Drought under global warming: A review. *Wiley Interdiscip. Rev. Clim. Chang.* 2:1209–1220. doi:10.1002/wcc.81.

Darwin, F. 1898. IX. Observations on stomata. *Philos. Trans. R. Soc. London. Ser. B, Contain. Pap. a Biol. Character*. 190. doi:10.1098/rstb.1898.0009.

Delmer, D.P. 1999. Cellulose biosynthesis: Exciting times for a difficult field of study. *Annu. Rev. Plant Biol.* 50. doi:10.1146/annurev.arplant.50.1.245.

Dick-Pérez, M., Y. Zhang, J. Hayes, A. Salazar, O.A. Zabotina, and M. Hong. 2011. Structure and interactions of plant cell-wall polysaccharides by two- and three-dimensional magic-angle-spinning solid-state NMR. *Biochemistry*. 50. doi:10.1021/bi101795q.

Doblin, M.S., I. Kurek, D. Jacob-Wilk, and D.P. Delmer. 2002. Cellulose biosynthesis in plants: From genes to rosettes. *Plant Cell Physiol.* 43:1407–1420. doi:10.1093/pcp/pcf164.

Doheny-Adams, T., L. Hunt, P.J. Franks, D.J. Beerling, and J.E. Gray. 2012. Genetic manipulation of stomatal density influences stomatal size, plant growth and tolerance to restricted water supply across a growth carbon dioxide gradient. *Philos. Trans. R. Soc. B Biol. Sci.* 367. doi:10.1098/rstb.2011.0272.

Dong, J., Y. Jiang, R. Chen, Z. Xu, and X. Gao. 2011. Isolation of a novel xyloglucan endotransglucosylase

(OsXET9) gene from rice and analysis of the response of this gene to abiotic stresses. *African J. Biotechnol.* 10. doi:10.5897/AJB11.1242.

Dumas, P., C. Hanson, J. Ranganathan, T. Searchinger, and R. Waite. 2019. Creating a Sustainable Food Future. *WRI - World Resour. Inst.* 1.

Dunn, J., L. Hunt, M. Afsharinafar, M. Al Meselmani, A. Mitchell, R. Howells, E. Wallington, A.J. Fleming, and J.E. Gray. 2019. Reduced stomatal density in bread wheat leads to increased water-use efficiency. *J. Exp. Bot.* 70:4737–4748. doi:10.1093/jxb/erz248.

Durand, C., M. Vicré-Gibouin, M.L. Follet-Gueye, L. Duponchel, M. Moreau, P. Lerouge, and A. Driouich. 2009. The organization pattern of root border-like cells of Arabidopsis is dependent on cell wall homogalacturonan. *Plant Physiol.* 150. doi:10.1104/pp.109.136382.

Earl, H.J. 2003. A precise gravimetric method for simulating drought stress in pot experiments. *In* Crop Science.

Ebringerová, A., and T. Heinze. 2000. Xylan and xylan derivatives - Biopolymers with valuable properties, 1: Naturally occurring xylans structures, isolation procedures and properties. *Macromol. Rapid Commun.* 21. doi:10.1002/1521-3927(20000601)21:9<542::AID-MARC542>3.0.CO;2-7.

Edwards, K., C. Johnstone, and C. Thompson. 1991. A simple and rapid method for the preparation of plant genomic DNA for PCR analysis. *Nucleic Acids Res.* 19. doi:10.1093/nar/19.6.1349.

Ehleringer, J.R., A.E. Hall, and G.D. Farquhar. 1993. Introduction: Water Use in Relation to Productivity. *In* Stable Isotopes and Plant Carbon-water Relations.

Ehleringer, J.R., and H.A. Mooney. 1978. Leaf hairs: Effects on physiological activity and adaptive value to a desert shrub. *Oecologia*. 37. doi:10.1007/BF00344990.

Einhorn-Stoll, U., H. Hatakeyama, and T. Hatakeyama. 2012. Influence of pectin modification on water binding properties. *Food Hydrocoll.* 27. doi:10.1016/j.foodhyd.2011.08.019.

Endo, A., Y. Sawada, H. Takahashi, M. Okamoto, K. Ikegami, H. Koiwai, M. Seo, T. Toyomasu, W. Mitsuhashi, K. Shinozaki, M. Nakazono, Y. Kamiya, T. Koshiba, and E. Nambara. 2008. Drought induction of Arabidopsis 9-cis-epoxycarotenoid dioxygenase occurs in vascular parenchyma cells. *Plant Physiol.* 147. doi:10.1104/pp.108.116632.

Fanourakis, D., H. Giday, R. Milla, R. Pieruschka, K.H. Kjaer, M. Bolger, A. Vasilevski, A. Nunes-Nesi, F. Fiorani, and C.O. Ottosen. 2015. Pore size regulates operating stomatal conductance, while stomatal densities drive the partitioning of conductance between leaf sides. *Ann. Bot.* 115. doi:10.1093/aob/mcu247.

Faye, L., K.D. Johnson, A. Sturm, and M.J. Chrispeels. 1989. Structure, biosynthesis, and function of asparagine-linked glycans on plant glycoproteins. *Physiol. Plant.* 75. doi:10.1111/j.1399-3054.1989.tb06187.x.

Feng, D., Y. Wang, J. Wu, T. Lu, and Z. Zhang. 2017. Development and drought tolerance assay of marker-free transgenic rice with OsAPX2 using biolistic particle-mediated co-transformation. *Crop J.* 5. doi:10.1016/j.cj.2017.04.001.

Feng, W., D. Kita, A. Peaucelle, H.N. Cartwright, V. Doan, Q. Duan, M.C. Liu, J. Maman, L. Steinhorst, I. Schmitz-Thom, R. Yvon, J. Kudla, H.M. Wu, A.Y. Cheung, and J.R. Dinneny. 2018. The FERONIA Receptor Kinase Maintains Cell-Wall Integrity during Salt Stress through Ca2+ Signaling. *Curr. Biol.* 28:666–675. doi:10.1016/j.cub.2018.01.023.

Ferguson, J.N., M. Humphry, T. Lawson, O. Brendel, and U. Bechtold. 2018. Natural variation of life-history traits, water use, and drought responses in Arabidopsis. *Plant Direct*. 2. doi:10.1002/pld3.35.

Fischer, R.A., D. Rees, K.D. Sayre, Z.M. Lu, A.G. Condon, and A. Larque Saavedra. 1998. Wheat yield progress associated with higher stomatal conductance and photosynthetic rate, and cooler canopies. *Crop Sci.* 38. doi:10.2135/cropsci1998.0011183X003800060011x.

Fleischer, A., M.A. O'Neill, and R. Ehwald. 1999. The pore size of non-graminaceous plant cell walls is rapidly decreased by borate ester cross-linking of the pectic polysaccharide rhamnogalacturonan II. *Plant Physiol.* 121:829–838. doi:10.1104/pp.121.3.829.

Forand, A.D., Y.Z. Finfrock, M. Lavier, J. Stobbs, L. Qin, S. Wang, C. Karunakaran, Y. Wei, S. Ghosh, and K.K. Tanino. 2022. With a Little Help from My Cell Wall : Structural Modifications in Pectin May Play a Role to Overcome Both Dehydration Stress and Fungal Pathogens.

Frank, J., H. Kaulfürst-Soboll, S. Rips, H. Koiwa, and A. Von Schaewen. 2008. Comparative analyses of Arabidopsis complex glycan1 mutants and genetic interaction with staurosporin and temperature sensitive3a. *Plant Physiol.* 148:1354–1367. doi:10.1104/pp.108.127027.

Franks, P.J., and D.J. Beerling. 2009. CO2-forced evolution of plant gas exchange capacity and water-use efficiency over the Phanerozoic. *Geobiology*. 7. doi:10.1111/j.1472-4669.2009.00193.x.

Franks, P.J., T. W. Doheny-Adams, Z.J. Britton-Harper, and J.E. Gray. 2015. Increasing water-use efficiency directly through genetic manipulation of stomatal density. *New Phytol.* 207.

doi:10.1111/nph.13347.

Fry, S.C. 1988. The growing plant cell wall: chemical and metabolic analysis. *New York*. 203.

Fuentes, S., N. Pires, and L. Østergaard. 2010. A clade in the QUASIMODO2 family evolved with vascular plants and supports a role for cell wall composition in adaptation to environmental changes. *Plant Mol. Biol.* 73. doi:10.1007/s11103-010-9640-5.

Fujita, M., and G.O. Wasteneys. 2014. A survey of cellulose microfibril patterns in dividing, expanding, and differentiating cells of Arabidopsis thaliana. *Protoplasma*. 251:687–698. doi:10.1007/s00709-013-0571-2.

Funakawa, H., and K. Miwa. 2015. Synthesis of borate cross-linked rhamnogalacturonan II. *Front. Plant Sci.* 6. doi:10.3389/fpls.2015.00223.

Le Gall, H., F. Philippe, J.M. Domon, F. Gillet, J. Pelloux, and C. Rayon. 2015. Cell wall metabolism in response to abiotic stress. *Plants*. 4:112–166. doi:10.3390/plants4010112.

Gardner, K.H., and J. Blackwell. 1974. The structure of native cellulose. *Biopolymers*. 13:1975–2001. doi:10.1002/bip.1974.360131005.

Geiger, D., S. Scherzer, P. Mumm, A. Stange, I. Marten, H. Bauer, P. Ache, S. Matschi, A. Liese, K.A.S. Al-Rasheid, T. Romeis, and R. Hedrich. 2009. Activity of guard cell anion channel SLAC1 is controlled by drought-stress signaling kinase-phosphatase pair. *Proc. Natl. Acad. Sci. U. S. A.* 106:21425–21430. doi:10.1073/pnas.0912021106.

Giannoutsou, E., P. Apostolakos, and B. Galatis. 2016. Spatio-temporal diversification of the cell wall matrix materials in the developing stomatal complexes of Zea mays. *Planta*. 244. doi:10.1007/s00425-016-2574-7.

Gille, S., and M. Pauly. 2012. O-acetylation of plant cell wall polysaccharides. *Front. Plant Sci.* 3. doi:10.3389/fpls.2012.00012.

Gille, S., A. de Souza, G. Xiong, M. Benz, K. Cheng, A. Schultink, I.B. Reca, and M. Pauly. 2011. O-acetylation of Arabidopsis hemicellulose xyloglucan requires AXY4 or AXY4L, proteins with a TBL an DUF231 domain. *Plant Cell*. 23. doi:10.1105/tpc.111.091728.

Gonçalves, B., A. Maugarny-Calès, B. Adroher, M. Cortizo, N. Borrega, T. Blein, A. Hasson, E. Gineau, G. Mouille, P. Laufs, and N. Arnaud. 2017. GDP-L-fucose is required for boundary definition in plants. *J. Exp. Bot.* 68:5801–5811. doi:10.1093/jxb/erx402.

Gou, J.Y., L.M. Miller, G. Hou, X.H. Yu, X.Y. Chen, and C.J. Liu. 2012. Acetylesterase-mediated deacetylation of pectin impairs cell elongation, pollen germination, and plant reproduction. *Plant Cell*. 24. doi:10.1105/tpc.111.092411.

Gribaa, A., F. Dardelle, A. Lehner, C. Rihouey, C. Burel, A. Ferchichi, A. Driouich, and J.C. Mollet. 2013. Effect of water deficit on the cell wall of the date palm (Phoenix dactylifera "Deglet nour", Arecales) fruit during development. *Plant, Cell Environ.* 36:1056–1070. doi:10.1111/pce.12042.

Guénin, S., A. Mareck, C. Rayon, R. Lamour, Y. Assoumou Ndong, J.M. Domon, F. Sénéchal, F. Fournet, E. Jamet, H. Canut, G. Percoco, G. Mouille, A. Rolland, C. Rustérucci, F. Guerineau, O. Van Wuytswinkel, F. Gillet, A. Driouich, P. Lerouge, L. Gutierrez, and J. Pelloux. 2011. Identification of pectin methylesterase 3 as a basic pectin methylesterase isoform involved in adventitious rooting in Arabidopsis thaliana. *New Phytol.* 192. doi:10.1111/j.1469-8137.2011.03797.x.

Guo, W., J. Zhao, X. Li, L. Qin, X. Yan, and H. Liao. 2011. A soybean β-expansin gene GmEXPB2 intrinsically involved in root system architecture responses to abiotic stresses. *Plant J.* 66. doi:10.1111/j.1365-313X.2011.04511.x.

Hafrén, J., G. Daniel, and U. Westermark. 2000. The distribution of acidic and esterified pectin in cambium, developing xylem and mature xylem of Pinus sylvestris. *IAWA J.* 21. doi:10.1163/22941932-90000242.

Hall, D.M., and R.L. Jones. 1961. Physiological significance of surface wax on leaves. *Nature*. 191. doi:10.1038/191095a0.

Hanstein, S.M., and H.H. Felle. 2002. CO2-triggered chloride release from guard cells in intact fava bean leaves. Kinetics of the onset of stomatal closure. *Plant Physiol.* 130. doi:10.1104/pp.004283.

Harb, A., A. Krishnan, M.M.R. Ambavaram, and A. Pereira. 2010. Molecular and physiological analysis of drought stress in arabidopsis reveals early responses leading to acclimation in plant growth. *Plant Physiol.* 154. doi:10.1104/pp.110.161752.

Harberd, N.P., E. Belfield, and Y. Yasumura. 2009. The angiosperm gibberellin-GID1-DELLA growth regulatory mechanism: How an "inhibitor of an inhibitor" enables flexible response to fluctuating environments. *Plant Cell*. 21. doi:10.1105/tpc.109.066969.

Harholt, J., J.K. Jensen, S.O. Sørensen, C. Orfila, M. Pauly, and H.V. Scheller. 2006. ARABINAN DEFICIENT 1 is a putative arabinosyltransferase involved in biosynthesis of pectic arabinan in arabidopsis. *Plant Physiol.* 140. doi:10.1104/pp.105.072744.

Harholt, J., J.K. Jensen, Y. Verhertbruggen, C. Søgaard, S. Bernard, M. Nafisi, C.P. Poulsen, N. Geshi, Y. Sakuragi, A. Driouich, J.P. Knox, and H.V. Scheller. 2012. ARAD proteins associated with pectic Arabinan biosynthesis form complexes when transiently overexpressed in planta. *Planta*. 236. doi:10.1007/s00425-012-1592-3.

Harholt, J., A. Suttangkakul, and H.V. Scheller. 2010. Biosynthesis of pectin. *Plant Physiol.* 153:384–395. doi:10.1104/pp.110.156588.

Hayashi, T. 1989. Xyloglucans in the Primary Cell Wall. *Annu. Rev. Plant Physiol. Plant Mol. Biol.* 40. doi:10.1146/annurev.pp.40.060189.001035.

Heffernan, O. 2013. The dry facts. *Nature*. 501:52–53. doi:10.1038/501S2a.

Van Hengel, A.J., and K. Roberts. 2002. Fucosylated arabinogalactan-proteins are required for full root cell elongation in arabidopsis. *Plant J.* 32. doi:10.1046/j.1365-313X.2002.01406.x.

Hepworth, C., T. Doheny-Adams, L. Hunt, D.D. Cameron, and J.E. Gray. 2015. Manipulating stomatal density enhances drought tolerance without deleterious effect on nutrient uptake. *New Phytol.* 208. doi:10.1111/nph.13598.

Hetherington, A.M., and F.I. Woodward. 2003. The role of stomata in sensing and driving environmental change. *Nature*. 424:901–908. doi:10.1038/nature01843.

Holloway, P.J. 1994. Plant Cuticles: Physicochemical Characteristics and Biosynthesis. *In* Air Pollutants and the Leaf Cuticle.

Houston, K., M.R. Tucker, J. Chowdhury, N. Shirley, and A. Little. 2016. The plant cell wall: A complex and dynamic structure as revealed by the responses of genes under stress conditions. *Front. Plant Sci.* 7:undefined. doi:10.3389/fpls.2016.00984.

Hsu, P.K., G. Dubeaux, Y. Takahashi, and J.I. Schroeder. 2021. Signaling mechanisms in abscisic acid-mediated stomatal closure. *Plant J.* 105. doi:10.1111/tpj.15067.

Hsu, P.K., Y. Takahashi, S. Munemasa, E. Merilo, K. Laanemets, R. Waadt, D. Pater, H. Kollist, and J.I. Schroeder. 2018. Abscisic acid-independent stomatal CO_2 signal transduction pathway and convergence of CO_2 and ABA signaling downstream of OST1 kinase. *Proc. Natl. Acad. Sci. U. S. A.* 115:9971–9980. doi:10.1073/pnas.1809204115.

Hu, H., R. Zhang, Z. Tao, X. Li, Y. Li, J. Huang, X. Li, X. Han, S. Feng, G. Zhang, and L. Peng. 2018. Cellulose synthase mutants distinctively affect cell growth and cell wall integrity for plant biomass production in arabidopsis. *Plant Cell Physiol.* 59:1144–1157. doi:10.1093/pcp/pcy050.

Huang, Y.C., H.C. Wu, Y. Da Wang, C.H. Liu, C.C. Lin, D.L. Luo, and T.L. Jinn. 2017. PECTIN METHYLESTERASE34 contributes to heat tolerance through its role in promoting stomatal movement. *Plant Physiol.* 174:748–763. doi:10.1104/pp.17.00335.

Hughes, J., C. Hepworth, C. Dutton, J.A. Dunn, L. Hunt, J. Stephens, R. Waugh, D.D. Cameron, and J.E. Gray. 2017. Reducing stomatal density in barley improves drought tolerance without impacting on yield. *Plant Physiol.* 174:776–787. doi:10.1104/pp.16.01844.

Hunt, L., S. Amsbury, A. Baillie, M. Movahedi, A. Mitchell, M. Afsharinafar, K. Swarup, T. Denyer, J.K. Hobbs, R. Swarup, A.J. Fleming, and J.E. Gray. 2017. Formation of the stomatal outer cuticular ledge requires a guard cell wall proline-rich protein. *Plant Physiol.* 174:689–699. doi:10.1104/pp.16.01715.

Iraki, N.M., R.A. Bressan, P.M. Hasegawa, and N.C. Carpita. 1989. Alteration of the Physical and Chemical Structure of the Primary Cell Wall of Growth-Limited Plant Cells Adapted to Osmotic Stress. *Plant Physiol.* 91:39–47. doi:10.1104/pp.91.1.39.

Isayenkov, S. V., and F.J.M. Maathuis. 2019. Plant salinity stress: Many unanswered questions remain. *Front. Plant Sci.* 10. doi:10.3389/fpls.2019.00080.

Ishii, T., T. Matsunaga, and N. Hayashi. 2001. Formation of rhamnogalacturonan II-borate dimer in pectin determines cell wall thickness of pumpkin tissue. *Plant Physiol.* 126:1698–1705. doi:10.1104/pp.126.4.1698.

Ishii, T., T. Matsunaga, P. Pellerin, M.A. O'Neill, A. Darvill, and P. Albersheim. 1999. The plant cell wall polysaccharide rhamnogalacturonan II self-assembles into a covalently cross-linked dimer. *J. Biol. Chem.* 274:13098–13104. doi:10.1074/jbc.274.19.13098.

Iwai, H., N. Masaoka, T. Ishii, and S. Satoh. 2002. A pectin glucuronyltransferase gene is essential for intercellular attachment in the plant meristem. *Proc. Natl. Acad. Sci. U. S. A.* 99. doi:10.1073/pnas.252530499.

Iwanoff, P.P. 1928. Die entwicklung der larvalsegmente bei den anneliden. *Zeitschrift für Morphol. und Ökologie der Tiere*. 10. doi:10.1007/BF00419279.

Jarvis, M.C. 1984. Structure and properties of pectin gels in plant cell walls. *Plant. Cell Environ.* 7. doi:10.1111/1365-3040.ep11614586.

Jones, L., J.L. Milne, D. Ashford, and S.J. McQueen-Mason. 2003. Cell wall arabinan is essential for guard

cell function. *Proc. Natl. Acad. Sci. U. S. A.* 100:11783–11788. doi:10.1073/pnas.1832434100.

Kardiman, R., and A. Ræbild. 2018. Relationship between stomatal density, size and speed of opening in Sumatran rainforest species. *Tree Physiol.* 38. doi:10.1093/treephys/tpx149.

Keegstra, K. 2010. Plant cell walls. *Plant Physiol.* 154:483–486. doi:10.1104/pp.110.161240.

Kiefer, L.L., W.S. York, A.G. Darvill, and P. Albersheim. 1989. Xyloglucan isolated from suspension-cultured sycamore cell walls is O-acetylated. *Phytochemistry*. 28. doi:10.1016/S0031-9422(00)97928-7.

Kim, S.H., C.M. Lee, and K. Kafle. 2013. Characterization of crystalline cellulose in biomass: Basic principles, applications, and limitations of XRD, NMR, IR, Raman, and SFG. *Korean J. Chem. Eng.* 30. doi:10.1007/s11814-013-0162-0.

Kim, S.J., B. Chandrasekar, A.C. Rea, L. Danhof, S. Zemelis-Durfee, N. Thrower, Z.S. Shepard, M. Pauly, F. Brandizzi, and K. Keegstra. 2020. The synthesis of xyloglucan, an abundant plant cell wall polysaccharide, requires CSLC function. *Proc. Natl. Acad. Sci. U. S. A.* 117. doi:10.1073/PNAS.2007245117.

Kimura, S., W. Laosinchai, T. Itoh, X. Cui, C.R. Linder, and R. Malcolm Brown. 1999. Immunogold labeling of rosette terminal cellulose-synthesizing complexes in the vascular plant Vigna angularis. *Plant Cell*. 11:2075–2086. doi:10.1105/tpc.11.11.2075.

Komalavilas, P., and A.J. Mort. 1989. The acetylation of O-3 of galacturonic acid in the rhamnose-rich portion of pectins. *Carbohydr. Res.* 189. doi:10.1016/0008-6215(89)84102-3.

Kramer, P.J., and J.S. Boyer. 1995. Water Relations in Plants and Soils. *Acad. Press*.

Kriedemann, P.E., B.R. Loveys, G.L. Fuller, and A.C. Leopold. 1972. Abscisic Acid and Stomatal Regulation. *Plant Physiol.* 49. doi:10.1104/pp.49.5.842.

Lahr, W., and K. Raschke. 1988. Abscisic-acid contents and concentrations in protoplasts from guard cells and mesophyll cells of Vicia faba L. *Planta*. 173. doi:10.1007/BF00958966.

Lau, J.M., M. McNeil, A.G. Darvill, and P. Albersheim. 1985. Structure of the backbone of rhamnogalacturonan I, a pectic polysaccharide in the primary cell walls of plants. *Carbohydr. Res.* 137:111–125. doi:10.1016/0008-6215(85)85153-3.

Lawson, T., and M.R. Blatt. 2014. Stomatal size, speed, and responsiveness impact on photosynthesis and water use efficiency. *Plant Physiol.* 164. doi:10.1104/pp.114.237107.

Leucci, M.R., M.S. Lenucci, G. Piro, and G. Dalessandro. 2008. Water stress and cell wall polysaccharides in the apical root zone of wheat cultivars varying in drought tolerance. *J. Plant Physiol.* 165:1168–1180. doi:10.1016/j.jplph.2007.09.006.

Levesque-Tremblay, G., J. Pelloux, S.A. Braybrook, and K. Müller. 2015. Tuning of pectin methylesterification: consequences for cell wall biomechanics and development. *Planta*. 242. doi:10.1007/s00425-015-2358-5.

Levy, S., W.S. York, R. Stuike-Prill, B. Meyer, and L.A. Staehelin. 1991. Simulations of the static and dynamic molecular conformations of xyloglucan. The role of the fucosylated sidechain in surface-specific sidechain folding. *Plant J.* 1:195–215. doi:10.1111/j.1365-313X.1991.00195.x.

Li, F., Y. Han, Y. Feng, S. Xing, M. Zhao, Y. Chen, and W. Wang. 2013. Expression of wheat expansin driven by the RD29 promoter in tobacco confers water-stress tolerance without impacting growth and development. *J. Biotechnol.* 163. doi:10.1016/j.jbiotec.2012.11.008.

Liang, Y., D. Basu, S. Pattathil, W.L. Xu, A. Venetos, S.L. Martin, A. Faik, M.G. Hahn, and A.M. Showalter. 2013. Biochemical and physiological characterization of fut4 and fut6 mutants defective in arabinogalactan-protein fucosylation in Arabidopsis. *J. Exp. Bot.* 64. doi:10.1093/jxb/ert321.

Lim, S., J. Park, N. Lee, J. Jeong, S. Toh, A. Watanabe, J. Kim, H. Kang, D.H. Kim, N. Kawakami, and G. Choi. 2013. ABA-insensitive3, ABA-insensitive5, and DELLAs interact to activate the expression of SOMNUS and other high-temperature-inducible genes in imbibed seeds in Arabidopsis. *Plant Cell*. 25. doi:10.1105/tpc.113.118604.

Locascio, A., M.A. Blázquez, and D. Alabadí. 2013. Genomic analysis of della protein activity. *Plant Cell Physiol.* 54. doi:10.1093/pcp/pct082.

Lösch, R. 1979. Responses of stomata to environmental factors-experiments with isolated epidermal strips of Polypodium vulgare - II. Leaf bulk water potential, air humidity, and temperature. *Oecologia*. 39:229–238. doi:10.1007/BF00348071.

Lü, P., M. Kang, X. Jiang, F. Dai, J. Gao, and C. Zhang. 2013. RhEXPA4, a rose expansin gene, modulates leaf growth and confers drought and salt tolerance to Arabidopsis. *Planta*. 237:1547–1559. doi:10.1007/s00425-013-1867-3.

Lund, C.H., A. Stenbæk, M.A. Atmodjo, R.E. Rasmussen, I.E. Moller, S.M. Erstad, A.K. Biswal, D. Mohnen, J. Mravec, and Y. Sakuragi. 2020. Pectin Synthesis and Pollen Tube Growth in Arabidopsis Involves Three GAUT1 Golgi-Anchoring Proteins: GAUT5, GAUT6, and GAUT7. *Front. Plant Sci.* 11. doi:10.3389/fpls.2020.585774.

MacMillan, C.P., S.D. Mansfield, Z.H. Stachurski, R. Evans, and S.G. Southerton. 2010. Fasciclin-like arabinogalactan proteins: Specialization for stem biomechanics and cell wall architecture in Arabidopsis and Eucalyptus. *Plant J.* 62:689–703. doi:10.1111/j.1365-313X.2010.04181.x.

Manabe, Y., M. Nafisi, Y. Verhertbruggen, C. Orfila, S. Gille, C. Rautengarten, C. Cherk, S.E. Marcus, S. Somerville, M. Pauly, J. Paul Knox, Y. Sakuragi, and H.V. Scheller. 2011. Loss-of-function mutation of REDUCED WALL ACETYLATION2 in Arabidopsis leads to reduced cell wall acetylation and increased resistance to Botrytis cinerea. *Plant Physiol.* 155. doi:10.1104/pp.110.168989.

Manabe, Y., Y. Verhertbruggen, S. Gille, J. Harholt, S.L. Chong, P.M.A. Pawar, E.J. Mellerowicz, M. Tenkanen, K. Cheng, M. Pauly, and H.V. Scheller. 2013. Reduced wall acetylation proteins play vital and distinct roles in cell wall O-acetylation in Arabidopsis. *Plant Physiol.* 163. doi:10.1104/pp.113.225193.

Marx-Figini, M. 1966. Comparison of the biosynthesis of cellulose in vitro and in vivo in cotton bolls [45]. *Nature*. 210:754–755. doi:10.1038/210754a0.

McAdam, S.A.M., and T.J. Brodribb. 2018. Mesophyll cells are the main site of abscisic acid biosynthesis in water-stressed leaves. *Plant Physiol.* 177. doi:10.1104/pp.17.01829.

McAdam, S.A.M., F.C. Sussmilch, and T.J. Brodribb. 2016. Stomatal responses to vapour pressure deficit are regulated by high speed gene expression in angiosperms. *Plant Cell Environ.* 39. doi:10.1111/pce.12633.

McAusland, L., S. Vialet-Chabrand, P. Davey, N.R. Baker, O. Brendel, and T. Lawson. 2016. Effects of kinetics of light-induced stomatal responses on photosynthesis and water-use efficiency. *New Phytol.* 211:1209–1220. doi:10.1111/nph.14000.

McCann, M.C., B. Wells, and K. Roberts. 1990. Direct visualization of cross-links in the primary plant cell wall. *J. Cell Sci.* 96:323–334.

McNeil, M., A.G. Darvill, S.C. Fry, and P. Albersheim. 1984. Structure and function of the primary cell walls of plants. *Annu. Rev. Biochem.* 53:625–663. doi:10.1146/annurev.bi.53.070184.003205.

Meents, M.J., Y. Watanabe, and A.L. Samuels. 2018. The cell biology of secondary cell wall biosynthesis. *Ann. Bot.* 121:1107–1125. doi:10.1093/aob/mcy005.

Melotto, M., W. Underwood, and Y.H. Sheng. 2008. Role of stomata in plant innate immunity and foliar bacterial diseases. *Annu. Rev. Phytopathol.* 46. doi:10.1146/annurev.phyto.121107.104959.

Miwa, K., S. Wakuta, S. Takada, K. Ide, J. Takano, S. Naito, H. Omori, T. Matsunaga, and T. Fujiwara. 2013. Roles of BOR2, a boron exporter, in cross linking of rhamnogalacturonan II and root elongation under boron limitation in arabidopsis. *Plant Physiol.* 163. doi:10.1104/pp.113.225995.

Mohnen, D. 2008. Pectin structure and biosynthesis. *Curr. Opin. Plant Biol.* 11. doi:10.1016/j.pbi.2008.03.006.

Moore, J.P., E.E. Nguema-Ona, M. Vicré-Gibouin, I. Sørensen, W.G.T. Willats, A. Driouich, and J.M. Farrant. 2013. Arabinose-rich polymers as an evolutionary strategy to plasticize resurrection plant cell walls against desiccation. *Planta*. 237. doi:10.1007/s00425-012-1785-9.

Mortimer, J.C., G.P. Miles, D.M. Brown, Z. Zhang, M.P. Segura, T. Weimar, X. Yu, K.A. Seffen, E. Stephens, S.R. Turner, and P. Dupree. 2010. Absence of branches from xylan in Arabidopsis gux mutants reveals potential for simplification of lignocellulosic biomass. *Proc. Natl. Acad. Sci. U. S. A.* 107. doi:10.1073/pnas.1005456107.

Mott, K.A., and T.N. Buckley. 2000. Patchy stomatal conductance: Emergent collective behaviour of stomata. *Trends Plant Sci.* 5. doi:10.1016/S1360-1385(00)01648-4.

Mott, K.A., F. Denne, and J. Powell. 1997. Interactions among stomata in response to perturbations in humidity. *Plant, Cell Environ.* 20. doi:10.1046/j.1365-3040.1997.d01-138.x.

Moura, J.C.M.S., C.A.V. Bonine, J. de Oliveira Fernandes Viana, M.C. Dornelas, and P. Mazzafera. 2010. Abiotic and biotic stresses and changes in the lignin content and composition in plants. *J. Integr. Plant Biol.* 52. doi:10.1111/j.1744-7909.2010.00892.x.

Murashige, T., and F. Skoog. 1962. A Revised Medium for Rapid Growth and Bio Assays with Tobacco Tissue Cultures. *Physiol. Plant.* 15. doi:10.1111/j.1399-3054.1962.tb08052.x.

Nadeem, M., J. Li, M. Yahya, A. Sher, C. Ma, X. Wang, and L. Qiu. 2019. Research Progress and Perspective on Drought Stress in Legumes: A Review. *Int. J. Mol. Sci.* 20. doi:10.3390/ijms20102541.

Nafisi, M., M. Stranne, L. Fimognari, S. Atwell, H.J. Martens, P.R. Pedas, S.F. Hansen, C. Nawrath, H. V. Scheller, D.J. Kliebenstein, and Y. Sakuragi. 2015. Acetylation of cell wall is required for structural integrity of the leaf surface and exerts a global impact on plant stress responses. *Front. Plant Sci.* 6. doi:10.3389/fpls.2015.00550.

Naran, R., G. Chen, and N.C. Carpita. 2008. Novel rhamnogalacturonan I and arabinoxylan polysaccharides of flax seed mucilage. *Plant Physiol.* 148. doi:10.1104/pp.108.123513.

Ndeh, D., A. Rogowski, A. Cartmell, A.S. Luis, A. Baslé, J. Gray, I. Venditto, J. Briggs, X. Zhang, A. Labourel,

N. Terrapon, F. Buffetto, S. Nepogodiev, Y. Xiao, R.A. Field, Y. Zhu, M.A. O'Neill, B.R. Urbanowicz, W.S. York, G.J. Davies, D.W. Abbott, M.C. Ralet, E.C. Martens, B. Henrissat, and H.J. Gilbert. 2017. Complex pectin metabolism by gut bacteria reveals novel catalytic functions. *Nature*. 544:65–70. doi:10.1038/nature21725.

Negi, J., K. Moriwaki, M. Konishi, R. Yokoyama, T. Nakano, K. Kusumi, M. Hashimoto-Sugimoto, J.I. Schroeder, K. Nishitani, S. Yanagisawa, and K. Iba. 2013. A dof transcription factor, SCAP1, is essential for the development of functional stomata in arabidopsis. *Curr. Biol.* 23. doi:10.1016/j.cub.2013.02.001.

Neumetzler, L., T. Humphrey, S. Lumba, S. Snyder, T.H. Yeats, B. Usadel, A. Vasilevski, J. Patel, J.K.C. Rose, S. Persson, and D. Bonetta. 2012. The FRIABLE1 gene product affects cell adhesion in arabidopsis. *PLoS One*. 7. doi:10.1371/journal.pone.0042914.

Newman, R.H., S.J. Hill, and P.J. Harris. 2013. Wide-angle x-ray scattering and solid-state nuclear magnetic resonance data combined to test models for cellulose microfibrils in mung bean cell walls. *Plant Physiol.* 163. doi:10.1104/pp.113.228262.

Nir, I., H. Shohat, I. Panizel, N. Olszewski, A. Aharoni, and D. Weiss. 2017. The tomato DELLA protein PROCERA acts in guard cells to promote stomatal closure. *Plant Cell*. 29. doi:10.1105/tpc.17.00542.

Novaković, L., T. Guo, A. Bacic, A. Sampathkumar, and K.L. Johnson. 2018. Hitting the wall—sensing and signaling pathways involved in plant cell wall remodeling in response to abiotic stress. *Plants*. 7:89. doi:10.3390/plants7040089.

O'Neill, M.A., S. Eberhard, P. Albersheim, and A.G. Darvill. 2001. Requirement of borate cross-linking of cell wall rhamnogalacturonan II for Arabidopsis growth. *Science (80-.)*. 294:846–849. doi:10.1126/science.1062319.

O'Neill, M.A., D. Warrenfeltz, K. Kates, P. Pellerin, T. Doco, A.G. Darvill, and P. Albersheim. 1996. Rhamnogalacturonan-II, a pectic polysaccharide in the walls of growing plant cell, forms a dimer that is covalently cross-linked by a borate ester. In vitro conditions for the formation and hydrolysis of the dimer. *J. Biol. Chem.* 271:22923–22930. doi:10.1074/jbc.271.37.22923.

Oehme, D.P., M.T. Downton, M.S. Doblin, J. Wagner, M.J. Gidley, and A. Bacic. 2015. Unique aspects of the structure and dynamics of elementary Iβ cellulose microfibrils revealed by computational simulations. *Plant Physiol.* 168. doi:10.1104/pp.114.254664.

Ogura, T., C. Goeschl, D. Filiault, M. Mirea, R. Slovak, B. Wolhrab, S.B. Satbhai, and W. Busch. 2019. Root System Depth in Arabidopsis Is Shaped by EXOCYST70A3 via the Dynamic Modulation of Auxin Transport. *Cell*. 178. doi:10.1016/j.cell.2019.06.021.

Orfila, C., F.D. Degan, B. Jørgensen, H.V. Scheller, P.M. Ray, and P. Ulvskov. 2012. Expression of mung bean pectin acetyl esterase in potato tubers: Effect on acetylation of cell wall polymers and tuber mechanical properties. *Planta*. 236. doi:10.1007/s00425-012-1596-z.

Pabst, M., R.M. Fischl, L. Brecker, W. Morelle, A. Fauland, H. Köfeler, F. Altmann, and R. Léonard. 2013. Rhamnogalacturonan II structure shows variation in the side chains monosaccharide composition and methylation status within and across different plant species. *Plant J.* 76. doi:10.1111/tpj.12271.

Pandey, A., U. Rajamani, J. Verma, P. Subba, N. Chakraborty, A. Datta, S. Chakraborty, and N. Chakraborty. 2010. Identification of extracellular matrix proteins of rice (Oryza sativa L.) involved in dehydration-responsive network: A proteomic approach. *J. Proteome Res.* 9:3443–3464. doi:10.1021/pr901098p.

Pandey, V., and A. Shukla. 2015. Acclimation and Tolerance Strategies of Rice under Drought Stress. *Rice Sci.* 22:147–161. doi:10.1016/j.rsci.2015.04.001.

Panter, P. 2018. Exploring the role of cell-wall pectin and cross-linking in freezing tolerance and guard cell dynamics in Arabidopsis thaliana. Durham University, Durham.

Panter, P.E., O. Kent, M. Dale, S.J. Smith, M. Skipsey, G. Thorlby, I. Cummins, N. Ramsay, R.A. Begum, D. Sanhueza, S.C. Fry, M.R. Knight, and H. Knight. 2019. MUR1-mediated cell-wall fucosylation is required for freezing tolerance in Arabidopsis thaliana. *New Phytol.* 224:1518–1531. doi:10.1111/nph.16209.

Park, S.Y., P. Fung, N. Nishimura, D.R. Jensen, H. Fujii, Y. Zhao, S. Lumba, J. Santiago, A. Rodrigues, T.F.F. Chow, S.E. Alfred, D. Bonetta, R. Finkelstein, N.J. Provart, D. Desveaux, P.L. Rodriguez, P. McCourt, J.K. Zhu, J.I. Schroeder, B.F. Volkman, and S.R. Cutler. 2009. Abscisic acid inhibits type 2C protein phosphatases via the PYR/PYL family of START proteins. *Science (80-.)*. 324:1068–1071. doi:10.1126/science.1173041.

Park, Y.B., and D.J. Cosgrove. 2012a. Changes in cell wall biomechanical properties in the xyloglucan-deficient xxt1/xxt2 mutant of Arabidopsis. *Plant Physiol.* 158. doi:10.1104/pp.111.189779.

Park, Y.B., and D.J. Cosgrove. 2012b. A revised architecture of primary cell walls based on biomechanical changes induced by substrate-specific endoglucanases. *Plant Physiol.* 158.

doi:10.1104/pp.111.192880.

Parkhurst, D.F., and O.L. Loucks. 1972. Optimal Leaf Size in Relation to Environment. *J. Ecol.* 60. doi:10.2307/2258359.

Pauly, M., P. Albersheim, A. Darvill, and W.S. York. 1999. Molecular domains of the cellulose/xyloglucan network in the cell walls of higher plants. *Plant J.* 20. doi:10.1046/j.1365-313X.1999.00630.x.

Pauly, M., S. Gille, L. Liu, N. Mansoori, A. de Souza, A. Schultink, and G. Xiong. 2013. Hemicellulose biosynthesis. *Planta*. 238:627–642. doi:10.1007/s00425-013-1921-1.

Pauly, M., and K. Keegstra. 2008. Physiology and metabolism "Tear down this wall." *Curr. Opin. Plant Biol.* 11:233–235. doi:10.1016/j.pbi.2008.04.002.

Pauly, M., and K. Keegstra. 2016. Biosynthesis of the Plant Cell Wall Matrix Polysaccharide Xyloglucan∗. *Annu. Rev. Plant Biol.* 67. doi:10.1146/annurev-arplant-043015-112222.

Peaucelle, A., R. Wightman, and H. Höfte. 2015. The Control of Growth Symmetry Breaking in the Arabidopsis Hypocotyl. *Curr. Biol.* 25. doi:10.1016/j.cub.2015.05.022.

Pelloux, J., C. Rustérucci, and E.J. Mellerowicz. 2007. New insights into pectin methylesterase structure and function. *Trends Plant Sci.* 12:267–277. doi:10.1016/j.tplants.2007.04.001.

Perrin, R.M., Z. Jia, T.A. Wagner, M.A. O'Neill, R. Sarria, W.S. York, N. V. Raikhel, and K. Keegstra. 2003. Analysis of xyloglucan fucosylation in arabidopsis. *Plant Physiol.* 132. doi:10.1104/pp.102.016642.

Perrone, P., C.M. Hewage, A.R. Thomson, K. Bailey, I.H. Sadler, and S.C. Fry. 2002. Patterns of methyl and O-acetyl esterification in spinach pectins: New complexity. *Phytochemistry*. 60. doi:10.1016/S0031-9422(02)00039-0.

Persson, S., K.H. Caffall, G. Freshour, M.T. Hilley, S. Bauer, P. Poindexter, M.G. Hahn, D. Mohnen, and C. Somerville. 2007. The Arabidopsis irregular xylem8 mutant is deficient in glucuronoxylan and homogalacturonan, which are essential for secondary cell wall integrity. *Plant Cell*. 19. doi:10.1105/tpc.106.047720.

Philippe, F., J. Pelloux, and C. Rayon. 2017. Plant pectin acetylesterase structure and function: New insights from bioinformatic analysis. *BMC Genomics*. 18:undefined. doi:10.1186/s12864-017-3833-0.

Piro, G., M.R. Leucci, K. Waldron, and G. Dalessandro. 2003. Exposure to water stress causes changes in the biosynthesis of cell wall polysaccharides in roots of wheat cultivars varying in drought tolerance. *Plant Sci.* 165:559–569. doi:10.1016/S0168-9452(03)00215-2.

Piskurewicz, U., Y. Jikumaru, N. Kinoshita, E. Nambara, Y. Kamiya, and L. Lopez-Molina. 2008. The gibberellic acid signaling repressor RGL2 inhibits Arabidopsis seed germination by stimulating abscisic acid synthesis and ABI5 activity. *Plant Cell*. 20. doi:10.1105/tpc.108.061515.

Placido, D.F., M.T. Campbell, J.J. Folsom, X. Cui, G.R. Kruger, P.S. Baenziger, and H. Walia. 2013. Introgression of novel traits from a wild wheat relative improves drought adaptation in wheat. *Plant Physiol.* 161. doi:10.1104/pp.113.214262.

Pollard, M., F. Beisson, Y. Li, and J.B. Ohlrogge. 2008. Building lipid barriers: biosynthesis of cutin and suberin. *Trends Plant Sci.* 13. doi:10.1016/j.tplants.2008.03.003.

Popper, Z.A., and S.C. Fry. 2008. Xyloglucan-pectin linkages are formed intra-protoplasmically, contribute to wall-assembly, and remain stable in the cell wall. *Planta*. 227:781–794. doi:10.1007/s00425-007-0656-2.

Prashar, A., and H.G. Jones. 2014. Infra-red thermography as a high-throughput tool for field phenotyping. *Agronomy*. 4. doi:10.3390/agronomy4030397.

Ralet, M.C., M.J. Crépeau, G. Lefèbvre, G. Mouille, H. Höfte, and J.F. Thibault. 2008. Reduced number of homogalacturonan domains in pectins of an Arabidopsis mutant enhances the flexibility of the polymer. *Biomacromolecules*. 9. doi:10.1021/bm701321g.

Rayon, C., M. Cabanes-Macheteau, C. Loutelier-Bourhis, I. Salliot-Maire, J. Lemoine, W.D. Reiter, P. Lerouge, and L. Faye. 1999. Characterization of N-glycans from arabidopsis. Application to a fucose-deficient mutant. *Plant Physiol.* 119:725–734. doi:10.1104/pp.119.2.725.

Reiter, W.D., C.C.S. Chapple, and C.R. Somerville. 1993. Altered growth and cell walls in a fucose-deficient mutant of Arabidopsis. *Science (80-.).* 261:1032–1035. doi:10.1126/science.261.5124.1032.

Reuhs, B.L., J. Glenn, S.B. Stephens, J.S. Kim, D.B. Christie, J.G. Glushka, E. Zablackis, P. Albersheim, A.G. Darvill, and M.A. O'Neill. 2004. L-galactose replaces L-fucose in the pectic polysaccharide rhamnogalacturonan II synthesized by the L-fucose-deficient mur1 Arabidopsis mutant. *Planta*. 219. doi:10.1007/s00425-004-1205-x.

Rhee, S.Y., E. Osborne, P.D. Poindexter, and C.R. Somerville. 2003. Microspore Separation in the quartet 3 Mutants of Arabidopsis Is Impaired by a Defect in a Developmentally Regulated Polygalacturonase Required for Pollen Mother Cell Wall Degradation. *Plant Physiol.* 133. doi:10.1104/pp.103.028266.

Ricardi, M.M., R.M. González, S. Zhong, P.G. Domínguez, T. Duffy, P.G. Turjanski, J.D. Salgado Salter, K.

Alleva, F. Carrari, J.J. Giovannoni, J.M. Estévez, and N.D. Iusem. 2014. Genome-wide data (ChIP-seq) enabled identification of cell wall-related and aquaporin genes as targets of tomato ASR1, a drought stress-responsive transcription factor. *BMC Plant Biol.* 14. doi:10.1186/1471-2229-14-29.

Riederer, M., and L. Schreiber. 2001. Protecting against water loss: Analysis of the barrier properties of plant cuticles. *In* Journal of Experimental Botany.

Roelfsema, M.R.G., S. Hanstein, H.H. Felle, and R. Hedrich. 2002. CO2 provides an intermediate link in the red light response of guard cells. *Plant J.* 32. doi:10.1046/j.1365-313X.2002.01403.x.

Roelofsen, P.A. 1966. Ultrastructure of the Wall in Growing Cells and its Relation to the Direction of the Growth. *Adv. Bot. Res.* 2:69–149. doi:10.1016/S0065-2296(08)60250-5.

Rosales, M.A., C. Maurel, and P. Nacry. 2019. Abscisic acid coordinates dose-dependent developmental and hydraulic responses of roots to water deficit. *Plant Physiol.* 180. doi:10.1104/pp.18.01546.

Rose, J.K.C., J. Braam, S.C. Fry, and K. Nishitani. 2002. The XTH family of enzymes involved in xyloglucan endotransglucosylation and endohydrolysis: Current perspectives and a new unifying nomenclature. *Plant Cell Physiol.* 43. doi:10.1093/pcp/pcf171.

Rui, Y., and C.T. Anderson. 2016. Functional analysis of cellulose and xyloglucan in the walls of stomatal guard cells of Arabidopsis. *Plant Physiol.* 170:1398–1419. doi:10.1104/pp.15.01066.

Rui, Y., Y. Chen, B. Kandemir, H. Yi, J.Z. Wang, V.M. Puri, and C.T. Anderson. 2018. Balancing strength and flexibility: how the synthesis, organization, and modification of guard cell walls govern stomatal development and dynamics. *Front. Plant Sci.* 9. doi:10.3389/fpls.2018.01202.

Ryden, P., K. Sugimoto-Shirasu, A.C. Smith, K. Findlay, W.D. Reiter, and M.C. McCann. 2003. Tensile properties of Arabidopsis cell walls depend on both a xyloglucan cross-linked microfibrillar network and rhamnogalacturonan II-borate complexes. *Plant Physiol.* 132:1033–1040. doi:10.1104/pp.103.021873.

Scheller, H.V., R. Lou Doong, B.L. Ridley, and D. Mohnen. 1999. Pectin biosynthesis: A solubilized α1,4-galacturonosyltransferase from tobacco, catalyzes the transfer of galacturonic acid from UDP-galacturonic acid onto the non-reducing end of homogalacturonan. *Planta*. 207. doi:10.1007/s004250050511.

Scheller, H.V., and P. Ulvskov. 2010. Hemicelluloses. *Annu. Rev. Plant Biol.* 61. doi:10.1146/annurev-arplant-042809-112315.

Schindelin, J., I. Arganda-Carreras, E. Frise, V. Kaynig, M. Longair, T. Pietzsch, S. Preibisch, C. Rueden, S. Saalfeld, B. Schmid, J.Y. Tinevez, D.J. White, V. Hartenstein, K. Eliceiri, P. Tomancak, and A. Cardona. 2012. Fiji: An open-source platform for biological-image analysis. *Nat. Methods*. 9. doi:10.1038/nmeth.2019.

Schroeder, J.I., and S. Hagiwara. 1989. Cytosolic calcium regulates ion channels in the plasma membrane of Vicia faba guard cells. *Nature*. 338:427–430. doi:10.1038/338427a0.

Schulz, P., K. Piepenburg, R. Lintermann, M. Herde, M.A. Schöttler, L.K. Schmidt, S. Ruf, J. Kudla, T. Romeis, and R. Bock. 2021. Improving plant drought tolerance and growth under water limitation through combinatorial engineering of signalling networks. *Plant Biotechnol. J.* 19. doi:10.1111/pbi.13441.

Sechet, J., S. Htwe, B. Urbanowicz, A. Agyeman, W. Feng, T. Ishikawa, M. Colomes, K.S. Kumar, M. Kawai-Yamada, J.R. Dinneny, M.A. O'Neill, and J.C. Mortimer. 2018. Suppression of Arabidopsis GGLT1 affects growth by reducing the L-galactose content and borate cross-linking of rhamnogalacturonan-II. *Plant J.* 96:1036–1050. doi:10.1111/tpj.14088.

Seifert, G.J., and K. Roberts. 2007. The biology of arabinogalactan proteins. *Annu. Rev. Plant Biol.* 58. doi:10.1146/annurev.arplant.58.032806.103801.

Seymour, G.B., G. Tucker, and L.A. Leach. 2004. Cell adhesion molecules in plants and animals. *Biotechnol. Genet. Eng. Rev.* 21. doi:10.1080/02648725.2004.10648051.

Shao, H.B., L.Y. Chu, C.A. Jaleel, and C.X. Zhao. 2008. Water-deficit stress-induced anatomical changes in higher plants. *Comptes Rendus - Biol.* 331:215–225. doi:10.1016/j.crvi.2008.01.002.

Shope, J.C., D.B. Dewald, and K.A. Mott. 2003. Changes in Surface Area of Intact Guard Cells Are Correlated with Membrane Internalization. *Plant Physiol.* 133. doi:10.1104/pp.103.027698.

Simmons, T.J., J.C. Mortimer, O.D. Bernardinelli, A.C. Pöppler, S.P. Brown, E.R. DeAzevedo, R. Dupree, and P. Dupree. 2016. Folding of xylan onto cellulose fibrils in plant cell walls revealed by solid-state NMR. *Nat. Commun.* 7. doi:10.1038/ncomms13902.

Stephen, A.M., and J.H. Cummings. 1979. Water-holding by dietary fibre in vitro and its relationship to faecal output in man. *Gut.* 20. doi:10.1136/gut.20.8.722.

Stranne, M., Y. Ren, L. Fimognari, D. Birdseye, J. Yan, M. Bardor, J.C. Mollet, T. Komatsu, J. Kikuchi, H. V. Scheller, and Y. Sakuragi. 2018. TBL10 is required for O-acetylation of pectic rhamnogalacturonan-I in Arabidopsis thaliana. *Plant J.* 96. doi:10.1111/tpj.14067.

Stuart, D.A., and J.E. Varner. 1980. Purification and Characterization of a Salt-extractable Hydroxyproline-

rich Glycoprotein from Aerated Carrot Discs. *Plant Physiol.* 66:787–792. doi:10.1104/pp.66.5.787.

Sun, T.P., and F. Gubler. 2004. Molecular mechanism of gibberellin signaling in plants. *Annu. Rev. Plant Biol.* 55. doi:10.1146/annurev.arplant.55.031903.141753.

Takenaka, Y., K. Kato, M. Ogawa-Ohnishi, K. Tsuruhama, H. Kajiura, K. Yagyu, A. Takeda, Y. Takeda, T. Kunieda, I. Hara-Nishimura, T. Kuroha, K. Nishitani, Y. Matsubayashi, and T. Ishimizu. 2018. Pectin RG-I rhamnosyltransferases represent a novel plant-specific glycosyltransferase family. *Nat. Plants*. 4. doi:10.1038/s41477-018-0217-7.

Tan, L., S. Eberhard, S. Pattathil, C. Warder, J. Glushka, C. Yuan, Z. Hao, X. Zhu, U. Avci, J.S. Miller, D. Baldwin, C. Pham, R. Orlando, A. Darvill, M.G. Hahn, M.J. Kieliszewski, and D. Mohnena. 2013. An Arabidopsis cell wall proteoglycan consists of pectin and arabinoxylan covalently linked to an arabinogalactan protein. *Plant Cell*. 25. doi:10.1105/tpc.112.107334.

Tanaka, Y., T. Nose, Y. Jikumaru, and Y. Kamiya. 2013a. ABA inhibits entry into stomatal-lineage development in Arabidopsis leaves. *Plant J.* 74. doi:10.1111/tpj.12136.

Tanaka, Y., S.S. Sugano, T. Shimada, and I. Hara-Nishimura. 2013b. Enhancement of leaf photosynthetic capacity through increased stomatal density in Arabidopsis. *New Phytol.* 198. doi:10.1111/nph.12186.

Taylor, N.G., R.M. Howells, A.K. Huttly, K. Vickers, and S.R. Turner. 2003. Interactions among three distinct CesA proteins essential for cellulose synthesis. *Proc. Natl. Acad. Sci. U. S. A.* 100. doi:10.1073/pnas.0337628100.

Thorlby, G., E. Veale, K. Butcher, and G. Warren. 1999. Map positions of SFR genes in relation to other freezing-related genes of Arabidopsis thaliana. *Plant J.* 17:445–452. doi:10.1046/j.1365-313X.1999.00395.x.

Toro, G., J. Flexas, and J.M. Escalona. 2019. Contrasting leaf porometer and infra-red gas analyser methodologies: an old paradigm about the stomatal conductance measurement. *Theor. Exp. Plant Physiol.* 31. doi:10.1007/s40626-019-00161-x.

Tryfona, T., T.E. Theys, T. Wagner, K. Stott, K. Keegstra, and P. Dupree. 2014. Characterisation of FUT4 and FUT6 α-(1→2)-fucosyltransferases reveals that absence of root arabinogalactan fucosylation increases arabidopsis root growth salt sensitivity. *PLoS One*. 9. doi:10.1371/journal.pone.0093291.

Turner, N.C., and A. Graniti. 1969. Fusicoccin: A fungal toxin that opens stomata. *Nature*. 223. doi:10.1038/2231070a0.

Uga, Y., K. Sugimoto, S. Ogawa, J. Rane, M. Ishitani, N. Hara, Y. Kitomi, Y. Inukai, K. Ono, N. Kanno, H. Inoue, H. Takehisa, R. Motoyama, Y. Nagamura, J. Wu, T. Matsumoto, T. Takai, K. Okuno, and M. Yano. 2013. Control of root system architecture by DEEPER ROOTING 1 increases rice yield under drought conditions. *Nat. Genet.* 45. doi:10.1038/ng.2725.

Umezawa, T., N. Sugiyama, M. Mizoguchi, S. Hayashi, F. Myouga, K. Yamaguchi-Shinozaki, Y. Ishihama, T. Hirayama, and K. Shinozaki. 2009. Type 2C protein phosphatases directly regulate abscisic acid-activated protein kinases in Arabidopsis. *Proc. Natl. Acad. Sci. U. S. A.* 106:17588–17593. doi:10.1073/pnas.0907095106.

Vanholme, R., B. Demedts, K. Morreel, J. Ralph, and W. Boerjan. 2010. Lignin biosynthesis and structure. *Plant Physiol.* 153:895–905. doi:10.1104/pp.110.155119.

Vanzin, G.F., M. Madson, N.C. Carpita, N. V. Raikhel, K. Keegstra, and W.D. Reiter. 2002. The mur2 mutant of Arabidopsis thaliana lacks fucosylated xyloglucan because of a lesion in fucosyltransferase AtFUT1. *Proc. Natl. Acad. Sci. U. S. A.* 99:3340–3345. doi:10.1073/pnas.052450699.

Varner, J.E., and L.S. Lin. 1989. Plant cell wall architecture. *Cell*. 56:231–239. doi:10.1016/0092-8674(89)90896-9.

Verger, S., S. Chabout, E. Gineau, and G. Mouille. 2016. Cell adhesion in plants is under the control of putative O-fucosyltransferases. *Dev.* 143. doi:10.1242/dev.132308.

Voelker, S.L., B. Lachenbruch, F.C. Meinzer, P. Kitin, and S.H. Strauss. 2011. Transgenic poplars with reduced lignin show impaired xylem conductivity, growth efficiency and survival. *Plant, Cell Environ.* 34:655–668. doi:10.1111/j.1365-3040.2010.02270.x.

Vogel, J.P., T.K. Raab, C. Schiff, and S.C. Somerville. 2002. PMR6, a pectate lyase-like gene required for powdery mildew susceptibility in Arabidopsis. *Plant Cell*. 14. doi:10.1105/tpc.003509.

Vogel, J.P., T.K. Raab, C.R. Somerville, and S.C. Somerville. 2004. Mutations in PMR5 result in powdery mildew resistance and altered cell wall composition. *Plant J.* 40. doi:10.1111/j.1365-313X.2004.02264.x.

Voragen, A.G.J., G.J. Coenen, R.P. Verhoef, and H.A. Schols. 2009. Pectin, a versatile polysaccharide present in plant cell walls. *Struct. Chem.* 20:263–275. doi:10.1007/s11224-009-9442-z.

Wang, T., Y.B. Park, M.A. Caporini, M. Rosay, L. Zhong, D.J. Cosgrove, and M. Hong. 2013a. Sensitivity-enhanced solid-state NMR detection of expansin's target in plant cell walls. *Proc. Natl. Acad. Sci. U.*

S. A. 110. doi:10.1073/pnas.1316290110.

Wang, T., Y.B. Park, D.J. Cosgrove, and M. Hong. 2015. Cellulose-pectin spatial contacts are Inherent to never-dried Arabidopsis primary cell walls: Evidence from solid-state nuclear magnetic resonance. *Plant Physiol.* 168. doi:10.1104/pp.15.00665.

Wang, T., O. Zabotina, and M. Hong. 2012. Pectin-cellulose interactions in the arabidopsis primary cell wall from two-dimensional magic-angle-spinning solid-state nuclear magnetic resonance. *Biochemistry*. 51. doi:10.1021/bi3015532.

Wang, Y., J.C. Mortimer, J. Davis, P. Dupree, and K. Keegstra. 2013b. Identification of an additional protein involved in mannan biosynthesis. *Plant J.* 73:105–117. doi:10.1111/tpj.12019.

Watanabe, Y., M.J. Meents, L.M. McDonnell, S. Barkwill, A. Sampathkumar, H.N. Cartwright, T. Demura, D.W. Ehrhardt, A.L. Samuels, and S.D. Mansfield. 2015. Visualization of cellulose synthases in Arabidopsis secondary cell walls. *Science (80-.).* 350. doi:10.1126/science.aac7446.

Wiethölter, N., B. Graeßner, M. Mierau, A.J. Mort, and B.M. Moerschbacher. 2003. Differences in the methyl ester distribution of homogalacturonans from near-isogenic wheat lines resistant and susceptible to the wheat stem rust fungus. *Mol. Plant-Microbe Interact.* 16. doi:10.1094/MPMI.2003.16.10.945.

Willats, W.G.T., L. Mccartney, W. Mackie, and J.P. Knox. 2001a. Pectin: Cell biology and prospects for functional analysis. *Plant Mol. Biol.* 47. doi:10.1023/A:1010662911148.

Willats, W.G.T., C. Orfila, G. Limberg, H.C. Buchholt, G.-J.W.M. van Alebeek, A.G.. Voragen, S.E. Marcus, T.M.I.E. Christensen, J.D. Mikkelsen, B.S. Murray, and J.P. Knox. 2001b. Modulation of the Degree and Pattern of Methyl-esterification of Pectic Homogalacturonan in Plant Cell Walls. *J. Biol. Chem.* 276. doi:10.1074/jbc.m011242200.

Wolf, S., G. Mouille, and J. Pelloux. 2009. Homogalacturonan methyl-esterification and plant development. *Mol. Plant*. 2. doi:10.1093/mp/ssp066.

Woolfenden, H.C., G. Bourdais, M. Kopischke, E. Miedes, A. Molina, S. Robatzek, and R.J. Morris. 2017. A computational approach for inferring the cell wall properties that govern guard cell dynamics. *Plant J.* 92:5–18. doi:10.1111/tpj.13640.

Wu, H.C., V.P. Bulgakov, and T.L. Jinn. 2018. Pectin methylesterases: Cell wall remodeling proteins are required for plant response to heat stress. *Front. Plant Sci.* 871. doi:10.3389/fpls.2018.01612.

Wu, Y., E.T. Thorne, R.E. Sharp, and D.J. Cosgrove. 2001. Modification of expansin transcript levels in the maize primary root at low water potentials. *Plant Physiol.* 126. doi:10.1104/pp.126.4.1471.

Xiang, Y., X. Sun, X. Bian, T. Wei, T. Han, J. Yan, and A. Zhang. 2021. The transcription factor ZmNAC49 reduces stomatal density and improves drought tolerance in maize. *J. Exp. Bot.* 72. doi:10.1093/jxb/eraa507.

Xiao, C., T. Zhang, Y. Zheng, D.J. Cosgrove, and C.T. Anderson. 2016. Xyloglucan deficiency disrupts microtubule stability and cellulose biosynthesis in arabidopsis, altering cell growth and morphogenesis1[OPEN]. *Plant Physiol.* 170. doi:10.1104/pp.15.01395.

Xiong, G., K. Cheng, and M. Pauly. 2013. Xylan O-acetylation impacts xylem development and enzymatic recalcitrance as indicated by the arabidopsis mutant tbl29. *Mol. Plant*. 6. doi:10.1093/mp/sst014.

Xiong, L., K.S. Schumaker, and J.K. Zhu. 2002. Cell signaling during cold, drought, and salt stress. *Plant Cell*. 14. doi:10.1105/tpc.000596.

Yamaguchi, S. 2008. Gibberellin metabolism and its regulation. *Annu. Rev. Plant Biol.* 59. doi:10.1146/annurev.arplant.59.032607.092804.

Yang, L., C.C. Wang, W.D. Guo, X.B. Li, M. Lu, and C.L. Yu. 2006. Differential expression of cell wall related genes in the elongation zone of rice roots under water deficit. *Russ. J. Plant Physiol.* 53:390–395. doi:10.1134/S1021443706030150.

Yapo, B.M., P. Lerouge, J.F. Thibault, and M.C. Ralet. 2007. Pectins from citrus peel cell walls contain homogalacturonans homogenous with respect to molar mass, rhamnogalacturonan I and rhamnogalacturonan II. *Carbohydr. Polym.* 69:426–435. doi:10.1016/j.carbpol.2006.12.024.

Yi, H., Y. Rui, B. Kandemir, J.Z. Wang, C.T. Anderson, and V.M. Puri. 2018. Mechanical effects of cellulose, xyloglucan, and pectins on stomatal guard cells of arabidopsis thaliana. *Front. Plant Sci.* 871. doi:10.3389/fpls.2018.01566.

Zablackis, E., J. Huang, B. Müller, A.G. Darvill, and P. Albersheim. 1995. Characterization of the cell-wall polysaccharides of Arabidopsis thaliana leaves. *Plant Physiol.* 107:1129–1138. doi:10.1104/pp.107.4.1129.

Zablackis, E., W.S. York, M. Pauly, S. Hantus, W.D. Reiter, C.C.S. Chapple, P. Albersheim, and A. Darvill. 1996a. Substitution of L-fucose by L-galactose in cell walls of Arabidopsis mur1. *Science (80-.).* 272. doi:10.1126/science.272.5269.1808.

Zablackis, E., W.S. York, M. Pauly, S. Hantus, W.D. Reiter, C.C.S. Chapple, P. Albersheim, and A. Darvill.

1996b. Substitution of L-fucose by L-galactose in cell walls of Arabidopsis mur1. *Science (80-.).* 272:1808–1810. doi:10.1126/science.272.5269.1808.

Zang, H., S. Xie, B. Zhu, X. Yang, C. Gu, B. Hu, T. Gao, Y. Chen, and X. Gao. 2019. Mannan oligosaccharides trigger multiple defence responses in rice and tobacco as a novel danger-associated molecular pattern. *Mol. Plant Pathol.* 20. doi:10.1111/mpp.12811.

Zeiger, E. 1983. The Biology of Stomatal Guard Cells. *Annu. Rev. Plant Physiol.* 34:441–475. doi:10.1146/annurev.pp.34.060183.002301.

Zeng, W., A. Brutus, J.M. Kremer, J.C. Withers, X. Gao, A.D. Da Jones, and S.Y. He. 2011. A genetic screen reveals Arabidopsis Stomatal and/or apoplastic defenses against pseudomonas syringae pv. tomato DC3000. *PLoS Pathog.* 7. doi:10.1371/journal.ppat.1002291.

Zentella, R., N. Sui, B. Barnhill, W.P. Hsieh, J. Hu, J. Shabanowitz, M. Boyce, N.E. Olszewski, P. Zhou, D.F. Hunt, and T.P. Sun. 2017. The Arabidopsis O-fucosyltransferase SPINDLY activates nuclear growth repressor della. *Nat. Chem. Biol.* 13. doi:10.1038/nchembio.2320.

Zhang, B., Y. Gao, L. Zhang, and Y. Zhou. 2021. The plant cell wall: Biosynthesis, construction, and functions. *J. Integr. Plant Biol.* 63. doi:10.1111/jipb.13055.

Zhang, J., and W.J. Davies. 1991. Antitranspirant activity in xylem sap of maize plants. *J. Exp. Bot.* 42. doi:10.1093/jxb/42.3.317.

Zhang, L., C. Gao, F. Mentink-Vigier, L. Tang, D. Zhang, S. Wang, S. Cao, Z. Xu, X. Liu, T. Wang, Y. Zhou, and B. Zhang. 2019a. Arabinosyl deacetylase modulates the arabinoxylan acetylation profile and secondary wall formation. *Plant Cell*. 31. doi:10.1105/tpc.18.00894.

Zhang, L., B.C. Paasch, J. Chen, B. Day, and S.Y. He. 2019b. An important role of l-fucose biosynthesis and protein fucosylation genes in Arabidopsis immunity. *New Phytol.* 222:981–994. doi:10.1111/nph.15639.

Zhang, L., Y. Takahashi, P.K. Hsu, H. Kollist, E. Merilo, P.J. Krysan, and J.I. Schroeder. 2020. FRET kinase sensor development reveals SnRK2/OST1 activation by ABA but not by MeJA and high CO2 during stomatal closure. *Elife*. 9. doi:10.7554/eLife.56351.

Zhang, T., S. Mahgsoudy-Louyeh, B. Tittmann, and D.J. Cosgrove. 2014. Visualization of the nanoscale pattern of recently-deposited cellulose microfibrils and matrix materials in never-dried primary walls of the onion epidermis. *Cellulose*. 21. doi:10.1007/s10570-013-9996-1.

Zhang, T., Di. Vavylonis, D.M. Durachko, and D.J. Cosgrove. 2017. Nanoscale movements of cellulose microfibrils in primary cell walls. *Nat. Plants*. 3. doi:10.1038/nplants.2017.56.

Zhang, X., P.G. Dominguez, M. Kumar, J. Bygdell, S. Miroshnichenko, B. Sundberg, G. Wingsle, and T. Niittylä. 2018. Cellulose synthase stoichiometry in aspen differs from arabidopsis and Norway spruce. *Plant Physiol.* 177. doi:10.1104/pp.18.00394.

Zheng, M., Y. Meng, C. Yang, Z. Zhou, Y. Wang, and B. Chen. 2014. Protein expression changes during cotton fiber elongation in response to drought stress and recovery. *Proteomics*. 14:1776–1795. doi:10.1002/pmic.201300123.

Zhong, R., and Z.H. Ye. 2015. Secondary cell walls: Biosynthesis, patterned deposition and transcriptional regulation. *Plant Cell Physiol.* 56. doi:10.1093/pcp/pcu140.

Zhu, X., Q. Cao, L. Sun, X. Yang, W. Yang, and H. Zhang. 2018. Stomatal conductance and morphology of arbuscular mycorrhizal wheat plants response to elevated co2 and NaCl Stress. *Front. Plant Sci.* 9. doi:10.3389/fpls.2018.01363.

Zlatev, Z., and F.C. Lidon. 2012. An overview on drought induced changes in plant growth, water relations and photosynthesis. *Emirates J. Food Agric.* 24. doi:10.9755/ejfa.v24i1.10599.

Zykwinska, A.W., M.C.J. Ralet, C.D. Garnier, and J.F.J. Thibault. 2005. Evidence for in vitro binding of pectin side chains to cellulose. *Plant Physiol.* 139. doi:10.1104/pp.105.065912.